UNIVERSITY OF SOUTHAMPTON

FACULTY OF ENGINEERING, SCIENCE AND MATHEMATICS

Optoelectronics Research Centre

Holey optical fibres for high nonlinearity devices

by

Walter Belardi

Thesis submitted for the degree of Doctor of Philosophy

December 2003

UNIVERSITY OF SOUTHAMPTON

ABSTRACT

FACULTY OF ENGINEERING, SCIENCE AND MATHEMATICS
OPTOELECTRONICS RESEARCH CENTRE

Doctor of Philosophy

HOLEY OPTICAL FIBRES FOR HIGH NONLINEARITY DEVICES

by Walter Belardi

This thesis describes the development of a novel type of optical fibre, namely holey optical fibre (HF), for its specific incorporation in optical devices based on fibre nonlinearity. The development of the fabrication technique to produce such a fibre is discussed, and the fibres produced are characterized and used in device applications, proving the advantages of HF technology in the implementation of highly nonlinear optical devices, as well as showing its limitations. The initial fabrication problems that hindered the production of HFs with a high nonlinearity are identified and several strategies are adopted for its solution, including an experimental study of the HF drawing parameters, the invention of a novel holey fibre fabrication design based on an air clad HF jacket, the introduction of HF preform pressurization by means of a sealing technique and the use of a HF silica jacket. Thus long and robust HFs with a high nonlinearity can be reliably fabricated. In parallel with the development of the HF fabrication technique, the first applications of HF technology to high nonlinearity devices are investigated, ranging from a 2R data regenerator, based on only 3.3 m of a HF, to a Raman amplifier and a Brillouin laser based on long and robust HFs with low confinement losses, high birefringence and high anomalous dispersion at the operating wavelength. The negative impact of anomalous dispersion on the BER performances of a wavelength converter, and the limitations in terms of wavelength tuning range and phase matching of a high dispersion HF, directs our research towards the development of a HF with a relatively low normal dispersion (about $-30\ ps/nm-km$) and an extremely high effective nonlinearity ($\gamma = 70\ W^{-1}km^{-1}$). 15 meters of this HF were used to provide a demonstration of the first wavelength converter based on FWM, which allows error free-penalty free wavelength conversion of 10 Gbit/s data signals over a 10 nm bandwidth. As shown by these experiments one major issue of our HFs is the high polarization mode dispersion. We suggest a possible route to the solution of this problem, by systematically investigating the feasibility of a spun HF. We first use some hollow tubes to study the effects of preform spinning on the spin pitch, on a central hole and on an off-centre hole. Those preliminary results lead us towards the successful fabrication of the first spun HF, which demonstrates the applicability of the preform spinning technique to HF technology.

Contents

List of Figures

DECLARATION OF AUTHORSHIP

I, **Walter Belardi** ,

declare that the thesis entitled

"Holey optical fibres for high nonlinearity devices"

and the work presented in it are my own. I confirm that:

- this work was done wholly or mainly while in candidature for a research degree at this University;
- where any part of this thesis has previously been submitted for a degree or any other qualification at this University or any other institution, this has been clearly stated;
- where I have consulted the published work of others, this is always clearly attributed;
- where I have quoted from the work of others, the source is always given. With the exception of such quotations, this thesis is entirely my own work;
- I have acknowledged all main sources of help;
- where the thesis is based on work done by myself jointly with others, I have made clear exactly what was done by others and what I have contributed myself;
- I have published, as part of my PhD work, some of the research material contained within this thesis as journal and conference papers (see "List of publications").

Signed: .....

Date: .....

Acknowledgements

I acknowledge the importance of the financial support of the EPSRC, which has allowed the realization of this research project.

I wish to thank my supervisor Prof. David J. Richardson for his research guidance over these years, for his patient support and his time spent in defining the goals and main purposes of my research project. A sincere "thank you" is owed to Dr Eleanor Tarbox for her support during my PhD and, especially, for her generous help with the technical writing of this thesis. Thanks are also due to Dr Tanya M. Monro for helping in my supervision during my PhD and for providing me with valuable advice on several occasions.

I owe a great deal of debt of gratitude to my great friend and best collaborator Dr Ju Han Lee, for his genuine friendship, authentic help and fundamental support, at work as in life. I wish to thank my collaborators Mr Zulfadzli Yusoff, Dr Periklis Petropoulos, Dr Jonathan Price, Mrs Joanne Baggett and Dr Morten Ibsen for their help, and the discussions undertaken for the understanding of various optical phenomena. I must thank the silica fibre fabricators Dr Jayanta Sahu, Dr Kentaro Furusawa, Dr Richard Williams and Dr Gilberto Brambilla for their help and constant advice during the days spent together in our cleanroom. Thank you especially to Eng. Paul Turner and Mr Grant Harris for teaching me the basic techniques for optical fibre fabrication and for their availability. Finally thanks to Dr Marco Romagnoli for great motivation at the beginning of my research project.

Moreover I wish to thank all the many friends that have been close to me over these years spent in Southampton. They all constitute for me a treasure of inestimable value and I may try to remember here only some of them, which have been particularly close to me: Matteo Fuochi, Fabio Ghiringhelli, Ron Haaksman, Christos Grivas, Katia Gallo, Francesca Parmigiani, Costantino Corbari, Angélique Favre, Yuh Tat Cho, Alessandro Busacca, Emiliano Rustighi. And, undoubtedly, a special tribute of gratitude is given to Lenka Šimanová for being very close to me through difficult periods of my stay in Southampton and because her lovely blue eyes let me always forget the grey sky of England.

Finally I would like to thank my parents, my brothers Antonio, Biagio and Riccardo and my friends Francesco Griseta, Paolo Lombardi, Marco Passerini and Gianluca Sala, who, even if far away, have been always close to me with their thoughts and support.

"...iudico potere essere vero che la fortuna sia arbitra della metà delle azioni nostre, ma che etiam lei ne lasci governare l'altra metà, o presso, a noi."

*"**Il principe**", Chapter 25*
Niccolò Machiavelli

Nomenclature

a	Fibre core radius
A_{eff}	Effective mode area
AFF	Air filling fraction (d/Λ)
$AOTF$	Acousto-optic tunable filter
B	Modal birefringence
BER	Bit error rate
CF	Conventional fibre
CW	Continuous wave
d	Hole size
D	Diameter
DCF	Dispersion compensating fibre
DFB	Distributed feedback
DSF	Dispersion shifted fibre
e_{12}	Elasto-optic coefficient
E	Electric field
$EDFA$	Erbium doped fibre amplifier
Er	Erbium
FBG	Fibre Bragg grating
FWM	Four wave mixing
g_B	Brillouin gain
g_R	Raman gain coefficient
Ge	Germanium
GVD	Group velocity dispersion
HC	Hollow core
HNL	Highly nonlinear holey fibre
HF	Holey fibre
I	Intensity
ID	Inner diameter
k_0	Propagation constant in the vacuum
L	Length
L_B	Beat length
LPG	Long period grating
$MCVD$	Modified chemical vapor deposition

$MTIR$	Modified form of total internal reflection
n	Refractive index
n_2	Nonlinear coefficient
NA	Numerical aperture
NRZ	Non-return to zero
$NZ-DSF$	Non-zero dispersion fibre
OD	Outer diameter
OSA	Optical spectrum analyzer
OVD	Outside vapor deposition
p	polarization
p_{nl}	Nonlinear polarization
P	Power
P_r	Pressure
PBG	Photonic bandgap
$PBGF$	Photonic bandgap fibre
PC	Photonic crystal
PCF	Photonic crystal fibre
PE	Polarization extinction
PM	Polarization maintaining
PMD	Polarization mode dispersion
r	Radius
R	Rotation speed
RF	Radio frequency
RZ	Return to zero
SBS	Stimulated Brillouin scattering
SEM	Scanning electron micrograph
SHG	Second harmonic generation
SOP	State of polarization
SPM	Self phase modulation
SRS	Stimulated Raman scattering
t	Time
T	Temperature
TIR	Total internal reflection
UV	Ultraviolet
v_g	Group velocity
VAD	Vapor-phase axial deposition
XPM	Cross phase modulation
w	Gaussian spot size of the optical mode
W_d	Drawing speed
W_f	Feed speed
WD	Waveguide dispersion

WDM	Wavelength division multiplexing
Yb	Ytterbium
$1D$	One dimension
$2D$	Two dimensions
$3D$	Three dimensions
α	Loss factor
β	Mode propagation constant
χ	Electric susceptibility
δ	Surface tension
$\Delta\phi$	Nonlinear phase change
ϵ_0	vacuum permittivity
γ	Effective nonlinearity
κ	Thermal conductivity
λ	Wavelength of the light
Λ	Hole pitch
μ	Viscosity
ν	Frequency
ω	Angular frequency
ρ	Density
τ	Time delay

Chapter 1

Introduction

Since the first development of low-loss optical fibers (20 dB/km at the He-Ne laser wavelength of 633 nm) in 1970 by "Corning Glass Works" in the United States (Kapron et al. [1970]), optical fibres have become a practical means for high capacity transmission of coherent light signals. Since then, major improvements have been made both in glass manufacturing and in optical communication systems. The introduction of novel optical fibre fabrication methods, such as MCVD (Nagel et al. [1982]), OVD and the VAD technique (Li [1985]) today enables the production of very low loss optical fibers (0.1484 dB/km at 1570 nm has recently been reported by Nagayama et al. [2002]). At the same time, the development of wavelength division multiplexed (WDM) optical communication systems based on optical amplification (Ghatak and Thyagarajan [1998]) (and of the parallel improvement of infrared transmitters and receivers) allows today the successful transmission of data at rates of 3.2 Tb/s over 1000 km in the 1550 nm telecommunication window (Gupta et al. [2002]).
The workhorse of optical fibers since 1983 has been conventional, dispersion-unshifted single mode fibers, such as SMF 28. Several million km of this fiber, optimized for operation at 1300 nm, were installed. However, the increasing demand for information-carrying capacity has led to the increase in the practical optical fibre transmission capacity, by operating at a wavelength around 1550 nm, which corresponds to the lowest loss of silica based optical fibres and to the gain band of the erbium doped fibre amplifier (EDFA) (Becker et al. [1999]). On the other hand the positive dispersion (about 16 $ps/nm-km$) of conventional optical fibres at 1550 nm compromises the correct transmission and receipt of the data, limiting the transmission bit rate (Agrawal [1997]). Thus it is necessary to compensate their dispersion with "dispersion compensating fibers" (DCFs), which at this wavelength have a high negative dispersion ($\sim -100 ps/nm-km$). To overcome the issue of optical fiber dispersion, other types of optical fibers have also been developed such as "dispersion shifted fibers"(DSFs), which have zero dispersion at 1550 nm, and "non-zero dispersion fibers" (NZ-DSFs) which have very low dispersion (of either sign) in the C-band (Agrawal [2001b]). However, to date, fibre dispersion remains a critical issue for the implementation of high capacity transmission systems, operating at very high bit rates (40 Gb/s and beyond) (Nelson [2003]).

Another significant special class of optical fibers is highly nonlinear (HNL) fibres (Agrawal [2001b]). They have a small core size (less than 5 μm) and a relatively high numerical aperture (NA) (up to 0.2). In such fibres, light is confined within a small effective area (A_{eff}) (about 20 μm^2), and the correspondingly high light intensity can enhance effective fibre nonlinearity. Nonlinear effects can be used for a very wide range of applications such as, for example, soliton generation (in which nonlinearity balances the effects of dispersion, leading to the theoretical propagation of an undistorted optical pulse over enormous fibre lengths), fast optical switching, broadband Raman amplification and efficient wavelength conversion. Thus HNL-fibres have a fundamental importance in the development of optical communication systems performing at a very high bit rate (Agrawal [2001b]).

The physical principle according to which light can propagate in all conventional optical fibres is known as "total internal reflection" (TIR). It relies on the fact that an electromagnetic wave, travelling from a higher refractive index medium to a lower refractive index medium, can be reflected when its incidence angle is greater than a critical angle given by Snell's law (Born and Wolf [1999]). Thus all standard optical fibres are, in the most simple scheme, constituted by two materials, one for the central core with a higher refractive index, and one for the outer cladding with a lower refractive index (Ghatak and Thyagarajan [1998]).

However other forms of optical guidance have been studied over the years. Already in 1977 Yeh et al. [1977] introduced a theoretical model to study the propagation of electromagnetic radiation in periodically stratified media. Their considerations led to the prediction of a "Bragg waveguide", in which light can be propagated in a low-index slab, provided that the bounding media, with indices of refraction higher than that of the inner slab, are periodic. In this case the physical principle of guidance relies on the Bragg effect (Born and Wolf [1999]), according to which light of a certain wavelength λ can be reflected when directed to a medium with a given refractive index periodicity, that precisely satisfies a "Bragg condition" $\lambda = 2n\Lambda$, where n is the average refractive index and Λ the period of the stratified media. Only a narrow frequency band is reflected and it is referred to as a "photonic band-gap" (PBG), in which light propagation through the periodic medium is forbidden. Thus, in the design of Yeh et al. [1977], light can propagate through a low index medium because of the presence of a PBG inside the low index central slab, which prevents light dissipation in the bounding media.

Yeh et al. [1978] extended their results to the prediction of a Bragg fiber, an optical fibre made with multiple periodic cladding layers around a lower refractive index core (Yariv and Yeh [1984]). Such a fibre has been successfully fabricated only in recent years (Brechet et al. [2000]) and demonstrates that their predictions were correct.

The Bragg reflection effect in optical fibers became increasingly important with the development of fibre Bragg gratings (FBGs). First discovered in 1978 (Hill et al. [1978]), their importance in optical communication systems and sensors was really recognized only in the '90s (Kashyap [1999], Othonos and Kalli [1999]) when novel techniques were

developed for their production (Meltz et al. [1989], Hill et al. [1993], Hill et al. [1990], Lemaire et al. [1993], Eggleton et al. [1994]), which rapidly led to their commercialization in 1995. In a FBG a one dimensional periodic refractive index along an optical fibre causes Bragg reflection for a narrow frequency band (PBG) and this effect finds applications in optical filters, mode converters, sensing and dispersion compensation (Agrawal [2001a], Agrawal [1997], Ibsen and Feced [2002]). FBGs are also used for pulse compression (Williams et al. [1995]), pulse shaping, optical switching and distributed-feedback (DFB) semiconductor lasers (Kashyap [1999]).

The importance of periodic optical structures in a three dimensional (3D) configuration was established in 1987 by the pioneering work of Yablonovitch [1987] and John [1987]. They theoretically predicted that in a 3D periodic structure a complete PBG could be created for light travelling in all directions, similar to what happens in a grating in 1D or in a Bragg fibre in 2D. Thus, if a defect is created inside such an otherwise periodic structure, light of certain wavelengths (i.e. within the PBG) becomes trapped in this defect, being unable to propagate anywhere. They developed their theory associating the behaviour of a photon in a 3D periodic structure to that of an electron in a semiconductor crystal (which also has an energy gap between the valence band and the conduction band), and thus they referred to this novel optical structure as a "photonic crystal" (PC) (Yablonovitch [1993], Russell [1992]).

To demonstrate the validity of his theory, Yablonovitch's group fabricated the first "photonic" crystal in 1991 at the "Navesink Research Centre" in New Jersey (Yablonovitch et al. [1991], Yablonovitch [1993]), following an earlier design of Ho et al. [1990] based on a "diamond structure". This first PC was made by direct drilling of several holes in a commercial dielectric material with a refractive index of 3.6 (Emerson & Cumming Stycast-12). Given the large scale of the PC, it could work only at microwave frequencies, which requires a PC crystal periodicity of the order of centimeters. The experiment was successful, demonstrating the existence of a full PBG between 13 and 16 GHz, and opened the way to a novel and promising branch of optoelectronics research.

Since then PCs have attracted great attention, because they provide the possibility to manipulate photons with an unprecedented degree of freedom (Joannopoulos et al. [1995], Joannopoulos et al. [1997]). Although the first motivation for a PC was the inhibition of spontaneous emission in a semiconductor laser (Yablonovitch [1987]), several other applications were very soon identified. In particular potential applications such as optical switches, microfabricated lasers, waveguides, light emitting diodes, telecommunications and others, motivated researchers to develop fabrication techniques for producing miniaturized PCs, to operate in the visible and infrared wavelengths. In the last 10 years this research has made massive advances, passing through fabrication techniques known as "woodpile structure" (Ho et al. [1994], Sozuer and Dowling [1994], Lin et al. [1998]), "woodpile by wafer fusion" (Noda et al. [2000]), "layer by layer" (Johnson and Joannopoulos [2000]), "stacking by micromanipulation" (Aoki et al. [2002]), "X-ray interference lithography" (Qi and Smith [2002]), "holographic lithography" (Sharp et al.

[2002]) and "colloidal crystal" (Lopez [2003]). The outstanding development in the fabrication technique of 3D PCs has led to the achievement of a full photonic bandgap up to infrared frequencies ($\lambda \sim 1.3\ \mu m$) (Noda et al. [2000]) and further improvements are expected soon (Aoki et al. [2002], Lopez [2003]). Excellent results have been obtained also with metallic 3D PCs, in which a PBG between 8 and 20 μm has recently been reported (Fleming et al. [2002]).

If the periodicity of a PC is restricted to only two dimensions (2D), then it can still block certain wavelengths of light at any angle in the plane of the PC device. However its production is much simpler than in the 3D case and mature fabrication techniques with high resolution (about 15 nm), such as e-beam lithography, can be readily employed, using semiconductor-based structures, such as GaAs/AlGaAs and silicon on insulator (SOI) (Krauss [2003]). 2D PCs with a photonic bandgap at near infrared wavelength have been demonstrated already (Krauss et al. [1996]) and currently the origin of their optical losses is being investigated.

PCs may lead to true photonic integration thanks to the miniaturization of the optical devices, which means they can operate over lengths on a wavelength scale, and to their functionality as optical delay lines, optical pulse compression/dilation and wavelength splitters. The realization of a nano-photonic integrated circuit operating at optical frequencies would have massive effects throughout the world of information technology (Krauss [2003], Yablonovitch [2002]).

According to the theory of PCs (Yablonovitch [1987]) the refractive index contrast in a PC required to obtain a PBG should be greater than 2. However, in 1995 Birks et al. [1995] predicted the feasibility of a 2D PC in a silica/air structured optical fibre, in which the refractive index contrast was less than 0.45. The idea was that, if light travelled perpendicularly to a 2D PC, then a PBG could be achieved with a much lower refractive index contrast.

The air/silica periodic structure modelled by Birks et al. [1995] consisted of a periodic array of air holes that run along the full length of the optical fibre, and thus is commonly called "photonic crystal fibre" (PCF). If a defect is created in this otherwise periodic transverse structure, for example by eliminating a hole, light of certain wavelengths may become confined in this defect by the PBG effect. This kind of fibre is also referred to as a "photonic bandgap fibre"(PBGF)(Knight et al. [1998b]), due to the nature of its guidance. However a defect maybe created also by increasing the size of one hole. In this case light guidance may be allowed inside this low refractive index air-hole, resulting in a specific type of PBGF, named "hollow core photonic crystal fibre" (HC-PCF).

The applications of HC-PCFs are of great interest. Theoretically the guidance of light in air could lead to a fibre with very low loss, theoretically at least much below that of actual conventional optical fibres (Xu and Yariv [2003]). Nonlinear effects in this fibre may be almost completely suppressed, allowing the transmission of very high optical powers in air (avoiding also the risk of glass breakdown). By filling the air hole with gas, vapor or a low index liquid, very strong interactions are possible with the light in

the guided mode; this could be useful in gas sensing and monitoring, and to enhance non linear effects in gas. Moreover a HC-PCF may be the ideal means to guide atoms or particles. Besides that, the narrow band performance of this fibre suggests that it could be used as a spectral filtering device.
In 1998 Philip Russell's group, at the University of Bath, in England, produced the first PCF whose guidance relies on the existence of a PBG effect. In this case the guiding medium was silica but, one year later, the same group reported the fabrication of a hollow core-PCF, in which light could be guided by a PBG effect inside an air core (Cregan et al. [1999]).
Only a few centimeters of these first PBGFs could be characterized because of the precise longitudinal uniformity of the structure required to observe a PBG effect. However, in recent years, major improvements have been made in the fabrication of HC-PCFs. A 1 meter long HC-PCF has been filled with hydrogen (a gas broadly adopted in gas based nonlinear optics) and successfully used by Russell's group for the demonstration of Stimulated Raman Scattering, to highlight the advantages of using HC-PCF technology. The energy required to achieve a 30% Raman conversion from a pump wavelength to a Stokes wavelength was 800 nJ, two orders of magnitude lower than previously reported experiments; thus moving gas-based nonlinear optics to previously inaccessible parameter regimes of intensity and interaction length (Bernabid et al. [2002]). At the same time "Corning Incorporated", in the USA, demonstrated a 100 m HC-PCF with a minimum loss of 13 dB/km at 1500 nm (Venkataraman et al. [2002], Smith et al. [2003]), opening up the way to practical applications of HC-PCFs in telecommunications.
As it happens, the first attempts at making a PBGF didn't work very well. The fabricated structure was not regular enough and the holes were not large enough to support photonic band gap guidance, as predicted by Birks et al. [1995]. However, even these first fibres were characterized and, surprisingly, even though they were formed of one single material and a PBG could not form, they guided a single optical mode over an extended wavelength range (Knight et al. [1996]). Almost by chance, Russell and his colleagues had discovered a new type of optical waveguide based on a single material, with extraordinary properties.
The first mathematical model to explain these unusual properties was developed by Birks et al. [1997]. The guidance of these novel optical fibres was related to the fact that the presence of the air holes in the fibre cladding lowers the effective cladding refractive index. Thus the principle of guidance of this structure is similar to the TIR effect and is often referred to as a "modified form of total internal reflection" (MTIR). The presence of holes around the fibre core acts as a "modal sieve" (Russell [2003]), which blocks the fundamental mode from escaping out of the core but allows higher order modes (with a smaller spatial distribution) to leak out of the core through the gaps between the air holes. This novel type of waveguide is often also referred to as PCF that guides by MTIR, although more often now, since its guidance doesn't rely on an exact periodicity of the structure (Monro et al. [2000]), the more generic term of "microstructured

fibre"(MF) or "holey fibre"(HF) is used.
Birks et al. [1997] demonstrated that a HF can be made single mode for all wavelengths. This dramatically novel behaviour of HFs is related to the strong wavelength dependence of the cladding refractive index. In a HF the V number (Ghatak and Thyagarajan [1998]) is given by $V = \frac{2\pi}{\lambda} a \sqrt{n_1^2 - n_{eff}^2(\lambda)}$ where a is the core radius, n_1 is the silica core refractive index and $n_{eff}(\lambda)$ is the effective cladding refractive index (λ dependent). When light with a longer wavelength travels inside a HF, it penetrates inside the cladding holes more than shorter wavelengths do, decreasing the effective cladding refractive index. Thus the inverse dependence of the V number on wavelength can be balanced by its direct dependence on the light wavelength through $n_{eff}(\lambda)$. This can happen only for small ratios d/Λ between the hole size d and the hole spacing Λ ($d/\Lambda \leq 0.4$, Nielsen and Mortensen [2003]).
It was shown in 1998 that this single mode behaviour is not related to the core size but only to the air filling fraction d/Λ (AFF) and that single mode HFs could be made using very large core sizes (Knight et al. [1998a]). As a consequence, HF technology offers a practical way to make large mode optical fibres for the delivery and the generation of very high optical powers (Knight et al. [1998a], Wadsworth et al. [2001]). Moreover HFs have been demonstrated with an effective area as large as 680 μm^2 and bend losses comparable with those of conventional optical fibers (CFs) (Baggett et al. [2001]). HFs offer the advantages of easier fabrication (depending only on the AFF of the HF and not on complex refractive index profiles as in CFs) and of single mode guidance over an extended range of wavelengths.
By using an air clad fabrication approach (Belardi et al. [2002a], Sahu et al. [2001], Espindola et al. [1999]), some dual-clad large mode area HF lasers have been fabricated by different research groups through HF doping with ytterbium (Yb)(Furusawa et al. [2001], Wadsworth et al. [2003], Limpert et al. [2003]), erbium(Er) (Simonneau et al. [2003]) or erbium/ytterbium (Er/Yb) (Bouwmans et al. [2003]). This approach allows a very high NA to be achieved for the inner cladding, which in turn provides efficient pump launching inside a small inner cladding, reduced pump thresholds, high pump absorption, the possibility to use shorter fibres and an extended tuning range. In particular, an output power as high as 80 W with a slope efficiency of 78% has been recently demonstrated using a 2.3 m long air-clad Yb doped HF, fabricated at "Crystal Fibre", in Denmark (Limpert et al. [2003]).
Besides high power lasers, other HF devices have been demonstrated that take advantage of the novel HF structure. Gratings have been written in a germanium (Ge) doped HF core (Espindola et al. [1999], Eggleton et al. [1999]) or in a pure silica HF core (Kakarantzas et al. [2002]). Russell's group demonstrated direct writing of a long period grating (LPG) in a pure silica core HF by mean of a CO_2 laser beam and, by writing such a LPG in a high birefringence HF, made a rocking filter (Kakarantzas et al. [2003]). On the other hand, Eggleton et al. [2000], at "Lucent Technologies", in the USA, demonstrated the first Ge doped HF gratings. By filling the HF holes with polymer, to

enhance the wavelength tuning with temperature, they could tune the resonance of a grating filter between 1450 and 1600 nm by varying the temperature of the fibre between 25 °C and 120 °C. The same group has also fabricated the first tapered HF (Chandalia et al. [2001]), showing efficient light coupling in the taper, and demonstrating a variable optical attenuator HF device incorporating a "grapefruit" HF filled with polymer and adiabatically tapered (Kerbage et al. [2001]).
The properties of the HF structure may also be employed for sensing applications (Monro et al. [2001]) and some applications of multicore HFs (Mangan et al. [2000]) for curvature sensing (MacPherson et al. [2001]) and Doppler difference velocimetry (MacPherson et al. [2003]) have already been demonstrated.

But probably one of the most important prospects offered by HF technology regards the possibility to make HFs with a nonlinearity 10-100 times greater than in conventional fibers (CFs) (Broderick et al. [1999a]), which is not possible using standard optical fiber technology. Indeed, by increasing the air filling fraction (AFF) of a HF, one can decrease the effective cladding refractive index and fabricate HFs with a very high numerical aperture (NA) (> 1). Thus small core HFs with a high NA can have an extremely small effective area (1.5 μm^2) (Monro et al. [1999b]) and their effective nonlinearity γ can be enhanced to values as high as 70 $W^{-1}km^{-1}$ (Belardi et al. [2002b]).
In Chapter 2, we will review in detail some of the main nonlinear effects that can be enhanced in a HF, and that we have investigated. In particular we discuss the origin of self phase modulation (SPM), cross phase modulation (XPM), four wave mixing (FWM), stimulated Raman scattering (SRS) and stimulated Brilluoin scattering (SBS). This chapter provides the necessary background to understand the HF nonlinear devices discussed in Chapter 4 and 5. In the same chapter, we also show how small core HFs, besides having a high nonlinearity, can have completely novel dispersion properties. These include anomalous dispersion at a wavelength less than 1.27 μm (Mogilevtsev et al. [1998], Monro et al. [1999b], Ranka et al. [2000], Knight et al. [2000]), broadband flat dispersion (Ferrando et al. [1999], Reeves et al. [2002], Monro et al. [1999a]) or very high normal dispersion at 1550 nm (Birks et al. [1999]). These novel dispersion characteristics have found a large number of applications in pulse compression (Price et al. [2001a]), soliton propagation (Wadsworth et al. [2000], Price et al. [2001a]) and soliton generation (Price et al. [2001b]) at short wavelengths.
The practical use of HF technology for high nonlinearity applications, and to access novel dispersion regimes, has been, for some time, hindered by difficulties in the fabrication of small core HFs with a very high AFF. HF fabrication, as for conventional fibres, relies on fibre drawing from a starting glass preform (Li [1985]). When, during the drawing stage, the hole dimensions are reduced to a very small size (about $1\mu m$), the surface tension acting on the inner walls of the holes, causes them to collapse. This and other fabrication issues have been faced and successfully solved through a systematic study of the HF drawing parameters and the introduction of novel fabrication techniques. The

HF fabrication problem and our approach to its solution are discussed in Chapter 3. The fabricated fibres have been characterized and some of the first HNL-HF devices have been demonstrated using them (chapters 4 and 5).

In chapter 4 we provide the first demonstration of HF technology applied to practical high nonlinearity devices. We first show the demonstration of a 2R data regenerator based on only 3.3 m of an air clad HF (Petropoulos et al. [2001a]). Then we develop our fabrication design to produce a long and robust HF with a silica outer jacket. We used this fibre to demonstrate, for the first time, pulse compression and soliton formation in a HF with anomalous dispersion at 1 μm. Subsequently, by fabricating a HF with 4 air hole rings and a core size of about 1.5 μm, we demonstrate some HFs with low confinement losses and a high birefringence (one order of magnitude higher than standard "Panda" fibres). By using one of these HFs, with an effective area of 2.8 μm^2 we show the first implementation of a HF Raman amplifier (Lee et al. [2001]) and a HF Brillouin laser (Yusoff et al. [2002b]).

In chapter 5 we focus our attention on HNL-HF devices providing wavelength conversion. We first develop a HF wavelength converter based on XPM in an anomalous dispersion HF (Lee et al. [2002b]), achieving wavelength conversion over 20 nm tuning range but obtaining a 4 dB power penalty in the wavelength converted soliton pulses transmitted at 10 Gbit/s data rate. We deduced that this power penalty was due to the high anomalous dispersion of our HF (Nakazawa et al. [1999]) and, by repeating the same experiment but using a normal dispersion HF (Lee et al. [2003b]), we confirm our assumption by obtaining error free, almost penalty free wavelength conversion of 10 $Gbit/s$ soliton control pulses.

Given the importance of high normal dispersion fibres in optical communications (Goyal et al. [2002], Gruner-Nielsen et al. [1999]), we fabricate a high normal dispersion fibre, following a design of Finazzi et al. [2003c], with an almost regular structure and low confinement losses, and confirm the interesting possibility of HF technology for dispersion compensating devices (Birks et al. [1999], Shen et al. [2003]). Moving further, toward the implementation of an efficient wavelength converter based on FWM, we fabricate a HF with a moderate negative dispersion (about $-30\ ps/nm-km$) and a record effective nonlinearity of about 70 $W^{-1}km^{-1}$. We finally use this HF for the demonstration of an efficient FWM based wavelength converter (Belardi et al. [2002b]).

However the use of small core HNL-HFs in highly nonlinear applications still presents problems. The polarization beat length of these small core HFs with high AFF is usually less than 1 cm, and the related problem of polarization mode dispersion (PMD)(Agrawal [2001b]) represents a major obstacle to the development of practical HNL-HF devices. Thus, in chapter 6 of this thesis, we address a possible route to the possible solution of this problem by demonstrating that the preform spinning technique (Payne et al. [1983]), previously applied since the '80s to CFs for the demonstration of very low birefringence fibres (Barlow et al. [1981]), can be successfully applied also to the fabrication of HNL-HFs.

Chapter 2

Small core holey optical fibres

2.1 Introduction

A holey fibre (HF) is an optical fibre that can be made by using a single material (typically ultra pure silica), in which the optical confinement is due to the presence of a matrix of air holes that runs along the full length of the fibre (Knight et al. [1996], Birks et al. [1997]). The critical holey fibre parameters that govern the guidance properties of a HF are the hole size d, the distance between adjacent holes Λ and their ratio d/Λ , called the air filling fraction (AFF), which is an indication of the air percentage inside the holey fibre (see Fig. 2.1).

Small core HFs are a particular class of HFs, which are of special interest, due to their potential to have a very high nonlinearity and novel dispersion properties.

In this thesis, we describe the fabrication, properties and some device applications of highly nonlinear holey fibers (HNL-HFs). Therefore this chapter aims to provide the background to understand the main properties and applications of small core HFs.

In particular, in Sect. 2.3, we explain why and how a HF can have a nonlinearity 10-100 times higher than conventional fibres.

In the following section, we discuss some of the main nonlinear effects which it is possible to enhance in a HF, such as self phase modulation (SPM), cross phase modulation (XPM), four wave mixing (FWM), Raman effect and Brillouin effect. All of these nonlinear effects have been used for the implementation of the various HF based nonlinear devices, described in chapter 4 and chapter 5.

In section 2.5, we discuss the novel dispersion properties of small core HFs, such as anomalous dispersion at a wavelength less than 1.3 μm and high normal dispersion at 1.55 μm, and outline for which kind of applications these properties can be used.

Finally, in section 2.6, we provide basic information on the birefringence of optical fibres, outlining why it is that small core HFs normally have a very high birefringence.

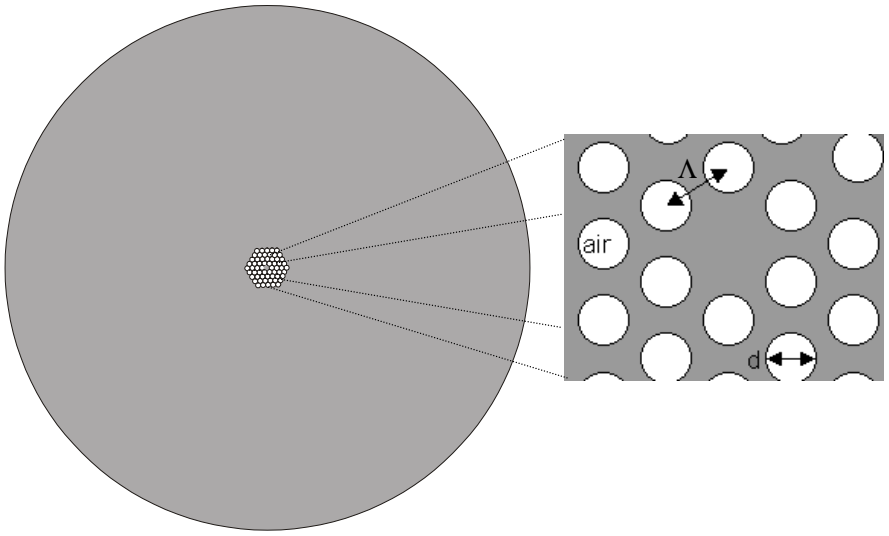

FIGURE 2.1: Sketch of a small core holey fibre. Λ is the hole distance, d is the hole size.

2.2 Optical confinement

A conventional optical fibre (CF) is made by using two different (but compatible) materials for the core and the cladding. The core material has a higher refractive index than the cladding material so that light can be confined inside the core by total internal reflection (TIR) (Ghatak and Thyagarajan [1998]).
Unlike CFs, in a HF both core and cladding can be made by using the same material (which is normally pure silica). However the presence of air holes in the cladding lowers the effective refractive index of the cladding leading to optical guidance within the fibre (Birks et al. [1997]). This effect is often referred to as a "modified form of total internal reflection" (MTIR). Moreover the average cladding refractive index can be modified by simply changing the hole size and does not require any periodicity of the holey structure (Monro et al. [2000]).
Note that it is possible to obtain guidance in holey fibres using photonic band gap effects but this requires a large air fill fraction and periodicity of the structure (Birks et al. [1995], Knight et al. [1998b], Cregan et al. [1999], Venkataraman et al. [2002]). However, we will not consider this form of guidance further within this thesis.

2.3 Effective area and numerical aperture

The effective core area A_{eff} of an optical fibre provides an effective measure of the area over which the fundamental mode is confined during its propagation within the fibre and is defined as (Agrawal [2001b]):

$$A_{eff} = \frac{[\int_{-\infty}^{\infty}\int_{-\infty}^{\infty}|E(x,y)|^2\,dxdy]^2}{\int_{-\infty}^{\infty}\int_{-\infty}^{\infty}|E(x,y)|^4\,dxdy} \tag{2.1}$$

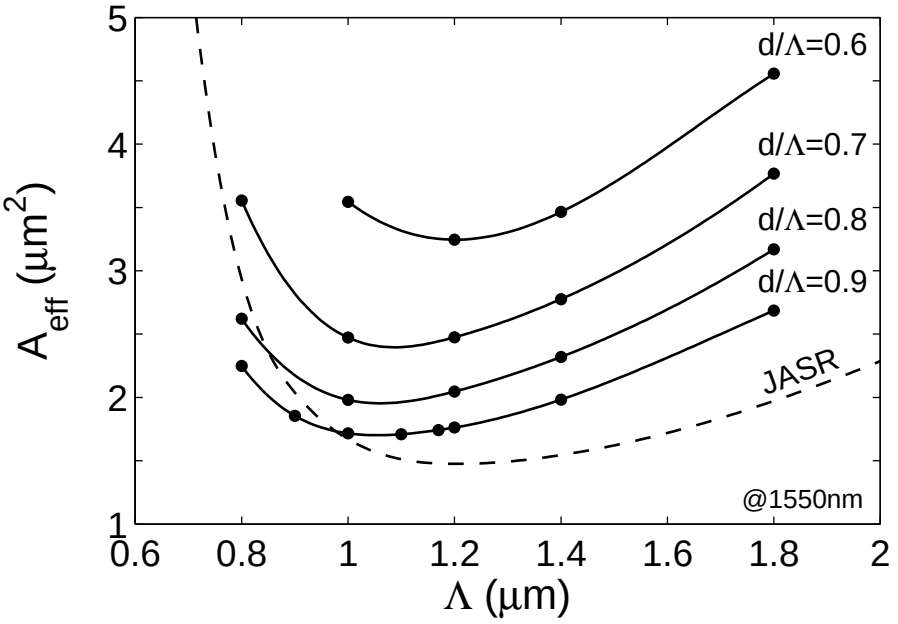

FIGURE 2.2: Predicted effective mode area as a function of hole-to-hole spacing Λ. Dashed curve, silica jacketed air-suspended rod (JASR) of diameter Λ (Finazzi et al. [2003c])

where $|E(x, y)|$ is the amplitude of the transverse electric field propagating inside the fibre. If E is approximated by a Gaussian distribution then $A_{eff} = \pi w^2$ where w is the Gaussian spot size of the mode.

The value of A_{eff} depends on the core diameter $2a$ of the fibre and its numerical aperture NA. For a given value of NA, A_{eff} reduces with decreasing core diameter $2a$ until a minimum value A^m_{eff}, corresponding to a core diameter $2a_m$ is reached. Beyond this point, once $2a$ becomes smaller than $2a_m$, A_{eff} increases because the fundamental mode becomes less confined within the core.

On the other hand, for a given core diameter $2a$, an increase of the NA reduces A_{eff} because the propagating mode can be better confined within the fibre.

Therefore the key to achieve very low A_{eff} values is to use the largest possible NA and to decrease the core diameter $2a$ to the value $2a_m$, corresponding to the minimum of the effective area A^m_{eff} (Finazzi et al. [2003c]).

Fig. 2.2 shows some theoretical predictions of Finazzi et al. [2003c] regarding small core HFs, obtained by using a multipole computational method (White et al. [2002b], Kuhlmey et al. [2002]). As we can see, HF technology offers an easy way to increase the NA by simply modifying d/Λ, and reducing the HF core size by reducing the hole pitch Λ. Fig. 2.2 also shows that the minimum value of the effective area theoretically achievable, with an extremely high AFF (ideally a jacket air-suspended rod (JASR)) and a hole pitch of about 1.2 μm, is about 1.5 μm^2. We will experimentally demonstrate this point in Sect. 5.5, where the measurement of such a small effective area in a practical HF will be shown.

At the other extreme, the possibility to fabricate single mode fibres with low NA, with

a $d/\Lambda < 0.4$ (Nielsen and Mortensen [2003]) and a large Λ (about 15 μm), allows also the production of single mode HFs with effective area as large as 680 μm^2 (Knight et al. [1998a], Monro et al. [1999b], Baggett et al. [2001]).
For standard fibres the range of achievable A_{eff} is limited by the practical possibility to fabricate CFs with high NA by means of silica core doping. In practice A_{eff} can vary between 20 μm^2 (Agrawal [2001b]) and about 450 μm^2 (Broderick et al. [1999b]) in the 1.5 μm region, depending on the fibre design. Thus HF technology allows this range of values to be greatly increased by means of simple modifications of the geometric characteristics of the HF.
Within this thesis we analyze the fabrication issues and the experimental properties of HFs with a very small effective area, thus with a very high air filling fraction AFF (d/Λ) and a small core size (about 1 μm). In these HFs, light can be confined very tightly to structural features of the order of the wavelength of the light, and which is simply not possible with any other optical fibre.

2.4 Nonlinearity

If light can be confined in an extremely small effective area, as in a high NA and small core HF, then the light power can be concentrated in a very small area, leading to very high optical intensities. At such a high optical intensities glass behaves nonlinearly and the total polarization $\mathbf{p}$ is given by (Agrawal [2001b]):

$$\mathbf{p} = \epsilon_0(\chi^{(1)}\mathbf{E} + \chi^{(2)}\mathbf{E}^2 + \chi^{(3)}\mathbf{E}^3 + ...) \tag{2.2}$$

where ϵ_0 is the vacuum permittivity and $\chi^{(j)}(j = 1, 2, ...)$ is the jth order "electric susceptibility". In general, $\chi^{(j)}$ is a tensor of rank j+1. The second order susceptibility $\chi^{(2)}$, which is responsible for such nonlinear effects as second harmonic generation, is non-zero only for media that lack an inversion symmetry at the molecular level. Thus $\chi^{(2)}$ vanishes for silica glass (Agrawal [2001b]) and the lowest order nonlinear effects in all silica based fibres originate from the third order susceptibility $\chi^{(3)}$.
In this section we describe in detail some of the most important physical effects that are caused by the optical fibre nonlinearity which we have used in the implementation of our HF based devices.

2.4.1 Self phase modulation

We first consider what happens when a single high intensity light beam travels inside an optical fibre.
The refractive index n, for a given wavelength of the light λ, in a silica based optical fibre can be written as (Ghatak and Thyagarajan [1998], Agrawal [2001b]) :

$$n = n_0 + n_2' I \tag{2.3}$$

with

$$n_0 \simeq 1.45\ (\lambda = 1550\ nm); \qquad n_2' = \frac{2n_2}{\epsilon_0 c n_0}; \qquad I = \frac{P}{A_{eff}} \tag{2.4}$$

where

$$n_2 = \frac{3Re(\chi^{(3)}_{xxxx})}{8n_0} \tag{2.5}$$

and c is the speed of light, P is the power carried by a mode in an optical fibre, A_{eff} is the effective area, I is the intensity, Re stands for real part and the optical field is assumed to be linearly polarized so that only one component $\chi^{(3)}_{xxxx}$ of the fourth-rank tensor contributes to the refractive index.
n_2 is called the "nonlinear coefficient" (also known as "Kerr nonlinearity coefficient") while the effective nonlinearity per unit length γ can be written as (Agrawal [2001b]):

$$\gamma = \frac{n_2 \omega_0}{A_{eff} c} \tag{2.6}$$

where ω_0 is the light frequency in vacuum and c is the speed of the light.
Thus from equation 2.3 and 2.4, we see that, by decreasing the effective area of an optical fibre, we can increase the intensity I and thereby the refractive index change Δn :

$$\Delta n = n - n_0 = n_2' I \tag{2.7}$$

Therefore we can increase the nonlinear phase change $\Delta\phi$ experienced by the light during propagation, which is given by (Agrawal [2001b], Ghatak and Thyagarajan [1998]):

$$\Delta\phi = \Delta n k_0 L = n_2' I k_0 L \tag{2.8}$$

where k_0 is the propagation constant in a vacuum and L is the fibre interaction length. The phenomenon which refers to the self induced phase shift experienced by an optical field during its propagation is called "self phase modulation" (SPM). Indeed, if we launch a Gaussian pulse with a temporal width $2t_0$ inside an optical fibre, we will have (Agrawal [2001b], Ghatak and Thyagarajan [1998]):

$$I = I_0 \exp\left(-\frac{2t^2}{{t_0}^2}\right) \tag{2.9}$$

and so the phase across the pulse is modulated by its own intensity envelope (SPM):

$$\Delta\phi = n_2' k_0 L I_0 \exp\left(-\frac{2t^2}{{t_0}^2}\right) \tag{2.10}$$

Since the frequency $\omega = \omega_0 - \frac{d\phi}{dt}$, we can see how the time dependent phase change experienced by optical signal pulses may alternatively be regarded as a change in the instantaneous frequency of the signal, which is referred to as frequency chirp. By substituting this expression in equation 2.10 and developing the calculations (see Agrawal [2001b]) it can be shown that SPM leads to spectral broadening of the pulse. Thus one

of the possible applications of this effect can be optical switching by use of a nonlinear fibre and of a spectral filter, as described in Sect. 4.2 (Petropoulos et al. [2001a]).
In a silica HF the nonlinear coefficient has roughly the same value as in a CF since this value depends only on the core material. However, the possibility to have a small effective area in a HF, leads to an increase in the light intensity I. Thus, from equation 2.8, we can see that the same nonlinear phase shift can be achieved by using a HF with a much shorter length than a CF. Due to the direct dependence of $\Delta\phi$ on both I and L, we can say that a HF with an effective area 10 times smaller than a highly nonlinear CF, can have a length 10 times shorter to achieve the same nonlinear performance. Indeed, by changing the A_{eff} of a HF it is possible to enhance the effective nonlinearity γ (equation 2.6), which is 1-10 $W^{-1}km^{-1}$ for a standard fibre ($A_{eff} = 20 - 100\ \mu m^2$), up to about 70 $W^{-1}km^{-1}$ for $A_{eff} = 1.5\ \mu m^2$. This implies that standard nonlinear devices using SPM, based on CFs with lengths of several hundred meters (Mamyshev [1998]), can be implemented by using only few meters of HF, opening up the possibility of more compact and cheaper nonlinear devices. An application of the SPM using a short HF (about 3 m) will be shown in Sect. 4.2 (Petropoulos et al. [2001a]).

2.4.2 Cross phase modulation

We now consider two optical signals propagating inside an optical fibre, interacting with each other through the fibre nonlinearity. Indeed each signal experiences SPM and they also influence each other by changing the refractive index experienced by the other signal, resulting in phase modulation. This phenomenon is known as "cross-phase modulation" (XPM). The nonlinear refractive index for each signal of a different frequency with the same polarization in an optical fibre can thus be expressed as (Agrawal [2001b], Ghatak and Thyagarajan [1998]):

$$n_i = n_i^L + n_2 I_i + 2n_2 I_j \tag{2.11}$$

$$n_j = n_j^L + n_2 I_j + 2n_2 I_i \tag{2.12}$$

where $n_{i,j}^L$ represents the linear refractive index for each signal and n_2 is the usual nonlinear coefficient. $I_{i,j}$ represents the optical intensities of the two signals, respectively. The factor of 2 on the right hand side of equation 2.11 and 2.12 shows that XPM is twice as effective as SPM for the same intensity. Given the direct dependence of the refractive index on the light intensity, the advantages of using HF technology to enhance this Kerr nonlinear effect are the same as for SPM, discussed above.
Electromagnetic theory can be adopted to explain the origin of both SPM and XPM. The rapidly varying part of the electric field can be written in the form:

$$\mathbf{E} = \frac{1}{2}\mathbf{x}[E_1 \exp(-i\omega_1 t) + E_2 \exp(-i\omega_2 t)] + c.c. \tag{2.13}$$

where $\mathbf{x}$ is the polarization unit vector, ω_1 and ω_2 are the centre frequencies of the two pulses. The amplitudes of E_1 and E_2 are assumed to be slowly varying functions of time. Remembering from equation 2.2 that the nonlinear part of the induced polarization $\mathbf{p}$ is $\mathbf{p}_{nl} = \epsilon_0 \chi \mathbf{E}^3$ and substituting equation 2.13, we can write (Agrawal [2001b]):

$$\begin{aligned}\mathbf{p}_{nl} = \frac{1}{2}\mathbf{x}\{&p_{nl}(\omega_1)\exp(-i\omega_1 t) + p_{nl}(\omega_2)\exp(-i\omega_2 t) \\ &+ p_{nl}(2\omega_1 - \omega_2)\exp[-i(2\omega_1 - \omega_2)t] + \\ &+ p_{nl}(2\omega_2 - \omega_1)\exp[-i(2\omega_2 - \omega_1)t]\} + c.c.\end{aligned} \tag{2.14}$$

where

$$p_{nl}(\omega_1) = \chi_{eff}(|E_1|^2 + 2\,|E_2|^2)E_1 \tag{2.15}$$

$$p_{nl}(\omega_2) = \chi_{eff}(|E_2|^2 + 2\,|E_1|^2)E_2 \tag{2.16}$$

$$p_{nl}(2\omega_1 - \omega_2) = \chi_{eff} {E_1}^2 {E_2}^* \tag{2.17}$$

$$p_{nl}(2\omega_2 - \omega_1) = \chi_{eff} {E_2}^2 {E_1}^* \tag{2.18}$$

with $\chi_{eff} = \left(\frac{3\epsilon_0}{4}\right)\chi^{(3)}_{xxxx}$ and the complex conjugates of E_1 and E_2 are E_1^* and E_2^*.
As we can see, the induced nonlinear polarization of equation 2.14 exhibits new frequency components at $2\omega_1 - \omega_2$ and $2\omega_2 - \omega_1$. These new components are generated from the phenomenon of four-wave mixing, which is discussed in Sect. 2.4.3, and are negligible unless special efforts are made to satisfy the associated phase matching condition. The remaining two terms contribute to the refractive index. $p_{nl}(\omega_j)$ can be written in the form $(j = 1, 2)$ (Agrawal [2001b])

$$p_{nl}(\omega_j) = \epsilon_0 \epsilon_j^{nl} E_j \tag{2.19}$$

After combining it with the linear part, the total induced polarization can be expressed as:

$$p(\omega_j) = \epsilon_0 \epsilon_j E_j \tag{2.20}$$

If the imaginary part of $\chi^{(3)}$ related to an absorption coefficient is ignored, the relative electric permittivity ϵ_j can be written as:

$$\epsilon_j = \epsilon_j^l + \epsilon_j^{nl} = (n_j^l + \Delta n_j)^2 \tag{2.21}$$

where n_j^l is the linear part of the refractive index and Δn_j is the change due to the third-order nonlinear effects. Under the approximation $\Delta n_j << n_j^l$ and the assumption

$n_1^l \simeq n_2^l = n_0$, the nonlinear part of the refractive index is found to be

$$\Delta n_j \approx \frac{\epsilon_j^{nl}}{2n_j} \approx n_2(|E_j|^2 + 2\,|E_{3-j}|^2) \tag{2.22}$$

As the signal pulse propagates through the fibre, it obtains an intensity-dependent nonlinear phase given by (Agrawal [2001b])

$$\phi_{nl}(t) = \frac{2\pi L_{eff} n_2}{\lambda}[|E_j|^2 + 2\,|E_{3-j}|^2] \tag{2.23}$$

The first term accounts for SPM and the second is responsible for XPM.
The XPM-induced coupling is also observed between optical waves of the same frequency but different polarization. Interestingly, XPM between the two waves of orthogonal polarization is less effective than that between two waves of different frequencies as it shows a factor of 2/3 rather than 2 in equations 2.11 and 2.12 although the qualitative behaviour is the same. The XPM effect in an optical fibre has a range of applications, for example a Kerr shutter based on XPM induced nonlinear birefringence (Asobe et al. [1992]), wavelength conversion using a dual wavelength loop mirror (Yu et al. [2000]), optical data demultiplexing (Yamamoto et al. [1998]) etc.
In particular HF technology can be applied to improve the performances of such nonlinear devices based on XPM in terms of power/length requirements. We have successfully demonstrated an efficient WDM wavelength converter based on XPM, in which a HF length of only 5.8 m has been used (Lee et al. [2003b])(see Sect. 5.3). This is an outstanding achievement when we compare it with similar experiments, using several hundred meters of dispersion shifted fibres (Ohlen et al. [2000]).

2.4.3 Four wave mixing

Another nonlinear effect of paramount importance in optical communication systems is "four-wave mixing"(FWM). It can occur when two or more frequencies of light propagate through an optical fibre. Providing a condition known as phase matching (momentum conservation) is satisfied, light is generated at new frequencies by converting optical power at the original signal wavelengths (Agrawal [2001b]). The equation that defines the frequency of a FWM product is given by

$$\omega_{ijk} = \omega_i + \omega_j + \omega_k \tag{2.24}$$

The generation of new frequencies from two partially non-degenerate input signals is shown schematically in Fig. 2.3. The main features of four-wave mixing can also be understood by taking into account the third-order polarization term in equation 2.2. Consider four optical waves oscillating at frequencies $\omega_1, \omega_2, \omega_3$ and ω_4 which are propagating in the same direction z and linearly polarized along the x axis. The total electric

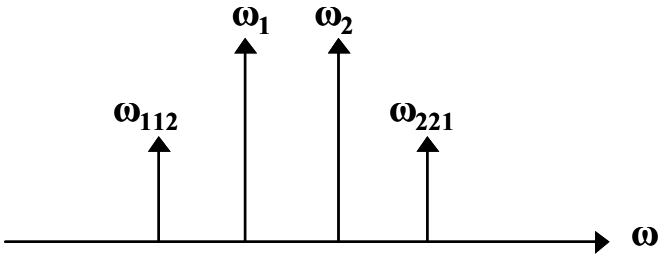

FIGURE 2.3: Schematic diagram of additional frequency generation through FWM for the partially non-degenerate case

field can be written as

$$\mathbf{E} = \mathbf{x}\frac{1}{2}\sum_{1}^{4} E_j \exp[i(k_j z - \omega_j t)] + c.c. \tag{2.25}$$

where $k_j = \frac{n_j \omega_j}{c}$ and n_j is the refractive index . After substituting equation 2.25 in the following equation

$$\mathbf{p}_{nl} = \epsilon_0 \chi^{(3)} \mathbf{E}^3 \tag{2.26}$$

$\mathbf{p}_{nl}$ exhibits the following form:

$$\mathbf{p}_{nl} = \mathbf{x}\frac{1}{2}\sum_{1}^{4} p_j \exp[i(k_j z - \omega_j t)] + c.c. \tag{2.27}$$

p_j is found to consist of a large number of terms involving the three products of three electric fields. For example, p_4 can be expressed as (Agrawal [2001b]):

$$\begin{aligned} p_4 = \frac{3\epsilon_0}{4}\{[|E_4|^2 + 2(|E_1|^2 + |E_2|^2 + |E_3|^2)]E_4 + \\ + 2E_1 E_2 E_3 \exp(i\theta_+) + 2E_1 E_2 E_3^* \exp(i\theta_-) + ...\} \end{aligned} \tag{2.28}$$

$$\theta_+ = (k_1 + k_2 + k_3 - k_4)z - (\omega_1 + \omega_2 + \omega_3 - \omega_4)t \tag{2.29}$$

$$\theta_- = (k_1 + k_2 - k_3 - k_4)z - (\omega_1 + \omega_2 - \omega_3 - \omega_4)t \tag{2.30}$$

The term proportional to E_4 in equation 2.28 accounts for SPM and XPM effects; the remaining terms are responsible for four-wave mixing. The efficiency of the FWM terms depends on the relative phase between E_4 and p_4 which is given by θ_+, θ_-. Efficient FWM requires frequency matching as well as phase matching. Of the two FWM terms in equation 2.28 the latter term is more readily used in optical fibre with high efficiency. In this case two photons at frequencies ω_1 and ω_2 are annihilated with the simultaneous creation of two photons at frequencies ω_3 and ω_4.

$$\omega_3 + \omega_4 = \omega_1 + \omega_2 \tag{2.31}$$

The phase matching condition to be achieved can be expressed as

$$\Delta k = k_3 + k_4 - k_1 - k_2 = \frac{n_3\omega_3 + n_4\omega_4 - n_1\omega_1 - n_2\omega_2}{c} = 0 \tag{2.32}$$

In the particular case of $\omega_1 = \omega_2$ (degenerate case), it is relatively easy to satisfy $\Delta k = 0$. The generation of new optical components has serious negative implications within wavelength division multiplexed (WDM) transmission systems, however it can be used to obtain data demultiplexing (Inoue and Toba [1992]), wavelength conversion (Clausen et al. [2001]) or dispersion compensation in long-haul optical fibre links (Watanabe et al. [1993]).
These highly nonlinear applications require the use of conventional fibers with low dispersion, high nonlinearity and a few hundreds meters length(Okuno et al. [1999]). Moreover it has been shown that efficient broadband wavelength conversion based on FWM requires the use of a short fibre length (Aso et al. [2000]). The use of HFs for this application can thus offer not only the advantage of more compact devices, but also should allow, in principle, the improvement of the performances of such devices. In Sect. 5.6 we demonstrate an efficient wavelength converter based on FWM using only 15 m of a HF with a record nonlinearity (Belardi et al. [2002b]).

2.4.4 Raman effect

SPM, XPM, and FWM are nonlinear effects that relate to the intensity dependence of the material refractive index. These are elastic nonlinear effects in the sense that there is no energy transfer among the light signals and the dielectric medium in which they propagate.
Another class of nonlinear phenomena is constituted by inelastic effects, in which a part of the propagating signal energy transfers to the medium or vice versa. Such effects are both the, so called, "Raman effect" and "Brillouin effect".
The Raman effect is based on energy transfer between the optical field propagating inside a nonlinear medium and the optical phonons of the medium (Agrawal [2001b]). This interaction can occur in two different directions. In the first, a photon of the incident field (called the pump) is annihilated to create a photon at a lower frequency (belonging to the Stokes wave) and a phonon with the right energy and momentum, to satisfy the total energy and momentum conservation.
In the second, a higher energy photon (at the so called anti-Stokes frequency) can also be created if a phonon loses part of its energy and momentum.
The initial growth of the Stokes wave can be described by (Agrawal [2001b]):

$$\frac{dI_z}{dz} = g_R I_P I_S \tag{2.33}$$

where I_S is the Stokes intensity, I_p is the pump intensity, and the Raman coefficient gain g_R is related, on a fundamental level, to the imaginary part of the third order nonlinear susceptibility $\chi^{(3)}$ (see Agrawal [2001b]). Its value for pure silica is $7 \cdot 10^{-14} m/W$. In

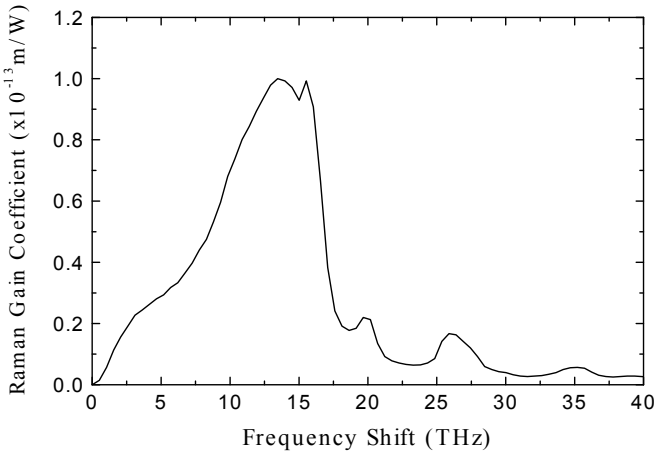

FIGURE 2.4: Raman-gain spectrum for fused silica at a pump wavelength $\lambda_p = 1\mu m$. The Raman gain scales inversely with λ_p (Agrawal [2001b]).

general, g_R depends on the composition of the fibre core and can vary significantly with the use of different dopants or using glasses other than silica (Stegeman et al. [2003]). Moreover there is an inverse dependence of g_R on the pump wavelength λ_P.
The Raman gain spectrum $g_R(\Omega)$, where Ω represents the frequency difference between the pump and the Stokes wave, extends in silica fibres over a large frequency range (up to 40 THz) with a broad peak located near 13 THz. Optical fibres can act as broadband amplifiers because of this feature. Indeed, if we consider a continuous wave (CW) pump beam at a frequency ω_P and a probe signal at a frequency ω_S co-propagating inside a fibre, the probe signal will be amplified because of the Raman gain, as long as the frequency difference $\Omega = \omega_P - \omega_S$ lies within the bandwidth of the Raman gain spectrum. The Raman threshold is defined as the input pump power P_0 at which the Stokes power P_S becomes equal to the pump power at the fibre output P_P:

$$P_s(L) = P_P(L) = P_0 \exp(-\alpha_P L) \tag{2.34}$$

where L is the fibre length and α_P is the pump loss factor. The critical pump power to reach the Raman threshold P_0^{cr} is found to be (see Agrawal [2001b]):

$$P_0^{cr} \simeq 16 \frac{A_{eff}}{L_{eff} \cdot g_R} \tag{2.35}$$

where L_{eff} is the effective interaction length which, because of pump absorption, is reduced from L to L_{eff}, where

$$L_{eff} = \frac{1 - \exp(-\alpha_P L)}{\alpha_P} \tag{2.36}$$

As the equation 2.35 shows, it is possible to decrease the critical pump power to reach the Raman threshold by decreasing the effective area of an optical fibre. Moreover the

gain of a Raman amplifier is given by (see Agrawal [2001b]):

$$G(dB) = 10 \lg \left(\exp \left(\frac{g_R P_0 L_{eff}}{A_{eff}} - \alpha_P L \right) \right) \tag{2.37}$$

Therefore the Raman gain can exponentially increase by decreasing the effective area. That's why a holey fibre, which can have an A_{eff} as small as a few μm^2, is particularly attractive to be used as a Raman amplifier and could overcome certain of the major disadvantages of Raman devices based on conventional fibres, i.e. the requirement for long lengths of fibre (about 10 km) and the related problems associated with double Rayleigh scattering (Namiki and Emori [2001]).
The demonstration of a Raman amplifier using a holey fibre will be shown in Sect. 4.6 (Yusoff et al. [2002a]).

2.4.5 Brillouin effect

Similar to the Stimulated Raman Scattering (SRS), the Stimulated Brillouin Scattering (SBS) is a nonlinear process based on the energy transfer between the optical field propagating inside a nonlinear medium and the acoustic phonons of the medium (Agrawal [2001b])
Thus the difference between the Raman effect and the Brillouin effect is the nature of the phonons involved. They are optical phonons in the case of the Raman effect, whereas they are acoustical phonons in the case of the Brillouin effect.
This basic distinction determines major differences between these SRS and SBS. For example the Stokes wave propagates backward when SBS occurs, while the SRS can occur in both directions.
SBS has normally a very narrow gain bandwidth and the Stokes shift in this case is normally of the order of 10 GHz, three orders of magnitude smaller than in the case of the Raman effect.
Moreover the threshold pump power for SBS depends on the spectral width associated with the pump wave and can be as low as 1 mW for a continuous wave (CW) or when the pump is in the form of relatively wide pump pulses (width$>$ 1 μs). In contrast it ceases to occur for short pump pulses (width$<$ 10 ns)(Agrawal [2001b]).
The process of SBS can be described classically as a nonlinear interaction between the pump and the Stokes fields through an acoustic wave. The confinement of the optical field within the fibre core creates a field gradient in the radial direction, which generates acoustic waves through electrostriction, a phenomenon that creates density variations in response to variations in the electric field. The acoustic wave modulates the refractive index of the medium. This pump-induced index grating scatters the pump light through Bragg diffraction. Scattered light is downshifted in frequency because of the Doppler shift associated with a grating moving at the acoustic velocity v_A (Agrawal [2001b]) (see Fig. 2.5).
Quantum-mechanically the SBS can be seen as the annihilation of a pump photon which

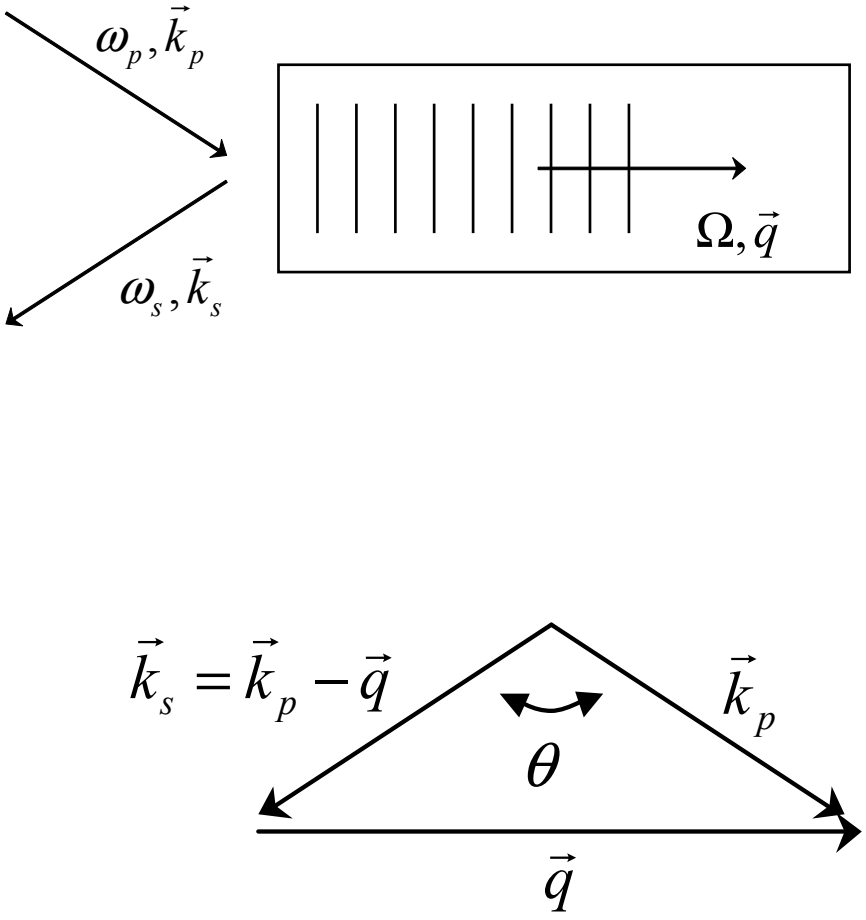

FIGURE 2.5: Illustration of the Stokes scattering based on Brillouin effect

generates a Stokes photon and an acoustic phonon simultaneously. Both the energy and the momentum must be conserved during this process:

$$\Omega_B = \omega_p - \omega_s, \qquad \mathbf{k}_A = \mathbf{k}_p - \mathbf{k}_s \tag{2.38}$$

where ω_p and ω_s are the frequencies, and $\mathbf{k}_p$ and $\mathbf{k}_s$ are the wave vectors, of the pump and Stokes respectively.
The frequency Ω_B and the wave vector $\mathbf{k}_A$ satisfy the standard dispersion relation:

$$\Omega_B = v_A \left|\mathbf{k}_A\right| \tag{2.39}$$

Since $|\mathbf{k}_p|$ is almost equal to $|\mathbf{k}_s|$ (because Ω_B is much smaller than ω_p), we can write (see Fig. 2.5):

$$\Omega_B = v_A \left|\mathbf{k}_A\right| = 2v_A \left|\mathbf{k}_p\right| \sin(\theta/2) \tag{2.40}$$

Equation 2.40 shows that the frequency shift of the Stokes wave depends on the scattering angle. Indeed the Stokes shift Ω_B is equal to zero for forward scattering and is maximum for backscattering ($\theta = \pi$). Thus, in an optical fibre, the Brillouin scattering should occur only in the backward directions. However a small amount of spontaneous or thermal

Brillouin scattering can occur in the forward direction due to the guiding nature of acoustic waves (Shelby et al. [1985]).
Using Equation 2.40 and that $|\mathbf{k}_p| = 2\pi n/\lambda_p$, the Brillouin frequency shift ν_B in the backward direction can be expressed as:

$$\nu_B = \frac{\Omega_B}{2\pi} = \frac{2n\nu_A}{\lambda_p} \tag{2.41}$$

where n and λ_p are the refractive index and the pump wavelength, respectively.
If we use $v_A = 5.96\ km/s$ and $n = 1.45$, the values appropriate for silica fibers, then $\nu_B = 11.1\ GHz$ at $\lambda_p = 1.55\ \mu m$.
The spectral bandwidth is associated with the damping time of the acoustic waves, or the phonon lifetime t_B. Assuming that an acoustic wave decays as $\exp(-t/t_B)$, the Brillouin gain coefficient g_B will exhibit a Lorenzian spectral profile as follows:

$$g_B(\nu) = \frac{\left(\frac{\Delta\nu_B}{2}\right)^2}{(\nu-\nu_B)^2 + \left(\frac{\Delta\nu_B}{2}\right)^2} g_B(\nu_B) \tag{2.42}$$

where $\Delta\nu_B$ is the 3 dB spectral bandwidth and can be expressed as $\Delta\nu_B = \frac{1}{\pi t_B}$. The peak value of the Brillouin gain coefficient g_p at $\nu = \nu_B$ is given by (Tang [1966]):

$$g_p = g_B(\nu_B) = \frac{2\pi n^7 {e_{12}}^2}{c\lambda_p \rho_0 \nu_A \Delta\nu_B} \tag{2.43}$$

where e_{12} is the longitudinal elasto-optic coefficient, ρ_0 is the material density, and λ_p is the pump wavelength.
The critical pump power P_0^{cr} to reach the Brillouin threshold is found to be (Smith [1972], Agrawal [2001b]):

$$P_0^{cr} \simeq 21 \frac{A_{eff}}{g_B L_{eff}} \tag{2.44}$$

where A_{eff} is the effective area (Eq.2.1) and L_{eff} is the effective fibre length (Eq.2.36). The numerical factor 21 is only approximate as it is a function of the Brillouin gain line-width.
For a conventional optical communication system operating at 1.55 μm,with $A_{eff} = 50\ \mu m^2, L_{eff} \simeq 20\ km$ and $g_B \simeq 5 \times 10^{-11} m/W$, equation 2.44 predicts a critical pump power $P_0^{cr} \simeq 1mW$. Such a low Brillouin threshold makes SBS a dominant nonlinear process in optical fibers.
Longitudinal variations in the Brillouin shift along the fibre length can reduce the effective Brillouin gain and increase the SBS threshold. This feature can be used to suppress SBS by intentionally changing the core radius along fiber length because $\Delta\nu_B$ depends on the core radius (Agrawal [2001b]).
In particular we have demonstrated the last point during our experiments regarding the investigation of the Brillouin effect in a HF (Lee et al. [2002a]). Moreover, due to the

very high nonlinearity of HF, we have demonstrated a HF Brillouin laser, based on only 73.5 m of our fabricated HF, which we discuss in Sect. 4.7.

2.5 Dispersion properties

Besides a high nonlinearity, small core HFs can have novel dispersion properties compared to CFs, and which can be employed in a wide range of applications. In this section we introduce the concept of dispersion, explain the reason for the novel dispersive behaviour of HNL-HFs and indicate some possible applications of these properties.
In an optical fibre the mode propagation constant β is a function of ω:

$$\beta(\omega) = n(\omega)\frac{\omega}{c} \tag{2.45}$$

where c is the speed of light in vacuum and $n(\omega)$ is the effective mode refractive index. Expanding β in a Taylor series about the frequency ω_0, we can write:

$$\beta = \beta_0 + \beta_1(\omega - \omega_0) + \frac{1}{2}\beta_2(\omega - \omega_0)^2 + ... \tag{2.46}$$

where $\beta_m = \left(\frac{d^m\beta}{d\omega^m}\right)_{\omega=\omega_0}$ with m=0,1,2,3,....

In particular $\beta_1 = \frac{1}{v_g}$ where v_g is called "group velocity" and represents the speed of the envelope of an optical pulse.
Instead, the "group velocity dispersion" (GVD) of a material is the phenomenon which results in different spectral components λ of a pulse travelling inside a fibre with different speeds. GVD is given by :

$$GVD = \frac{d}{d\lambda}\left(\frac{1}{v_g}\right) \tag{2.47}$$

The total dispersion inside a single mode optical fibre can be evaluated by the addition of two contributions, namely the material dispersion and the waveguide dispersion. The waveguide contribution (WD), takes into account that the effective mode index of an optical fibre is slightly lower than the core material index $n(\omega)$, the difference itself being ω dependent.
In a standard optical fibre the WD is relatively small and can shift the zero dispersion wavelength from 1.27 μm (zero material dispersion) to 1.31 μm. WD depends on fiber-design parameters such as core radius and numerical aperture. In particular, it is possible to fabricate fibres with more complex cladding refractive index profiles (Li [1985]) and to shift the zero dispersion wavelength λ_0 to 1.55 μm (dispersion shifted fibres DSFs) or beyond (nonzero dispersion shifted fibres). This shift in zero dispersion can be large and can result in large values of normal dispersion at 1550 nm. For example "dispersion compensating fibres" (DCF) have a negative dispersion at 1.55 μm (up to $-100\ ps/nm-km$) and therefore they can compensate the dispersion of standard optical fibres (which is about 16 ps/km-nm at 1550 nm), although long lengths are still required.

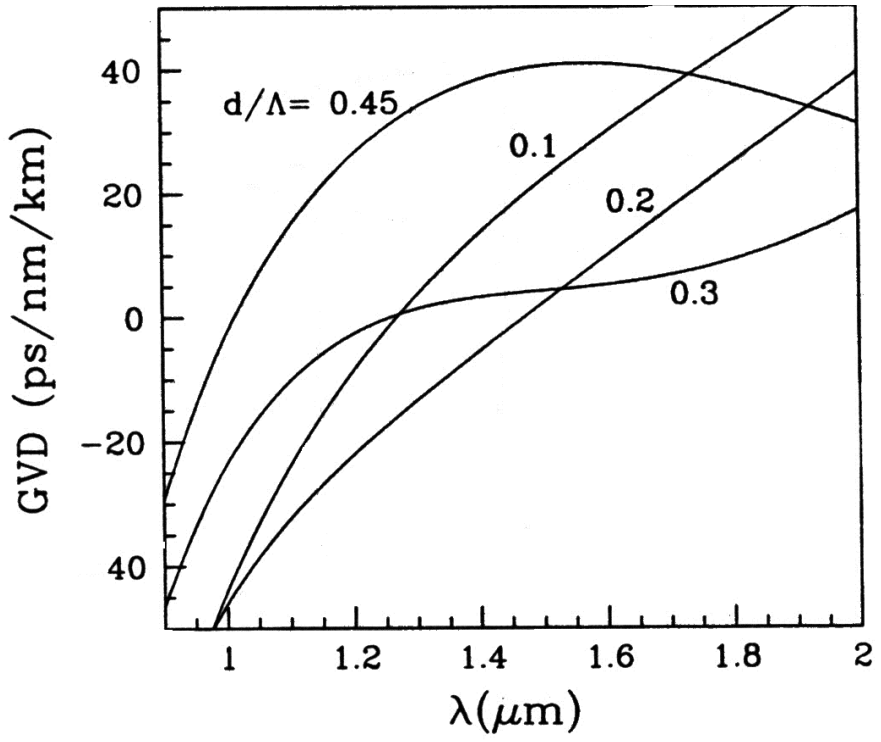

FIGURE 2.6: Total dispersion of a holey fibre with $\Lambda = 2.3\ \mu m$ (Monro et al. [1999b])

It is also possible to design dispersion-flattened optical fibres having low dispersion over a relatively broad wavelength range ($1.3 - 1.6\ \mu m$). This is achieved by using multiple cladding layers (Li [1985]).
Holey fibres can exhibit novel dispersion properties compared with standard single mode fibres. For example since they can have a very large NA and a very small fibre core; the hole distribution in the cladding gives rise to a wide range of completely new cladding refractive index profiles. Therefore the waveguide dispersion of a holey fibre can exhibit novel behaviour relative to that of all other types of optical fibre (Mogilevtsev et al. [1998], Birks et al. [1999], Monro et al. [1999a], Ferrando et al. [2000]).
In Fig. 2.6 we show some examples of the sort of novel HF dispersion properties, considering a HF with an hole pitch $\Lambda = 2.3\ \mu m$ (Monro et al. [1999b]). As we can see, when $d/\lambda = 0.45$ the dispersion is anomalous for wavelengths much shorter than $1.3\ \mu m$ and when $d/\lambda = 0.3$ the GVD is almost flat over a broadband range.

2.5.1 Anomalous dispersion

A HF can be designed to have anomalous dispersion ($GVD > 0$) for wavelengths shorter than $1.3\ \mu m$ while remaining single mode (Mogilevtsev et al. [1998], Monro et al. [1999b]), which is impossible for any kind of conventional optical fibre. This feature has been first predicted and demonstrated by the work of Ranka et al. [2000] and Knight et al. [2000]. In Fig. 2.7 some theoretical predictions and experimental measurements made by Knight et al. [2000] are shown, which refer to a two ring small core HF with a core size of about $1.5\ \mu m$ and an air hole size of $0.62\ \mu m$. At the ORC we have fabricated

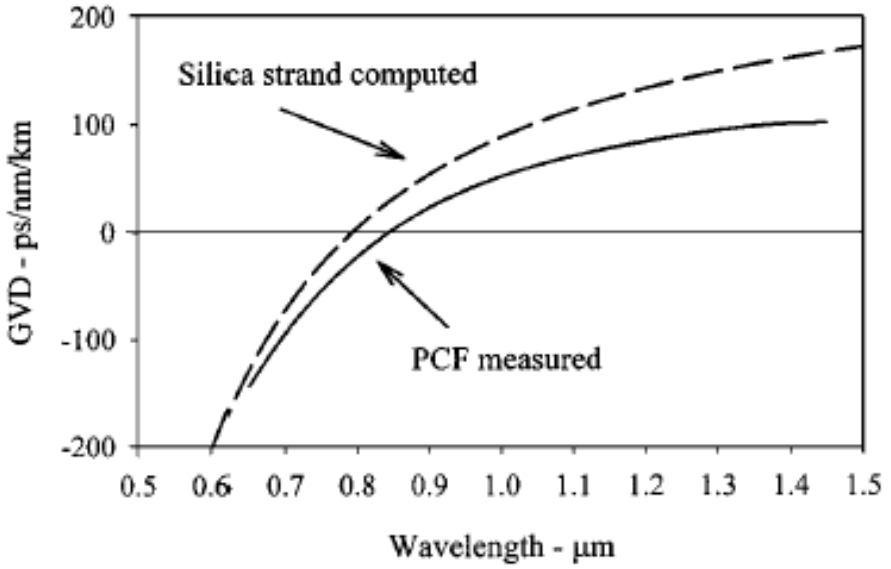

FIGURE 2.7: Computed GVD for a silica strand (AFF=1)with a core size of 1.5 μm (dotted line) and measured GVD for a PCF with a core size of 1.5 μm and an hole size of 0.62 μm (solid line) (Knight et al. [2000])

a HF with similar characteristics (see Sect. 4.3) and we have demonstrated how this HF can be used to achieve pulse compression and soliton formation at a wavelength of 1 μm (Price et al. [2001a])(see Sect. 4.3).

2.5.1.1 Pulse Compression

When a pulse is propagating inside a dispersive optical fibre, the instantaneous frequency within the pulse envelope changes with time (Agrawal [2001b]). Such a pulse is termed a "chirped pulse" (Agrawal [2001b], Ghatak and Thyagarajan [1998]).
If the dispersion is anomalous ($GVD > 0$) then the instantaneous frequency within the pulse increases with increasing time and we obtain a "negative chirp".
If the dispersion is normal ($GVD < 0$) then the instantaneous frequency within the pulse decreases with increasing time and we obtain a "positive chirp".
In a linear dispersive medium chirping is always associated with a temporal broadening of the pulse (while the optical spectrum is unaltered).
When a positively chirped pulse is launched inside a positive dispersive fibre ($GVD > 0$), its dispersion can be compensated during its propagation and therefore its original broadening in time can be cancelled, leading to pulse compression.
Since HFs can have a high anomalous dispersion in a regime in which conventional fibres have normal dispersion ($\lambda < 1.3\ \mu m$), short lengths can be used for dispersion compensation at these wavelengths and to achieve pulse compression. This will be shown in Sect. 4.3.

2.5.1.2 Soliton formation

Self phase modulation in a nonlinear nondispersive medium leads to the generation of new frequencies without generating any temporal broadening (Agrawal [2001b], Ghatak and Thyagarajan [1998]). This spectral broadening is always associated with a chirping of the pulse, in which the instantaneous frequency within the pulse decreases with increasing time (as for a positive chirp).
Therefore the effects of the anomalous dispersion and SPM can compensate each other and allow the propagation inside the fibre of a stable "soliton pulse", that broadens in neither the temporal domain nor the spectral domain.
Holey fibres can be used to achieve soliton formation at wavelengths less than 1.3 μm, which is not possible with conventional fibres (Sect. 4.3). Moreover the power levels required are relatively low, due to the very high nonlinearity that it is possible to achieve in HFs (see Sect. 5.5).

2.5.2 Normal dispersion

The dispersion of conventional fibres (CFs) used in telecommunications is about $16ps/(km-nm)$ in the third window of silica ($\lambda = 1.55\ \mu m$). The dispersion becomes quite high after several km and compromises the correct interpretation of the transmitted signals at the receiver, limiting the bit rate.
The dispersion of CFs can be compensated by combining them with fibres that have normal dispersion at 1550 nm according to this relation:

$$D_t = D_1 L_1 + D_2 L_2 / (L_1 + L_2) \tag{2.48}$$

Where D_t is the average total dispersion and which is ideally as small as possible, D_1 and D_2 are the dispersion of the first and the second fibre, L_1 and L_2 are the lengths of the first and the second fibre.
DCFs can have a dispersion lower than $-100\ ps/(km-nm)$ and therefore 1 km of DCF can compensate 8-10 km of standard fibre.
Holey fibres can be designed to have a very high normal dispersion (Birks et al. [1999]). A precise design has been provided by the work of Finazzi et al. [2003c]. Fig. 2.8 shows one of the results of this theoretical work. As we can see, when the hole pitch Λ is reduced to values of 1 μm or less, and 2 (or more) hole rings are used, the dispersion values of HNL-HFs go down to values of less than -400$ps/nm-km$ at 1.55 μm. Similar results have been obtained also from Shen et al. [2003], which have predicted a dispersion value of $-474.4\ ps/nm-km$ at 1.55 μm for a HF with $\Lambda = 0.932\ \mu m$ and $d/\Lambda = 0.893$.
Because of the possibility to have very high normal dispersion, HFs could be used as powerful dispersion compensators. Moreover the increasing need to compensate the dispersion of many transmission channels in modern WDM systems (Nelson [2003], Goyal et al. [2002]) requires the use of optical fibres with normal dispersion and a negative slope of the GVD, which is also achievable using holey fibres (Hansen et al. [2003]).

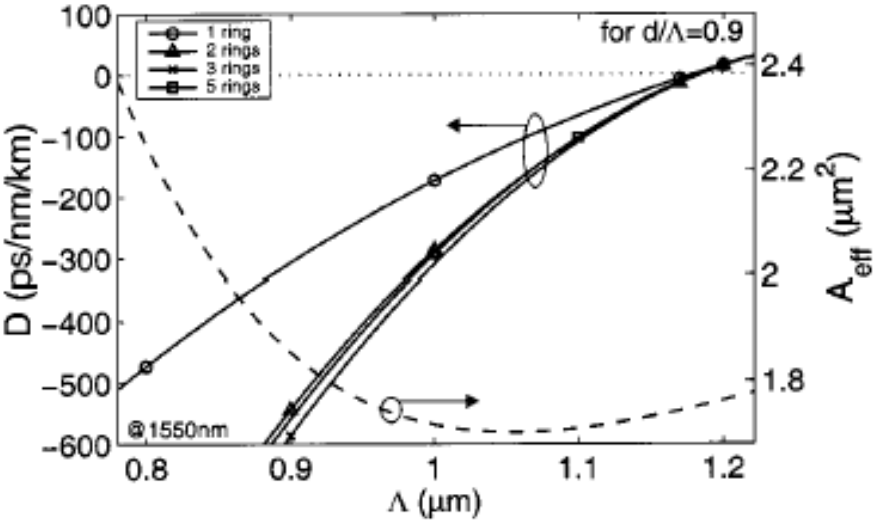

FIGURE 2.8: Dispersion and effective mode area at a wavelength of 1.55 μm as a function of hole-to-hole spacing Λ for different numbers of rings for large air-filling fraction HFs (Finazzi et al. [2003c])

We will show in Sect. 5.4 the first measurement of highly normal dispersion in a HF at 1.55 μm.

2.6 Birefringence

In this section, we would like to introduce the concept of fibre birefringence and see how in a small core HF, together with a high nonlinearity and novel dispersion properties, unprecedent levels of birefringence can be achieved.

Generally speaking, even a single mode fibre is not truly single mode because it can support two degenerate modes that are polarized in two orthogonal directions (Agrawal [2001b]). Under ideal conditions (perfect cylindrical symmetry and stress-free fibre) these modes have the same propagation constants and do not couple to each other. But in practical single mode fibres, small departures from cylindrical symmetry of the core and the presence of stress, twists or bends, leads to a difference between the two propagation constants of the two degenerate modes. Such a phenomenon is referred to as "modal birefringence".

The birefringence is defined as (Agrawal [2001b]) :

$$B = \frac{|\beta_x - \beta y|}{k_0} = |n_x - n_y| \tag{2.49}$$

where β_x and β_y are the propagation constants and n_x and n_y are the modal refractive indices for the two orthogonally polarized states.

Because of the different propagation constants, the two orthogonal polarization modes experience a phase difference between them. Thus, because of the beating of the two polarization modes, light changes its state of polarization (SOP) during its propagation

inside an optical fibre with a period :

$$L_b = \frac{2\pi}{|\beta_x - \beta_y|} = \frac{\lambda}{B} \tag{2.50}$$

where L_b is called "beat length" and is the minimum fibre length after which SOP repeats itself.

In standard optical fibres, B is not constant along the fibre length but changes randomly because of fluctuations in the core shape and anisotropic stress. As a result the SOP of the light launched in the fibre changes in a random fashion. This is an issue for optical communication systems when short pulses are transmitted over long lengths. The random change of the SOP results in a broadening of the pulse and this phenomenon is referred as "polarization mode-dispersion" (PMD). However the random changes of birefringence occurring along the fibre tend to equalize each other so that PMD induced pulse broadening is relatively small compared with GVD effects. PMD becomes a limiting factor only for high speed communication systems designed to operate over long distances near the zero dispersion wavelength of the fibre (Agrawal [2001b]).

On the other hand the random change of the SOP creates problems when single mode fibres have to be used in coherent communications, in fibre optic phase change sensors, in nonlinear optical devices and in applications in which the fibre has to be coupled to polarization sensitive devices. To overcome these problems special fibres, such as elliptic core fibres, and stress-induced high-birefringence fibres have been developed. In standard single mode fibres the beat length is of the order of 1-10 m. However birefringence can be enhanced in CFs either by a modification of the symmetry of the structure, for example by adopting elliptical core fibres (with a beat length of about 1 m), or by applying a stress on the guiding material, by developing stress induced fibres (with an L_B the order of cm).

Holey fibre technology offers an easy and reliable way to make very highly birefringent fibres. As it is been shown by Ortigosa-Blanch et al. [2000] and by Suzuki et al. [2001], HFs can be fabricated with a structural asymmetry by simply modifying the air hole size of some of the holes surrounding the HF core. Moreover the high NA and very small core features of HFs play a fundamental role in increasing the birefringence. That is why all of our HNL-HFs present a beat length of the order of 1 mm and this value is further reduced for some particular asymmetric HFs. As an example, in Sect. 4.5, we will describe the beat length measurement of a polarization maintaining fibre (very high B) with a beat length as small as 0.44 mm.

2.7 Conclusions

In this chapter we have provided a theoretical background to this thesis, describing the main properties and applications of small core holey fibers.

First of all, in Sect. 2.3, we have highlighted how HF technology allows in particular the fabrication of small core optical fibres with a very high refractive index difference

between the core and the cladding (up to 0.4) and thus an effective area as small as 1.5 μm^2 (and an effective nonlinearity γ up to 70 $W^{-1}km^{-1}$)(Finazzi et al. [2003c], Belardi et al. [2002b]).
We have then explained, in Sect. 2.4, which are the main nonlinear effects we have used for the demonstration of the first highly nonlinear HF based devices, discussed in detail in Chapter 4 and 5. These effects are "self phase modulation" (SPM), "cross phase modulation", "four wave mixing"(FWM), "stimulated Raman scattering" (SRS) and "stimulated Brillouin scattering" (SBS).
In the following Sect. 2.5, we have highlighted that small core HFs, besides having a very high nonlinearity, can have dispersion properties completely different from conventional optical fibres. In particular HFs with anomalous dispersion at wavelengths less than 1.3 μm can be made, and these HFs can be used to achieve pulse compression and soliton formation at short wavelengths (Wadsworth et al. [2000], Price et al. [2001a]). On the other hand HFs can also be designed to have very high negative dispersion (Finazzi et al. [2003c], Shen et al. [2003]). This feature is of fundamental importance for the realization of dispersion compensating devices.
Finally, in Sect. 2.6, we have shown how HF technology offers the possibility to produce optical fibres with a very high birefringence (a beat length less than 1 mm, an order of magnitude less than stress-induced high birefringence conventional optical fibres). This important characteristic is related to the high NA, small core size and structural asymmetry, which it is possible to obtain using HFs.

Chapter 3

Fabrication of highly nonlinear holey optical fibres

3.1 Introduction

The first single material silica optical fibres were made as early as 1974 by Kaiser and Astle [1974]. They were proposed as low loss single-mode fibers and consisted of a tubular cladding shell connected to a central core, with a diameter between 10 and 25 μm, by thin webs of glass, as shown in Fig.3.1(a). Using a slightly different approach, sketched in Fig. 3.1(b), a three core fibre was also fabricated. It already involved the preparation of the fibre preform by stacking of a few capillary tubes inside an outer jacket tube, and the final core diameters were about 10 μm.

A lowest loss of about $3dB/km$ at a wavelength of 1.1 μm was obtained using a fiber 130 m long. However, those fibres proved very hard to make, and work on them was abandoned with the advent of novel optical fibre fabrication methods, like MCVD (Nagel et al. [1982]), OVD and VAD (Li [1985]) which today enable fibre losses as low as 0.148 dB/km at a wavelength of 1550 nm (Nagayama et al. [2002]).

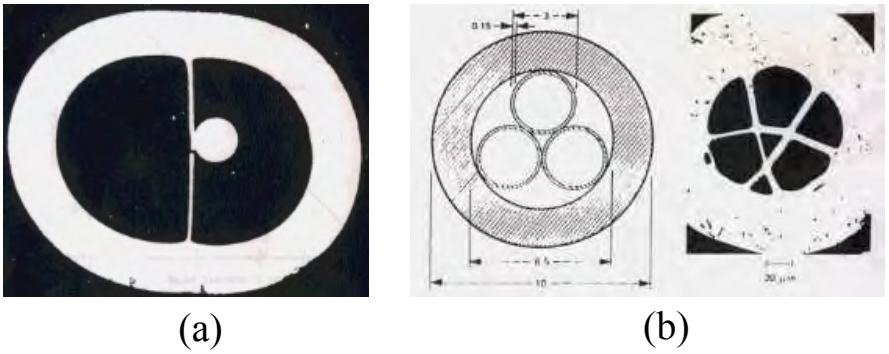

(a) (b)

FIGURE 3.1: Some samples of the first single material optical fibers made by Kaiser and Astle [1974].(a)Single core optical fibre with air clad. (b) Preform design (on the left) of a three core single material fibre and fabricated fibre (on the right).

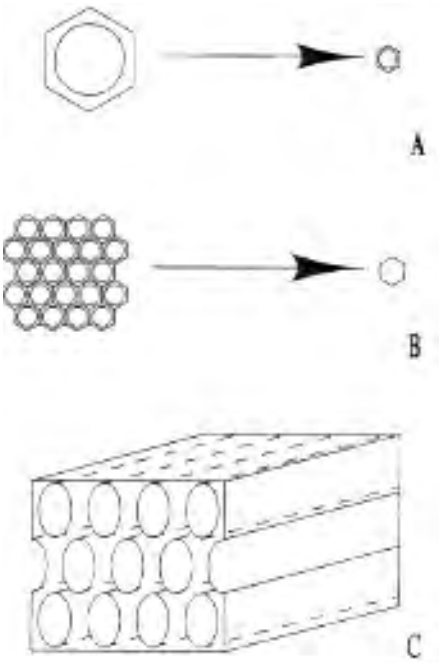

FIGURE 3.2: Schematic diagram indicating the steps for fabricating the NCG array (Tonucci et al. [1992]).(A)Cladding and acid-etchable core glass are reduced in diameter to a fine filament by drawing the glass composite at elevated temperatures.(B)After stacking the filaments into a bundle forming an array, the bundle is further drawn to reduce its overall diameter again to a filament. The process is repeated until the desired diameter of the channel glass is achieved.(C)A magnified view of the final product of an array of acid-etchable cores embedded in the matrix glass.

In 1992 Tonucci et al. [1992] developed a method for the production of a nanochannel glass (NCG) array , containing a regular parallel array of submicrometer capillaries ($\sim 33\ nm$), arranged in a two-dimensional hexagonal close packed configuration. Such structures were designed to be used in ultra-small and ultradense electronic devices (see Appenzeller et al. [1991]).
Fig 3.2 shows the basic steps for fabricating such a NCG array, and Fig. 3.3 shows a SEM of the final nanostructure. As shown in Fig.3.2, their fabrication technique involved stacking and drawing of glass channels and allowed the production of channel diameters as small as 33 nanometers and packing densities as high as 3×10^{10} channels per square centimeter.

At the same time the photonic band gap(PBG) was becoming a really hot topic. The concept of the PBG was originally proposed in 1987 by Eli Yablonovitch (Yablonovitch [1987]) and Sajeev John (John [1987]), and concerns the creation of a frequency band in a three dimensional dielectric structure in which electromagnetic waves are forbidden, irrespective of the propagation direction in space. In 1991 Yablonovitch and his colleagues fabricated the first band-gap material (operating at microwave frequencies) by drilling holes 1 mm in diameter in a block of material with a refractive index of 3.6 (Yablonovitch et al. [1991]).

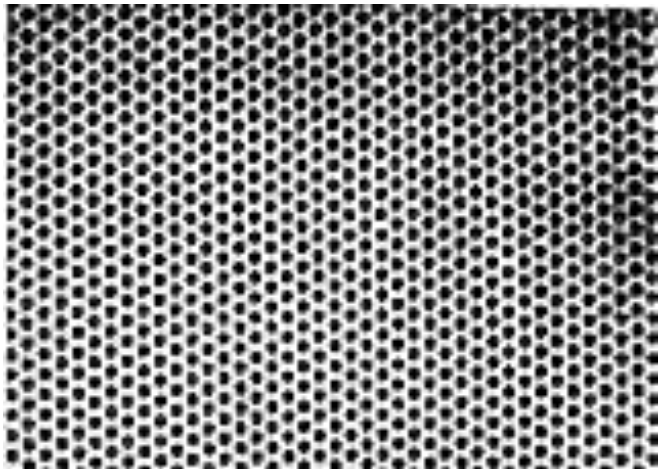

FIGURE 3.3: SEM of 450 nm diameter hollow channels arranged in a hexagonal close packing array configuration contained within the matrix glass(Tonucci et al. [1992]).

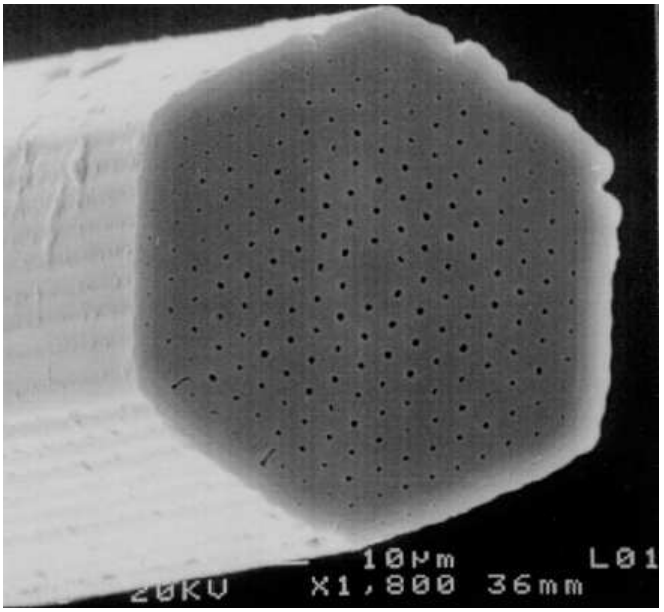

FIGURE 3.4: The first holey fibre was made by Knight et al. [1996]. It had a hole pitch of 2.3 μm and the fibre dimension was about 40 μm.

Around the same period, Philip Russell developed the idea to realize a photonic band-gap in an optical fibre. According to Russell's idea, this photonic band-gap fibre exhibited a periodic index modulation in the cladding region by means of large air holes and a unique hexagonal symmetry. This PBG-fibre was realized in Russell's group only some years later in 1999 (Cregan et al. [1999]) but the first successful attempt at making a microstructured optical fibre had already happened in 1995(Birks et al. [1995],Knight et al. [1996]). Unlike the first single material fibers (Kaiser and Astle [1974]), this fibre substantially differs from them by having an almost periodic index modulation in the cladding region and an hexagonal symmetry. A SEM of this fibre is shown in Fig. 3.4. The fabrication approach used for the manufacture of this fibre involves, similar to the

work of Tonucci et al. [1992], the stacking of several silica capillaries in a hexagonal pattern, the insertion of a silica rod in the middle of the bundle and the final drawing of the stack, to reduce its dimensions.
This first holey fibre (HF) had a pitch of 2.3 μm, a core size greater than 3 μm and an external fibre diameter of only 40 μm.
The fabrication of this fibre constitutes a milestone in the history of microstructured optical fibres. Russell's group soon realized that this fibre could not experience a photonic band-gap effect, due to the small air filling fraction and relatively poor regularity of the structure. However, surprisingly, they found that this fibre was single-mode over an extended wavelength range (Birks et al. [1997]). They tried to understand this "strange" behaviour and developed the first mathematical models to explain their observations (Birks et al. [1997], Mogilevtsev et al. [1998], Birks et al. [1999]), and they found that this novel optical fibre may also possess completely novel and tailorable dispersion properties, besides a very high nonlinearity (see also Monro et al. [1999b]). This generated a high level of excitement in many research groups and gave strong motivation to the improvement of the holey fibre fabrication technique.

The very small size of the first holey fibre (40 μm, see Fig. 3.4) is related to the particular technique used to fabricate it, which involve the stacking of several capillary tubes. It is difficult to handle capillaries with a size less than 1 mm and so, since the maximum HF preform size that could be drawn was about 30 mm, a very small fibre size was required to achieve a final structure having micrometer holes. As can be easily understood, such small dimension fibres are not easy to handle and this problem constituted a major limitation to the further reduction of hole size.
Another issue was the observed collapse of the fibre inner holes during the drawing process, due to the effect of the surface tension acting on the inner walls of the capillaries. In particular these problems complicated the fabrication of a very highly nonlinear HF, which simultaneously requires a very small hole pitch Λ and a very high AFF.

To solve the issue of the small outer fibre dimension, Bennett et al. [1999], working at the ORC, introduced a two step drawing technique: in the first step an initial HF preform, made as suggested by Knight et al. [1996] (see also Fig. 3.4), is drawn to produce a cane with a diameter of about 1 mm. The final HF preform was obtained by inserting the cane inside a thick vycor tube, with a diameter of about 20 mm.
Then a second drawing step was required to produce a final HF, with an outer dimension of about 300 μm.
The fibre fabricated by Bennett is shown in Fig. 3.5. It represents an important step towards the fabrication of highly nonlinear holey fibres (HNL-HFs), which require a core size comparable with the wavelength of the light. Indeed this fibre allowed the first measurements of nonlinearity in a HF (Broderick et al. [1999a]) and had an effective area as small as 4.5 μm^2.

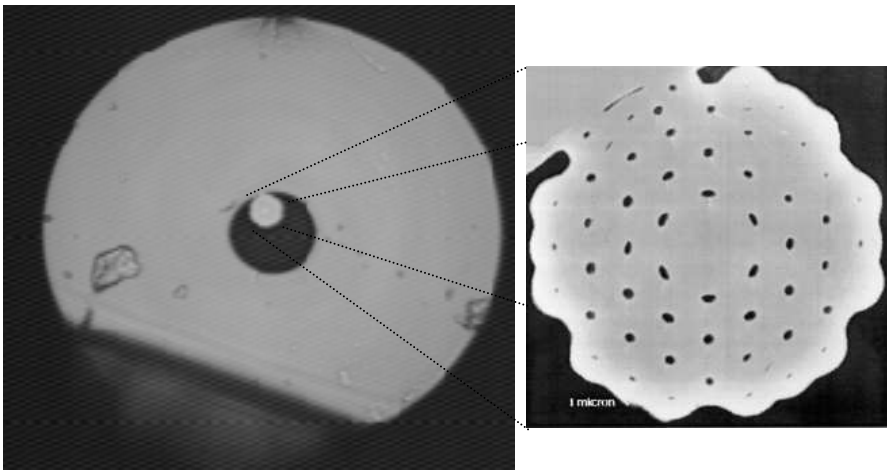

FIGURE 3.5: One of the first highly nonlinear HF was fabricated by Bennett et al. [1999]. It had a hole pitch of 1.8 μm, a hole size of 0.34 μm and a fibre dimension of about 300 μm. It was fabricated by using a two steps drawing technique.

However this fabrication approach presented numerous problems. As we can see from Fig. 3.5, the inner structure of this fibre presented only two contact points with the external silica jacket, which make it fragile, unstable and unsuitable for the implementation in optical devices.

Moreover the HF length was limited to only a few meters and, as observed also in the first HF (see Fig. 3.4), during the final drawing stage the inner holes collapsed, due to the inner surface tension. Indeed , in its best section, the fibre has quite a small core size of about 1.8 μm but an air filling fraction (AFF) of only 0.2. A much higher AFF would be desirable for a HNL-HF.

Finally, but most importantly, the fabrication of this unique HF could not be repeated by Bennett.

I became personally involved in this research shortly after Peter Bennett left the ORC and tried to improve his fabrication technique and solve some of the issues he had faced. This chapter concerns the fabrication of highly nonlinear silica HFs and is a direct development of the fabrication techniques discussed above. We aim, on one hand, to provide a better understanding of the fabrication process of highly nonlinear HFs, and to obtain a reliable HF fabrication method that allows the manufacture of long lengths of robust HFs with a small core size and a large AFF and standard external dimensions.

In Sect. 3.2, the characteristics of the drawing tower are described. The following Sect. 3.3 is a summary of the HF fabrication technique, briefly describing general issues, such as choice of the silica material, uniformity of the capillaries, the two drawing step technique and manufacture of the HF jacket.

After this introductory part, in Sect. 3.4, I analyze the main holey fibre fabrication problems and address the way for their solution.

In the following sections, I present, in chronological order, which improvements were performed to achieve a better understanding of the HF fabrication process and to ob-

tain a reliable HF fabrication method for highly nonlinear HFs.
I first started a study regarding the influence of the drawing parameters, such as feed speed and temperature, on the HF structure. This point is discussed in Sect. 3.5.
I then invented a novel holey fibre fabrication design, based on a air holey fibre structure (Belardi et al. [2002a]), which facilitates the manufacture of highly nonlinear HFs, and, at the same time, showed interesting applications. I describe this method in Sect. 3.6.
The following Sect. 3.7, concerns the introduction of holey fibre pressurization by sealing the top of the preform prior to the final HF drawing. In particular, the introduction of this technique has allowed the reliable fabrication of HFs with a very high nonlinearity (up to 70 $W^{-1}km^{-1}$), by creating an external force which directly balances the surface tension of the inner fibre holes .
To improve the strength of our HFs I adopted a silica jacket, developing the method of Bennett et al. [1999], based on the use of a Vycor one. The advantages of the silica jacket are shown in Sect. 3.8.
In Sect. 3.9, I discuss some technical issues regarding the pressurization of a HF preform, and, in particular, I outline why the sealing technique leads to a pressure instability, during the HF drawing.
Finally, in Sect. 3.10, I discuss some of the HF preform fabrication issues, regarding the stacking, the cleaning procedures and the "drop" choice, and show how I have partially improved these fabrication stages.

3.2 Drawing tower

A sketch of the drawing tower is shown in Fig. 3.6(see Paek [1999]). The preform is held in the vertical position by the chuck of a motorized stage and then fed, at a well determined feed speed (controlled up to 17 mm/min), into a graphite resistance furnace, with an aperture of 33 mm. The furnace hot zone length is approximately 300 mm and has the temperature profile sketched in Fig. 3.6 (measured for a maximum temperature T_{MAX} of about 1600 °C), with the hottest temperature reached at a position 146 mm below the top aperture. A continuous flow of dry argon gas through the furnace keeps it purged, and two adjustable irises, at the top and at the bottom of the furnace, prevent ingress of air and oxidation of the heating element (see Li [1985]). The iris apertures must be kept fixed during the drawing because their aperture modifies the dynamics of the gas flow, which results in fast fluctuations in the fibre diameter (Imoto et al. [1989]).
After the insertion of the preform inside the furnace, the temperature is increased by means of a controller unit. Typical drawing temperatures for conventional silica optical fibres are around 2100 °C but, when drawing holey preforms, the drawing temperature must be adjusted, to control the air filling fraction (AFF) (as we will explain later). Usually temperatures as low as 1740 °C can be used (i.e. for unpressurized capillaries) or as high as 2100 °C (in the pressurized case).
Once the preform has reached the set temperature, the glass softens at the hottest point,

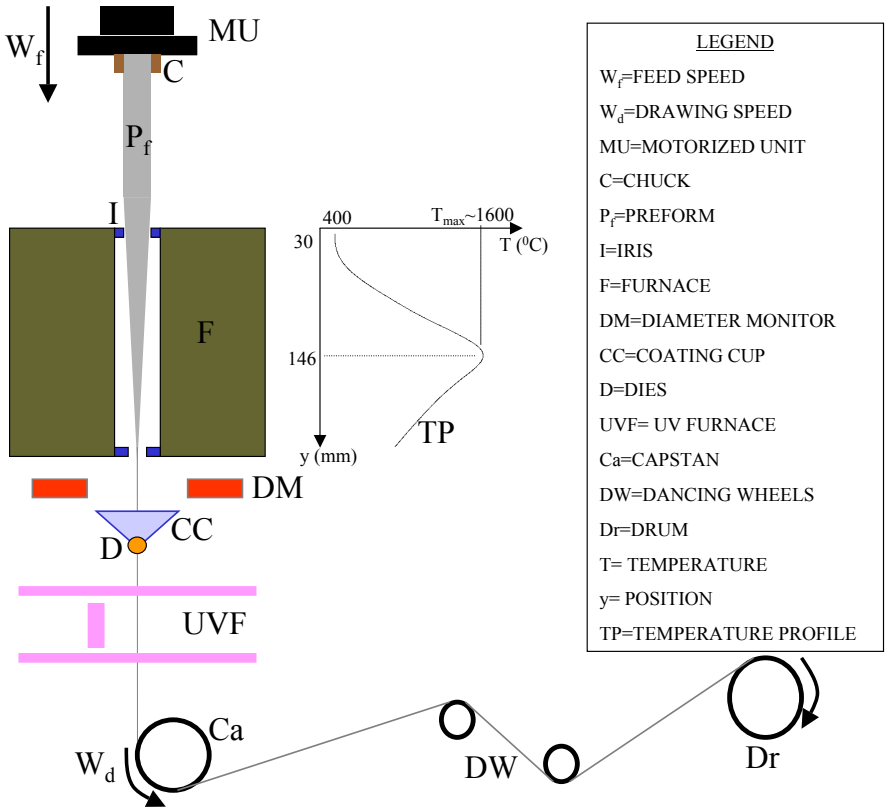

FIGURE 3.6: Drawing tower

and the preform begins to "neck down", while the part of the preform beneath the neck (the so called "drop") falls due to its own weight. This causes a natural elongation of the preform.

After the "drop" has emerged from the bottom aperture of the furnace, it is cut and the fibre is pulled, by using pliers, until is firmly fixed on a computer-controlled capstan. Drawing speeds allowed from our capstan range from 2-3 m/min to 40-50 m/min. For the drawing of capillaries or rods, the use of much lower drawing speeds is often required. In this case the capillaries are drawn by a tractor unit, with drawing speed between 0.1 and 1.5 m/min.

A diameter gauge at the bottom of the furnace monitors the diameter of the drawn fibre, as well as the ellipticity, and a feedback control unit can be activated to automatically modify the drawing speed, to keep a set fibre diameter.

Below the diameter gauge there is a coating cup that allows the application of a protective polymer coating to the fibre. This can be cured by using a UV curing unit, positioned below the coating cup. The size of the dies in the coating cup is typically around twice the fibre diameter.

Finally the drawn fibre is wound on a drum. A tensioner, constituted by some "dancing wheels", is used between the capstan and the drum to avoid breaking of the fibre during the drawing, as usually the drum and capstan radius are not the same, nor is their rotation speeds.

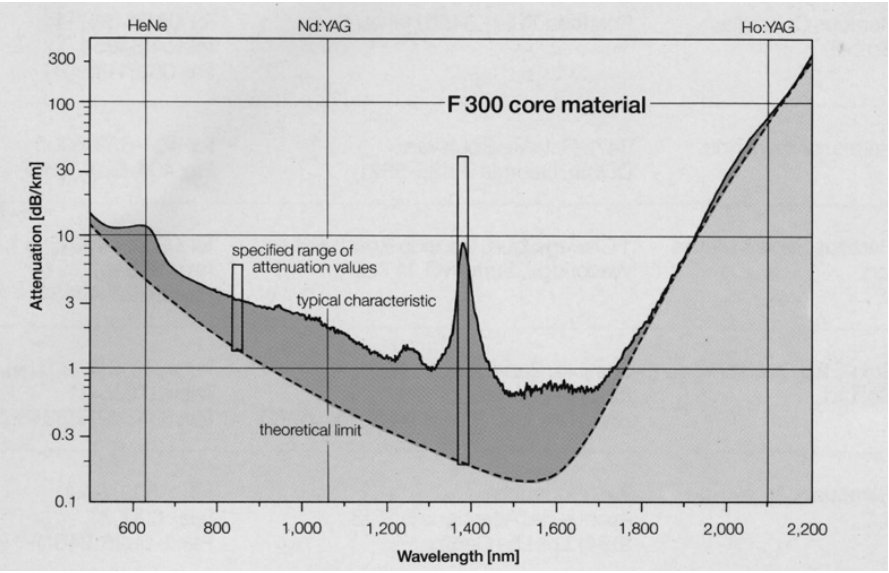

FIGURE 3.7: F300 attenuation versus wavelength (from Heraeus data).

3.3 Basic holey fibre fabrication technique

An HF preform can be fabricated by inserting a number of silica capillaries and rods, with a diameter of around 1-2 mm, inside a silica tube, with a inner diameter of around 20 mm. Therefore the first step in the fabrication of a holey fibre consists of the drawing of silica capillaries and rods from commercially available silica tubes and rods, normally with an outer diameter between 18 and 30 mm.

Glass quality should be chosen to provide the lowest loss, most perfect circularity and uniformity. Suprasil F300 silica offers these characteristics when we require optical guidance at 1550 nm. F300 is a synthetic fused silica glass created through a chemical deposition process after which the level of impurities is reduced below 0.1% (in particular 0.005% of Al_2O_3 and less than 0.001 % of both Na_2O_3, K_2O and CaO (Pfaender [1996])). Moreover Suprasil F300 has a very low OH content (less than 1 ppm) and its transmission characteristic is shown in Fig. 3.7. Suprasil F100 glass, offers comparable losses to F300 silica in the visible range, as shown in Fig. 3.8, and thus would be preferred in this regime, due to its much lower cost. However its high OH content (600 to 800 ppm), makes it unsuitable to use in the telecommunication window, due to the high hydroxyl absorption at this wavelength.

Material losses are clearly an issue related to the guidance of the final HF, while perfect circularity and uniformity are key issues for obtaining a high quality, regular geometry within the HF preform. The ovality of silica F300 tubes is as small as 0.08% while diameter variations along F300 tubes and rod lengths are of the order of 0.2%.

The final capillaries are obtained by drawing them by means of a tractor unit, which basically consists of 2 aligned rotating wheels that transfer their motion to the glass by gripping it, as shown in the sketch of Fig. 3.9.

We generally achieved variations along 1 metre length of a capillary, with a 1-2 mm

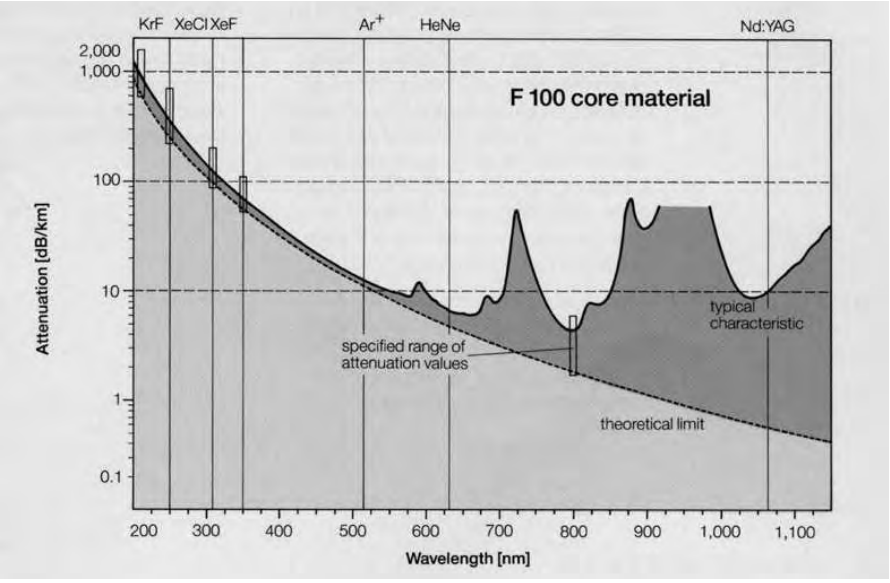

FIGURE 3.8: F100 attenuation versus wavelength (from Heraeus data).

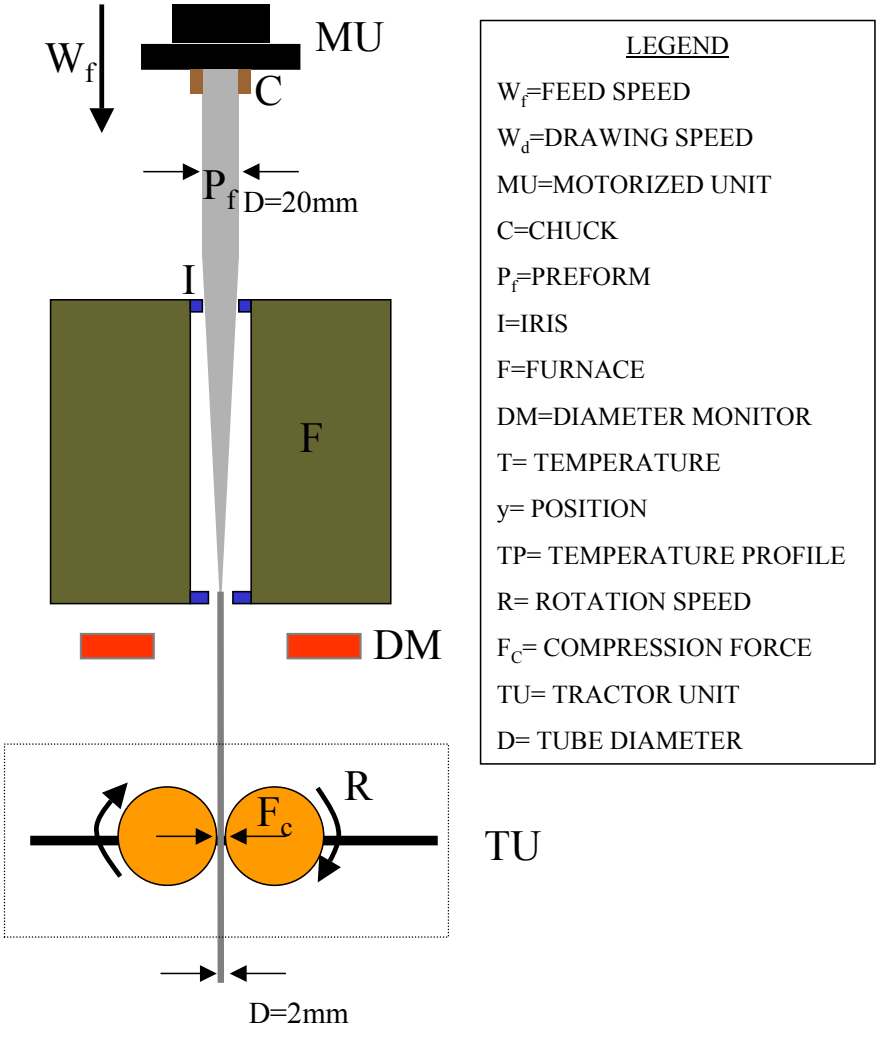

FIGURE 3.9: Sketch of tractor unit operation

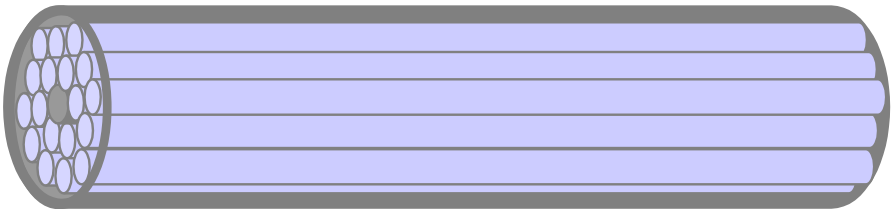

FIGURE 3.10: Stacking

diameter, of order 2-3%. But often, in practice, we make short HF preforms (only 20-25 cm long) so that the actual variations along this length can be mostly reduced to less than 1%.

Once the required capillaries and rods, with a diameter between 1 and 2 mm, have been drawn, they are inserted inside a silica tube of about 20-25 mm OD, as shown in Fig. 3.10. One of the silica rods produced will act as core in the final HF, and is inserted in the middle of the bundle. Choice of the exact capillary sizes, to provide a snug fit in the jacket, is essential to provide a good geometry, and their AFF defines the refractive index difference between the HF core and the HF clad.

After finishing the stacking, the HF preform can be drawn to produce a final HF. Depending on the final core size required, one or two drawing steps may be necessary. For example, let's assume that, as in the case of a large mode HF, the required hole pitch Λ be 15 μm and that we require 6 rings of holes n around the central core. Let us also assume that we would like to stack capillaries with an outer diameter d of 1.2 mm. We can write:

$$\Lambda = 15\mu m; \quad n = 6; \quad d = 1200\mu m; \quad \frac{d}{\Lambda} = F = 80; \tag{3.1}$$

where F has to be the dimension ratio between the preform and the final fibre. Therefore, if we use an outer tube jacket with an inner diameter ID, an outer diameter OD and an air filling fraction AFF_D of 0.8, we need to have:

$$ID = (2n+1)\cdot d = 15.6\ mm; \quad OD = \frac{ID}{AFF_D} = 19.5\ mm; \quad D_f = \frac{OD}{F} = 243\mu m; \tag{3.2}$$

where D_f is the final fibre dimension.

Now let's consider the case of a small core HF, with $\Lambda = 2\ \mu m$ and n=6. Let us again assume we use again $d = 1200\ \mu m$ (F=600) and $AFF_D = 0.8$. Making the same calculations as in 3.2, we obtain:

$$ID = 15.6\ mm; \quad OD = 19.5\ mm; \quad D_f = 32.5\mu m; \tag{3.3}$$

Therefore, as we can see, in this case we need to produce a fibre with a very small fibre diameter, just as happened in the production of the first HF (see Fig. 3.4). As explained in Sect. 3.1, such a fibre would be very difficult to handle and so is not practical.

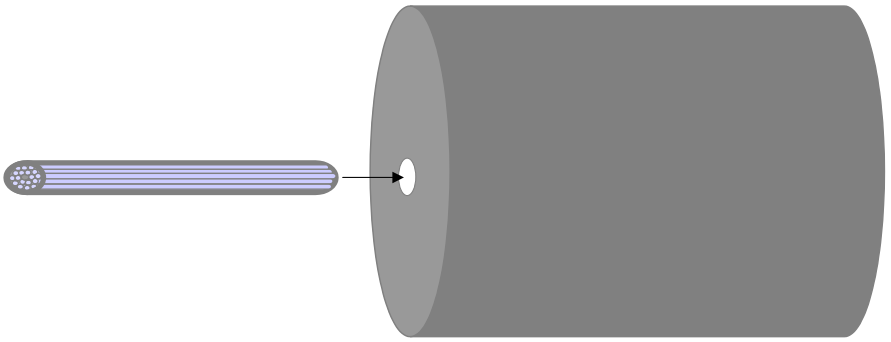

FIGURE 3.11: Cane insertion

As we can see from the previous examples:

$$F = \frac{d}{\Lambda} \tag{3.4}$$

$$D_f = \frac{OD}{F} \tag{3.5}$$

and substituting 3.4 in3.5, we obtain that the fibre diameter D_f is:

$$D_f = \Lambda \frac{OD}{d} \tag{3.6}$$

There are practical limitations on the size of the capillaries d and on the outer tube diameter OD The first is limited by the ability to stack very small capillaries, which are indeed very difficult to handle. As a reference value, we can say that in practice d should not be less than 1 mm. On the other hand, the outer tube diameter OD is limited by the bore of the furnace of our drawing tower, which is about 33 mm. So if we require a HF with a hole pitch Λ of 2 μm we can obtain the following maximum fibre diameter D_f:

$$D_f = \Lambda \frac{OD}{d} = 2\mu m \cdot \frac{33\ mm}{1\ mm} = 66\mu m \tag{3.7}$$

which is still too small compared to a standard fibre diameter of 125 μm.
Thus we need to divide the drawing process into two stages: the first to fabricate a HF cane of 1-2 mm and the second to make the final HF drawing.
The fabricated cane is normally inserted into an external solid jacket, as shown in Fig. 3.11, with a diameter between 10-20 mm and with a central hole of the same size as the cane. The fit of the cane inside the jacket should be very tight to avoid slippage of the cane during the fibre drawing, which would produce a different feed speed between the cane and the jacket, as well as a strong instability of the HF structure and non-circularity.
The jacket can be obtained by drilling a hole of the same size as the holey cane (1.5-2 mm) inside a silica rod with a diameter of around 20 mm, using a rotary ultrasonic drilling machine. Particular care must be taken in this phase since a fast drilling of the glass can result in a fracture due to the stress applied. We usually use a low feeding

speed (about 1.5mm/min) of the diamond core drill, for drilling a silica rod with a diameter of 15 mm. The hole size fluctuations are limited to 1% and its depth is usually around 150 mm.
Alternatively the silica jacket can be fabricated by collapsing a silica tube, using a standard lathe, which allows more freedom in terms of jacket length and dimensions. Since an exact fit of the cane into the jacket can often be difficult to achieve, it is sometimes good practice to produce first the silica jacket and then the cane, testing its fit while drawing it down.
Following the insertion of the cane in the silica jacket, a second drawing step of the so formed final HF preform leads to a HF with a core size comparable with the wavelength of the light.
(It's worth briefly noting that, as we will explain in all this chapter and in particular in Sect. 3.7, we have consistently improved this basic fabrication technique through the introduction of HF preform pressurization prior to the fibre drawing, which can be obtained either by sealing the cane before its insertion in the external jacket or by sealing the single capillaries prior to stacking them).

3.4 The main holey fibre fabrication problem

As outlined in Sect. 3.1, the highly nonlinear HF produced at the ORC by Bennett et al. [1999] couldn't be reproduced. Further attempts to make a similar fibre, with a higher AFF and a smaller core size (to enhance its nonlinearity), and a better jacketing (to improve the strength and the fibre length), resulted in a negative outcome.
I faced the problem of the fabrication of a highly nonlinear HF, and tried, first of all, to analyze and experimentally investigate the reasons for the previous failed fabrication attempts. In this way I hoped to find new fabrication techniques to successfully produce HNL-HFs.
In Fig. 3.12 I have highlighted the main physical parameters, which affect the closure of a glass fibre hole.

Some of these parameters are related to the intrinsic characteristics of the glass we intend to draw, such as the glass viscosity μ, surface tension δ and thermal conductivity κ. My work has focused on the fabrication of HNL-HFs made in silica material, although recently HNL-HFs have been made, at the ORC, from different glasses (Ebendorff-Heidepriem et al. [2004], Feng et al. [2003], Petropoulos et al. [2003]) which have different intrinsic physical parameters.
In contrast, we can refer to the drawing temperature T, the feed speed W_f, the drawing speed W_d and the internal hole pressure Pr, as external physical parameters.
It is important here to establish, for the production of a HNL-HF, how these physical parameters influence the closure of a small hole. Indeed several attempts, previous to this work, to draw a HF with a hole pitch Λ less than 2 μm demonstrated that the internal fibre holes completely collapsed.

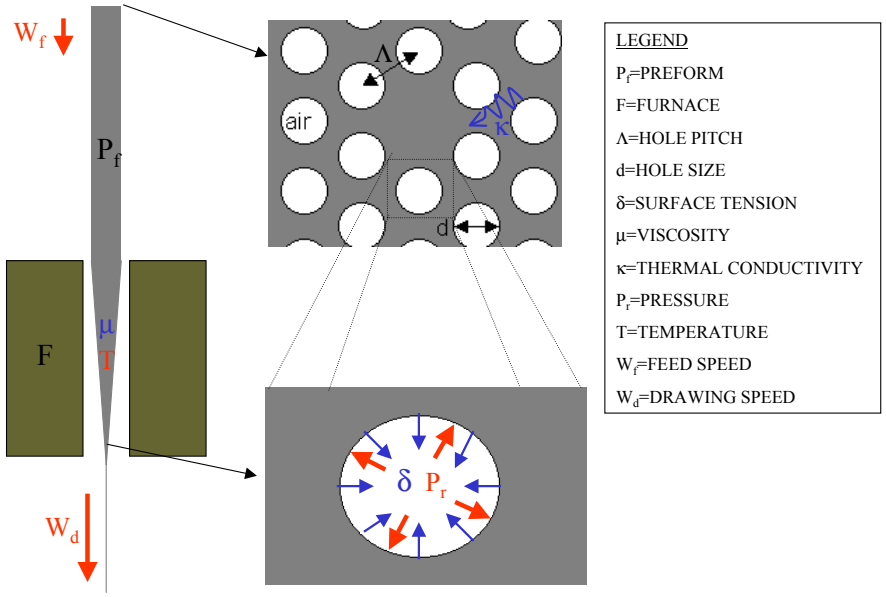

FIGURE 3.12: Closure of the HF holes during the drawing

The collapse of the internal fibre holes was also experienced during the fabrication of the first HFs by Knight (Birks et al. [1995]) and Bennett (Bennett et al. [1999]), although in this case the hole collapse was not complete.
The physical reason for the hole collapse relates to surface tension δ that acts on the inner walls of the fibre holes, and which naturally leads the hole to collapse. The value of the surface tension δ for silica is 0.3 N/m (Bansal and Doremus [1986]). As we will show in Sect. 3.7, the surface tension effects can be balanced by applying an internal hole pressure Pr.

The viscosity μ of the glass is also of fundamental importance in relation to the closure of the fibre hole. Fig. 3.13 shows how the silica glass viscosity is related to temperature. In particular five temperature values, which correspond to five viscosity values, are of fundamental importance in the production of a glass fibre (Doremus [1994]). The first is the "melting point", which is the melting temperature of the glass and corresponds to a glass viscosity of 10^2 P. The second is the "working point", which is the temperature corresponding to a viscosity value of $10^4 P$. At this temperature, the glass can be readily formed or sealed. The third is the "softening point", which is the temperature corresponding to a viscosity value of $10^{7.6} P$. At this viscosity, a rod about 24 cm long elongates 1 mm/min under its own weight. The fourth point is the "annealing point", with a temperature corresponding to a viscosity of $10^{13.4} P$, at a which point a glass transforms from an elastic state to a viscous state (Pfaender [1996]). The last temperature value is indicated as the "strain point", corresponding to a viscosity value of $10^{14.6} P$.
As we will discuss in Sect. 3.5.2, we investigated the relations between the drawing fibre temperature and the fibre hole size. Indeed at a lower temperature the glass viscosity is

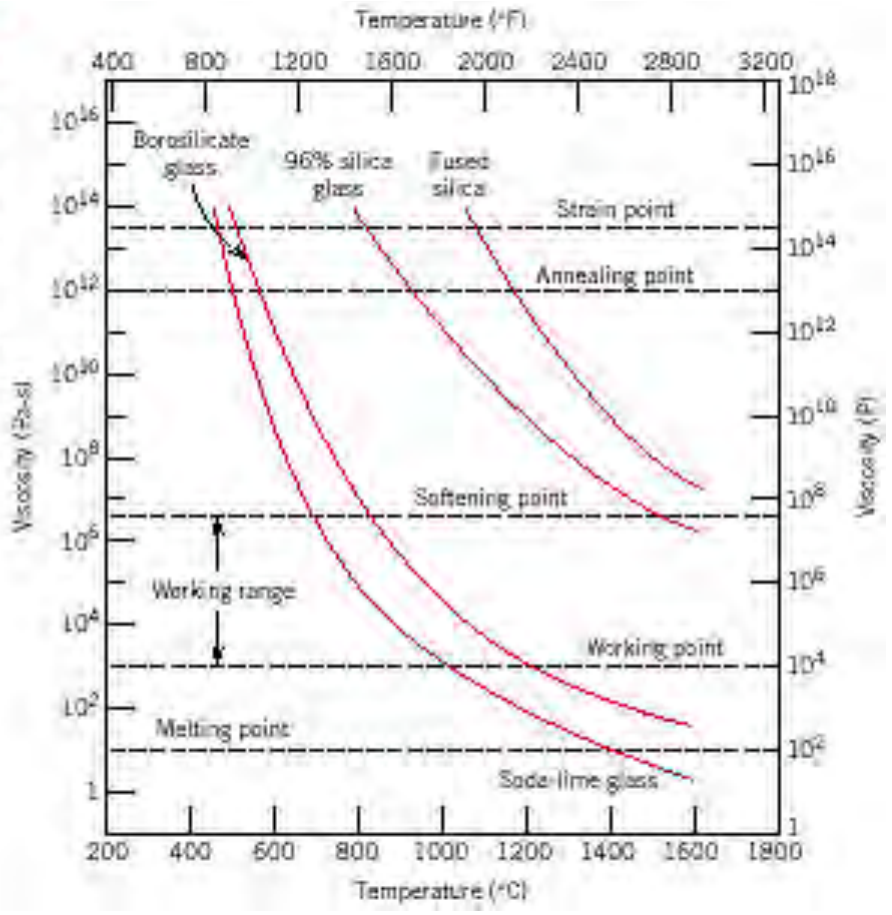

FIGURE 3.13: Logarithm of viscosity versus temperature for fused silica and several silica glasses. As we can see, Vycor (96% silica glass) has a lower viscosity than fused silica (from Shand [1968]).

higher and, intuitively, the hole collapse should be less effective.

On the other hand, as we will explain in Sect. 3.8, we also investigated the possibility to use different glass compositions for the fabrication of a HF, to take advantage of their different viscosity values. Thus, beside fused silica glass, we also used Vycor glass for the jacketing of HF. The different properties of this glass compared to silica are highlighted in Fig. 3.13 (Shand [1968]) and Fig. 3.14 (Weber [2003], Pfaender [1996]). As we can see the softening point of Vycor is 120 °C lower than that for silica. This means that a Vycor fibre can be drawn at a much lower temperature than a silica fibre. Thus the use of a Vycor jacket in the production of a HF may offer two main advantages.

First of all, we should consider that the drawing temperature of a composite glass, constituted by two different glasses, has a value, in general, between the drawing temperatures of the two glasses alone. However, as is intuitive, the drawing temperature is closer to the drawing temperature of the glass that occupies the greatest volume in the composite glass. Since the Vycor jacket has a much higher volume than the internal silica cane, the drawing temperature of a Vycor jacketed HF is determined predominantly by the Vycor viscosity. That's why it is possible to draw such composite HF preform at a lower

	FUSED SILICA	VYCOR
COMPOSITION	SiO_2 (99%)	SiO_2(96%) B_2O_3(<3.5%)
ANNEALING TEMPERATURE (^{0}C)	1100	1050
SOFTENING TEMPERATURE (^{0}C)	1650	1530
COEFFICIENT OF THERMAL EXPANSION α(20-300^{0}C) (10^{-6}/K)	0.54	0.75
DENSITY (g/cm^3)	2.21	2.18
HARDNESS KNOOP (kg/mm^2)	500	487
ELASTICITY MODULUS (10^3N/mm^2)	66	68

FIGURE 3.14: Comparison between main physical characteristics of fused silica and Vycor glass (Weber [2003], Pfaender [1996]).

temperature than when using a silica jacket. The reduction of the drawing temperature, as explained above, means that the silica hole viscosity is higher, and which helps to keep the internal holes open in the core region of the HF.
A second advantage concerns the fusion of the external silica jacket to the internal cane. Due to its low viscosity and high thermal expansion (see Fig. 3.14), a Vycor jacket can completely collapse onto the internal cane during the fibre drawing, even if the initial fit of the cane to the jacket is not very good. We will discuss both these points in Sect. 3.8, showing some experimental proofs.

The final physical parameter of fundamental importance in the production of HFs is the thermal conductivity κ. Indeed, when the preform is in the furnace, a certain heat is applied on the external walls of the preform and, from there, transfers to the centre of the preform (Papamichael and Miaoulis [1994]). The thermal conductivity κ is a measure of how well the heat transfers through the glass. The value of κ for fused silica is 1.38 $W/m \cdot K$ (Weber [2003]).
We investigated the possibility to adopt a HF jacket with a lower thermal conductivity (see Sect. 3.6). Indeed in this case, although the drawing temperature may be as high as 2050 °C, the effective temperature of the internal cane is lower, so that the actual viscosity of the glass around the fibre holes is higher and the holes can be preserved. Our novel idea was the introduction of an air jacket (Belardi et al. [2002a]). Indeed the thermal conductivity of the air is only 0.0262 $W/m \cdot K$ and so the internal cane is thermally well isolated from the jacket, especially when the feed speed used is quite high.

Besides that, we also point out that the reduction of the glass volume in the jacket lowers the compressive force acting on the internal cane while the preform is being stretched. This point will be discussed in detail in Sect. 3.6.
In parallel with all these experimental investigations, a mathematical model for the fabrication of silica capillaries has been proposed by Fitt et al. [2002]. Some of the conclusions of this model regarding the hole pressure and instability, as well as the drawing and feed speed, may be useful for a more accurate comprehension of the HF fabrication problem. In the following sections I will sometimes refer to this model. The fundamental assumption of this model is that the problem of capillary drawing can be treated as the flow of an incompressible fluid, whose evolution is ruled by the following Equations (see, for example, Round and Garg [1985]):

$$\nabla \mathbf{v} = 0 \tag{3.8}$$

$$\rho \frac{d\mathbf{v}}{dt} = -\nabla P_r + \mu \nabla^2 \mathbf{v} + \rho \mathbf{g} \tag{3.9}$$

where ρ is the fluid density, g is the gravity acceleration, μ is the fluid viscosity, Pr is the pressure, $\mathbf{v}$ is the fluid velocity. Equation 3.8 represents the incompressibility, i.e. that there is no change of density in time. Equation 3.9 represents the so called "Navier-Stokes" equation, which is derived from the momentum conservation of the fluid.
To take account of the temperature variation, another equation should be added, which accounts for energy conservation:

$$\rho c_p \frac{dT}{dt} = \nabla(\kappa \nabla T) + S \tag{3.10}$$

where T is the absolute temperature, S represents the heat source, c_p is the specific heat and κ is the thermal conductivity.
By applying these general equations to specific cases, Fitt et al. [2002] obtained important conclusions regarding the influence of pressure, feed speed and viscosity (thus temperature) on the fabrication of a hollow fibre, which fits well with our experimental results. We are going to review some of their results in the following sections. In particular they also demonstrated that, "whatever the dependence of μ on temperature, the absence of surface tension and internal hole pressurization means that the initial fibre geometry is always preserved throughout the pull, and there is no question of hole closure or fibre explosion" (Fitt et al. [2002]).
Now that the main fabrication problem of a HNL-HF has been addressed, I can proceed in the discussion of our experimental investigation, which aimed, first of all, to find the correct drawing parameters and practical fabrication techniques to avoid closure of the HNL-HF holes during the drawing process. Thus, we first investigated the influence of the feed speed and the drawing temperature on the final holey fibre structure. Then we invented, introduced and developed new fabrication techniques to reliably produce long and robust HNL-HFs.

3.5 Holey fibre drawing parameters

The choice of the right drawing parameters is found to be of fundamental importance for the successful fabrication of a HF, because they have a direct influence on the collapse ratio of the fibre holes.
In this section, I describe some systematic experiments, which investigate the influence of the feed speed and of the drawing temperature on the AFF of a holey fibre. In particular, in Sect. 3.5.1, I analyze the relation between the feed speed and the AFF in the simplest case of a hollow fibre. This leads to considerations regarding the influence of this drawing parameter on the complex HF structure and a practical feed speed value is indicated.
In the following Sect. 3.5.2, I explain how the drawing temperature determines the AFF of a HF, once the other drawing parameters are fixed. It is to be noted that even small changes in the drawing temperature can lead to HFs with completely different optical properties.

3.5.1 Feed speed

I have experimentally investigated the effects of the feed speed on a hollow fibre, to monitor the influence of this drawing parameter on the most simple holey structure.
A Suprasil F300 silica tube, with an outer diameter of 9.95 mm and a inner diameter of 2.85 mm (AFF=0.286), has been drawn, using different feed speed values, a constant drawing speed Wd of 6m/min, and a drawing temperature T of 2150 °C. The results are shown in Fig. 3.15. I have measured the fibre diameter and the hole size by means of an optical microscope. As expected, they both increase with increasing rate of feed glass into the furnace (Fig. 3.15(a)). However the increasing expansion rate of the hole size is much higher than that of the fibre diameter. As shown in Fig. 3.15(b), the AFF of the hollow fibre increases linearly with the feed speed.
This experimental data leads to the conclusion that the (preform) feed speed is a critical parameter in the fabrication of a HF. Very low feed speed values tend to produce a collapse of the HF holes and thus should be avoided. In contrast, high values of the feed speed can be advantageous and, as explained in Sect. 3.5.2, may allow a higher drawing temperature. However the feed speed cannot be increased too much, since the fibre diameter must be kept around 125 μm. Indeed, for optical fibre drawing, the following relation is valid (mass conservation law):

$$W_f = \left(\frac{D_f}{D}\right)^2 W_d \tag{3.11}$$

where W_f,W_d, D_f, D are respectively the feed speed, drawing speed, fibre diameter, and preform diameter. As we can see, besides the feed speed, the fibre diameter is also determined by the drawing speed and preform size. However even for these factors there are limits.

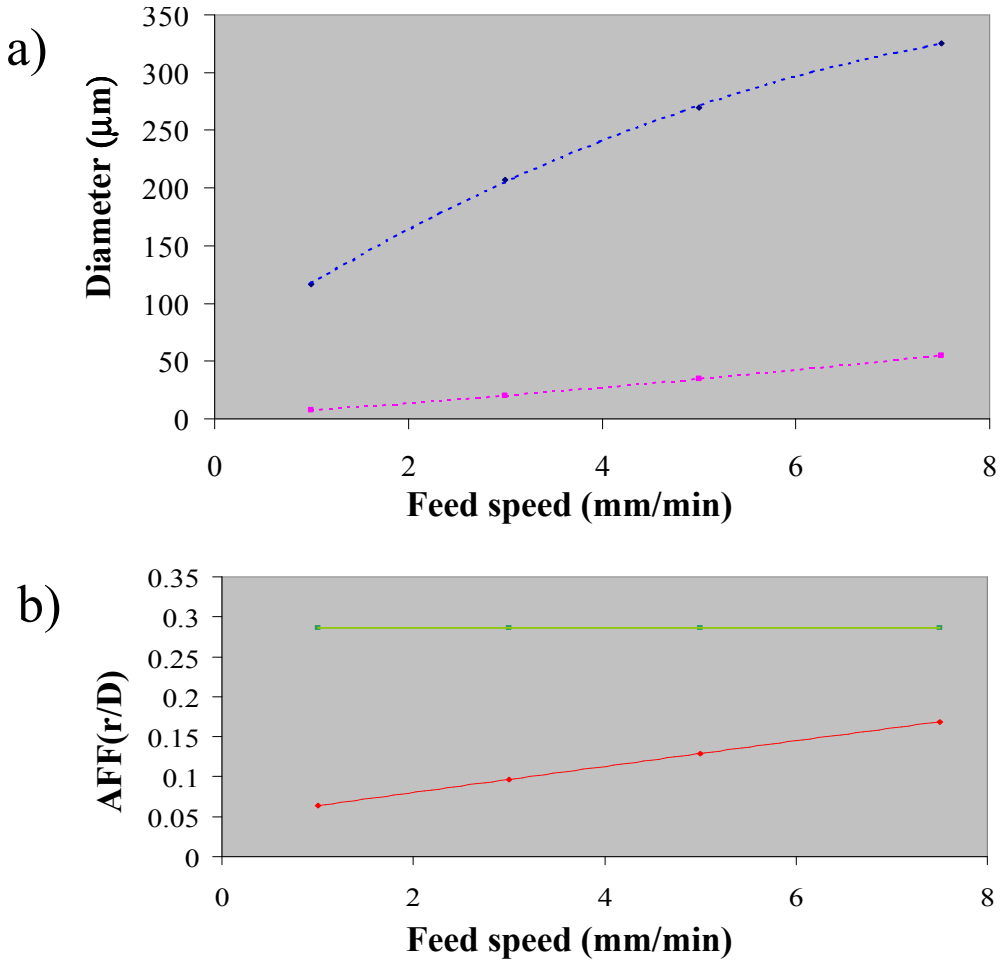

FIGURE 3.15: a)Hole(purple)and fibre(blue)diameter versus feed speed.b)AFF versus feed speed(red) and preform AFF (green).

The drawing speed in practice cannot be higher than 50 m/min, otherwise, by using our 5 m drawing tower the fibre coating can not be consistently applied to the fibre, due to the short cooling time prior to the coating application (Paek [1999], Kyriacou et al. [1990]).

The preform size can be reduced to a diameter of only few millimeters. However, in this case the production of long lengths of holey fibre would imply the use of very long preforms, of around 1 metre length or more. As we will explain in more detail in Sect. 3.7, the HF preform is normally internally pressurized and, in particular, during the drawing, such internal pressure changes are related to the preform length, which causes non-uniformity along the fibre length (see also Fig. 3.30). Hence the use of a very long preform should be avoided.

From our experience, a practical value of the feed speed used during the HF drawing is about 2 mm/min, when a final HF preform with a diameter of 20 mm, a length of 150 mm and a drawing speed between 20 and 40 m/min is being used (corresponding to an outer fibre diameter between 140 μm and 200 μm).

The theoretical model on capillary drawing developed by Fitt et al. [2002] confirms the

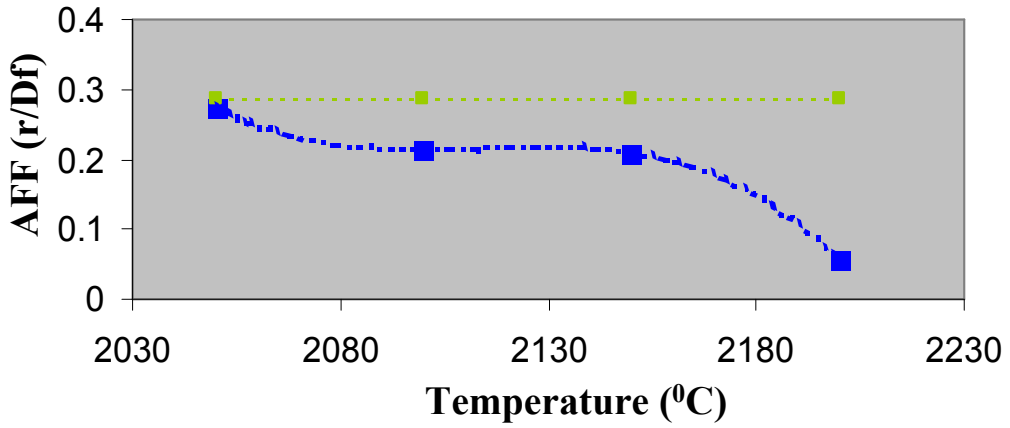

FIGURE 3.16: AFF of a hollow fibre versus temperature(blue line). Original AFF of the preform (green line)

importance of the feed speed W_f in the fabrication of a hollow fibre. Indeed the model predicts that, if we assume a large draw ratio $W_d/W_f \gg 1$, consider the surface tension to be small and do not include pressure, the hole collapse occurs when:

$$\mu W_f \ln(\frac{W_d}{W_f}) \leq \frac{\delta L r_{20}}{r_{10}(r_{20} - r_{10})} \tag{3.12}$$

where L is the hot zone length in the fibre drawing furnace, r_{20} and r_{10} are the outer and inner preform diameter, δ is the surface tension ($\delta \simeq 0.3N/m$ for silica) and μ is the glass viscosity. As we can see by equation 3.12, the hole collapse is more sensitive to the feed speed W_f than to the drawing speed W_d. We also observe that the hole closure is sensitive to the temperature through the glass viscosity μ. We investigate this point in the next section.

3.5.2 Temperature

I experimentally investigated the direct effects of the drawing temperature on the air filling fraction of a HF.

Firstly I drew a silica F300 tube, with an outer diameter OD of 9.95 mm, and an inner diameter ID of 2.85 mm, at a fixed feed speed W_f of 5 mm/min and a fixed drawing speed W_d of 6 m/min. I used different drawing temperatures T and experimentally observed the relationship between the AFF of the drawn hollow fibre and T, as shown in Fig. 3.16. As we can see, the air filling fraction decreases nonlinearly with an increase in the drawing temperature. In particular, at a very high drawing temperature ($> 2150\,^{\circ}$C), the hole rapidly tends to collapse. We can logically extend this result, obtained by using a hollow tube, to a more complex HF structure.

I have also studied directly the geometric effects of the drawing temperature on the fabrication of a large mode HF, with a core size of about $15 - 20\ \mu m$. In this case I used a Vycor outer jacket with an outer diameter of 15 mm and an inner diameter of about 12 mm.

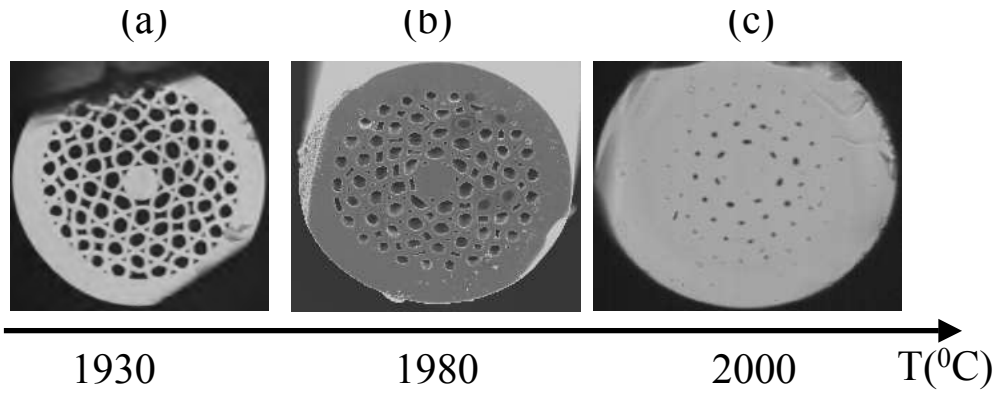

FIGURE 3.17: 3 large mode holey fibers drawn from the same preform and with the same fabrication parameters, but different temperatures.

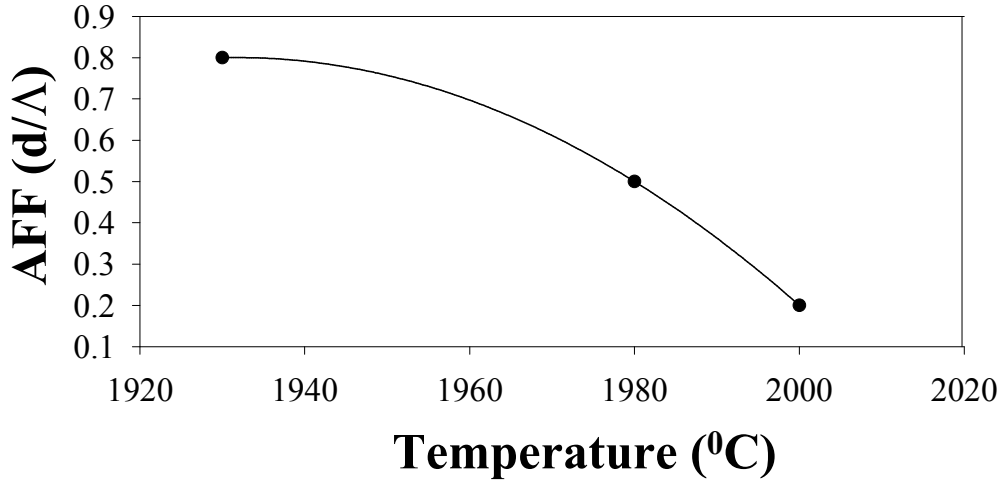

FIGURE 3.18: Average AFF of 3 different large mode HFs versus their drawing temperatures.

In Fig. 3.17, I compare the AFF of three different HFs, obtained during the same fibre drawing, using three different temperatures, while keeping the other fabrication parameters fixed. It is clear that a change in the temperature of only 20 degrees, between the fibres of Fig. 3.17(b) and (c), generates a huge change in the air filling fraction, especially when the temperature is quite high.

The results of the previous experiments are readily understandable. The viscosity μ of silica glass is related to its temperature T from the approximated relation 3.13, valid in the range between 1600 and 2500 °C (Bansal and Doremus [1986]).

$$\log \mu = -6.24 + \frac{2.69 \cdot 10^4}{T} \; [poise] \tag{3.13}$$

where T is the absolute temperature. Thus the viscosity is an exponential function of the temperature, and we can easily realize that a small change in the temperature can imply a quite big change in terms of viscosity. For example if the temperature increase from $T_1 = 1950°$ C to $T_2 = 1980°$ C, then, applying equation 3.13 the viscosity will

decrease from $\mu_1 = 10^{5.86} P(poise)$ to $\mu_2 = 10^{5.7} P$.

The drawing temperature is not such a critical parameter for the fabrication of conventional single mode optical fibres, usually drawn at about 2100 °C. On the contrary, the drawing temperature is a fundamental parameter for successful fabrication of a holey optical fibre. Indeed the viscosity of the glass (and thus the temperature) plays a major role in keeping the fibre holes open during the drawing. In particular, a high drawing temperature (thus a low viscosity) leads to the collapse of the internal fibre holes. On the other hand, reducing the drawing temperature to relatively small values (e.g. $1850 - 1900$ °C) can make it difficult to draw an optical fibre, due to the increased viscosity of the glass and the resulting high tension, and may cause a break of the fibre during the drawing, if the preform is not carefully prepared.

In practice, to allow reliable fibre drawing, the temperature cannot be lower than about 1900 °C, for a solid preform with a diameter of about 20 mm. Even so, due to the high fibre tension, HF fabrication involves a significant risk of a breaking point at any drawing temperature between 1900 and 2000 °C.

I now give some reference values for the correct temperature to be used during the drawing of a HF or of a holey fibre cane (resulting from my technical experience).

A HF cane made with pressurized capillaries (see Sect. 3.9.1) can be drawn usually at a temperature as high as 2050 °C, due to the big size of the preform capillaries (1-2 mm), with the consequent high pressure generated by sealing.

By contrast, a HF cane fabricated using unpressurized capillaries should usually be drawn at about 1800 °C (in the production of a 1 metre long cane, drawn by the tractor unit, we can use a temperature as low as 1740 °C).

For the final drawing of a silica jacketed highly nonlinear HF (see Sect. 3.8), the drawing temperature is about $1920 - 1950$ °C (considering a standard preform size of 20 mm). The temperature can be lowered, if the preform size is smaller, due to the reduced amount of glass. The reduction of the preform size turns out to be very useful when drawing a silica jacketed HF at a temperature less than 1920 °C, for complex structures, or when a very high air filling fraction is required (e.g. > 0.9).

In Sect. 3.8 we will see that the use of a Vycor HF jacket can reduce the HF drawing temperature. In fact Vycor has a much lower viscosity than silica (see Fig. 3.14), and so the drawing, in the HF drawing temperature regime, doesn't involve the risk of a fibre break. However a Vycor jacketed HF is more fragile (hardness of Vycor is 487 kg/mm^2, while for silica is 500 kg/mm^2).

Finally, using an "air jacketed HF" fabrication method, instead of a solid jacket, which I will describe in the next Sect. 3.6, we can draw a pressurized HF preform at a much higher temperature, about 2050 °C, without compromising the inner structure of the HF.

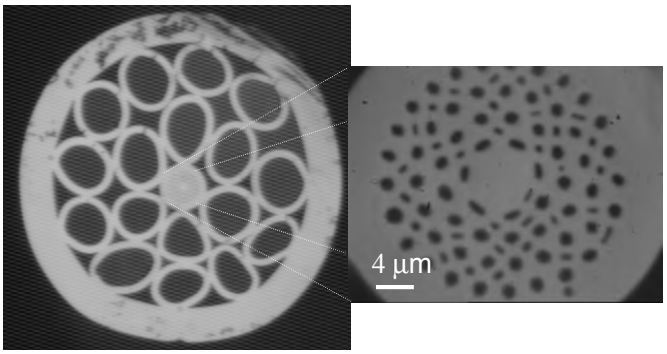

FIGURE 3.19: Air jacketed holey fibre. A magnified view of the inner cladding is shown on the right hand side.

3.6 A novel holey fibre fabrication design

The investigation of the empirical relations between the drawing parameters and the AFF of a holey fibre gave us some indications about the correct feed speed and, in particular, the drawing temperature we need to use to fabricate a highly nonlinear HF. I then invented a novel fabrication design for a HF, to facilitate the HF drawing, in terms of the required drawing temperature (Belardi et al. [2002a]). It consists of the use a two sized ring structure, as shown in Fig. 3.19. The cane is supported by a certain number of silica capillaries instead of a full silica jacket. This method has the disadvantage that the final HF is more fragile and difficult to handle than a full solid jacketed HF. However it has got some advantages both in terms of fabrication and in terms of optical properties. Indeed, since the thermal conductivity of the air is only 0.0262 $W/m \cdot K$ (while in silica is 1.38 $W/m \cdot km$), the use of an air jacket allows a very good thermal isolation of the central cane. That's why, although the actual temperature of the outer "two ring" jacket is about 2000 ^{0}C, the actual temperature of the internal cane is expected to be lower, especially when the feed speed used is quite high. Besides that, the reduction of the amount of glass in the preform lowers the compressive force of the jacket on the internal cane, while the preform is being stretched. In this way, a HF can be drawn at high temperatures without involving the risk of a fibre break but at the same time, the viscosity of the internal cane can be high enough to preserve the HF inner holes.
Another thing to consider is that the actual glass volume of our air jacketed HF preform is very much reduced in comparison with a full silica jacketed preform. Therefore the drawing temperature used can be reduced.
Using this method, a highly nonlinear HFs can be drawn (without using pressurization), if the drawing temperature is reduced to less than 1950 °C . However, as we can see from Fig. 3.19, the holes are still very small and the surface tension still causes their collapse.
Another advantage of this method is that it allows a perfect fusion of the cane to the outer "two ring jacket". This is a very important point, as I have experimentally observed that the insertion of the cane in a solid jacket can cause problems of slippage of the cane.

This can result in different actual feed speeds for the cane and the jacket, which leads to very strong instabilities, compromising the maintenance of the HF inner structure.
The new method enables the fabrication of HFs with novel optical properties. In particular this novel structure, comprised of different sized holes that surround the core, can be used to achieve more complex refractive index profiles for a holey fibre. Recently a double clad HF laser has been made at the ORC (Furusawa et al. [2001]), which uses the "two ring" fabrication approach. At the same time, this novel fabrication design has also allowed poling of a holey fibre, in which two electrodes, with a diameter of about 30 μm, can be inserted into two of the larger holes within the jacket. This has led for the first time to second harmonic generation in a HF (Faccio et al. [2001])

3.7 Pressurization of the holey fibre preform

The invention of the "two ring jacket" method allowed the reliable fabrication of small core HFs, because of the possibility to use a drawing temperature of about 1950 °C.
However it presented several disadvantages also. First of all the HF structures have a very small AFF (~ 0.2), which is undesirable for a highly nonlinear HF. Moreover the fibres produced were fragile and of only a few meters in length.
Thus I explored other ways to make, in a reliable fashion, long and robust small core HFs with a high AFF.
As outlined in Sect. 3.4, the main holey fibre fabrication problem is related to the closure of the holes, due to the surface tension acting on their inner walls. I thought of creating a pressure inside the holes, which would provide a radial force that could oppose and resist the effects of the surface tension.
The theoretical model developed by Fitt et al. [2002] shows that, "though internal hole pressurization might be employed to prevent hole collapse, it may lead to drawing processes that are harder to control". Indeed this model also provided a reference pressure condition that should be satisfied to achieve a controlled hollow fibre manufacturing process:

$$P_r < \frac{2W_f \mu \beta \log\left(\frac{ID}{OD}\right)}{L(e^{-\beta} - 1)} \tag{3.14}$$

where $\beta = \ln\left(\frac{W_d}{W_f}\right)$, ID is the inner preform diameter and OD is the outer preform diameter. Although equation 3.14 is obtained by neglecting the effects of surface tension, it indicates that large hot zone lengths L, small viscosities μ and a small feed speed W_f decrease the critical value of the pressure P_r to obtain controlled hollow fibre fabrication.
Some studies of externally-controlled HF preform pressurization were made at the ORC prior to this work, and they resulted in the conclusion that it was extremely hard to control the drawing process.
I thought of a novel way to pressurize the HF preform, which involves the sealing of the top of the cane or of the single capillaries prior to HF drawing. The sealing provides a self-controlled pressurization and, in that, is fundamentally different from the

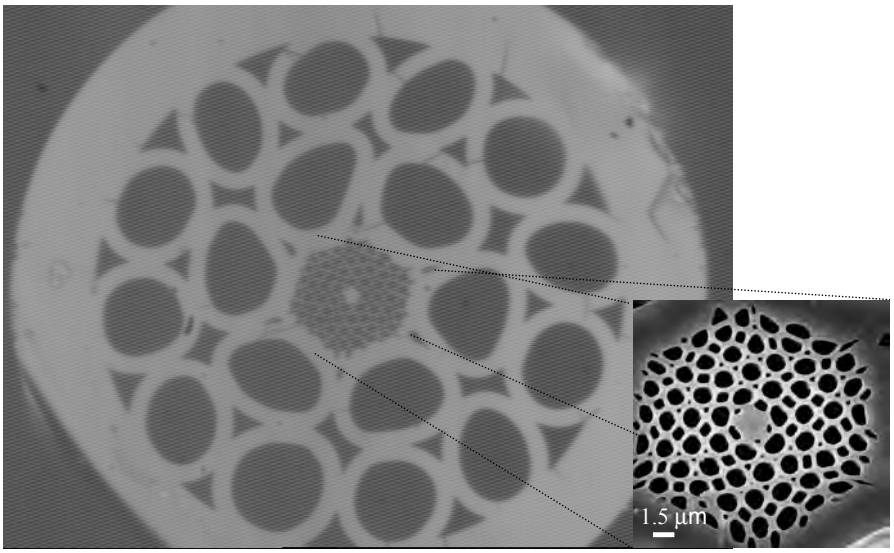

FIGURE 3.20: Pressurized "air jacketed" holey fibre

externally-controlled pressurization technique.
I first tested the method on an "air jacketed" HF. I sealed the top end of the central cane prior to the fibre drawing and I obtained the fibre in Fig. 3.20 In the manufacture of this fibre I used a quite high temperature of 2050 $°C$ and was able to obtain an AFF of about 0.8 and a core size of about 1.5 μm. Due to the high drawing temperature used, I could draw a fibre length of several hundreds of meters.
Thus the introduction of the sealing technique to pressurize a HF preform was found to provide a successful means to fabricate HNL-HFs. Numerous fibres were subsequently made using this technique which highlights the reliability of this method.

3.8 Holey fibre jacket

The fibres produced combining the sealing technique and the "air jacket" method, were however still very fragile and difficult to handle.
Thus I investigated the possibility to improve the strength of the fibre, by using a solid jacket in the hope that this would allow the fabrication of long and robust HNL-HFs.
By using the self-pressurization technique I performed several experiments on different types of jacket (Vycor and silica) and tried different techniques to insert the cane into the jacket.
I investigated two different possibilities for preparing a solid outer jacket for the HF. In the first I drilled a hole inside a solid rod with a diameter of 20 mm using a rotary ultrasonic drilling machine. We normally needed to drill a hole with a diameter of about 1.4 mm and thus required the use of a drill bit with the same diameter. However, the rotating small dimension drill would vibrate if longer than about 150 mm, compromising the uniformity of the hole. This limited the practical hole length I was able to drill with

this method.
The second possibility I investigated was to collapse a tube, by using a lathe, until its internal hole reaches the required dimension. In this case the hole length is limited by the lathe length, but, in practice, a hole with a dimension of about 1 mm and 600 mm length can be reliably made. However the collapse of a hole using a lathe should be made in such a way to maintain its circularity. The tube should be secured well in the chucks of the lathe, and its oscillations during rotation should be reduced to the minimum level. Active internal pressurization can be also used to maintain the circularity of the hole, although this requires a longer process and usually higher collapsing temperature. Tube collapsing can also improve the circularity of the jacket, especially when the material used has a high degree of ovality, like Vycor tubes for example.

The use of a Vycor jacket had already been tried by Bennett et al. [1999]. The choice of Vycor was particularly suitable for the manufacture of a HF, because of the lower melting temperature of Vycor compared to silica. Thus, while drawing the HF, the Vycor jacket should collapse on the cane. However, in Bennett's fibre full collapse of the jacket was not achieved (see Fig. 3.5).
I however found that a Vycor jacket collapses onto the HF cane during the drawing process, even at relatively low temperatures (e.g. 1920 °C), due to the lower viscosity of this glass compared to silica (see Fig. 3.14). Even if the initial fit of the cane into the jacket is very poor, this doesn't compromise maintenance of the HF structure, although I typically observed an enlargement of the holes in the inner structure of the HF, as shown in Fig. 3.21. By using a Vycor jacket the drawing of a HF can be made at a

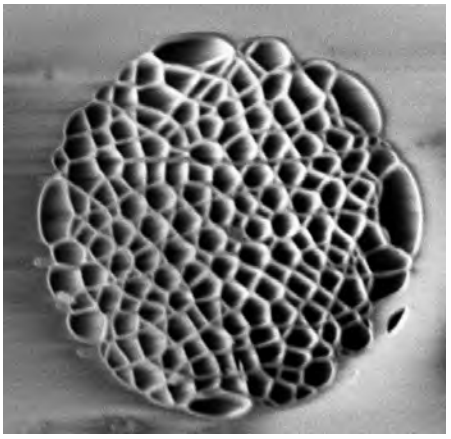

FIGURE 3.21: Example of an holey fibre in which the fit of the cane inside the solid Vycor jacket is very poor. A strong enlargement of the holes is observed.

sufficiently low temperature, that the risk of a breakage is small. Indeed the actual drawing temperature of a fibre depends upon the material of the preform. In the case of a Vycor jacketed HF, Vycor is largely responsible for the drawing temperature because the volume of the Vycor HF jacket is much greater than the volume of the internal silica cane. In this way this Vycor jacketed HF can be drawn at a lower temperature than a

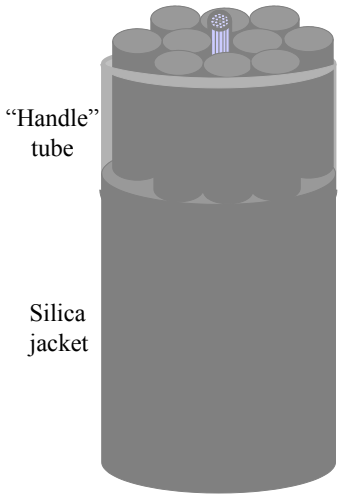

FIGURE 3.22: Slippage of the holey fibre cane inside the silica jacket can be avoided holding the cane by few rings of rods in the "handle" tube.

silica jacketed HF.

The manufacture of HFs made by using Vycor glass, resulted in more robust HFs than the previous "air jacketed" HFs, but they were still relatively fragile compared to conventional fibres, due to the low quality of the jacket material.

I attempted to make silica jacketed HFs. In this case, as the jacket material was the same as the cane material, we could not rely on the collapse of the outer jacket on the inner cane. Thus two main issues had to be addressed.

The first concerns the elimination of the air gap between the cane and the jacket, as, for example, occurred in Bennett's fibre (see again Fig. 3.5).

The second issue regards the different feed speeds, which would be experienced by the cane and the jacket, in the case of "slippage" of the cane into the jacket.

Thus a good fit of the cane into the jacket is of particular importance, because the collapse is not as strong as in the previous case. Accuracy can be obtained by careful choice of the jacket hole dimensions and of the cane dimension and uniformity.

Moreover, to avoid problems of "slippage" of the cane into the jacket, during the drawing stage, I introduced a new technique to hold the cane, as shown in Fig. 3.22. The cane is secured to the "handle" of the HF preform, by stacking a few rods inside the "handle" that hold the cane firmly, in a similar way to the preform of a "air jacketed" HF.

Our first fabricated HNL-HF made by using a full silica jacket is shown in Fig. 3.23. It had a core size of about 1.5 μm, an AFF of about 0.8, a standard outer fibre dimension of 125 μm and it was as long, strong and robust as a standard optical fibre, due to the thick protective silica layer around the microstructured region.

3.9 Pressurization issues

In the previous sections I have described how it has been possible to fabricate long and robust HNL-HFs, by introducing a sealing technique to pressurize the HF preform and

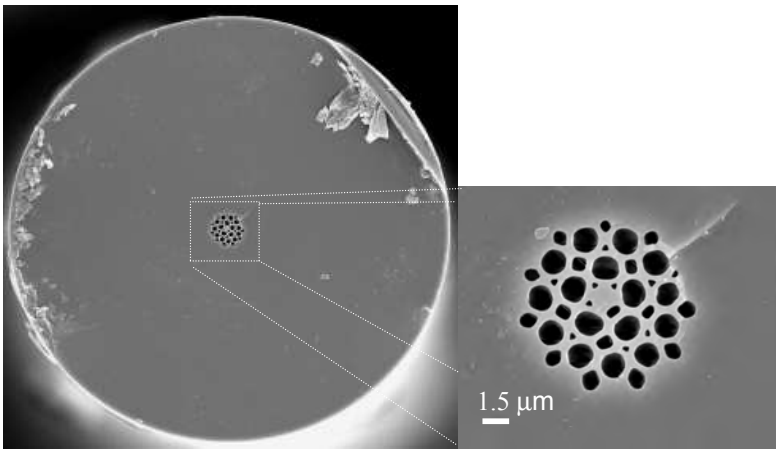

FIGURE 3.23: A full solid silica jacketed holey fibre

jacketing the microstructure region with a solid silica jacket.
In this section, I specifically discuss some of the issues related to the sealing technique both in terms of preform preparation and in terms of HF structure uniformity.
In particular, in Sect. 3.9.1 I discuss how the sealing of the cane, prior to its insertion in the jacket, can be performed.
In Sect. 3.9.2 I describe the main issues related to the pressurization of the single capillaries.
In Sect. 3.9.3, I show some systematic data that indicate that the sealing technique leads to a non-uniform pressure build up as the preform is fed into the furnace.

3.9.1 Pressurization of the cane

The cane can be pressurized prior to the final drawing stage simply by sealing the top end of the cane using a H_2/O_2 gas torch. There is no need to seal the bottom end of the cane because it will be closed naturally at the beginning of the fibre draw (as the starting drawing temperature is as high as 2100 °C).
The sealing of the cane is a straightforward technique which is easy to apply and, at the same time, fundamental for the success of HF fabrication. However it presents some disadvantages. In particular it should be observed that the amount of pressure inside the cane is related to the cane length, as will be indirectly demonstrated in Sect. 3.9.3. Usually a cane length between 150 and 300 mm is used but, as the drawing process proceeds, the preform length reduces and the amount of internal pressure increases (see Fig. 3.30). In this way an increasing pressure can lead to non-uniformity of the hole size along the fibre length, as well as an instability in the fabrication process.
A simple mass conservation equation can be written as:

$$\rho\pi r^2 l = \rho\pi R^2 L \tag{3.15}$$

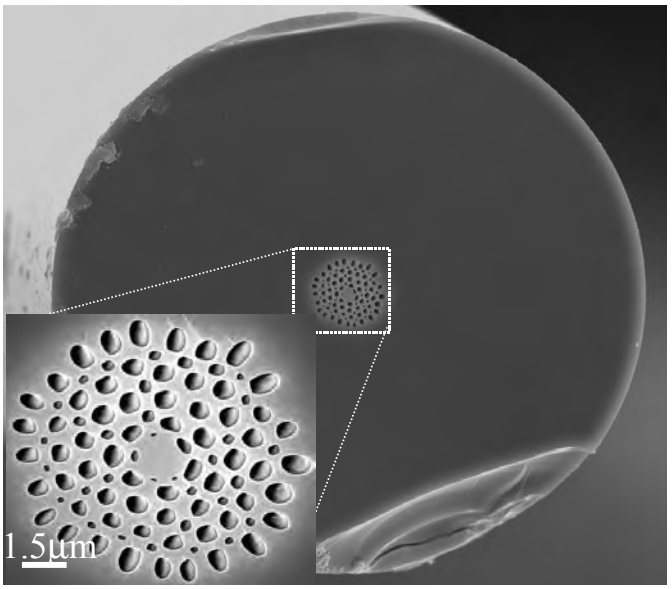

FIGURE 3.24: Holey fibre made by pressurizing the cane

where ρ is the glass density, R and r are the preform radius and fibre radius, L and l are the preform length used and the fibre length obtained. From equation 3.15, we can understand that it would be preferable to use a HF preform with a large radius R, so that, keeping the same fibre radius r and length l, a HF preform with a shorter length L can be used, and, due to the relatively small increase of the internal pressure, the fibre uniformity can be maintained. For example if we use a preform radius of about 5 mm we can obtain 250 m of a conventional fibre with a radius of 72.5 μm by using a preform length of about 5.3 cm. On the other hand, using a preform with a radius of 10 mm (double that before), we can obtain about 250 m of a conventional size HF by using only 1.3 cm of preform length. However, in practice, when using bigger preform sizes, we also need a cane with a diameter greater than 1.5-2 mm, if it contains 4 rings of holes, and which is produced at a very low drawing speed (about 0.5 m/min).
The sealing of a cane leads to a final HF of the kind shown in Fig. 3.24. As we can see, the interstitial holes between the capillaries remain open, as well as their internal holes. Indeed the sealing is for all the cane and so all the air holes are pressurized. Interstitial holes can be useful optically in terms of mode shape (Monro et al. [2000]) and in terms of nonlinearity (because the actual fibre numerical aperture increases). However most mathematical models, that predict HF's properties, assume a HF structure in which interstitial holes are absent. So some means to close there up is desirable.

3.9.2 Pressurization of the capillaries

To make HFs in which interstitial holes are absent, we need to seal the starting capillaries before making their assembly, so that the difference in pressure between the capillary holes and the interstitial holes will cause the capillary holes to remain open and the interstitial holes to collapse.

In this case pressurization is applied even during the production of the cane. Normally, in the absence of pressurization, the cane fabrication is usually made at a very low temperature, usually less than 1800 °C. In contrast, in the case of pressurized capillaries, the drawing temperature can be as high as 2050 °C, which indicates a large amount of internal pressure in the capillaries. At such a high temperature, the interstitial holes, which are not pressurized, collapse.
At this point the cane can be sealed as normal, before being inserted into the protective silica jacket, and pulled. Fig. 3.25 shows the different structure of the final HF obtained

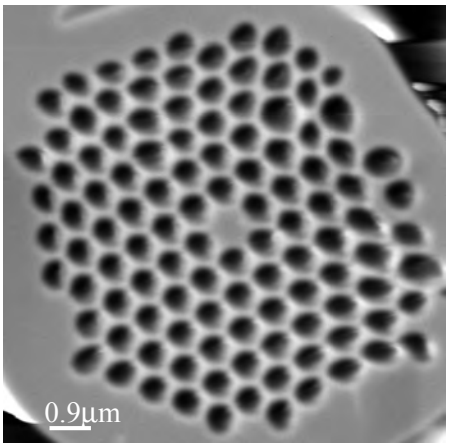

FIGURE 3.25: Holey fibre made by pressurizing the capillaries

by using this technique. As we can see, the resulting HF holes are more circular in shape and the interstitial holes are absent. However, the sealing of single capillaries is quite a long operation, depending on the number of capillaries required, and involves additional cleaning procedures on the singular capillaries, as I will explain in Sect. 3.10.2. Moreover their length should be accurately matched in the bundle, as shown in Fig. 3.26, otherwise they will experience different internal pressures. In practice the length matching

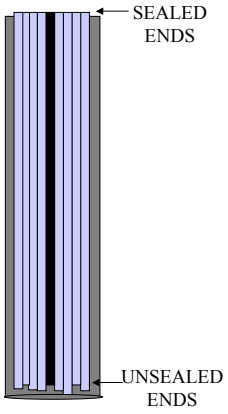

FIGURE 3.26: Length matching of sealed capillaries

is achieved by inserting one by one the capillaries from one side of the external outer tube, and controlling their length from the other side, by using a silica rod of the right dimensions. This operation requires that the sealed end of the capillaries is exactly

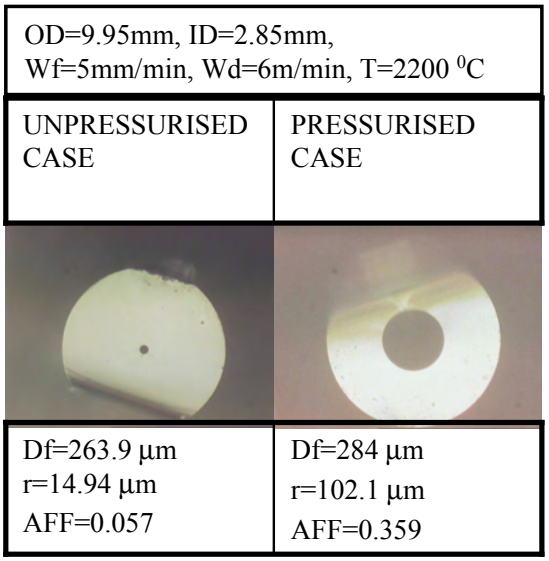

FIGURE 3.27: Pressurization of the hollow preform leads to a dramatic increase of the AFF

straight, because if the capillary end bends or blows out during the sealing operation, the exact alignment of the capillaries is made more complicated. So additional technical skills and care should be taken during the sealing stage.
In Sect. 3.10.2 the particular precautions which must be taken will be explained. Avoiding trapping contaminants inside the capillaries during cleaning is particularly important. If this happens, the capillaries may blow up during the HF drawing, due to the formation, at high temperature, of a powder inside the holes, which can block them.
Finally, we can also apply the sealing technique to the tubes used for drawing capillaries. This allows capillaries to be drawn at a much higher temperatures (about 2100 $^{\circ}C$), which results in an improved strength of the glass, due to the faster cooling (Anderson [1958], Bateson [1958]). An enhanced strength of the capillaries can be important for the stacking operation. Indeed, if the capillaries are very fragile, they are likely to break when they are closely packed.

3.9.3 Pressure instability

Pressurization of the HF preform is the most important factor for reliable fabrication of long, robust, highly nonlinear HF. Indeed HF pressurization, by sealing the top end of the HF preform, generates a dramatic increase in the AFF, as we can see from Fig. 3.27. The same hollow tube has been drawn twice using the same drawing parameters (feed speed W_f,drawing speed W_d, temperature T). In the first case (on the left) the top end of the preform has not been sealed, while in the second case (on the right) it has been sealed. The huge difference in terms of AFF, demonstrates the importance of pressurization in order to retain the HF structure.
The amount of pressure that is generated by the sealing of the preform is not easily measurable, but it clearly depends, in my experience, on the preform hole size and

length. In the case of a larger AFF of the preform, the pressure generated is certainly greater. According to Fitt et al. [2002] the pressure generated in a capillary with a outer diameter of 0.8 mm and an inner diameter of 0.64 mm is of the order of 0.25 psi (1 psi = 6894.76 Pa = $6.8046 \cdot 10^{-2}$ atm). So, in the actual fabrication of a HF, in which sealed capillaries with a similar size (1-2 mm) are used, we believe the pressure to be of the same order as this reference value.

However, the sealing technique to pressurize the HF preform has some major disadvantages, which are related to the pressure instability along the fibre length and to its dependence on the preform length.

The beginning of HF drawing is characterized by a gradual decrease of the drawing temperature, from the drop temperature of 2080 °C to a temperature regime that allows retention of the HF structure. After reaching this temperature the drawing process can remain unstable for more than 15 mins (depending mainly on the preform size and jacketing, as discussed in Sect. 3.5.2). Fig. 3.28 gives an idea of the dynamics of the

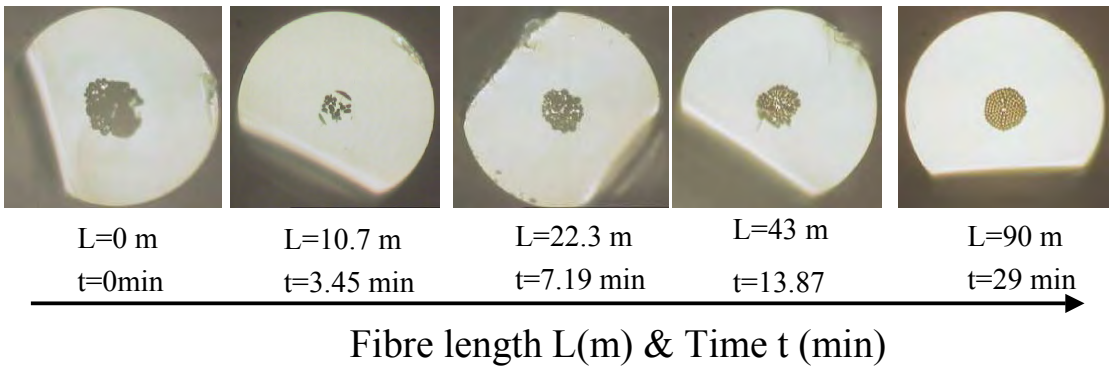

FIGURE 3.28: Stabilization evolution of a highly nonlinear holey fibre

pressure stabilization which takes place in a HF. Subsequent pictures of the transverse section of a HF have been taken during successive time intervals. The HF evolves from a hole structure, in which the overpressure causes the explosion of all the fibre holes (L=0, t=0), to the final HF with well defined structure (L=90m, t=29min).

However, even after a very long time (i.e. some hours), a small amount of pressure instability remains. I have drawn two hollow tubes, one sealed and the other not, with exactly the same dimensions and with very similar drawing parameters, to directly compare the stability of the unsealed case with the instability of the sealed one. The results are shown in Fig. 3.29. As we can see, the AFF in the unsealed case is stable along the full fibre length (60 m). In the sealed case we observe a variation of the AFF as great as as 11%.

For further investigation of the origin of this instability, I have monitored the AFF evolution of a sealed tube over a long time (about an hour), and related it to the preform length. The result is shown in Fig. 3.30. As we can see the AFF (and thus the internal pressure) increases with decrease of the preform length, as the preform is fed at constant speed into the furnace. The AFF (thus the internal pressure) increases with an almost

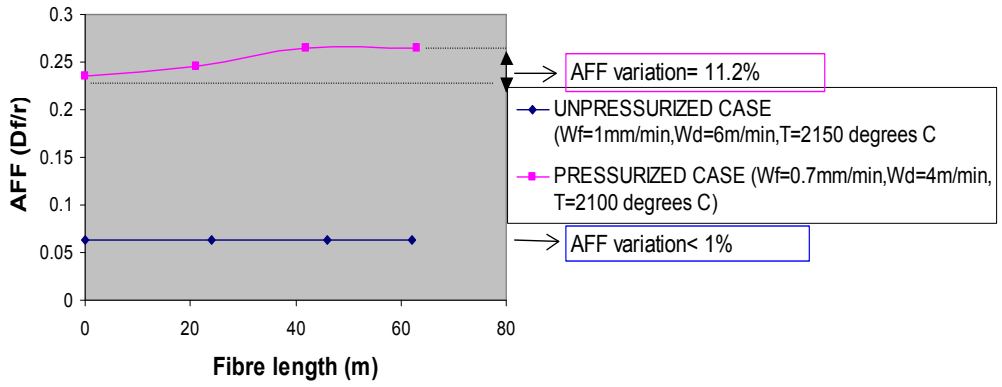

FIGURE 3.29: Comparison between the stability of the unpressurized case with the instability of the pressurized case.

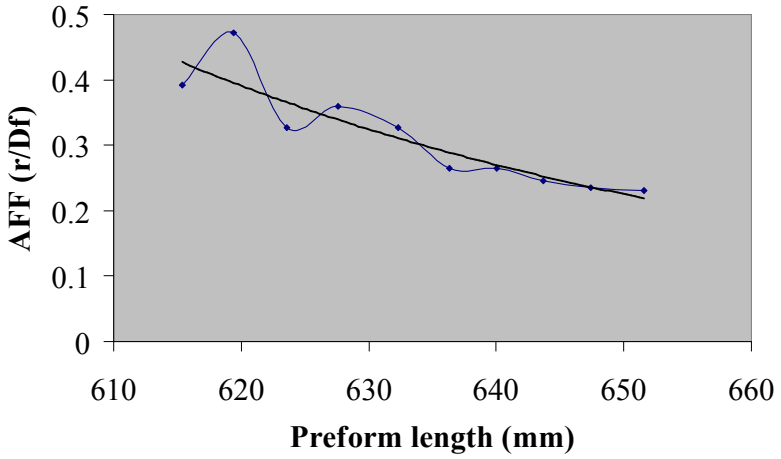

FIGURE 3.30: AFF versus preform length. The blue line shows the amount of instability observed during the hollow fibre drawing. The black line shows the trend of the AFF value with the remaining preform length

linear trend (see black line in Fig. 3.30), however the instability observed during this process can be quite high.

3.10 Preform fabrication issues

In this section I discuss some issues related to the fabrication of a HF preform. My considerations have often only a qualitative nature, because they derive from our technical experience and personal observations; but they can offer a technical guide for the production of a HF.

Firstly, in Sect. 3.10.1, I describe in detail the main technical issues involved in the stacking procedure and how I attempted to overcome them.

In Sect. 3.10.2, I explain how the cleaning of the preform from contaminants is performed in practice, and how it can be important for a successful HF fabrication process.

Finally Sect. 3.10.3 concerns the problems related to the correct choice of length of the drop, attached to the HF preform prior to drawing. This is an important issue because

an incorrect length of the drop can lead to failure of the HF draw.

3.10.1 Stacking

The assembly of the capillaries is made manually by inserting capillaries with a diameter of around 1-2 mm one by one inside a tube with an inner diameter generally around 18-20 mm and with an outer diameter around 20-25 mm.
Depending on the HF design, the capillaries can be thin, with an AFF as high as 0.8, or thick, with an AFF as low as 0.2. The main differences in the stacking concerns the fragility of the capillaries. Although thin capillaries are a fundamental requirement for the fabrication of highly nonlinear holey fibres, due to their high AFF, it has been noted that they are more likely to bend or break during the stacking, because they are more fragile. However they have some advantages. In particular due to their higher elasticity, when at the end of the stacking, the fit of the bundle inside the outer tube has to be made tight. Indeed a bundle of thicker capillaries may even require an extra collapse of the outer jacket, to tighten the assembly.
The outer tube, which is used to keep the capillaries packed together is generally thin (AFF about 0.9), and can be of silica or Vycor.
The use of a Vycor outer jacket can be advantageous. Indeed during the caning,the fit of the capillaries can be tightened at a temperature of only 1740 °C, because the Vycor jacket collapses on the bundle, due to its lower viscosity relative to silica(see Fig. 3.31).
However the use of a Vycor jacket can be disadvantageous because of the low quality

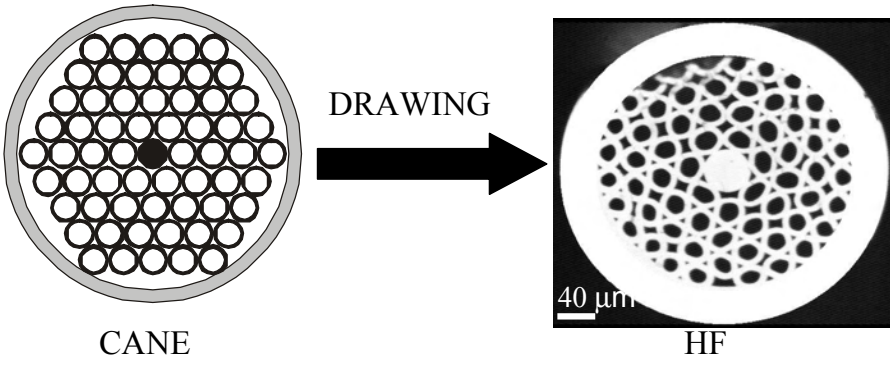

FIGURE 3.31: Holey fibre made by using a Vycor outer jacket. The external jacket collapses on the bundle of unsealed silica capillaries, due to its lower viscosity.

of this glass, in terms of uniformity and circularity. This can complicate the stacking of precise geometric HF structures. For this reason the use of a high quality silica glass, such as Suprasil F300, provides the best solution in terms of circularity and uniformity. In particular, to avoid a loose fit of the outer silica jacket to the bundle, the capillaries can be sealed. In this case the drawing of the cane can be performed at a much higher temperature (about $2050°C$), which facilitates the collapse of the external silica jacket onto the bundle.
A typical stacking procedure is sketched in Fig. 3.32. If the HF has to have n rings of

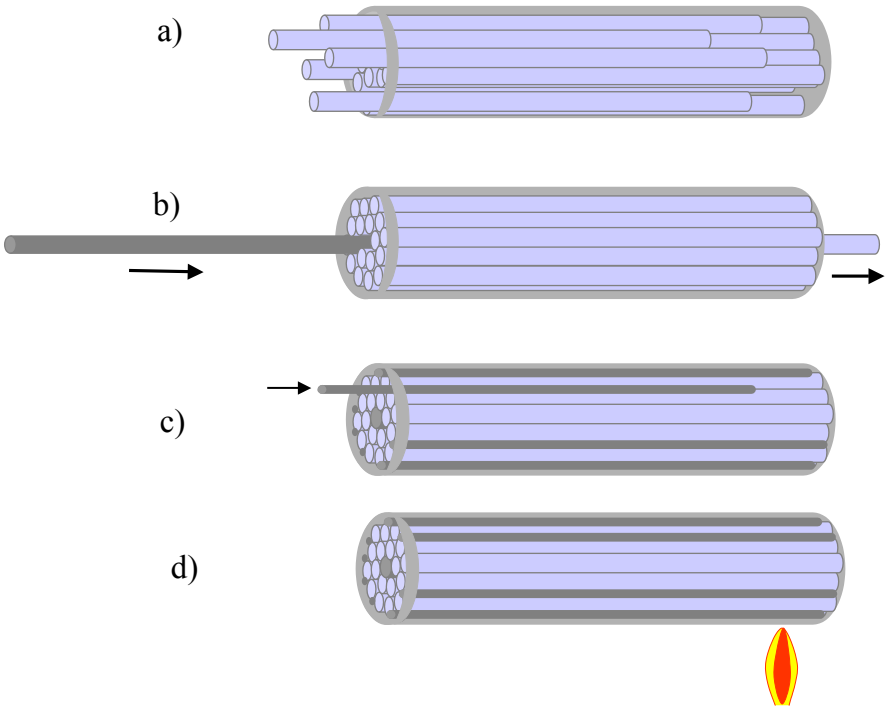

FIGURE 3.32: Stacking technique. a)Capillaries are first inserted one by one. b)A rod is inserted by pushing the central capillary. c)The fit is made tight by inserting smaller size rods. d)The preform is heated at one extremity, so that the outer jacket collapses on the internal bundle.

holes in an hexagonal structure, then the number of capillaries that need to be inserted in the tube is 3n(n+1). These capillaries can be first inserted one by one in the tube, to avoid their bending.

A rod of the same size as the capillaries is inserted into the middle of the assembly in the following way. First an extra capillary (of the same size as the others) is inserted in the bundle. Then, when the capillaries are all packed together, by looking at the preform transversal section, using a magnifying lens, the centre of the bundle is determined. The silica rod (which will act as the core in the HF) in inserted by pushing a selected capillary in the middle of the bundle, so that this can can be made to protrude from the other side of the tube and be extracted.

Capillaries are chosen carefully to ensure that they are uniform along their length and of the same size. However they normally don't fit tightly inside the outer tube, due also to the imperfect circularity of the jacket. The insertion of additional rods, with smaller dimensions, at the extremities of the capillary bundle improves the fit within the jacket. These rods are inserted, if possible, in a symmetric way, so that the hexagonal shape of the bundle can be kept.

Moreover, to secure the fit of the bundle to the jacket, it is good practice to slightly collapse the jacket onto the bundle at its lower extremity. Although this operation is simple in the case of a Vycor outer jacket, sometimes it is not simple to avoid damage to the preform in the case of a silica jacket, because of the high collapse temperature required.

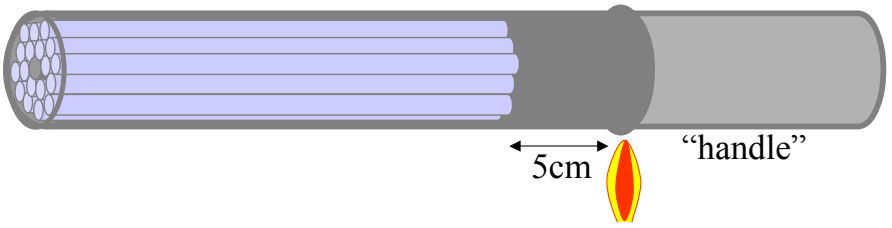

FIGURE 3.33: The connection between the holey fibre preform and the "handle" tube should be separated about 5 cm from the sealed ends of the capillaries.

Extreme care must be taken to avoid bending, or breaking of the capillaries (especially if they are thin), and to avoid external contamination.
Careful observation of the transversal section of the stack is fundamental to achieve a good structure (usually using just a magnifying lens). For the same reason, the sealing of only one end of the capillaries is preferred, so that the monitoring of the structure is easier and clearer.
As explained in Sect.3.9.3, the sealed capillaries have to be exactly aligned, so that they experience the same internal pressure. This is usually achieved by using a rod, a flat layer or a hand to hold the capillaries at one end of the tube, while inserting them at the other end.
Especially important is the correct sealing of the capillaries. The sealed end of a capillary should be straight and not blown up, otherwise both good stacking and good alignment are compromised.
Once the stacking has been completed, the bundle is connected to a so called "handle" tube, which is directly placed in the chuck of the drawing tower. This standard assembly operation, performed using a lathe, has to be made with care to avoid possible damage to the HF preform. The insertion in the stack of extra layers of rods can be helpful to protect the inner capillaries. For the same reason, it is good practice to connect the external "handle" tube to a point around 5 cm away from the sealed ends of the capillaries, as shown in Fig. 3.33, so that the joint is far enough from the bundle.
The stacking operation is actually performed manually, and so the geometric precision of the preform structure, as well as the contamination level within the preform, varies depending on the technical skills of the fabricator. In particular, an exact reproduction of a given preform structure is hard to achieve.
It's useful to point out that the stacking technique could be automated in the future in almost the same way as imaging fibres are produced. For example, the "Autofib" system of the Anglo-Australian Observatory (AAO), used for multi-object spectroscopy, basically consists of a bundle of hundreds of optical fibres, in which each fibre has been exactly located by a fibre positioning robot (Parry and Gray [1986]).

3.10.2 Cleaning procedures

Cleaning procedures are of fundamental importance not only to obtain a low loss HF, but also to get a good holey structure. Indeed contamination within the HF preform

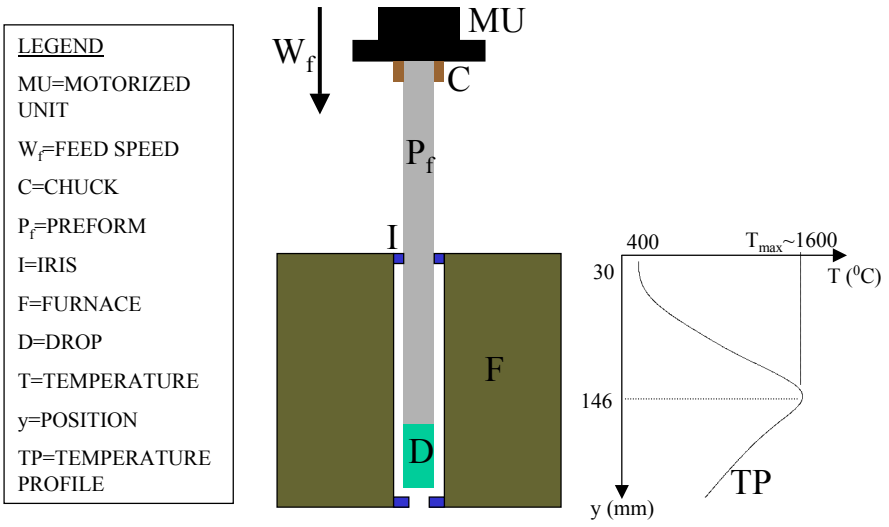

FIGURE 3.34: A "drop" is normally attached to the bottom end of the preform, prior to fibre drawing

may cause a complete failure in the HF fabrication, both during the cane drawing and the final HF drawing. Actually, a critical part of the cleaning is to avoid particles (water or gas) becoming trapped inside the capillary holes or the cane holes prior to drawing. If this happens, at elevated temperatures, these particles transform into a powder that can cause strong instabilities during the drawing.

Capillaries are cleaned first with acetone, which removes water and contaminants, and then with isopropanol, which removes acetone and then evaporates. Small diameter capillaries (e.g. 1 mm) are especially difficult to clean internally and also detergents are difficult to remove once applied. If they are not removed properly, this can result in the formation of a powder inside the holes, which causes great instabilities during the drawing and can lead to the holes blowing up. It is preferred to clean the capillaries only on their outer walls. However, even so, some contaminants, in gas form, can flow inside the holes. To avoid this, they could be sealed at both ends just after their drawing.

However, after finishing the cleaning of their outer walls, one sealed end of the capillaries must be chopped off. In this way water contamination, which results from assembly work on the HF preform at high temperature, can evaporate from the inner surfaces.

It is good practice to scan the capillaries multiple times (sealed on only one end) along a $H_2 - O_2$ flame, so that contaminants can evaporate out of the holes.

Cleaning of the HF cane follows the same rules as the capillaries. Moreover it is also efficient to leave the cane to dry in air for many hours or days, so that it naturally dehydrates.

3.10.3 Drop

The last technical consideration, in the fabrication of a HF, concerns the size of the drop that is attached to the preform, prior to drawing (see Fig. 3.34).

Normally, a large drop would be preferable in terms of time saving, because the starting

drawing temperature (i.e. the "drop temperature") can be lower. In this way the stabilization of the HF structure at low temperature can be reached faster. However, the use of a too long a drop would cause an excessive elongation of the HF preform and a large amount of wastage.
On the other hand, the use of too small a drop leads to a long stabilization process. The major disadvantage is though that it reduces the tension experienced at the bottom end of the preform. As I empirically observed, in this case the pressurized holes can expand without the control of an opposite force, and the HF preform blows up at its bottom end. Therefore the use of a correct amount of drop is of particular importance for successful fabrication of a HF. Usually, for a 20-25 mm OD preform, the drop is a low quality silica rod about 40 mm long with a diameter of 20 mm.

3.11 Conclusions

In this chapter I have described the fabrication of highly nonlinear holey optical fibers (HNL-HFs).
Firstly, I have given a background introduction to the subject. I have discussed how the first single material air-silica optical fibers were already made by Kaiser et al. in 1974 (Kaiser and Astle [1974]), and how the basic technique for the fabrication of the first holey optical fiber (Knight et al. [1996]) originated from the technology used for the manufacture of nanochannel glass (NCG) array (Tonucci et al. [1992]).
I have also outlined that our work is a direct development of the work of P. J. Bennett (Bennett et al. [1999]) regarding the manufacture of HFs with a very high nonlinearity.
After introductory sections, about the drawing tower used and the basic fabrication techniques for HF, I have described the main HF fabrication problems and described various technical solutions.
In the following sections I have described how I improved the fabrication of HNL-HFs.
I first investigated the relationship between the feed speed and the drawing speed on the manufacture of a HF. This work led to some practical values of the drawing parameters, to use during HF drawing.
Then I introduced a novel HF fabrication approach, involving the manufacture of an "air jacketed" HF (Belardi et al. [2002a]). This method allowed the fabrication of very short and fragile HFs with a small core size, and showed interesting applications.
The key to fabricate very highly nonlinear HFs was the introduction of HF preform pressurization, by sealing the top of the preform prior to fibre drawing. I first applied this method to the fabrication of a pressurized "air jacketed" HF, but, afterwards, I introduced a full silica jacket for a HF and highlighted its advantages in terms of fibre strength compared to the use of a Vycor jacket. In this way I was able to produce very long and robust HNL-HFs.
Finally, in the last two sections, I have discussed some general issues.
The first issues concern my pressurization technique by means of sealing, which, in

particular, results in a pressure instability during the fibre drawing. This causes non-uniformity of the hole size along the fibre length.
Finally, the technical issues regarding the preform preparation are discussed, such as the stacking, the cleaning procedures and the correct amount of drop to attach to the preform, prior to drawing.

Chapter 4

High nonlinearity devices based on holey fibre technology

4.1 Introduction

In chapter 3 I explained how I could fabricate HFs with a very small core ($\sim 1.5\ \mu m$) and a very high air filling fraction AFF (~ 0.8). The successful development of a reliable HNL-HF fabrication method allowed me to investigate the properties of such fibres and use them for the demonstration of some of the first HF devices. By doing so, it was possible to better understand the actual problems in the implementation of HF technology in optical communication systems and address the group's research to practical solutions.

One of the first HNL-HFs I produced, based on an air-clad fabrication approach (see Fig. 3.20), was used for the demonstration of the first application of HF technology to optical switching. This fibre, because of the air jacket, was quite fragile and, although a long length was produced, only few meters of it could be used in actual experiments. Due to the very small effective area of this fibre (about 2.8 μm^2), even a short length (about 3 m) was enough for the implementation of the first 2R regenerator based on HF technology. In Sect. 4.2 I discuss this experiment, which, to our knowledge, constitutes the first demonstration of the practical application of HFs to optical communication systems. I acknowledge the main contribution of Dr Periklis Petropoulos to this work (Petropoulos et al. [2001a]).

After this first experiment, I tried to overcome some of the practical difficulties in the use of HFs, by developing the ability to fabricate HFs with a solid silica jacket (Sect. 3.8). This jacket provides strength to the fibre and hundred meters of fibre could not only be produced but actually be used in practical applications. Values of core size (about 1.5 μm) and air filling fraction (about 0.8) were chosen to get a HF with anomalous dispersion at 1 μm (see Fig. 2.7). Due to this completely novel dispersion behaviour we could demonstrate, in collaboration with Mr Jonathan Price (Price et al. [2001a]), nonlinear pulse compression and soliton formation at the unprecedented wavelength of

1 μm. I discuss this work in Sect. 4.3.
Although as robust as a CF, the newly fabricated solid jacket HF with only two rings of air holes (see Fig. 3.23) was very lossy (about 1000 dB/km). The actual investigation of certain nonlinear devices, for example a Raman amplifier, cannot readily be made with such a loss level. The origin of these large losses was found to be mainly attributable to confinement losses (White et al. [2001], Finazzi et al. [2002]). Thus my fabrication efforts were directed to increasing the number of air hole rings of our HF, keeping the same core diameter and AFF, to reduce the level of confinement losses in our HFs. I show in Sect. 4.4 that Finazzi et al. [2003b] predicted that, with a core size of 1.5 μm and an AFF of 0.8, the confinement losses should be reduced to a level below 0.2 dB/km (typical losses of CFs) by adopting 4 rings of holes. Thus I fabricated a silica jacketed HF with 4 air hole rings and I could achieve losses in this fibre of 40 dB/km and mainly limited to absorption losses (Li [1985]).
Two different fibres were produced from the same preform, the first with a core diameter of about 1.5 μm and the second with a core diameter of about 2 μm. In particular, this second fibre had a quite evident asymmetry of the core and thus I discuss, in Sect. 4.5, the beat length measurement on this fibre ($L_B = 0.44\, mm$), which outlines the extremely high birefringence that it is possible to achieve by means of HF technology. Precise designs to obtain such a high birefringence have also been proposed by Ortigosa-Blanch et al. [2000].
The produced fibres were now suitable for actual applications to nonlinear HF devices using several tens of meters fibre lengths. The first such device we investigated was a Raman amplifier. Due to the increasing importance of Raman amplification in optical communication systems (Namiki and Emori [2001]), we thought of exploring the feasibility and possible advantages of applying HF technology to Raman amplification (Yusoff et al. [2003]). In Sect. 4.6, we demonstrate a HF Raman device (Yusoff et al. [2002a]) based on only 75 m of a HF with a nonlinearity γ of 32 $W^{-1}km^{-1}$, obtaining internal gains of over 42 dB and a noise figure of $\sim$ 6 dB. Moreover we achieved an extinction ratio of 11 dB in a Raman induced all-optical modulation experiment. The results highlight how, due to the high nonlinearity feature of our small core HFs, the critical power to reach the Raman threshold (eq. 2.35) could be reduced in a HF and a much shorter fibre length could be used. This is very useful for the reduction of the deleterious impact of double Rayleigh scattering on Raman amplifier noise (Nissov et al. [1999]). I would like to acknowledge the fundamental contributions to this work of Dr Ju Han Lee and Mr Zulfadzli Yusoff.
Finally in Sect. 4.7, we use the same HF to investigate the Brillouin effect in a HF (Tanaka and Hotate [1997]). In particular we implement the first HF Brillouin laser containing 73.5 m of a HNL-HF and obtain a threshold of 125 mW and a slope efficiency of $\sim$ 70%. Moreover we show that the high lasing threshold is mainly due to reduction of the effective gain coefficient by structural non-uniformity along the fibre length (Lee et al. [2002a]). I wish to acknowledge the particular contribution to this

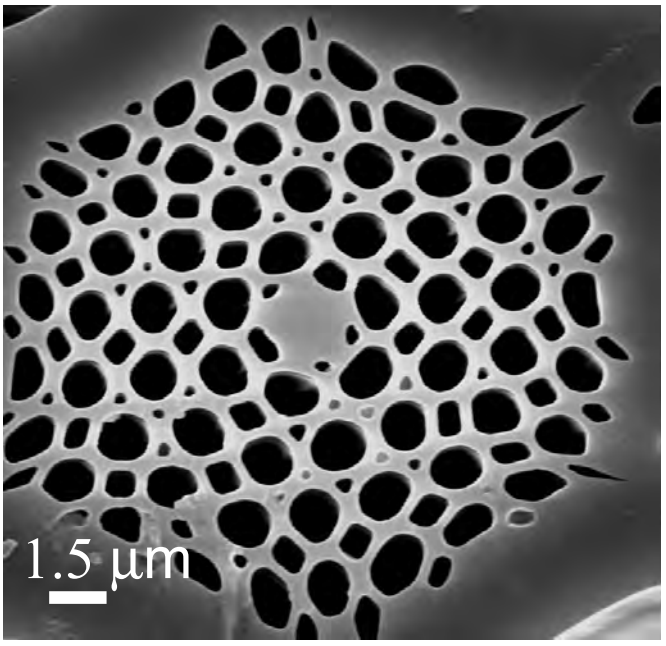

FIGURE 4.1: SEM of the HF used for a 2R regeneration experiment.

work of Dr Ju Han Lee and Mr Zulfadzli Yusoff.

4.2 A 2R data regenerator

As discussed in Sect. 3.6 and 3.7, the introduction of the air jacketed HF fabrication approach and of HF pressurization led to the successful production of HFs with a small core size and high AFF. We used one of these fibres for the first implementation of HF technology in a nonlinear device for optical switching (Petropoulos et al. [2001a]).
The fibre used in this experiment is shown in Fig. 4.1 , and has got a core size of $\sim 1.5\ \mu m$ and an air fill fraction of ~ 0.72. The measured beat length is only $1\ mm$ at $1550\ nm$ (polarization maintaining fibre) and its dispersion is highly anomalous at $1550\ nm$ (about $130\ ps/(km-nm)$). We also measured the nonlinear coefficient per unit length γ of the holey fibre using a pulsed, dual-frequency beat-signal nonlinear spectral enrichment technique (Boskovic et al. [1996]). Assuming the Kerr nonlinearity coefficient for silica to be $n_2 = 2.16 \times 10^{-20}\ m^2/W$ and considering negligible the fraction of optical power within the air holes (Broderick et al. [1999a]), we calculated the effective area of the fibre to be $A_{eff} = 2.8\ (\pm 0.5)\ \mu m^2$.
To demonstrate the practical advantages to be obtained through the use of holey fibers in fiber-based nonlinear devices we constructed a 2R regenerative optical switch from the fiber (Petropoulos et al. [2001b]). 2R regeneration requires both pulse reshaping and data bit amplitude restoration. The ideal pulse energy transfer characteristic of a regenerator is a binary function that provides zero transmission for pulses with a peak intensity below a certain threshold value while limiting the transmitted pulse energy for pulses with a peak intensity above the threshold value. Such a characteristic can be

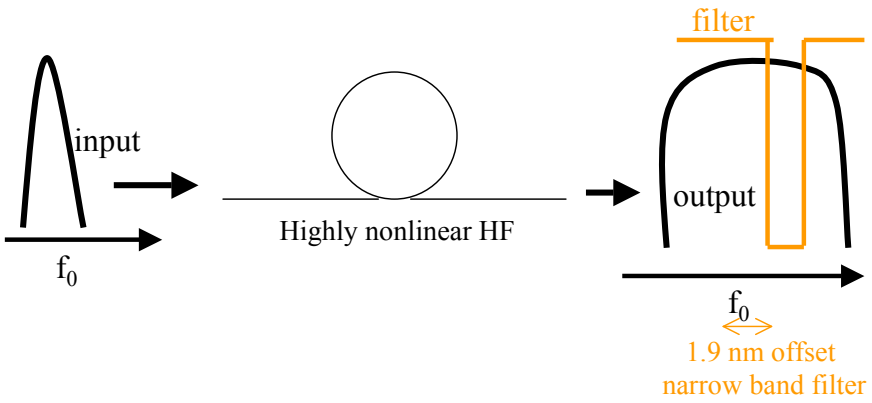

FIGURE 4.2: Sketch showing the broadening of an input pulse passing through a highly nonlinear optical fibre.

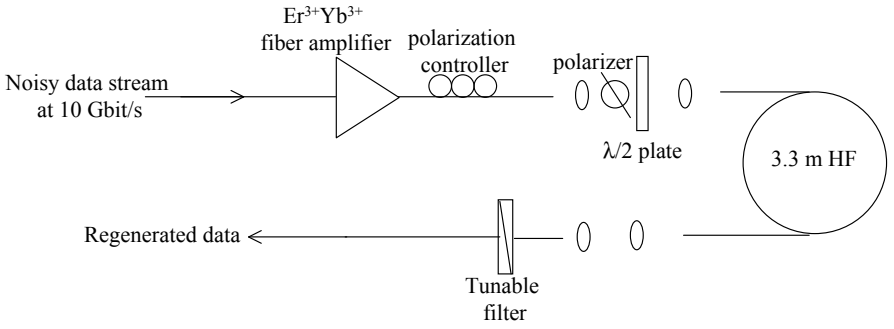

FIGURE 4.3: Experimental setup for the demonstration of a 2R regenerative switch.

obtained by use of a relatively simple scheme based on the nonlinear spectral broadening of pulses through self-phase modulation (SPM), followed by bandwidth-limited, offset spectral filtering (Mamyshev [1998]). Within this scheme the (noisy) data stream is first amplified and then fed through a nonlinear medium in which SPM takes place. The regenerated signal is obtained by filtering the spectrally broadened data signal with a narrow-band filter that has its central wavelength offset relative to the peak wavelength of the incident signal, as sketched in Fig. 4.2. Low-intensity input signal components do not generate significant SPM and are largely rejected by the filter. High intensity signal components, by contrast, generate significant SPM within the filter pass band, resulting in significant transmitted light. It can be shown that, in an appropriately designed system, the intensity of the output pulses becomes independent of the intensity of the input pulses once it is above a certain threshold value (Mamyshev [1998]). Moreover, the spectral shape of the filter defines the shape of the filtered pulses, thereby providing the required pulse-reshaping function.

Previous demonstrations of such a switch used kilometer lengths of dispersion-shifted fiber as the nonlinear medium. In our experiments we used just 3.3 m of HNL-HF to generate the necessary SPM effects. Our experimental set-up is shown in Fig. 4.3. Soliton pulses of 2-ps duration and a repetition rate of 500 MHz were amplified with an erbium ytterbium-doped fiber amplifier. The saturated average output power of the amplifier

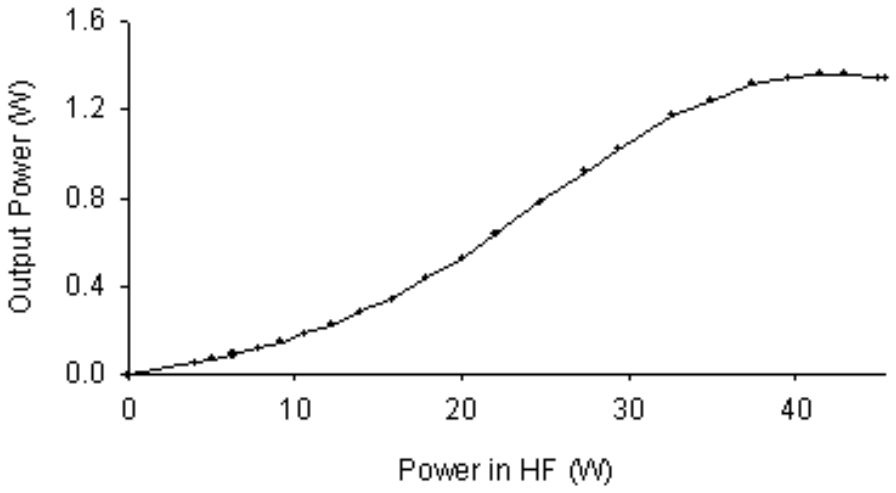

FIGURE 4.4: Transfer function of the switch.

was 70 mW. A combination of a polarization controller, a polarizer, and a half-wave plate was used to ensure that light was coupled onto one of the principal polarization axes of the HF. An angle-tuned dielectric filter with a 3 dB bandwidth of 1.3 nm was used to extract the switched regenerated optical pulses. This choice of transmission bandwidth ensured that the reshaped output pulses were of roughly the same duration as the input pulses. The power transfer characteristic of the device is shown in Fig. 4.4. The figure shows how the peak power of the output (filtered) pulses varies with the peak power of the input signal. The gradient of the transfer characteristic clearly decreases for both low-intensity and high-intensity pulses as required for beneficial regenerative effects to be derived. One can achieve a better approximation of the idealized binary response by cascading a number of such devices; moreover, the inherent wavelength shift associated with this operating principle can also be eliminated in this fashion. The peak power $\times$ length product of the device at the optimum operating point is about 0.13 $W \cdot km$, as opposed to a value of > 3.6 $W \cdot km$ reported by Mamyshev [1998]. The measurement shown in Fig. 4.4 was taken for a filter with its peak transmission centered 1.93 nm away from the central wavelength of the original signal, which represented the optimal operating point. In Fig. 4.5 we show the spectra of the input pulses, of the spectrally broadened signal pulses just before filtering, and of the corresponding filtered output. The optimum wavelength offset for the filter represents a trade-off between minimizing the switching power and ensuring adequate suppression of the input spectrum of the pulses to be regenerated. An autocorrelation trace of the filtered pulses is shown inset of Fig. 4.5, which shows a full width half maximum (FWHM) of 2.65 ps. Given the 1.3 nm bandwidth of the filter, this duration corresponds to that expected for transform-limited Gaussian pulses.

To provide a more visual demonstration of the regenerative effects of the switch, we artificially created pulse amplitude noise by using a suitably gated lithium niobate modulator to create pairs of 10 Gbit/s pulses with slightly different amplitudes; the unequal pulse amplitudes served to simulate noisy one bits. At the same time we detuned the dc

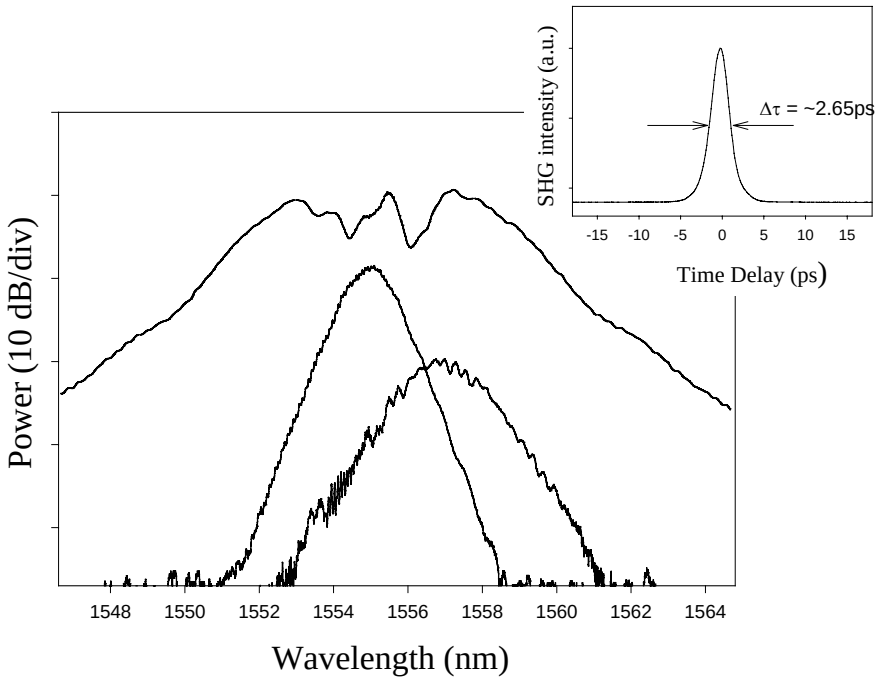

FIGURE 4.5: Measured optical spectra of the input signal(λ_{center} = 1554.0 nm), the signal at the output of the HF, and the output signal after spectral filtering (λ_{center} = 1555.9 nm). An autocorrelation trace of the regenerated pulses is shown in the inset. SHG, second-harmonic generation.

bias of the modulator to generate relatively low intensity pulses in bit slots adjacent to the relatively high amplitude pulse pairs. These low-intensity pulses were used to simulate noisy zero bits. The one bit pulse pairs were gated down to an effective repetition rate of 600 MHz to ensure that the peak powers of the amplified signal were adequate to operate the switch. In this way we were able to generate sequences of two one bits with an amplitude variation of about 10% and to reduce the extinction between the zero bit and the one bit levels by 10%. An example of the noisy data so generated before the switch is shown in Fig. 4.6(a). An oscilloscope trace of the regenerated output is shown in Fig. 4.6(b). The trace clearly shows that the noisy zero bit pulses that precede the one bits have been extinguished and that the amplitude of noisy one bits has been equalized. Note that the pulse structure shown after the one bits in Fig. 4.6 is due to ringing of the detector.

4.3 Demonstration of anomalous dispersion at 1 μm

The HF used in the demonstration of the HF based 2R regenerator was too fragile to be easily handled and this made difficult its employment for longer highly nonlinear devices. Thus we thought to adopt a silica jacket to improve the robustness of the HF (Sect. 3.8). Moreover we were seeking applications in the anomalous GVD regime at wavelengths less than 1.3 μm. Following an earlier design of Knight et al. [2000] (see Sect. 2.5.1 and Fig. 2.7) I fabricated the HF shown in Fig. 3.23. It is a silica jacketed

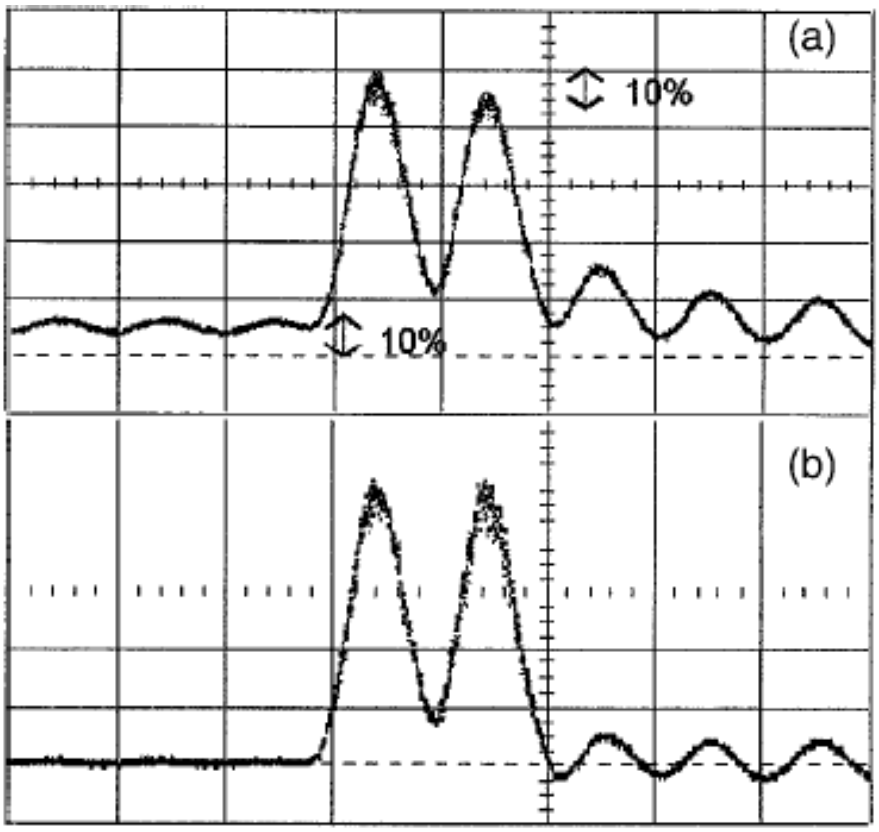

FIGURE 4.6: (a) Experimental simulation of 10 Gbit/s noisy packets of data. (b) The same data after nonlinear switching in the HF.

HF with two rings of air holes, a core dimension of 1.5 μm and a measured beat length of 1.15 mm at 1.06 μm.
In order to demonstrate the novel nonlinear and dispersive properties of this fibre, we used the experimental setup sketched in Fig. 4.7 to measure its dispersion and to achieve, for the first time, pulse compression and soliton formation at 1 μm. We used positively chirped pulses with a duration of 2.4 ps, an energy of about 60 pJ and a repetition rate of 54 MHz (about 3 mW average power) from a mode-locked laser and launched these into a short length of the HF. We achieved approximately 30% coupling efficiency into the HF, giving a maximum transmitted pulse energy of about 20 pJ. Using this experimental set-up, we could perform experiments in both the linear and the nonlinear compression regime (Price et al. [2001a],Price et al. [2002]).

In the linear regime, we attenuated the input pulses by inserting a neutral density filter before the HF. In this way the energy of the pulses travelling inside the fibre was attenuated from 20 pJ to only 1 pJ (and the pulse peak power of the compressed pulse was 6 W). With such low intensities self phase modulation (SPM) doesn't take place inside the fibre. Therefore the anomalous dispersion of the fibre compensates the positive chirp of the input pulses, leading to linear pulse compression (see Sect. 2.5.1.1, Ghatak and Thyagarajan [1998]). The 2.4 ps input pulses were compressed down to 170 fs using

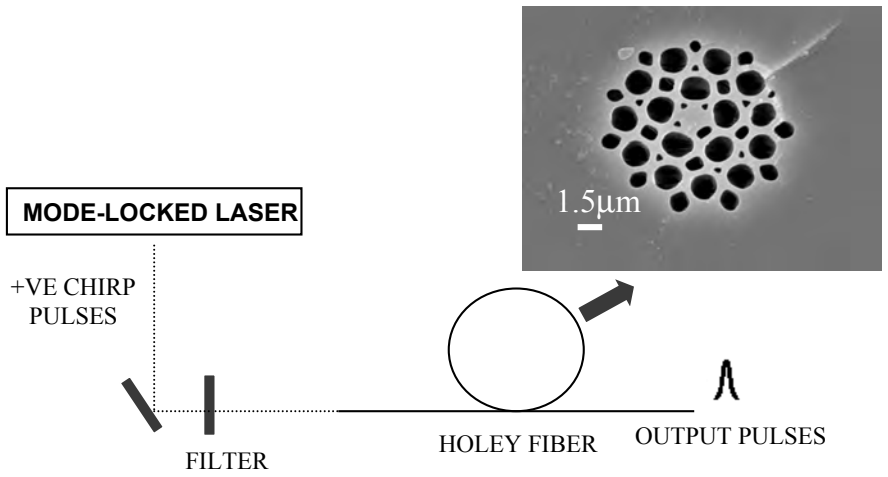

FIGURE 4.7: Sketch of the experimental setup used for the demonstration of anomalous dispersion at 1 μm.

just 1.1 m of holey fibre, as shown in Fig. 4.8 (a). The spectrum of the output pulse is not broadened (see Fig. 4.8(b)) and confirms linear propagation. We tested linear pulse compression in fibres with lengths up to 2.6 metres and from these measurements (see Fig. 4.8(c)), we estimated the dispersion of the fibre to be 150 $ps/nm - km$ (Agrawal [2001b]).

We then moved on to explore the nonlinear regime. We removed the neutral density filter form our set-up so that the launched input pulses had a pulse energy of 20 pJ (average power $\sim 1mW$, peak power $\sim 130\ W$). In this case the input intensity is high enough to generate SPM. Therefore the effect of SPM and anomalous dispersion are combined and balance each other, leading to soliton formation (see Sect. 2.5.1.2, Agrawal [2001b]). The spectrum in Fig. 4.9(a) shows the output pulse in the temporal domain after 2 m of HF, which demonstrates that soliton formation is achieved. Fig. 4.9(b) confirms the nonlinear propagation. Measuring the pulse width with different lengths of the fibre, we were able to obtain the plot of Fig. 4.9(c), which clearly shows soliton propagation without temporal broadening over 2.6 metres of holey fibre, which we calculated to be 20 soliton periods. Moreover, in this case, the shortest compressed pulse had a duration of 60 fs.

4.4 Confinement losses in holey optical fibres

The measured losses in our HF used for the demonstration of pulse compression and soliton formation at 1 μm (inset of Fig. 4.7) were as high as 1 dB/km. The origin of these high losses has been theoretically investigated by Finazzi et al. [2002].

A single material structure, which guides light by means of total internal reflection, with a finite inner cladding, is not truly a perfectly guiding medium. Indeed the outer cladding of a single material optical fibre, such as a HF, has got the same refractive index as the core material. Thus an electromagnetic wave, which is not well confined

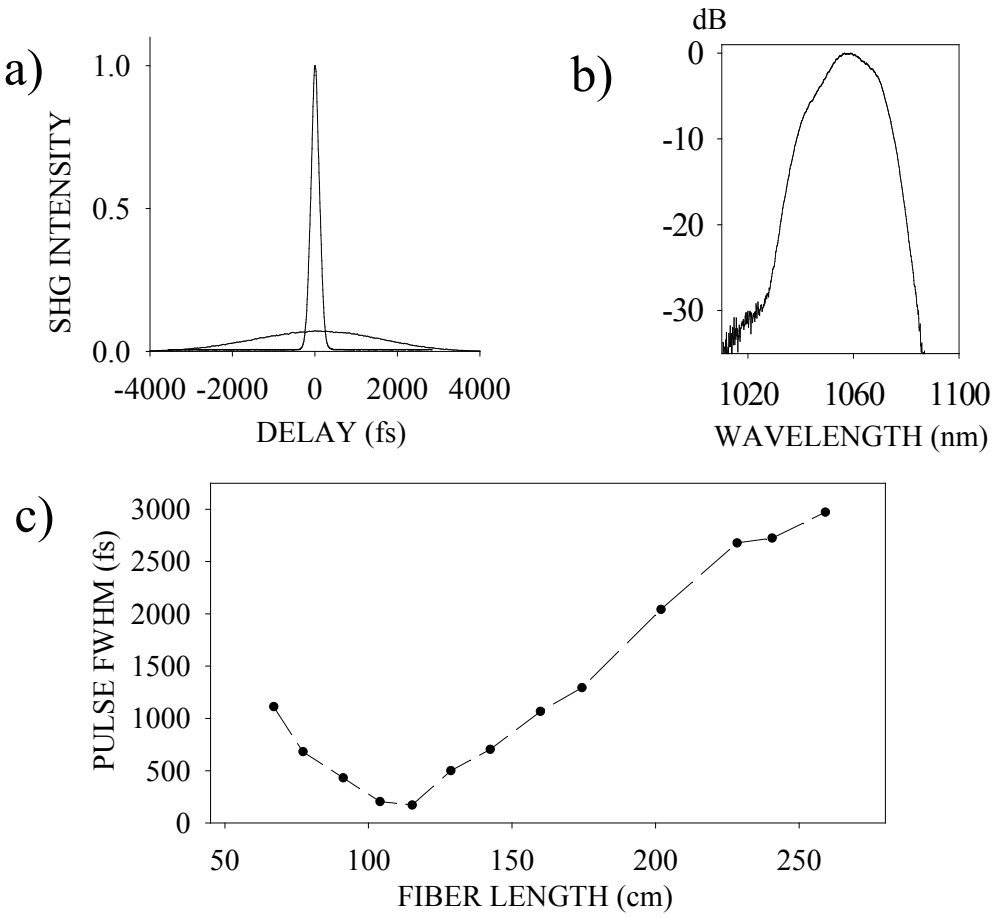

FIGURE 4.8: Experimental results in the linear regime. (a)Second harmonic autocorrelation traces of input and output pulse after 1.1 m of HF. (b)Output pulse spectra. (c)Pulse width versus fibre length.

within the core and inner cladding of the fibre, can leak out of the fibre through the outer cladding. This effect is referred to as "frustrated total internal reflection" and can cause high losses of optical power (Ghatak and Thyagarajan [1998]).
Confinement losses have been studied in HFs (White et al. [2001]) and a precise computational model to develop HNL-HFs with low confinement losses has been implemented by Finazzi et al. [2003b]. A theoretical result of this model is shown in Fig. 4.10. Considering a $d/\Lambda = 0.9$ and a core size between 0.8 and 1.8 μm, this figure shows, on the right side, that confinement losses of HNL-HFs can be highly improved by adding few air hole rings to the HF structure. The HF with two rings we had produced (Sect. 4.3), with a hole pitch of 1.5 μm (and a high AFF), had losses of about 1000 dB/km. However it appears from the plot that these losses are mainly due to confinement losses, which may be reduced below 0.2 dB/km by fabricating a HF with 4 hole rings. On the left side of Fig. 4.10, it is also shown that, for a HF structure with 4 rings of holes, the level of confinement losses depends also on the air filling fraction of the cladding (and thus on the HF numerical aperture). As we can see, within this structure, HF confinement losses go below 0.2 dB/km at 1550 nm, by adopting a d/Λ of 0.8 and a hole pitch greater

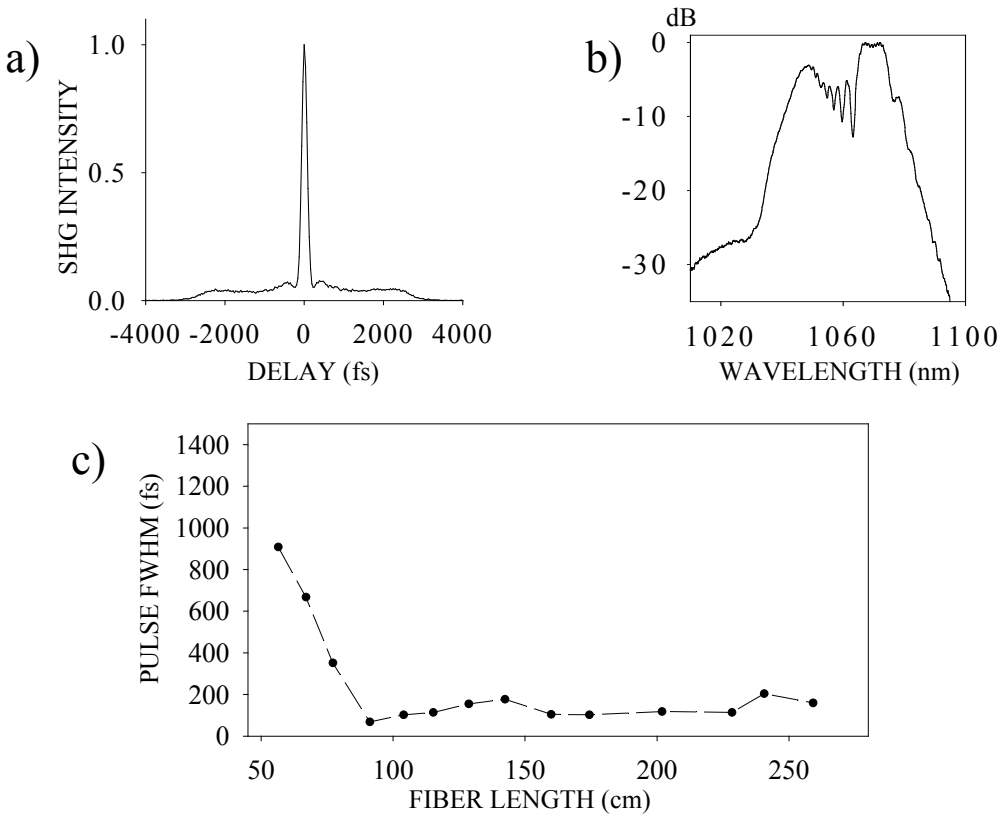

FIGURE 4.9: Experimental results in the nonlinear regime. (a)Second harmonic autocorrelation trace of the output pulse after 2m of HF. (b)Output pulse spectra. (c)Pulse width versus fibre length.

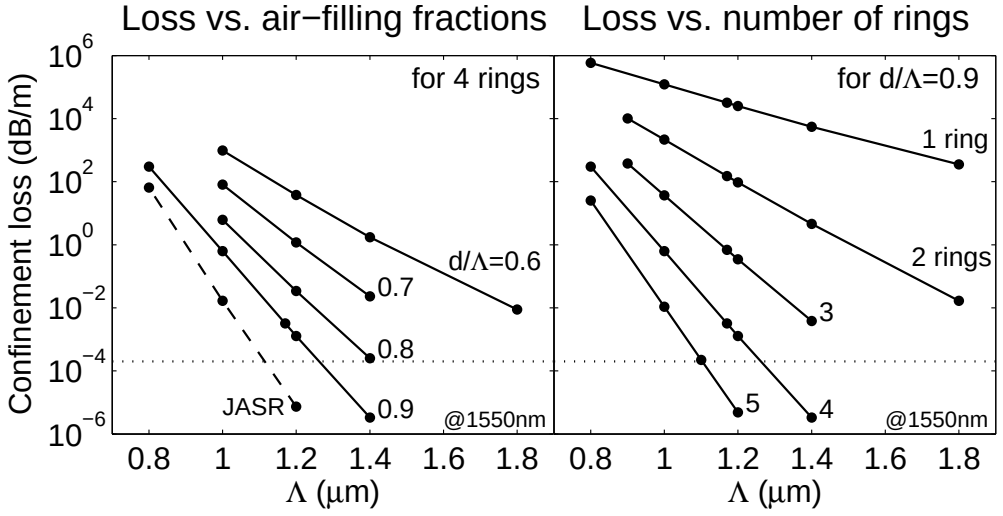

FIGURE 4.10: Confinement losses for different air-filling fraction (left) and different number of rings of holes (right) as a function of Λ. The dotted line represents the loss of conventional fibers (0.2 dB/km) (Finazzi et al. [2003b]).

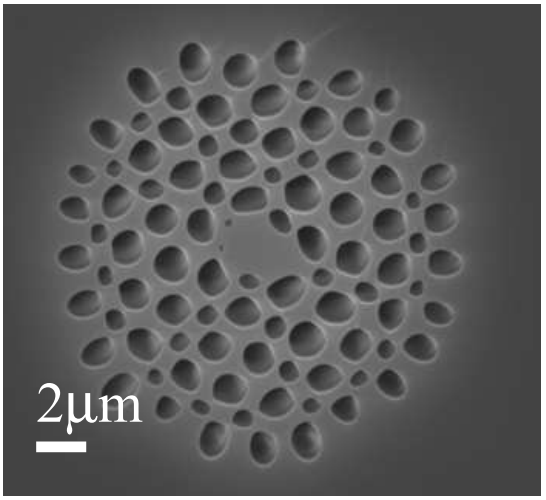

FIGURE 4.11: SEM of a HF with a beat length of only 0.44 mm.

than 1.4 μm.

We then thought of adopting a HF structure with 4 air hole rings, a hole pitch greater than 1.4 μm and a d/Λ of 0.8 to fabricate a HNL-HF with low confinement losses. The silica jacketed HF we produced had a $\Lambda \sim 2\mu m$, $AFF \sim 0.8$ and the structure shown in Fig. 4.11. The losses of this fibre (measured by means of a standard cut-back technique) were about 40 dB/km at 1550 nm limited we believe by material/scattering losses. Clearly, the contribution of confinement losses has been drastically reduced.

4.5 High birefringence

The fabricated HF with 4 rings of air holes (Fig. 4.11) had quite evident structural asymmetry and an elliptical core of about 2 μm. We can use this fibre to demonstrate that small core HFs can have a much higher birefringence than conventional fibres, because of the small core size, structural asymmetry and high NA. In this section, we describe the birefringence measurements of our elliptical core HF, whose beat length is found to be only 0.44 mm, more than 10 times less than conventional high birefringence optical fibres (Noda et al. [1986]). Note that precise designs for high birefringence HFs have been proposed by Ortigosa-Blanch et al. [2000] and that a structural asymmetry of HFs can be easily achieved during the fabrication stage by modifying the size of the holes surrounding the core.

We performed our beat length measurement using the experimental set-up shown in Fig. 4.12. We used a broadband source at 1550 nm and launched light into 1.1 m of the HF shown in Fig. 4.11. Between the source and the coupling lenses there was an optical polarizer, which ensured that the light polarization at the fibre input was aligned at about 45° to the main polarization axis of the fibre. After passing through a second polarizer, which acts as a polarization analyzer, the fibre output is measured through an optical spectrum analyzer (OSA). We obtained the graph shown in Fig. 4.13.

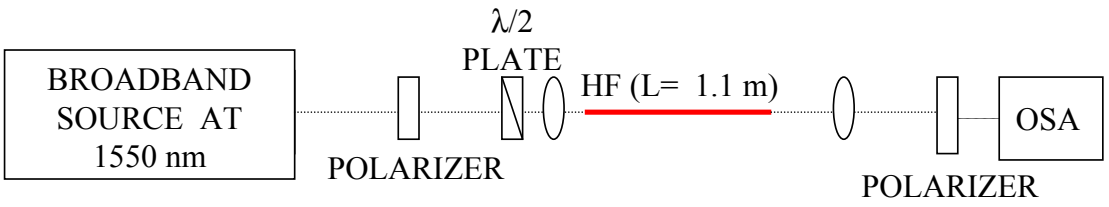

FIGURE 4.12: Experimental setup for the measurement of fibre birefringence

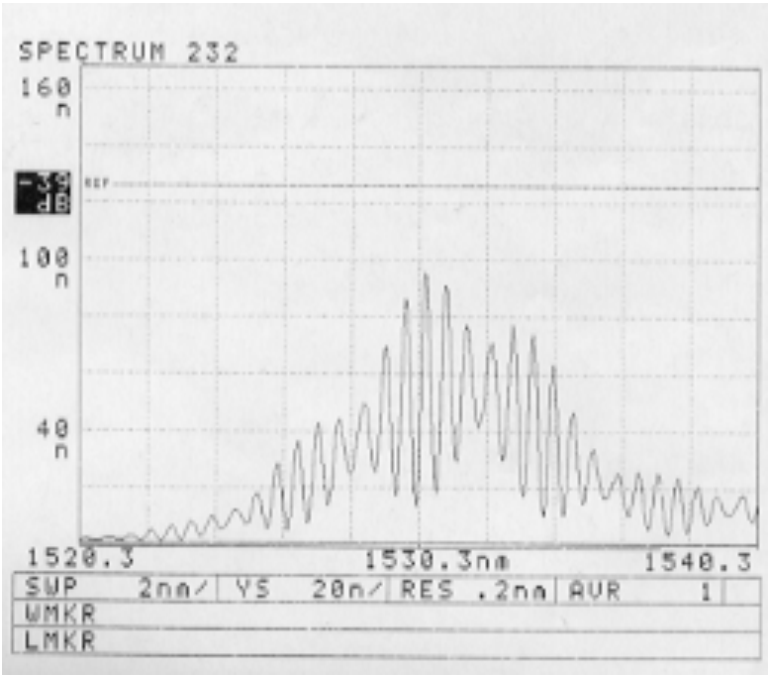

FIGURE 4.13: HF output spectrum.

We are now going to show that the beat length L_b of a fibre is given by the following relation:

$$L_b = L\frac{\Delta\lambda}{\lambda_0} \tag{4.1}$$

where L is the fibre length under test, $\Delta\lambda$ is the wavelength separation between two adjacent peaks in the optical spectrum in Fig. 4.13, and λ_0 is the wavelength of the first peak considered. We first assume that the fibre length L is equal to n times L_b:

$$L = nL_b \tag{4.2}$$

Then we compare the phase change at the wavelengths of two adjacent peaks, which are:

$$2\pi n = \delta\beta L_b = \delta n L_b \frac{2\pi}{\lambda_0} \tag{4.3}$$

$$2\pi(n-1) = \delta n L_b \frac{2\pi}{\lambda_0 + \Delta\lambda} \tag{4.4}$$

Where $\delta\beta = \beta_y - \beta_x$ with β_x and β_y being the mode propagation constants for the modes polarized in the x and y directions.
Dividing the two equations 4.3 and 4.4, we get:

$$\frac{n}{n-1} = \frac{\lambda_0 + \Delta\lambda}{\lambda_0} \tag{4.5}$$

which means that :

$$\lambda_0 = \Delta\lambda(n-1) \tag{4.6}$$

Now we can assume that :

$$n - 1 \simeq n \tag{4.7}$$

because n is very high (the beat length is usually very short compared to the fibre length under test L, as from equation 4.2).Therefore it is :

$$\lambda_0 = n\Delta\lambda \tag{4.8}$$

and using equation 4.2 we finally obtain that:

$$L = nL_b = \frac{\lambda_0}{\Delta\lambda}L_b \tag{4.9}$$

From the equation above and the graph in Fig. 4.13, we calculate a beat length of 0.442 mm, for $\Delta\lambda = 0.62\ nm$ and $\lambda = 1530\ nm$ (L_b is supposed not to be appreciably different at 1550 nm). Since the modal birefringence is given by (Agrawal [2001b]):

$$B_m = \frac{\mid \beta_x - \beta_y \mid}{k_0} = \mid n_x - n_y \mid = \frac{\lambda_0}{L_b} \tag{4.10}$$

we obtain the result that the birefringence of this fibre is about $3.5 \cdot 10^{-3}$ at about 1550 nm, which is almost 10 times higher than in standard polarization maintaining fibres (Noda et al. [1986]).
We also performed a measurement of the polarization extinction ratio PE_r, which measures how well the polarization can be maintained on the main polarization axis of a fibre. It is given by:

$$PE_r = 10\log\frac{P_{MAX}}{P_{min}} \tag{4.11}$$

where P_{MAX} and P_{min} are the maximum and minimum power output obtained by rotating the output polarizer. We found an extinction ratio of 20 dB for this fibre.

4.6 A Raman amplifier and modulator

The adoption of four rings of air holes surrounding the central core of our HF resulted in a dramatic decrease of the HF losses. Thus we now had some robust and long silica jacketed HNL-HFs with acceptable losses to allow the demonstration of HNL-HF devices based on effects such as stimulated Raman scattering (SRS) and stimulated Brillouin

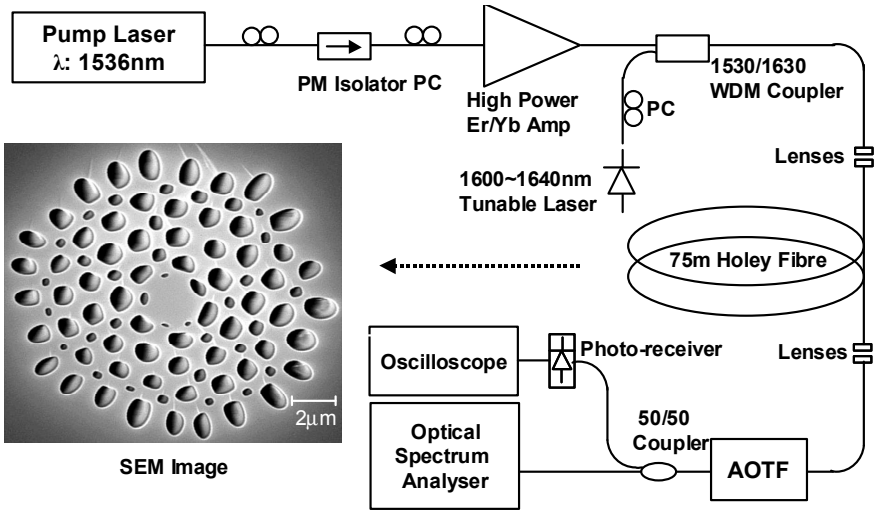

FIGURE 4.14: Experimental setup for the Raman amplification experiment.

scattering (SBS). We describe, in this section, the first demonstration of a HF Raman amplifier and, in Sect. 4.7, the first demonstration of a HF based Brillouin laser. In both these experiments we used the HF shown in Fig. 4.14 with 4 air hole rings, a core size of 1.5 μm, an AFF of about 0.8 and theoretical confinement losses just less than 0.2 dB/km.

The fibre diameter was ~ 100 μm, the measured effective area about 2.85 μm^2 and the losses about 40 dB/km.

Our experimental Raman amplifier set-up is shown in Fig. 4.14. A pump laser operating at 1536 nm generates 20 ns square pulses at 500 kHz repetition rate. Pump and signal are combined together in a wavelength division multiplexing (WDM) coupler before launching them in our 75 m long holey fibre. The signal light is a continuous wave signal generated from a laser tunable in the range 1600-1640 nm. The maximum peak pump power we could launch inside the HF was 6.7 W, while the maximum launched signal was of 0.1 mW. We placed an acousto-optic tunable filter (AOTF) at the output of the HF, whose high isolation (> 60 dB) allowed accurate gain measurements. The Raman gain measurements were made by analyzing the temporal response of the signal beam to the pulsed pump beam. A typical (high gain) spectral output is shown in Fig. 4.15(b).

By fixing pump/signal powers, we could obtain various internal Raman gains and noise figure for various probe signal wavelengths. As shown in Fig. 4.15(a) we could obtain higher gains and lower noise figure as we approached the peak of the Raman shift around 1650 nm, corresponding to the peak of the Raman shift of 13.2 THz.

We also measured the internal gain as a function of pump peak power for a signal wavelength of 1635 nm (see Fig. 4.15(c)), measuring a gain efficiency of 6 dB/W. Since the effective length of this fibre was only 54 m, and using equation 2.37, we calculated the gain coefficient g_R at the gain peak to have a value of 7.6×10^{-14} m/W, in good agreement with the number for pure silica (Agrawal [2001b]).

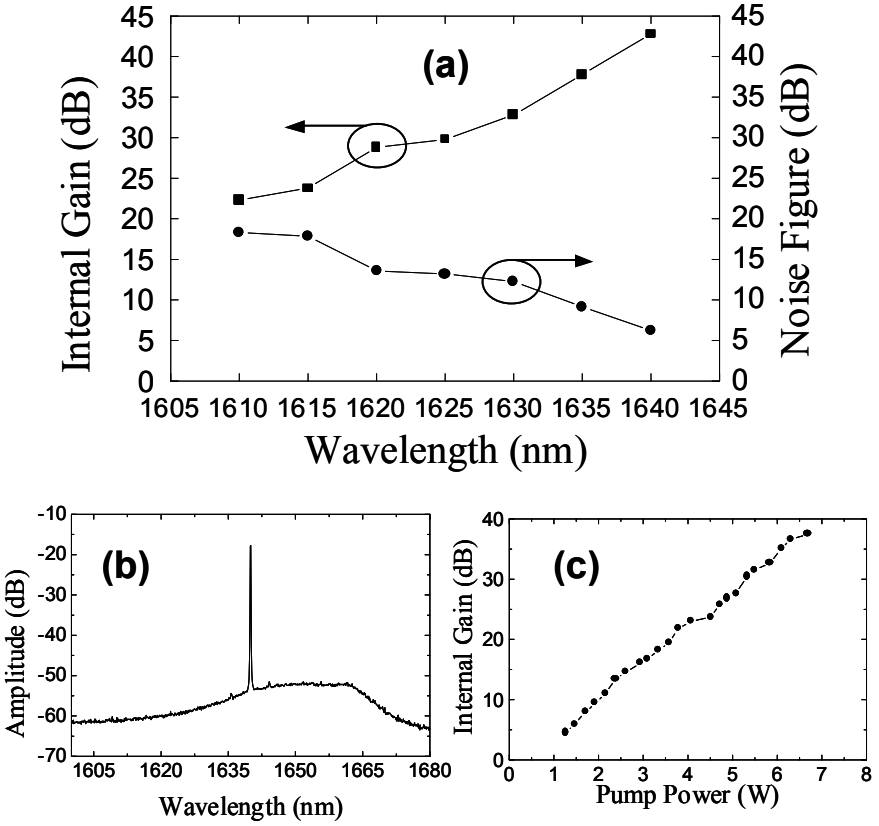

FIGURE 4.15: (a) Internal Raman gain and noise figure for various probe signal wavelengths (signal power: -10 dBm, pump peak power: 6.7 W). (b) Typical (high gain) amplifier spectrum showing Raman ASE spectrum. (c) Internal gain vs pump power at 1635 nm

By replacing our 1600 nm tunable signal source with a 100 mW, 1458 nm CW semiconductor diode laser, we inverted the previous situation because now the pump wavelength was greater than the signal wavelength. In this way, it is the signal beam that experiences stimulated Raman scattering and it is thus this that loses part of its energy. This results in an effective nonlinearly induced loss of the signal with the consequent formation of "dark" pulses in the time domain, as shown in Fig. 4.16(a,b).
We measured the modulator extinction ratio (which is the hole depth relative to the background CW level) as a function of pump peak power, as shown in Fig. 4.16(c). As we can see, we found an extinction ratio of 11 dB for peak powers of 5 W and above.

4.7 A Brillouin laser

The previous experiment on the implementation of a HF based Raman amplifier showed the clear advantage of using HF technology in terms of fibre length required. While conventional Raman amplifiers may require km fibre lengths (Nissov et al. [1999]), we only used 75 m of HNL-HF. In order to reinforce this point, we describe in this section the adoption of the same HF, used in Sect. 4.6, for the demonstration of a Brillouin based laser (Smith et al. [1991]). Moreover we exploit some of the particular features of

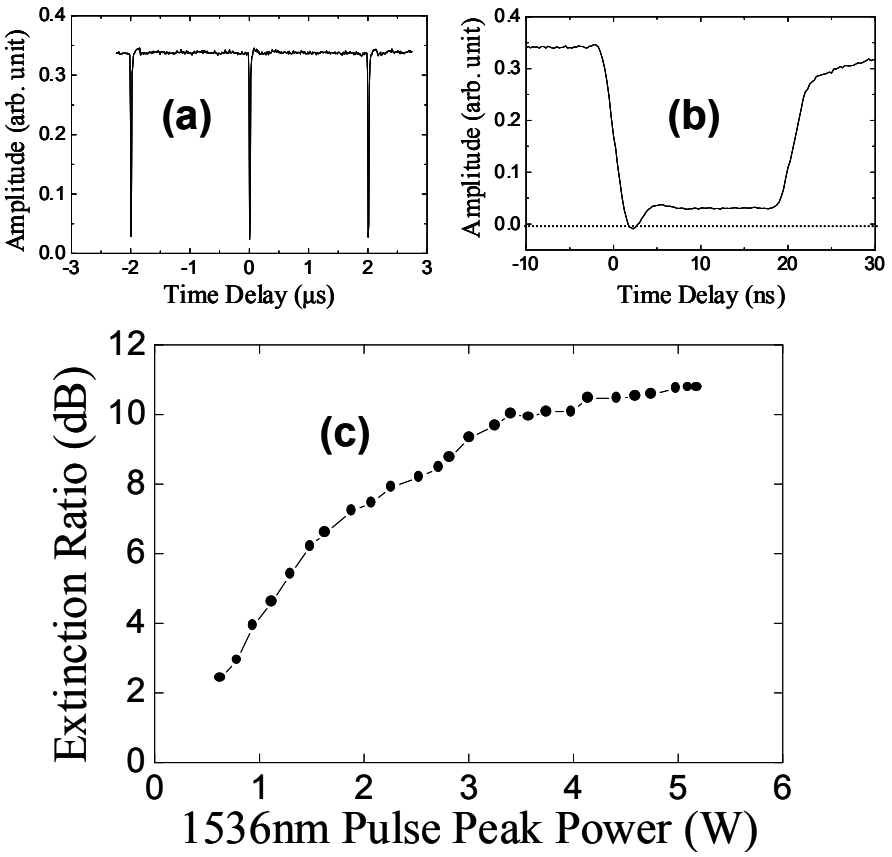

FIGURE 4.16: (a) Temporal profile of dark pulses at the SRS modulator output. (b) Close up view of the square-shaped dark pulse (the temporal dip at the falling edge is due to ringing of the photo-receiver). (c) Extinction ratio of SRS based signal modulation vs pump pulse peak power.

the Brillouin effect in a HF, which brings us to consider HF uniformity along its length (Shiraki et al. [1996]).

For the demonstration of the first Brillouin laser, we used a length of 73.5 m of the same fibre used in the previous experiment (Sect. 4.6), shown in the inset of Fig. 4.17. Our experimental set-up is shown in Fig. 4.17. The pump source is based on an erbium fiber DFB laser followed by an high power Er/Yb amplifier. The source has a line-width of $\sim$ 35 kHz, a center wavelength of 1552.1 nm and provides a maximum output power of $\sim$ 750 mW. The Fabry-Perot resonator incorporates a 73.5 m long HF ($L_{eff} = 53\ m$), a lens-coupled high reflectivity (HR) cavity mirror and a 96% output coupler defined by the Fresnel reflection from the cleaved fiber facet at the pump launch end of the cavity. Both polarization controllers and a polarization maintaining (PM) isolator were used in order that the pump beam could be lens-coupled onto one of the principal axes of the HF. A launch efficiency of 50% was measured. A 92:8 beam splitter was located at the pump launch end of the HF to monitor both the Brillouin laser output, and the incident pump power. A mechanical chopper was located in front of the HR mirror to facilitate alignment of the cavity.

In order to confirm the laser operation rather than stimulated scattering, we modu-

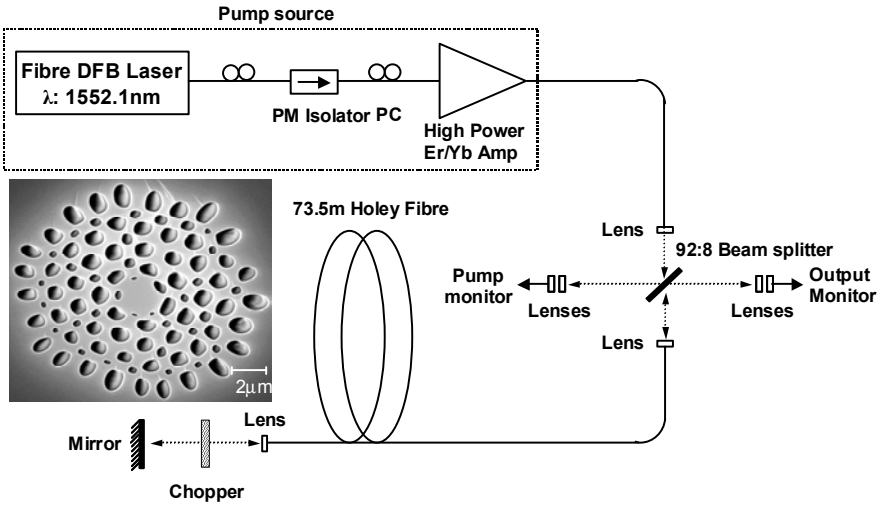

FIGURE 4.17: Experimental set-up used for the demonstration of a Brillouin laser. In the inset is shown the HF used in this experiment. PC=polarization controller.

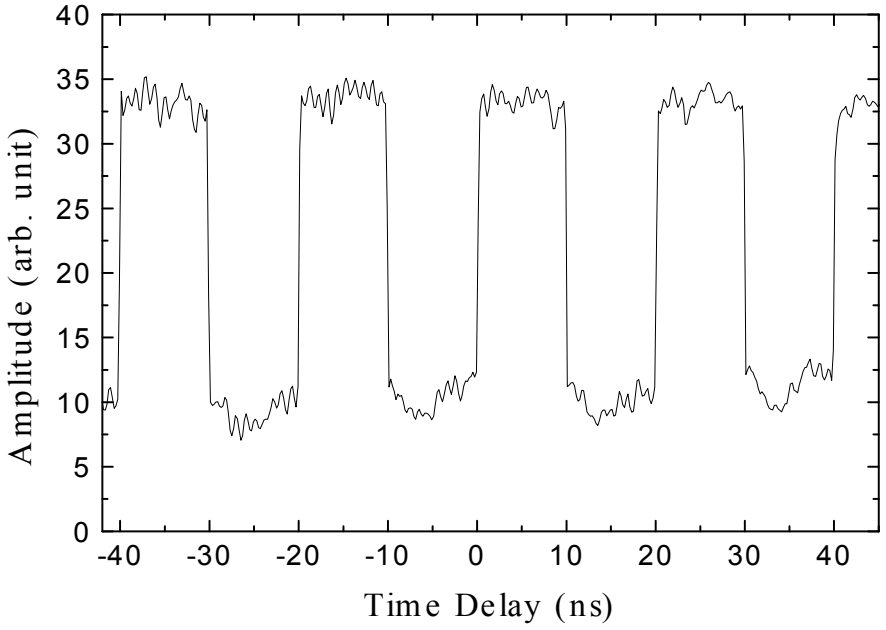

FIGURE 4.18: Modulated laser output obtained by using the free space chopper.

lated the cavity loss by using the free space chopper, and looked for the corresponding modulated laser output(see Fig.4.18). The RF spectrum of the beat signal between the laser output and the pump beam was measured using an RF spectrum analyzer, which showed that the frequency of the Brillouin laser output was downshifted by 10.6 GHz relative to the pump frequency, as shown in Fig. 4.19.

We measured the Brillouin laser output power as a function of the input pump power, as shown in Fig. 4.20. The laser threshold was found to be 125 mW, and the slope efficiency was $\sim 70\%$.

In the same Fig. 4.20, is also shown the SBS threshold within the HF. Feedback from the HR mirror was removed, and any possibility of Fresnel reflection was eliminated

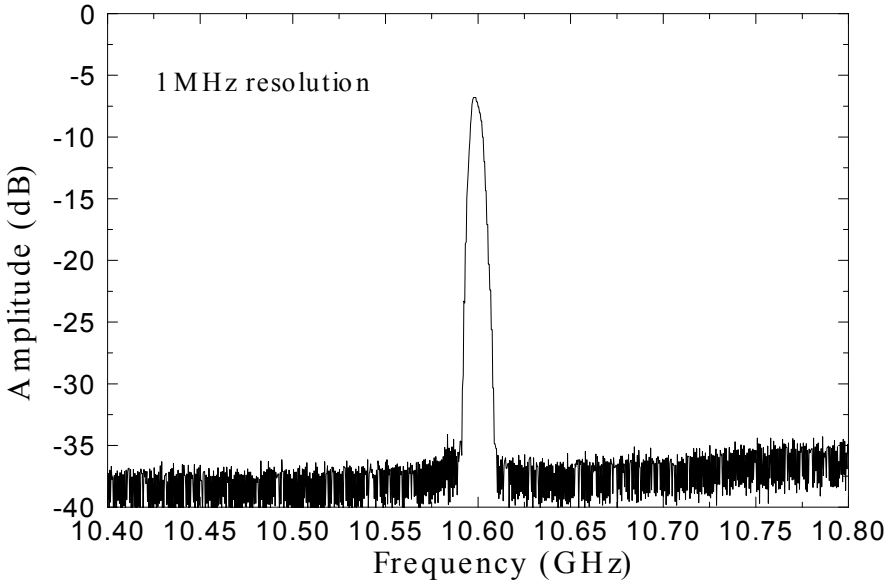

FIGURE 4.19: RF frequency trace of the beat signal between the Stokes and the pump beams.

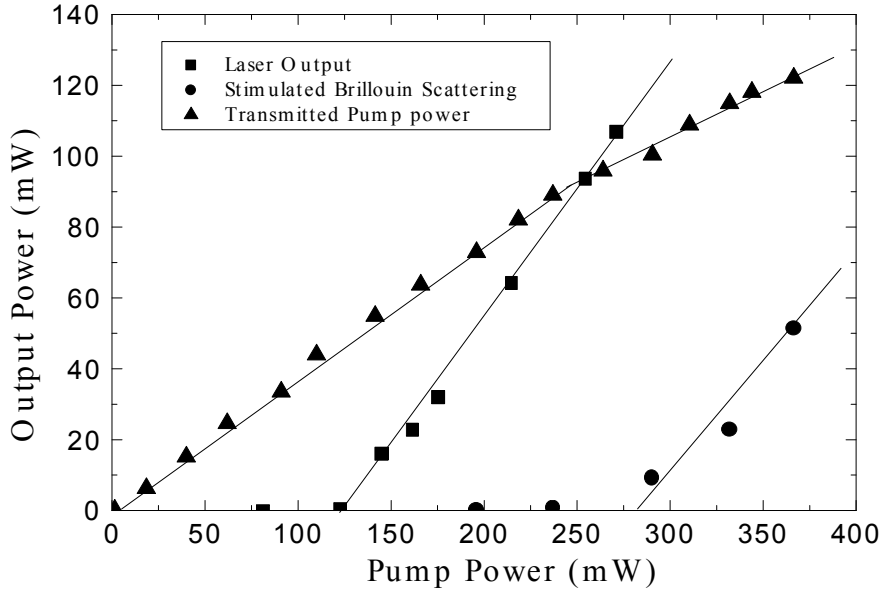

FIGURE 4.20: (a)Laser output.(b)Stimulated Brillouin scattering (backward).(c) Transmitted pump power as a function of launched pump power (stimulated scattering only).

by immersing the fibre in index matching liquid. We experimentally observed an SBS threshold of $\sim 280\ mW$.

Such a Brillouin threshold is substantially higher (by about an order of magnitude) than expected by a simple estimation based on the established Brillouin gain coefficient for pure silica, and the measured values of HF mode area and loss (Agrawal [2001b]). We thought that this was due to the structural variations along the HF length (Shiraki et al. [1996]), which was drawn without an active diameter control during the drawing process.

Theoretically if the pump laser line-width is negligible relative to the Brillouin gain bandwidth, the SBS threshold P_{th} can be approximated by the following equation, as suggested by Shiraki et al. [1996]:

$$P_{th} \simeq 21 \frac{K A_{eff}}{G(\nu_{max})} \tag{4.12}$$

The effective gain coefficient $G(\nu)$ is expressed as

$$G(\nu) = \int_0^L g_B(\nu, z) \exp(-\alpha z) dz \tag{4.13}$$

and K and A_{eff} are the polarization factor (K=1 for a polarization maintaining fiber) and the effective area of the fiber, respectively. ν_{max} represents the frequency at which $G(\nu)$ is maximized. $g_B(\nu, z)$ is the Brillouin gain spectrum whose Lorentzian profile is given by

$$g_B(\nu, z) = \frac{g_0}{1 + \left(\frac{\nu - \nu_B(z)}{\Delta\nu_B/2}\right)} \tag{4.14}$$

where ν_B is the Brillouin frequency shift at the location of z, $\Delta\nu_B$ is the intrinsic Brillouin gain bandwidth, and g_0 is the peak Brillouin gain coefficient.

Thus for a uniform fibre, the effective Brillouin gain coefficient, from Eq. 4.13, is

$$G(\nu_{max}) = g_0 L_{eff} \tag{4.15}$$

but, due to the irregular Brillouin shift distribution along the HF, $g_B(\nu, z) < g_0$, from Eq. 4.14. As a result $G(\nu) < G(\nu_{max})$ and, from Eq. 4.12, the Brillouin threshold increases.

We demonstrated this point by measuring the spontaneous Brillouin scattering line-shape for two different HF lengths (73.5 m and 40 m), using an heterodyne-detection technique that relies upon beating the spontaneously scattered light with the pump beam (Tkach et al. [1986]). We also compared these results to those of a standard DSF fibre. Our Brillouin gain band-width measurements are summarized in Fig. 4.21.

The bandwidth of the 73.5 m HF is about 7 times broader than the one for a DSF, in terms of 3-dB bandwidth.

The bandwidth of the 40 m HF ($L_{eff} = 33\ m$) is approximately half the value found in the 73.5 m length. We notice in addition a small increase in the Brillouin frequency shift,

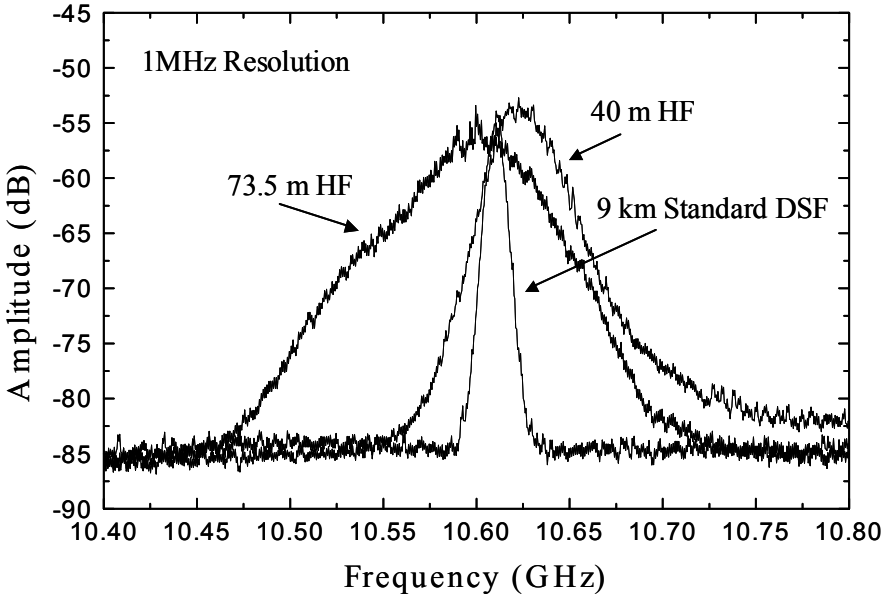

FIGURE 4.21: RF frequency trace of the beat signals between spontaneous Brillouin scattered beam and the pump for 73.5 m HF, 40 m HF, and a 9 km standard DSF fiber.

which represents a proof that structural variations along the length are responsible for the variations in the Brillouin frequency shift and corresponding line-width broadening, and consequently the increase in the SBS threshold. Moreover this 40 m HF had a SBS threshold of 290 mW, comparable to that of the 73.5 m HF.
Thus use of HF in the investigation of the Brillouin effect has some interesting and useful features, since pronounced structural variations along the fibre length may be useful for Brillouin suppression applications (Shiraki et al. [1996], see also Sect. 5.6).

4.8 Conclusions

Our desire to demonstrate various telecom devices based on HNL-HFs has directed our fabrication efforts towards the production of long, robust, HNL-HFs with low confinement losses. In this chapter I have reviewed some HNL applications of HFs and highlighted their novel properties and their advantages.
In Sect. 4.2 I have discussed the application of a 3.3 m long air clad HF to a 2R data regenerator, showing the improvements of using HFs in place of CFs, in terms of power-length product (0.13 $W \cdot km$ compared to 3.6 $W \cdot km$).
However the HF used in this experiment was too fragile to be used in longer lengths. I then improved our fabrication technique by adopting the use of a silica jacket (and pressurization), which allowed the production of HFs as robust as CFs. I produced a HF with two air hole rings in order to obtain anomalous dispersion at 1 μm wavelength. In Sect. 4.3, I have shown that this fibre could be used for the demonstration of pulse compression and soliton formation at 1 μm.
A multipole calculation method was adopted by Finazzi et al. [2002] to theoretically

investigate the origin of confinement losses in HFs. In Sect. 4.4, I have shown some of the results of this computational method. In particular, we have seen that the origin of high losses in our 2 air hole rings HF (about 1000 dB/km) was due mainly to confinement losses. It was also found that, by adopting a similar core size and AFF, and 4 air-hole rings, the theoretical confinement losses of less than 0.2 dB/km are achievable. Thus I fabricated some HFs by adopting this design and successfully achieved losses of 40 dB/km in these new structures with similar core size and AFF.

One of the silica jacketed HF produced with 4 air hole rings presented evident structural asymmetry. I have shown in Sect. 4.5 the beat length measurement of this HF ($L_B = 0.44$ mm at 1550 nm) and demonstrated how HF technology can be employed for the production of optical fibers with a birefringence one order of magnitude higher than conventional highly birefringent fibers (Noda et al. [1986]).

Taking advantage of the improved performances of our HFs in terms of robustness and confinement losses, we have demonstrated, in Sect. 4.3 the first HF Raman amplifier (Yusoff et al. [2002a]), using a 75 m HNL-HF with a core size of about 1.5 μm. We have obtained internal Raman gains of over 42 dB and a noise figure of about 6 dB. Moreover, using the same fibre, we have achieved an 11 dB extinction ratio in Raman induced all-optical modulation experiments. This experiment has highlighted the fundamental importance of HFs as a means to make short Raman amplifiers, which may overcome some of the fundamental limitations of Raman amplifiers based on conventional fibres, such as double Rayleigh scattering (Nissov et al. [1999]).

Finally we have shown, in Sect. 4.7 the first demonstration of a HF Brillouin laser (Lee et al. [2002a]), built by using a simple Fabry-Perot resonator scheme. It was based on 73.5 m of HF and we achieved a good laser power efficiency of 70% and a Brillouin shifted output power of 110 mW, at a wavelength of 1552.2 nm. In particular we investigated the stimulated Brillouin characteristics of the HF and established that structural variations along the particular HF used were responsible for broadening the Brillouin gain line-shape, and consequently for increasing the Brillouin power threshold.

Chapter 5

Wavelength conversion using highly nonlinear holey optical fibres

5.1 Introduction

In chapter 4 I have discussed some of the first applications of HF technology to practical highly nonlinear devices. In this chapter we focus our attention on a particular application of highly nonlinear fibres, namely "wavelength conversion", which is of fundamental interest in high speed WDM optical communication systems (Watanabe and Futami [2001], White et al. [2002a], Asghari et al. [1997]). I address some of the issues concerning the employment of a HF as a wavelength converter, describe ways to solve them and develop a specific fibre design for efficient wavelength conversion.
In Sect. 5.2, I discuss the application of an anomalous dispersion HF in a WDM wavelength conversion experiment based on XPM (Sakamoto et al. [2001], Sharping et al. [2002a]). We demonstrate, for the first time, a wavelength converter based on just 6 m of HNL-HF, proving the advantage of HF technology in terms of fibre length requirement, over conventional fibre technology (Yu and Jeppersen [2001], Ohlen et al. [2000]). Moreover, although wavelength conversion was achieved over a broad bandwidth of 20 nm, when we launched 10Gbit/s soliton control pulses in our HF wavelength converter, we obtained a 4 dB power penalty in the converted signals. The reason for this penalty we believed to be related to the high anomalous dispersion of our HF (Nakazawa et al. [1999]).
In order to overcome the power penalty associated with our first wavelength conversion experiment, we needed to design a HF with a normal dispersion at 1550 nm. Following the design of Birks et al. [1999] relating to high normal dispersion fibres (for dispersion compensation), I fabricated a HF with a core size of about 1 μm (with a high structural asymmetry) and an air filling fraction AFF of about 0.95. This fibre had a negative dispersion of about $-350\ ps/nm-km$. Thus, by using the same set-up as in

the previous experiment, we demonstrate, in Sect. 5.3, wavelength conversion through XPM in a normal dispersion HF. We successfully proved the benefits of using normal dispersion in this nonlinear device and achieved error-free, almost penalty-free (0.5 dB power penalty), wavelength conversion of 10 Gbit/s soliton control pulses.
Given the importance of high normal dispersion fibres in optical communications (Goyal et al. [2002], Gruner-Nielsen et al. [1999]), I consistently improved the manufacture of HFs by fabricating a negative dispersion HF with an almost regular structure, without interstitial holes and low confinement losses. Following the mathematical predictions of Finazzi et al. [2003c], I demonstrate, in Sect. 5.4, a long HF with the highest normal dispersion at 1550 nm ever reported in a HF (about $-453\ ps/nm-km$). Our experimental results have also been confirmed theoretically in a recent paper by Shen et al. [2003] and show the suitability of HFs for dispersion compensation.
Our HF wavelength converter based on XPM in a normally dispersive HF had a tuning wavelength range of 15 nm. I knew we could increase this range by adopting a HF with a lower normal dispersion. Indeed this would also have diminished the negative walk off effects (Agrawal [2001b]), due to the fibre dispersion. Indeed the use of a low dispersion HF is of fundamental importance for the implementation of a wavelength converter based on FWM (Okuno et al. [1999], Watanabe and Futami [2001]). Thus I aimed to fabricate a HF with a reduced amount of normal dispersion.
Finazzi et al. [2003c] predicted that a lower value of negative dispersion could have been achieved by slightly increasing the hole pitch in our previous fibre to about 1.2 μm. Moreover their theoretical results show that with such Λ and a very high AFF (close to 1) the effective area of a HF reaches the smallest possible theoretical value. It has also been shown that a HF with these geometric characteristics should have more than 4 air hole rings to decrease the confinement losses below 0.2 dB/km (Fig. 4.10). Thus, after several attempts, I fabricated a 6 rings HF with a core size of about 1.2 μm and an AFF of about 0.9, which had a negative dispersion at 1550 nm of about $-30\ ps/nm-km$ (significatively lower than in our previous HFs) and a record nonlinearity of 70 $W/km-nm$ (Belardi et al. [2002b]). This fibre has the highest nonlinearity ever reported for a silica based fibre and I describe its nonlinearity measurement in Sect. 5.5.
Finally, in Sect. 5.6, I use this fibre for the demonstration, for the first time, of a HF wavelength converter based on FWM (Belardi et al. [2002b]). Highly efficient, broadband wavelength conversion based on FWM in optical fibre requires high nonlinearity, small dispersion and a short fibre length to reduce the phase mismatch between the interacting waves (Inoue and Toba [1992], Aso et al. [2000], Sharping et al. [2001]). Thus our HF with a record nonlinearity, a reduced amount of normal dispersion, and low confinement losses (due to the 6 air hole rings) was the best candidate to exploit the advantages of HF technology in the realization of an efficient wavelength converter. I went on to achieve error-free wavelength conversion over $\sim 10\ nm$ bandwidth of a 10 Gb/s non-return-to-zero (NRZ) data rate. Due to the normal dispersion of our HF, modulation instability related amplitude noise, associated with the wavelength conver-

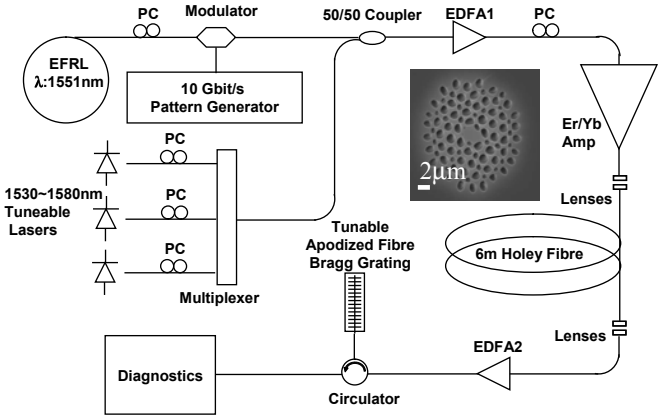

FIGURE 5.1: Experimental set-up for the WDM wavelength converter based on XPM. Inset: cross-sectional SEM image of the HF used in this experiment.

sion process, is successfully avoided (Grosz et al. [1999]).

Moreover the reduction of stimulated Brillouin scattering (SBS) effects is another key issue in a wavelength converter device and is required to suppress SBS-induced pump power loss (Hansryd et al. [2001]). In our experiment, we ensure a high SBS threshold of our HF, due to broadening of the Brillouin lineshape, through structural variation along the fiber length (Lee et al. [2002a]). The measured SBS threshold in the 15 m long HF, used in this experiment, is more than 130 mW, which is over three times higher than that of a uniform pure silica fiber. This characteristic of our HF is of fundamental importance for the performance of our wavelength converter, showing another advantage of our approach.

5.2 A WDM holey fibre wavelength converter based on XPM

In this section we describe the first application of a HF to achieve WDM wavelength conversion based on XPM and spectral filtering (Yu and Jeppersen [2001], Ohlen et al. [2000]).

The experimental set up is shown in Fig. 5.1. 2.5 ps pulses at a repetition rate of 10 GHz are first generated using a regeneratively mode-locked erbium fiber ring laser (EFRL) operating at a wavelength of 1551 nm. These pulses are then modulated to obtain a 10 Gb/s 2^{15} pseudorandom control pulse stream. We combined the control pulses and three probe beams together using a combination of 50/50 couplers prior to launching the light into the HF. The probe beams were generated from CW external cavity lasers tunable in the range 1530-1580 nm. Polarization controllers were included on both the control and probe launching paths into the HF so that all of the beams could be launched onto a single polarization axis of the polarization-maintaining HF. Both the control and probe signals were amplified using an Er-Yb amplifier with a maximum saturated output power of $\sim 800mW$, and were then lens coupled into a 6 m length of HF with a coupling

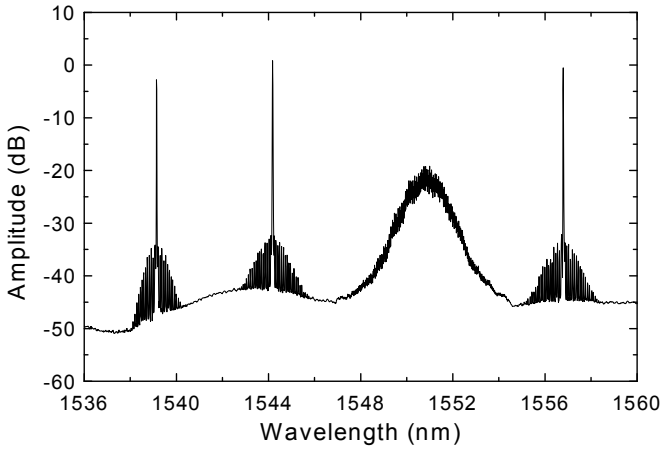

FIGURE 5.2: Measured optical spectrum of the three probe signals with control pulses after the HF.

efficiency of 40%.

A cross sectional SEM profile of the highly nonlinear HF used in this experiment is shown in the inset of Fig. 5.1. The core diameter is about 2 μm and the outer diameter is 125 μm. The measured dispersion at the wavelength of 1550 nm was $+100\ ps/nm{-}km$ and the measured loss was about 40 dB/km. From a measurement of the SPM induced nonlinear phase shift versus launched optical power (Boskovic et al. [1996]), we obtained an estimated value of $\gamma = 31\ W^{-1}{\cdot}km^{-1}$ for the nonlinearity coefficient and an estimated effective area of $A_{eff} = 2.93(\pm 0.3)\mu m^2$. This nonlinearity is $\sim$ 20 times higher than that of a conventional dispersion shifted fibre.

XPM between the control signal and the CW beams results in chirping of the CW laser beam where these beams overlap temporally within the fiber. This frequency chirping can then be converted to a frequency converted signal by passing this chirped signal through a narrow-band filter which serves to eliminate the residual unchirped CW signal as well as to select one of the two XPM-induced side bands (Ohlen et al. [2000]). The measured output spectrum from the HF is shown in Fig. 5.2. It is clearly evident that each probe beam is spectrally broadened due to XPM induced by the control signal. The control signal itself also shows a small amount of spectral broadening caused by SPM. (Note that XPM between three CWs and SPM of each CW could in principle be generated to some degree. However, the corresponding frequency chirping is small in practice compared to that due to XPM between the CW beams and pump due to the lower peak powers of the CW pumps).

In our experiment, we used an apodized FBG for the spectrum-slicing filter. The filter has a 3 dB bandwidth of 0.55 nm and a 30 dB bandwidth of 1.5 nm. The FBG was embedded in a layered flexible plate that, when bent, allowed for 20 nm wavelength tuning of the filter's central wavelength due to the resulting compressive strain applied to the FBG (Set et al. [2001]). The FBG provides both high precision and high efficiency spectral slicing as well as significant suppression of all residual CW components, pump beams, and adjacent wavelength channels, as shown in the spectrum of Fig. 5.3. Initially,

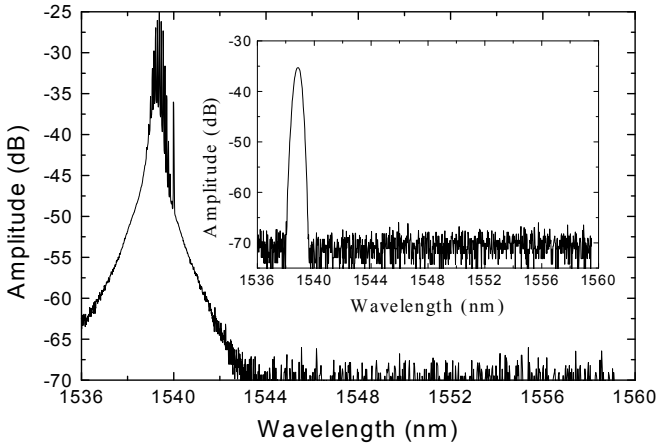

FIGURE 5.3: Measured optical output spectrum after HF and the grating filter; Inset: spectral response of the apodized fiber Bragg grating filter used (3 dB bandwidth of 0.55 nm, 30 dB bandwidth of 1.5 nm)

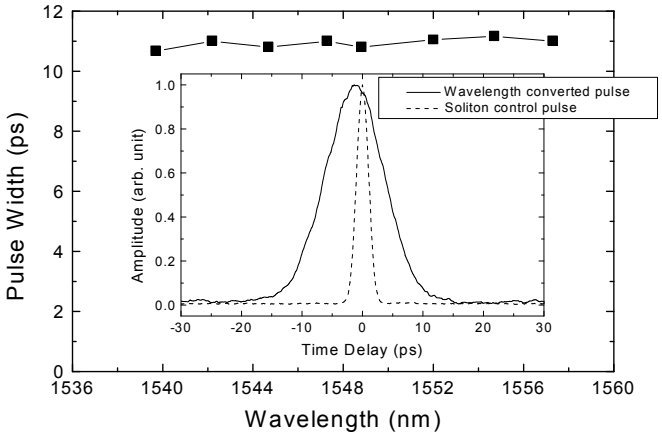

FIGURE 5.4: Measured full-width at half maximum of the wavelength converted pulses as a function of the probe beam wavelength for the case of wavelength conversion of a single channel. The inset shows the SHG autocorrelation traces of the wavelength converted pulses at 1540 nm, and the input pulses.

we characterized the performance of our wavelength converter in the temporal domain using a second harmonic generation (SHG) autocorrelator ($\leq$ 100 fs resolution). The measured temporal width of the wavelength-converted pulses as a function of probe-beam wavelength is plotted in Fig. 5.4. The pulse widths of the converted pulses were observed to be almost constant at $\sim$ 11 *ps* over the full $\sim$ 20 *nm* tuning wavelength range of our FBG. The walk-off between pump and signal was indeed quite significant and would have generated uneven output pulse widths over the 20 nm tuning range without bandwidth reduction. However, the use of a narrow bandpass filter (0.5 nm 3 dB bandwidth) restricted the output signal spectrum such that the temporal pulse shape was almost entirely determined by the filtered spectral bandwidth. The time-bandwidth product of the converted pulses was 0.5 which, although somewhat larger than that of the original control soliton pulses (0.32, transform-limited), still indicates high-quality pulses.

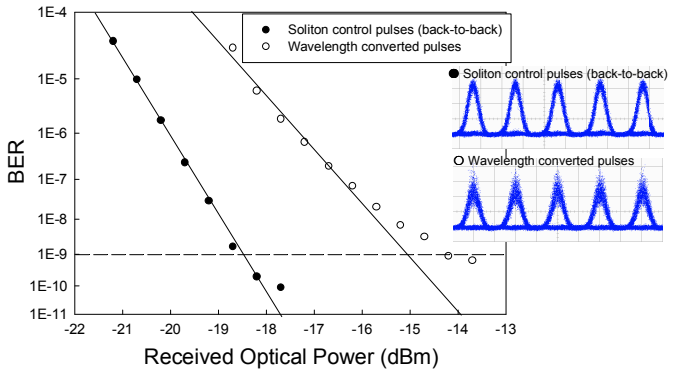

FIGURE 5.5: Measured BER versus received optical power for wavelength conversion of 10-Gb/s data pulses to a wavelength of 1540 nm.

However, a degree of amplitude noise was observed on the converted signals. Its origin was believed to be due to coherence degradation due to the anomalous dispersion of our HF (Nakazawa et al. [1999]). By incorporating in our set up a semiconductor optical amplifier (which can reduce intensity noise to a significant extent, Kim et al. [1999]), we could perform some BER measurements on one channel at a wavelength of 1540 nm. Fig. 5.5 shows both the measured BER and eye diagrams for the soliton control and wavelength-converted 10 Gb/s pulses. We observed an approximately 4 dB power penalty and an error floor at the 10^{-9} BER level relative to that of the soliton control pulses.

5.3 A wavelength converter based on XPM in a normal dispersion holey fibre

We believed that the 4 dB power penalty of our HF based XPM wavelength converter was due to a coherence degradation related to the anomalous dispersion of our fibre (Nakazawa et al. [1999]). In order to demonstrate this point, we decided to fabricate a HF with a normal dispersion, and use it in a similar WDM wavelength conversion experiment.

Already in 1999 Birks et al. [1999] theoretically predicted that HFs with a core size of about 1 μm and a very high AFF (close to 1) would have a normal dispersion at 1550 nm (and would be suitable for dispersion compensation). Thus I fabricated the HF shown in the inset of Fig. 5.6 by adopting a pressurization of the cane, to increase the AFF of the HF (see Sect. 3.9.1) and a Vycor jacket, which could allow an "expansion" of the fibre holes (see Sect. 3.8). The core is elliptical in shape (axis ratio ~ 1.5) with a minimum axis dimension of $\sim 1\mu m$. The outer diameter of the HF is 100 μm. The measured dispersion at the wavelength of 1550 nm was $\sim -350\ ps/nm-km$ and the measured loss was 300 dB/km. From a measurement of the SPM-induced non-linear phase shift versus launched optical power (Boskovic et al. [1996]), we obtained an estimated value of $\gamma \sim 60W^{-1}km^{-1}$ for the nonlinearity coefficient. This nonlinearity is $\sim$ 30 times

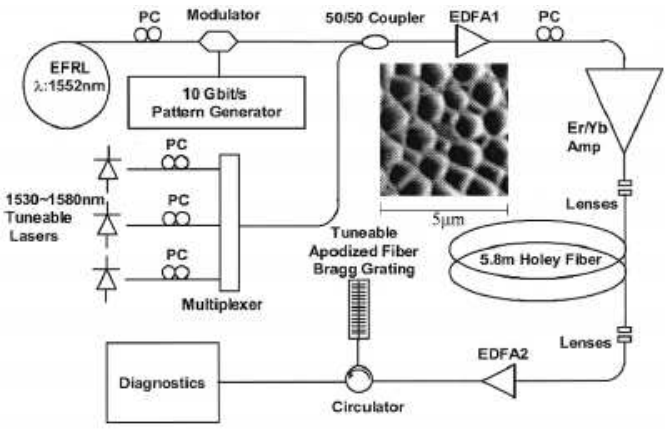

FIGURE 5.6: Experimental setup for the wavelength converter based on XPM. Inset: cross-sectional SEM image of the normal dispersion HF used in this experiment.

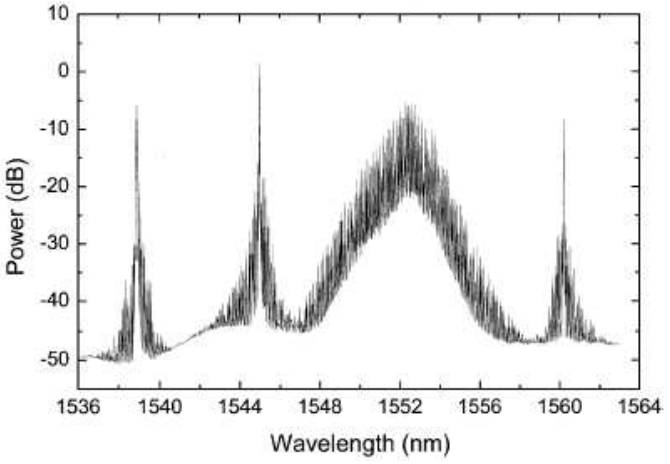

FIGURE 5.7: Measured optical spectrum of the three wavelength-converted signals and of the control pulses after the HF.

higher than that of a conventional dispersion-shifted fiber.

5.8 meters of this HF were employed in the set-up shown in Fig. 5.6, which is basically the same used in the previous WDM wavelength conversion experiment (with an anomalous dispersion HF). In this case the pump wavelength was 1552 nm and the coupling efficiency in this small core HF was of only 30%.

Fig. 5.7 shows the measured optical spectrum of the three wavelength converted pulses and of the control pulses after the HF. Also in this case, we measured the control pulse width versus the signal wavelength, tuned over a 15 nm wavelength range, observing an almost flat behaviour around 11 ps width (Fig. 5.8).

Although all the other characteristics of this wavelength converter based on a normal dispersion HF were very similar to those achieved by adopting an anomalous dispersion HF, the difference was clear when we performed some BER measurements on this device at a wavelength of 1545 nm. Fig. 5.9 shows both the measured BER and eye diagrams for the soliton control and wavelength-converted 10 Gb/s pulses. We obtained error-free, almost penalty-free (0.5-dB power penalty), wavelength conversion performance. Thus

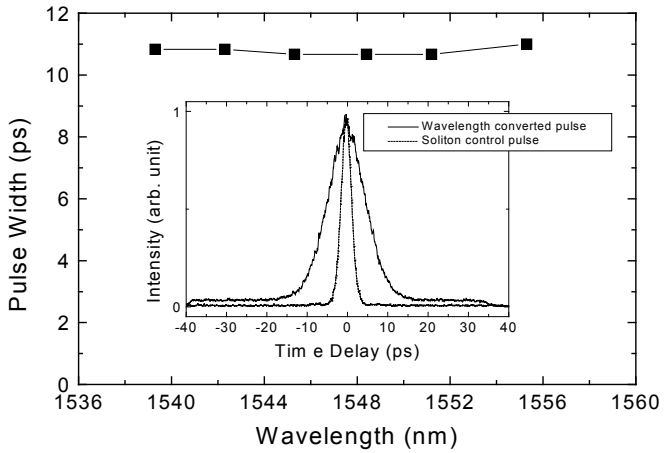

FIGURE 5.8: Measured full-width at half maximum of the wavelength converted pulses as a function of the probe beam wavelength for the case of wavelength conversion of a single channel. The inset shows the SHG autocorrelation traces of the wavelength converted pulses at 1545 nm, and the input pulses.

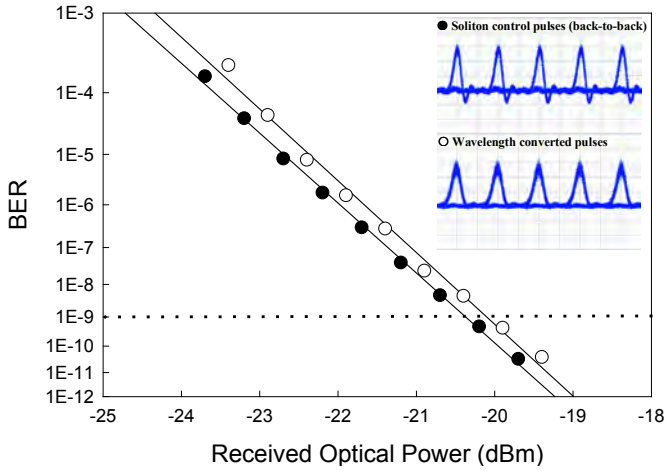

FIGURE 5.9: Measured BER versus received optical power for wavelength conversion of 10-Gb/s data pulses to a wavelength of 1545 nm.

our expectations of the advantage in using a normal dispersion HF were confirmed, because we could eliminate the source of coherence degradation of the signals.
Moreover, compared to the performance of the conventional highly nonlinear fiber-based wavelength converters (Yu and Jeppersen [2001]), we can see a benefit of using HF in terms of length/power product since our result shows a lower value of 1.2 $m \cdot W$ relative to the value of 10 $m \cdot W$ reported by Yu and Jeppersen [2001] . Both of the results show output pulse widths that are almost constant over the device operating bandwidth, although relatively broader output temporal pulse widths are observed in our HF-based wavelength converter due to the relatively high value of dispersion.

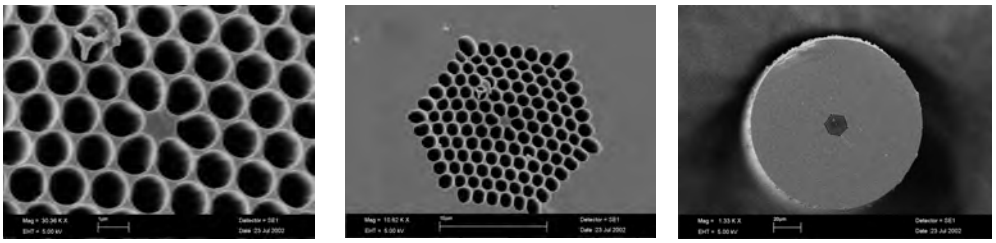

FIGURE 5.10: SEM of the transversal section of a highly normal dispersion HNL-HF with a core size of about 1 μm

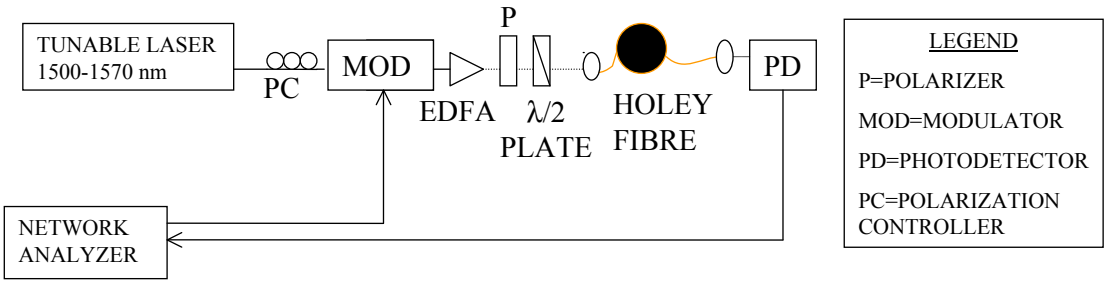

FIGURE 5.11: Experimental set-up for dispersion measurements.

5.4 Demonstration of high normal dispersion at 1.55 μm

Given the importance in actual HF devices of using a normal dispersion fibre at 1550 nm, we experimentally investigated the normal dispersion HF regime further.

Finazzi et al. [2003c] developed accurate theoretical predictions concerning the geometric parameters of HFs with negative dispersion (see Fig. 2.8). This model confirms some of the first predictions of Birks et al. [1999], concerning the possibility to use HFs for dispersion compensation in the telecommunications window. We already had produced a HF with a normal dispersion of $-350\ ps/nm-km$ (Sect. 5.3, inset of Fig. 5.6). However this fibre presented a very high structural asymmetry, an elliptical core, interstitial holes and had losses of about 300 dB/km. In order to confirm our theoretical model and, at the same time, prove the feasibility of a high normal dispersion HF, we fabricated the HF shown in Fig. 5.10, which has got a core size of 0.95 μm, a fibre diameter of 125 μm and a very large AFF of 0.95. A very similar design has also been suggested recently by Shen et al. [2003] as suitable for HF dispersion compensation in the 1550 nm telecommunication window.

Our HF has an almost regular structure (see Sect. 3.10.1), without interstitial holes (see Sect. 3.9.2) and with low confinement losses (Sect. 4.4, Fig. 4.10). The measured HF losses of this silica jacketed HF are 175 dB/km. Given the outstanding negative dispersion value (-453 ps/nm-km at 1550 nm, on one polarization axis) of this HF, we now describe in detail its dispersion measurement, which represents the first experimental demonstration of high normal dispersion in a HF.

We used the experimental set-up shown in Fig. 5.11. The network analyzer generates an electrical signal, which modulates the fibre input beam, and compares this signal with

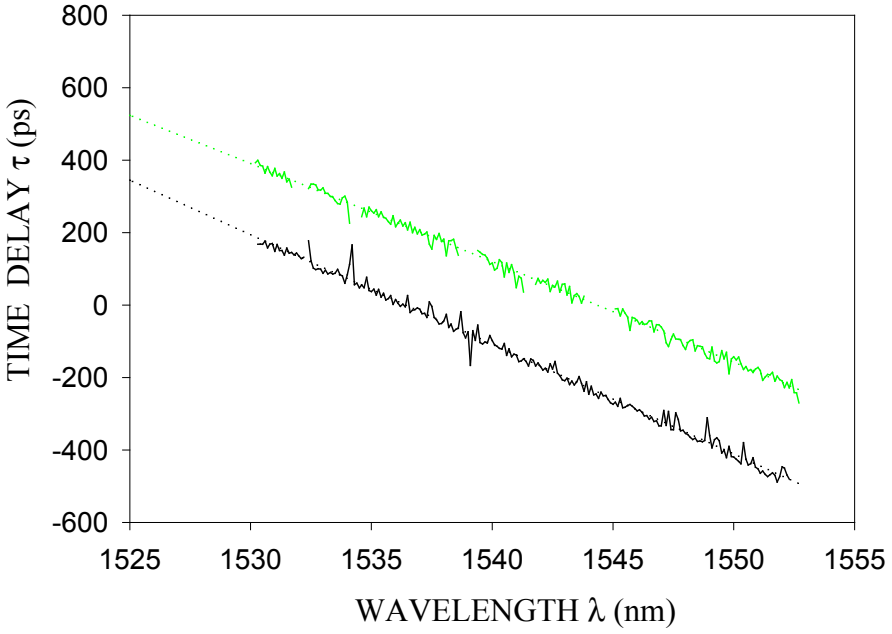

FIGURE 5.12: Time delay versus wavelength in the case of input signal polarized on the main polarization axis (green) or on the orthogonal polarization axis (black) of the 67 m long HF tested. The dotted lines represent the quadratic fit of the data.

the one generated from the photo-detector at the fibre output. The time delay between these two signals represents the group time delay τ_g experienced by the light during its propagation within the fibre, and is given by :

$$\tau_g = \frac{L}{v_g} \tag{5.1}$$

where L is the fibre length and v_g is the group velocity. The tunable laser allows measurement of the time delay for a range of wavelengths λ. The group velocity dispersion (GVD) is given by:

$$GVD = \frac{d}{d\lambda}(\frac{1}{v_g}) = \frac{d\tau_g}{L\ d\lambda} \tag{5.2}$$

We used 67 m of this fibre and measured the GVD both in the case of light polarized on the principal polarization axis of the fibre and in the case of orthogonally polarized light.

The time delay measurements are shown in Fig 5.12 . The quadratic fit of the time delay τ measured gives us the group time delay τ_g which is :

$$\tau_{gMAIN}[ps] = -0.0329 \cdot (\lambda[nm])^2 + 73.98 \cdot \lambda[nm] - 35733 \tag{5.3}$$

$$\tau_{gORT}[ps] = -0.0049 \cdot (\lambda[nm])^2 - 15.23 \cdot \lambda[nm] + 34911 \tag{5.4}$$

where λ is expressed in nm and τ in ps.

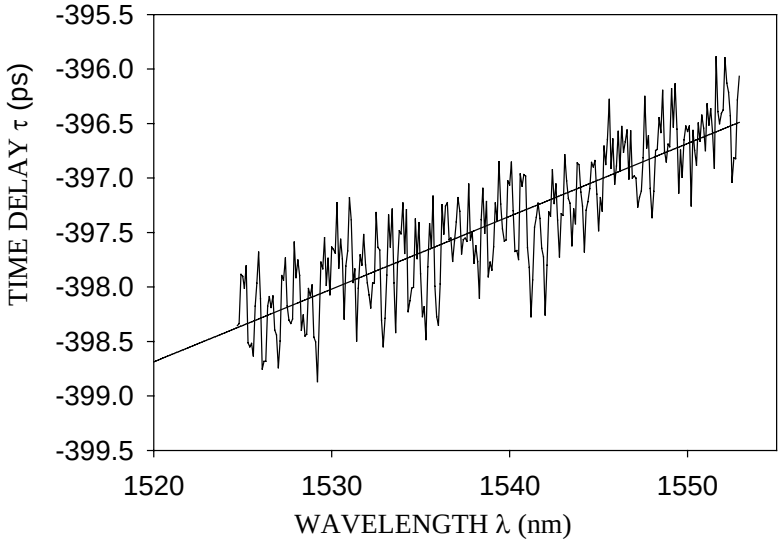

FIGURE 5.13: System time delay.

We then measured the time delay of the system, bypassing the HF in the set-up of Fig. 5.11. We obtained the time delay in Fig. 5.13
and the system group time delay τ_{gSYS} was:

$$\tau_{gSYS}[ps] = 0.07\lambda[nm] - 500 \tag{5.5}$$

By subtracting equation 5.5 from equation 5.3 and 5.4, we finally obtained the net group time delay τ_{ghf} :

$$\tau_{ghfMAIN}[ps] = -0.0329 \cdot (\lambda[nm])^2 + 74.05 \cdot \lambda[nm] + 36233 \tag{5.6}$$

$$\tau_{ghfORT}[ps] = -0.0049 \cdot (\lambda[nm])^2 - 15.17 \cdot \lambda[nm] + 34410 \tag{5.7}$$

Finally we calculated the derivative of the previous expression and divided the expression by the fibre length, to find the GVD (Fig. 5.14):

$$GVD_{hfMAIN}[ps/nm/km] = \frac{-0.0658 \cdot \lambda[nm] + 74.05}{67\ [m]} \tag{5.8}$$

$$GVD_{hfORT}[ps/nm/km] = \frac{-0.0098 \cdot \lambda[nm] - 15.16}{67\ [m]} \tag{5.9}$$

Therefore the calculated value of the GVD at 1.55 μm is -417 ps/nm-km for the main polarization axis and -453 ps/nm-km for the orthogonal axis. This value is about 20 times the dispersion of conventional fibres and a record for a HF. The GVD slope was found to be negative and more than 10 times higher than that of conventional fibers. This feature could be used for the compensation of dispersion on many transmission channels in a WDM system.

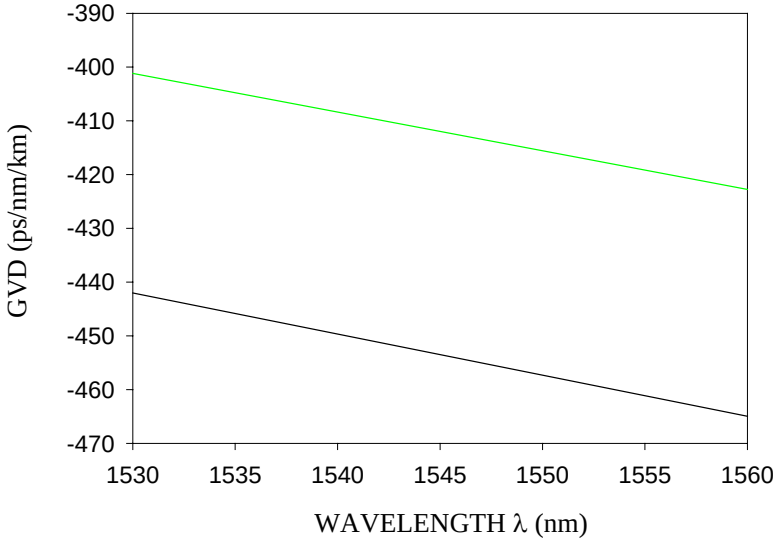

FIGURE 5.14: Group velocity dispersion (GVD) versus wavelength in the case of light polarized along the main fibre polarization axis (green line) or along the orthogonal polarization axis (black line).

Our measurements of dispersion of small core HFs in the telecommunication window show that dispersion compensation by using HFs could be achieved in principle. However HF losses are a major limit for the successful implementation of HFs as dispersion compensators. They are being reduced currently by some research groups worldwide (Tajima et al. [2003], Farr et al. [2002]) and HFs with losses of 0.28 dB/km at 1550 nm have been reported when the hole size is of the order of 4 μm and hole pitch is about 8 μm. However HF losses in the small scale regime are limited by the mode confinement and by losses due to surface scattering (Finazzi et al. [2003c]). Moreover, in this regime, some issues related to coupling losses and polarization need also to be addressed (Finazzi et al. [2003a]).

5.5 A moderate negative dispersion holey fibre with a record effective nonlinearity

In Sect. 5.3 we could achieve a wavelength conversion based on XPM in a HF, over a 15 nm wavelength range. The dispersion of the HF used was normal, to avoid coherence degradation of the signal (Nakazawa et al. [1999]), but it had a high absolute value (about $-350\ ps/nm-km$).
A high dispersion is not desirable in a wavelength converter based on XPM. Indeed, due to the fibre dispersion, pulses at different wavelengths propagate at different speeds. The nonlinear interaction between two optical pulses ceases to occur when the faster moving pulse completely walks through the slower moving pulse. We can define a "walk-off parameter" $d_{1,2}$ (Agrawal [2001b]):

$$d_{1,2} = v_g^{-1}(\lambda_1) - v_g^{-1}(\lambda_2) \tag{5.10}$$

where λ_1 and λ_2 are the center wavelengths of two pulses and $v_g(\lambda)$ is the group velocity of the pulse at a wavelength λ. If the pulse width is T_0 then the walk-off length is defined as:

$$L_W = \frac{T_0}{|d_{12}|} \tag{5.11}$$

Thus it is possible to increase the walk-off length and improve the operations of our devices by developing HFs with a lower dispersion value. This would allow the tuning range and also the efficiency of our HF based devices to be increased. Moreover HF technology may offer a big advantage over standard technology because of the possibility to develop HNL devices based on a very short HF length, which should, in principle, diminish the walk-off effects.

A similar argument can be made when we refer to the development of wavelength converters based on FWM. In this case the low dispersion value of the fibre used is of fundamental importance to satisfy the phase matching condition required for the occurrence of FWM (see Sect. 2.4.3). That's why conventional wavelength converters are normally based on HNL fibres with almost zero dispersion at the operating bandwidth (Okuno et al. [1999], Watanabe and Futami [2001]).

In order to fabricate a HF with lower negative dispersion, I followed the theoretical predictions of Finazzi et al. [2003c]. As shown in Fig. 2.8, a low negative dispersion fibre should have a hole pitch of about 1.2 μm and an AFF of about 0.9. Moreover, as we can see from Fig. 2.2, a HF with such parameters would have an A_{eff} incredibly close to the minimum theoretical value. Moreover, from Fig. 4.10, we can observe that the theoretical confinement losses of such a fibre with 5 or more air hole rings would be well below 0.2 dB/km.

However, as we can see from Fig. 2.8, the dispersion value, in this regime, is extremely sensitive to the exact hole pitch. Even a 100 nm error (or non-uniformity) in the HF inner structure, may result in a difference of tens of $ps/nm-km$, in terms of dispersion. Thus, given the practical difficulties in fabricating HFs with such a precise uniformity (see Sect. 3.9.3), I could only follow this design as a guideline. I fabricated the HF shown in Fig. 5.15, which has a core size of 1.2 μm and an average AFF of about 0.9.

This HF has a measured group velocity dispersion of about $-30\ ps/nm-km$. Moreover, as predicted by Finazzi et al. [2003c], its effective nonlinearity is almost 70 $W^{-1}km^{-1}$. This is the maximum effective nonlinearity ever achieved in a silica based optical fibre. I now describe in detail the nonlinearity measurement of this HF, which clearly proves the impact of HF technology on the development of highly nonlinear optical fibres.

The method I have used to measure the nonlinearity of our HF is the one of Boskovic et al. [1996], which is based on the measurement of the nonlinear phase shift experienced by a dual frequency beat signal travelling inside an optical fibre.

When two beating signals are launched simultaneously into a highly nonlinear optical fibre, the fibre output spectrum is of the type in Fig. 5.16 . The two beating signals generate new side frequencies due to the effect of FWM. In particular the intensity of the side signals is proportional to the nonlinearity of the optical fibre. The ratio between

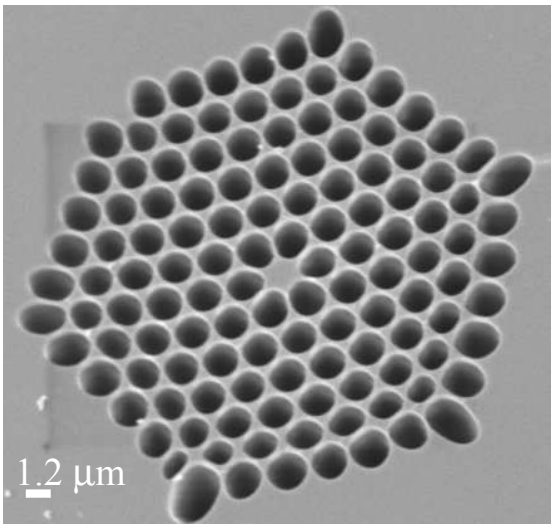

FIGURE 5.15: SEM of a normal dispersion holey fibre (about $-30\ ps/nm/km$) and a record nonlinearity ($\gamma \sim 70\ W^{-1}km^{-1}$).

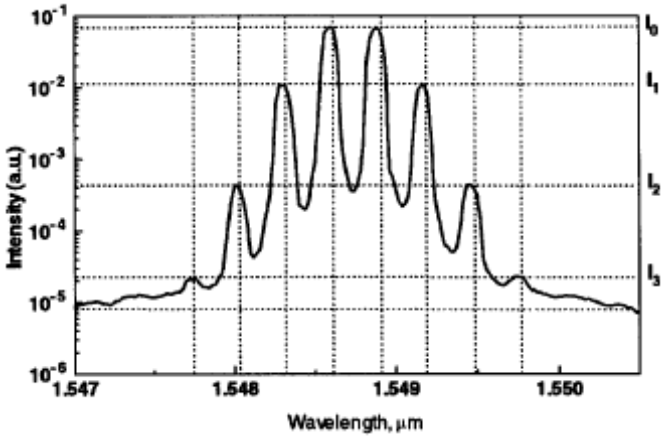

FIGURE 5.16: Typical SPM spectrum generated by the propagation of a beat signal in a fiber (Boskovic et al. [1996])

the intensities of the fundamental frequencies and of the first order sidebands is directly related to the nonlinear phase shift, according to the following relation:

$$\frac{I_0}{I_1} = \frac{J_0^2(\frac{\varphi_{SPM}}{2}) + J_1^2(\frac{\varphi_{SPM}}{2})}{J_1^2(\frac{\varphi_{SPM}}{2}) + J_2^2(\frac{\varphi_{SPM}}{2})} \tag{5.12}$$

where I_0 and I_1 are the intensities of the fundamental frequency and of the first sideband frequency, J_0, J_1 and J_2 are the Bessel functions of the zero, first and second order and φ is the phase shift. Therefore, the measurement of the ratio between the intensities of the fundamental frequency and of the first sideband frequency is an indirect measurement of the phase shift.

Once the phase shift has been calculated, the effective area A_{eff} can be obtained by the

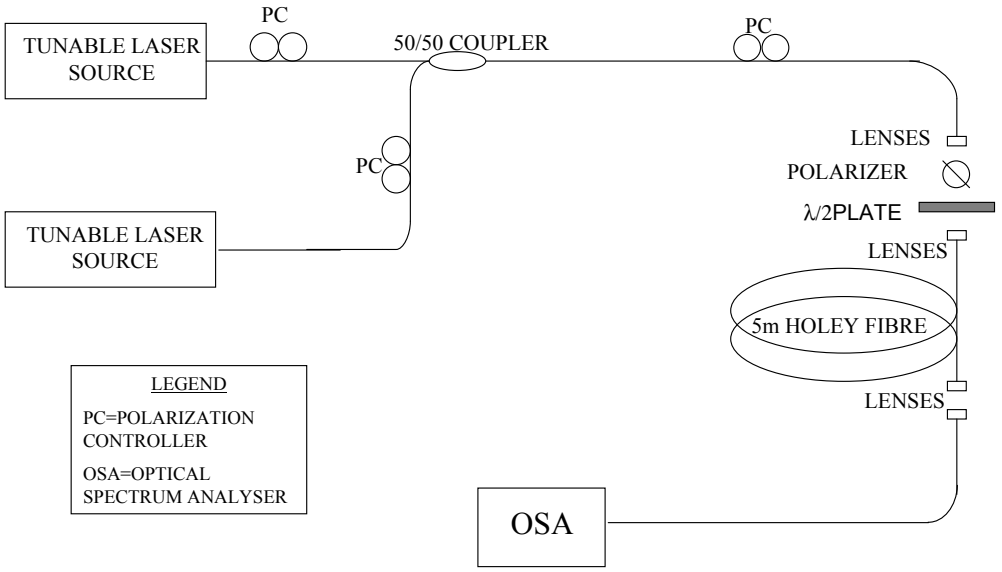

FIGURE 5.17: Experimental set-up used for the HF nonlinearity measurement

following relation (Boskovic et al. [1996]):

$$\varphi_{SPM} = \frac{2\omega_0 n_2 L_{eff} P_{avg}}{c A_{eff}} \tag{5.13}$$

where ω_0 is the fundamental frequency, c is the light speed, n_2 is the nonlinear refractive index of the fibre, L_{eff} is the effective fibre length and P_{avg} is the input average power of the signal.

As we can see, a correct nonlinearity measurement requires first the measurement of the ratio between I_0 and I_1, for the calculation of φ, secondly the measurement of the fibre loss, to calculate the effective fibre length L_{eff}, and then the measurement of the input average power P_{avg}. After these measurements, A_{eff} can be easily calculated by using equation 5.13.

The outline of our measurement setup is shown Fig. 5.17 . The HF length used was only 5 meters while the fibre loss was measured to be 190 dB/km, by using a cut-back measurement technique. The input beating signals were derived from tuneable, continuous wave, external cavity lasers and had respectively a wavelength of 1549.57 nm and 1550 nm. They were simultaneously launched inside our HF, by means of a 50/50 coupler and a pair of lenses with a coupling efficiency of 20%. The average output power was measured by using a thermal power meter at the end of our HF.

Fig. 5.18 shows the measurements of the intensity ratios versus the fibre output power, and versus the calculated phase shift and input power. Fig. 5.19 shows the linear relation between the nonlinear phase shift and the input average power.

The slope of the line gives γ and which is directly proportional to the fibre nonlinearity n_2/A_{eff}, as from relation 5.13, and is found to be 0.68. Thus we can measure the

Output average power (W)	**Intensity ratio (dB)**	**Input average power (W)**	**Nonlinear phase shift (rad)**
0	0	0	0
0.127	31.2	0.158	0.110
0.1465	29.9	0.182	0.127
0.16	29.7	0.199	0.130
0.185	28.1	0.230	0.157

FIGURE 5.18: Experimental data for the nonlinearity measurement.

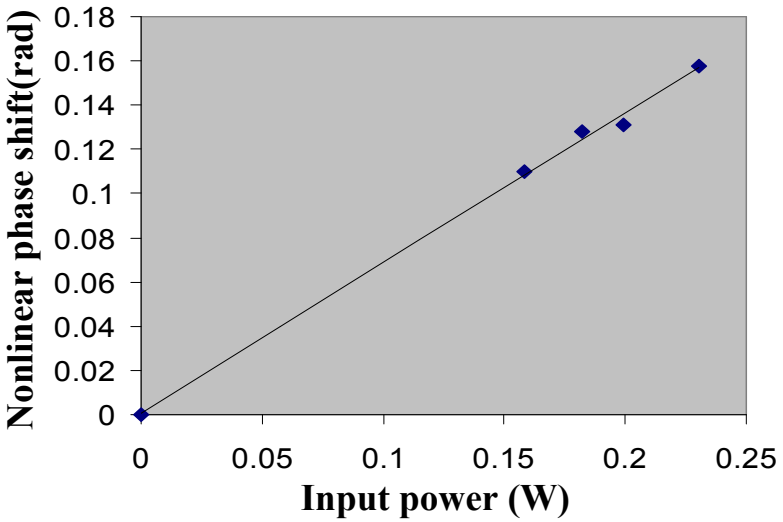

FIGURE 5.19: Linear relation between the nonlinear phase shift and the input average power.

effective nonlinearity γ (Agrawal [2001b]):

$$\gamma = \frac{2\pi n_2}{\lambda A_{eff}} \tag{5.14}$$

Indeed, by using equation 5.13 and equation 5.14, we can obtain:

$$\gamma = \frac{\varphi_{SPM}}{2P_{avg}L_{eff}} \tag{5.15}$$

where the effective length L_{eff} is given by:

$$L_{eff} = \frac{1 - exp(-\alpha L)}{\alpha} \tag{5.16}$$

the HF loss α is 190 dB/km and the HF length under test L is $5m$.
Our measured γ is of about 73 $W^{-1}km^{-1}$, which is the highest nonlinearity ever achieved in a silica based optical fibre (see Okuno et al. [1999]).
If we assume negligible the fraction of optical power localized within the inner fibre holes (Broderick et al. [1999a]), we can calculate the effective area A_{eff} directly from

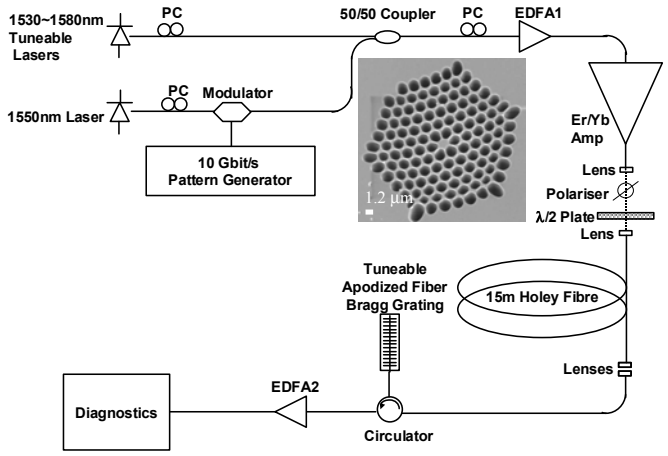

FIGURE 5.20: Experimental set-up for our HF wavelength converter based on FWM.

equation 5.13, finding that:

$$A_{eff} = \frac{4\pi n_2 L_{eff}}{\lambda \frac{\varphi}{P_{avg}}} = 1.45\mu m^2 \tag{5.17}$$

where we used a value $n_2 \sim 2.7 \cdot 10^{-20} m^2/W$ for a bulk silica glass (Agrawal [2001b]). Our nonlinearity measurement may be affected by experimental error. We estimate that in this case the error in the value of γ may be as large as 10 $W^{-1}km^{-1}$. Indeed, the accurate derivation of the nonlinear coefficient from the measured phase shift is dependent on measurements of the fiber loss and optical coupling. These measurements are somewhat more difficult to measure with accuracy using HF, and thus, the error quoted is somewhat larger than might be considered usual for the technique when applied to standard fiber types.
(It should also be noted here that, recently, Finazzi et al. [2003c] have shown how the definition of A_{eff} given in equation 2.1 should be modified in this regime, to take into account the fraction of the optical mode that travels in the inner air cladding of the HF. However our direct measurement of the nonlinear phase shift from equation 5.12 gives a good estimate of the effective nonlinearity γ.)

5.6 A holey fibre wavelength converter based on FWM

In order to take advantage of the newly developed HF with a reduced amount of normal dispersion and a record nonlinearity, I demonstrated, for the first time, an efficient wavelength converter based on FWM in a short HF.
The schematic of our experiment is shown in Fig. 5.20. Both the pump and the signal beams were derived from tunable continuous-wave (CW) external cavity lasers operating in the range $1530 \sim 1580\ nm$. The signal beam at a fixed wavelength of 1550 nm was modulated with a $2^{15} - 1$ pseudorandom data sequence at a data rate of 10 Gb/s and then combined with the pump beam using a 50/50 coupler. The two beams were then

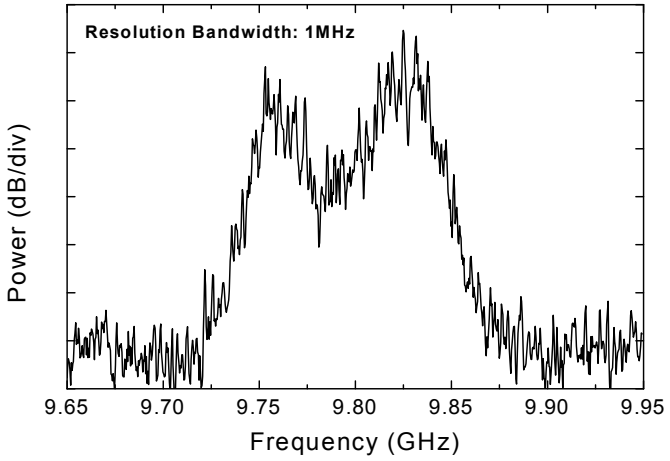

FIGURE 5.21: Radio frequency trace of the beat signals between spontaneous Brillouin scattered beam and the pump, using the 15 m long HF described in Fig. 5.20.

amplified using an Er/Yb amplifier with a maximum saturated power of 700 mW and then lens coupled into our 15 m long HF with a coupling efficiency of 20%. Polarization controllers (PCs), a polarizer, and a $\lambda/2$ plate were used to ensure that both beams were launched onto a single polarization axis of our polarization maintaining HF, which had a beat length of 0.5 mm and a polarization extinction ratio of 17 dB.

I obtained a highly nonlinear HF with a high SBS threshold by ensuring structural non-uniformity along its length during the fiber fabrication process through variation of the external fiber diameter (Lee et al. [2002a]). The structural variation of the HF was not precisely specified in this instance. I simply switched off the active diameter feedback control ordinarily used when drawing fiber. This resulted in a HF with larger than normal diameter fluctuations.

Since the measured HF loss was 190 dB/km at 1550 nm, the effective length of the 15 m HF was only 11 m. The high nonlinearity of this HF (about 70 $W^{-1}km^{-1}$) allows for a reduction in the device length which is one of the key factors required in order to achieve broad-band wavelength conversion (Aso et al. [2000],Sharping et al. [2001]). The measured group velocity dispersion (GVD) of the HF is $\sim -30ps/nm-km$ at a wavelength of 1550 nm. Due to the relatively short length of the fiber, and relatively narrow operating bandwidth of our measurement set-up, I was unable to get a reliable measurement of the dispersion slope. Our best estimate from numerical simulations of the structure would be that the average zero-dispersion wavelength along the fiber is located around 1550 nm, although it should be appreciated that this is likely to vary along the fiber length due to the structural non-uniformity. The predicted average dispersion slope is approximately $0.6ps/nm-km$.

We then characterized the SBS properties of the 15 m long HF. We first measured the spontaneous Brillouin scattering line shape of the 15 m HF using a heterodyne-detection technique that relies upon beating the spontaneously scattered light with the pump beam (Lee et al. [2002a]). Fig. 5.21 shows the measured spontaneous Brillouin

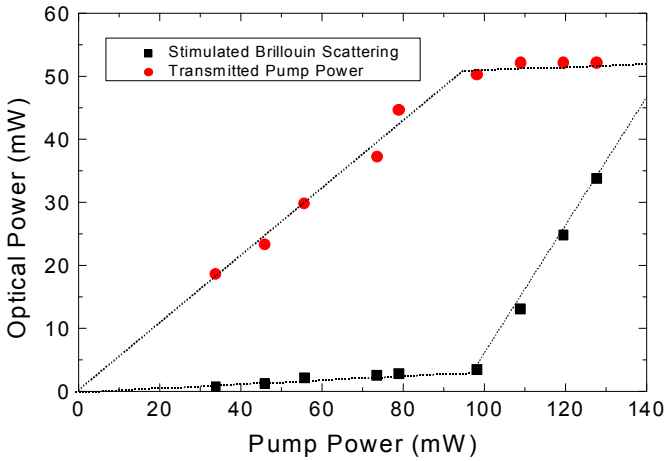

FIGURE 5.22: SBS and transmitted pump power as a function of launched pump power, using a 20 m length of nominally the same fiber.

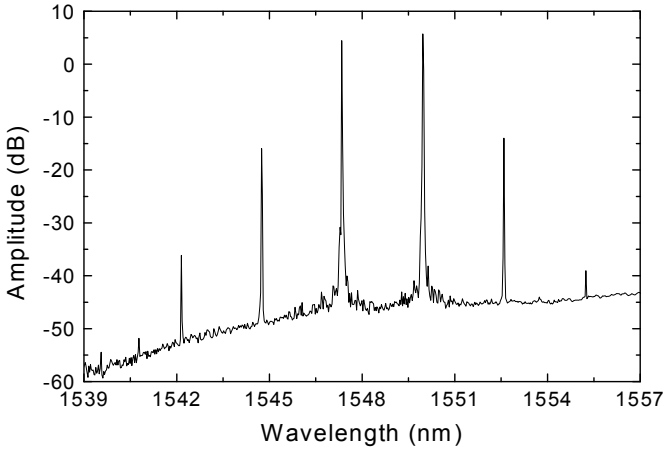

FIGURE 5.23: Output FWM spectrum after the HF only (input signal at $\lambda = 1550\ nm$, pump at $\lambda = 1547\ nm$)

spectrum. A non-Lorentzian line shape comprising two distinct peaks with 75 MHz frequency separation is clearly observed and results from the structural non-uniformity along the fiber length. The spontaneous Brillouin 3 dB bandwidth of one of the two peaks is seen to be approximately 50 MHz, which is over five times broader than would be expected for a silica fiber with a uniform cross-sectional profile (Lee et al. [2002a]). The SBS threshold of the 15 m HF we used for wavelength conversion was estimated to be higher than 130 mW since we were unable to observe SBS due to the limited output power of our amplifier (maximum pump power inside the HF: 130 mW). The SBS threshold of a 20 m length of nominally the same fiber was measured to be 100 mW, as shown in Fig. 5.22, which is around two times higher than would be expected for a silica fiber with a uniform cross-sectional profile.

The HF output spectrum is shown in Fig. 5.23. The wavelengths of the initial signal and the pump beams are 1550 and 1547 nm, respectively. A strong FWM wavelength converted signal is clearly evident at a wavelength of 1544 nm despite the short fiber

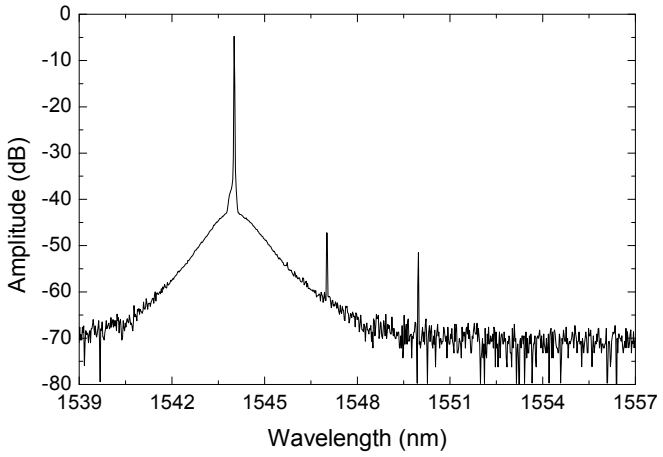

FIGURE 5.24: Wavelength converted signal spectrum after the apodized fibre Bragg grating filter.

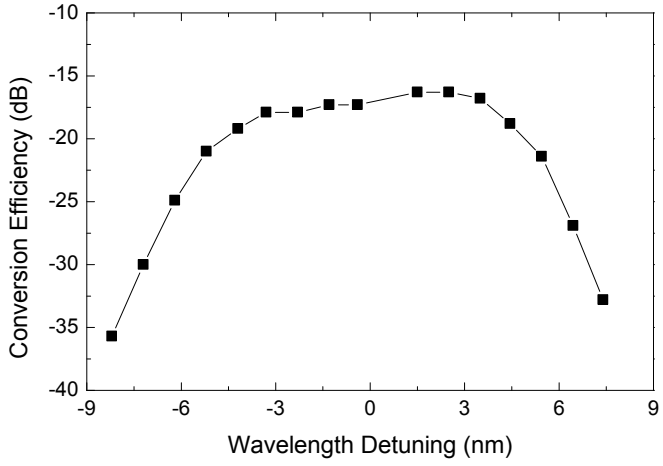

FIGURE 5.25: Conversion efficiency versus wavelength detuning relative to a fixed signal wavelength of 1550 nm

length used and both second- and third-order idler beams are also observable. After the HF, we used a compression-tunable two-stage apodized fiber Bragg grating (FBG) filter with a 3-dB bandwidth of 0.55 nm and a 30-dB bandwidth of 1.5 nm to efficiently suppress the input signal and pump beams and to pick out the wavelength converted signal. As shown in Fig. 5.24, a 40-dB extinction ratio between the idler and the pump was achieved. Fig. 5.25 shows the measured conversion efficiency, which is defined as the ratio of output wavelength-converted signal power to the input signal power. A maximum conversion efficiency of 16 dB was achieved over a 3-dB bandwidth of 10 nm. In order to analyze the system impact of using our HF-based FWM wavelength converter in practical WDM applications, we performed bit-error-rate (BER) measurements on the wavelength converted channel at 1544 nm. Fig. 5.26 shows the measured BER and eye diagrams for both the 10Gb/s NRZ input signal and wavelength converted output signal. We obtained error-free (BER) wavelength conversion performance with a 2 dB power penalty relative to that of the back-to-back input signal. The conversion efficiency will

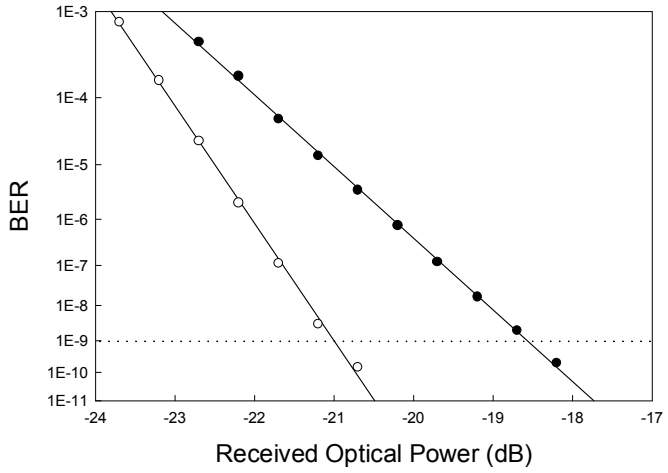

FIGURE 5.26: Measured BER versus received optical power for wavelength conversion of a 10 Gb/s NRZ signal at a wavelength of 1544 nm.

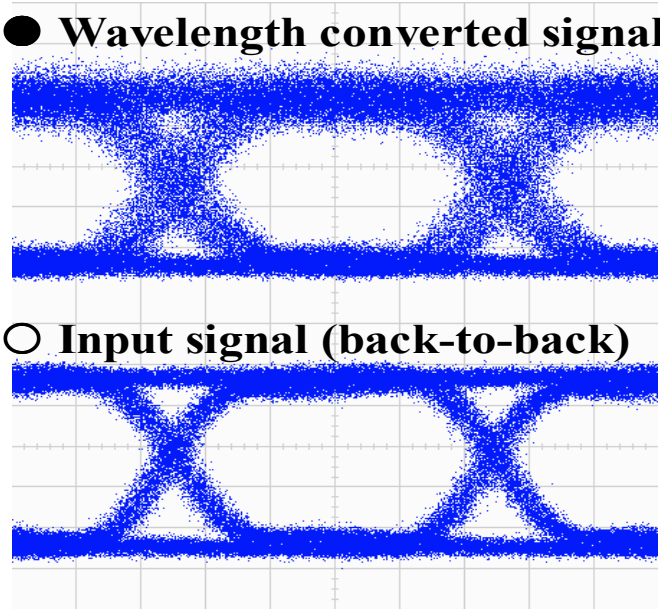

FIGURE 5.27: Eye diagrams of the input signal and of the wavelength converted output signal.

be a function of pump wavelength, and the BER performance will also depend on the pump and signal wavelengths since the HF is operated in a wavelength regime in which the dispersion slope is relatively high and the net GVD is small. In Fig. 5.27 we show the eye diagrams of both the input signal and the wavelength converted output signal. We can observe a small amount of timing jitter and intensity noise, which we believe to be due to polarization coupling in this highly birefringent small core fiber (Finazzi et al. [2003a]). However, since the fiber had normal dispersion, no modulation-instability-induced intensity noise was observed (Grosz et al. [1999]). In order to ensure the benefits of the use of normal dispersion fibers in the realization of this sort of nonlinear fiber device, I performed similar FWM-based wavelength conversion experiments using a HF

with an anomalous dispersion of 10 ps/nm/km. The intensity noise, which can be attributed to modulation instability in the anomalous dispersion regime, was so severe that BER measurements could not be performed.

5.7 Conclusions

In this chapter we have focused our attention on the application of HF technology to a particular high nonlinearity fibre device, namely the wavelength converter. Indeed the enhanced nonlinearity, which it is possible to obtain in a HF, gives rise to the possibility to develop a wavelength converter based on a very short HF length.
Wavelength conversion can be achieved either by using the XPM or FWM effect. We have first investigated, in Sect. 5.2, the feasibility of a HF wavelength converter based on XPM and spectral filtering (Yu and Jeppersen [2001], Ohlen et al. [2000]). We obtained WDM wavelength conversion over 20 nm tuning range by using a combination of 6 meters of a HF, with an anomalous dispersion of $+100\ ps/nm-km$, and an apodized FBG filter. When we launched 10 Gbit/s soliton pulses inside our small core HF, we obtained a 4 dB power penalty in the converted signals. We attributed this penalty to the positive dispersion of our HF, which caused a coherence degradation of the transmitted signals (Nakazawa et al. [1999]).
Thus I aimed to fabricate a HF with a negative dispersion at the operating wavelength of 1550 nm. I followed some earlier designs (Birks et al. [1999]) to produce a HF with a dispersion of $-350\ ps/nm-km$. By using 5.8 m of this normally dispersive HF, we repeated our experiment on wavelength conversion based on XPM and spectral filtering. This time, we could achieve error-free, almost penalty-free (0.5 dB power penalty) multiple wavelength conversion of 10 Gb/s return-to-zero data pulses over a 15-nm bandwidth, confirming the advantage of adopting a negative dispersion HF.
Given the importance of normal dispersion fibres in optical communications (Goyal et al. [2002], Gruner-Nielsen et al. [1999]), I tried to fabricate a HF with a high normal dispersion, but also with lower confinement losses, a more regular structure and without interstitial holes (to allow an easier modelling). I followed a recent design of Finazzi et al. [2003c] and fabricated a HF with 6 air hole rings and an almost regular structure, with a normal dispersion as high as $-453\ ps/nm-km$ at 1550 nm (on one polarization axis). In Sect. 5.4, I have shown the dispersion measurement of this HF and demonstrated, for the first time, high normal dispersion in a HF, which could be implemented for dispersion compensation (Birks et al. [1999]). Moreover, our fabricated structure confirms also a recent design of Shen et al. [2003].
In order to improve our results on wavelength conversion, I needed to fabricate a HF with a lower negative dispersion, to increase the walk off fibre length. This would have been useful also for the implementation of a wavelength converter based on FWM, in which a low dispersion value is of fundamental importance to achieve phase matching (Agrawal [2001b]). Thus I followed the model of Finazzi et al. [2003c] and fabricated a

HF with a core size of 1.2 μm and an AFF of about 0.9, which had a normal dispersion of about $-30\ ps/nm-km$. The computational model of Finazzi et al. [2003c] predicts, for this HF, an effective area very close to the minimum theoretical limit. Indeed, as shown in Sect. 5.5, I measured, in this HF, an effective nonlinearity of about 70 $W^{-1}km^{-1}$, which is the highest nonlinearity ever measured in a silica based optical fibre.
By using this small core HF, with a moderate normal dispersion and a record nonlinearity, I demonstrated, in Sect. 5.6, a HF-based tunable wavelength converter using FWM. Error-free wavelength conversion of 10 Gb/s NRZ data signals over a 10 nm bandwidth was reliably achieved using just 15 m of highly nonlinear HF with a high SBS threshold. Although our HF based FWM wavelength converter shows slightly worse performance in terms of conversion efficiency and tuning bandwidth compared to the results achieved with highly nonlinear fiber (Aso et al. [2000]), the use of a highly nonlinear HF with lower and flatter GVD should allow for further improvements. However, non-uniform HF technology offers significant advantages in terms of reduced device length, reduced power requirements, and ease of use since it eliminates the need for active schemes to reduce pump power loss caused by Brillouin scattering.

Chapter 6

Spinning of holey optical fibres

6.1 Introduction

In the previous chapters, we have demonstrated how HFs can be implemented in a wide range of nonlinear devices and require a much shorter length than conventional optical fibres.

I attempted to take the maximum advantage of the HF nonlinearity, by making HFs with very small cores ($\sim 1.2\mu m$) and very large AFF, achieving very high nonlinearity values (Belardi et al. [2002b]).

However, our experiments also highlighted several limitations that affect HFs when the hole pitch Λ is smaller than the wavelength λ. In particular we noticed that holey fibre losses, coupling efficiency and polarization extinction ratio dramatically decrease in this regime. For example, for the fibre of Fig. 5.15, used to demonstrate a HF wavelength converter (Belardi et al. [2002b]), I found an extinction ratio of only 17 dB (although the measured beat length was only 0.5 mm), I achieved a coupling efficiency of only 20% and the fibre losses were as high as 190 dB/km. Following this work, a study of these limits has been carried out and a precise model has been developed to better understand some fundamental properties of HNL-HFs (Finazzi et al. [2003a]) and their relative trade-offs as a function of fibre design (Finazzi et al. [2003c]).

The polarization properties of HFs are particularly problematic for certain applications since, as I pointed out previously, any slight structural asymmetry can lead to high values of fibre birefringence. Moreover, as the mode size is made small and approaches the wavelength of light the polarization modes begin to exhibit significant curvature of the field across the mode profile and which serves to degrade the polarization extinction ratio, when working with linearly polarized input/output beams (Finazzi et al. [2003a]). Means to control the birefringence properties of holey fibers are thus important. In particular it is desirable to be able to produce HNL-HFs with low effective values of birefringence and polarization mode dispersion (PMD).

PMD has deleterious effects in optical communication systems operating at high bit rates Agrawal [2001b]). For this reason some fabrication techniques have been optimized to reduce the PMD contribution. In particular, in the early 80s', Payne et al.

[1983] invented and developed an optical fibre fabrication technique based on preform spinning, which consists of the rotation of the preform during the drawing process.
Characteristic parameters involved in the spinning process are the spin speed, which is the rotation rate of the preform (measured in rotations per minute, rpm), and the spin pitch, which is the distance between successive twists in the fibre. In particular preform spinning has been successfully applied for the demonstration of very low birefringence optical fibres (Barlow et al. [1981]). Novel optimized spinning techniques are now being studied to develop low PMD optical fibers (Galtarossa et al. [2003a], Galtarossa et al. [2003b]).

I consider investigating the possibility to apply the preform spinning technique also to the fabrication of HNL-HFs. In particular there were some open issues regarding the feasibility to spin a holey fibre at a very low temperature, and some open questions regarding the effects of spinning on the fibre holes.
In this chapter I face these problems and try to solve them.
In Sect. 6.2 I discuss some technical issues related to the spinning of optical fibres in general and HFs in particular, describing the major factors that need to be considered to achieve a very high spin speed, and consequently a small spin pitch.
Using our spinning facility, I performed some experiments on simple holey structures.
In Sect. 6.3, I studied the relations between the fabrication parameters involved in the spinning and the spin pitch, demonstrating that the spin pitch is given simply by the ratio between the drawing speed and the rotation speed.
In Sect. 6.4 I applied preform spinning to a hollow tube, and studied the relationship between the AFF and the spin speed. I found that preform spinning doesn't affect the hole circularity but leads to hole expansion.
In Sect. 6.5, I investigated the effects of preform spinning on an off-centre hole, finding that the hole circularity is still not affected by spinning and that, also in this case, preform spinning leads to an expansion of the hole size with an increase of the rotation speed.
Finally in Sect. 6.6, I demonstrate the fabrication of the first spun HF and analyze its characteristics.

6.2 Technical issues

Our spinning capability is provided by a simple spinning motor, which is connected to the motorized stage on the top of our drawing tower, as shown in Fig. 6.1. The fibre preform is inserted in the internal chuck of our spinning motor for a total length of about 300 mm, and then secured. In this way the preform can be rotated while it is being fed into the furnace. The rotation of the preform can be controlled with a precision of 5 rpm and can reach a maximum spin speed of 2000 rpm.
The maximum preform "handle" diameter, which can be inserted in the chuck, is about

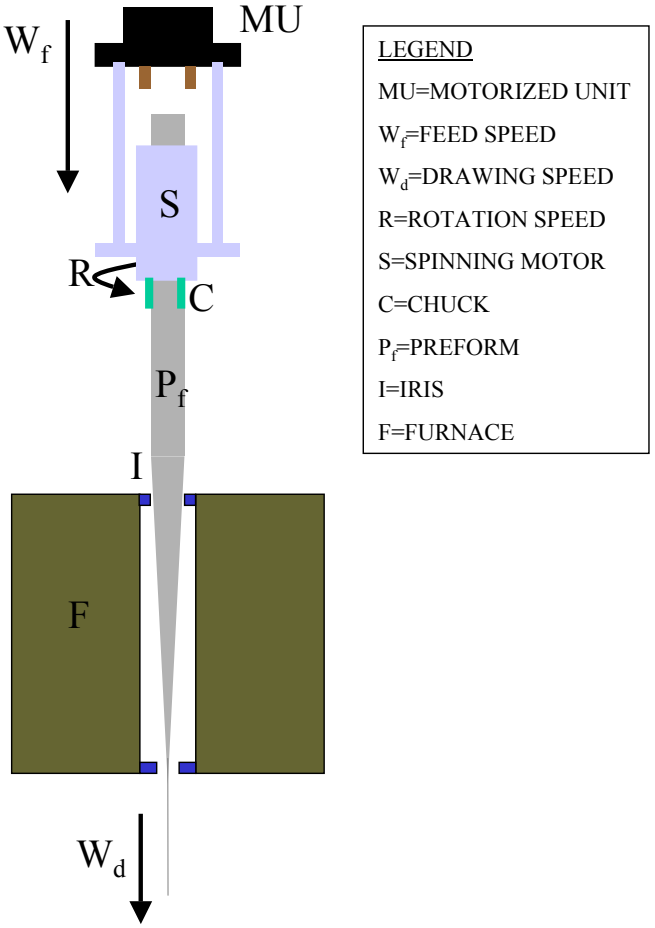

FIGURE 6.1: Sketch of our spinning facility.

10 mm. One can clearly attach to the "handle" a bigger size preform. However, in this case the joint should be as straight as possible, to preserve the alignment of the preform to the motor. In the case when the joint is not well made, I observe a very large oscillation of the preform during its rotation, which makes the fibre drawing hard to control.

The preform dimensions are critical to obtain high spin speeds. Indeed, when a small diameter preform is used, it can be directly inserted inside the motor, without the need for a joint. This ensures the absolute straightness of the preform, especially when high quality silica is used, which has got good uniformity and circularity properties.

The preform length is also an important factor for achieving high rotation speeds. The longer the preform is, the more likely it is to oscillate during the spinning. I usually use a maximum total preform length of 650 mm. Of this length about 300 mm are inserted inside the spinning motor. The separation between the chuck of the motor and the centre of the furnace can be a minimum of 150 mm. Thus only 200 mm of the preform are effectively being drawn.

In my experiments, which will be discussed in the following sections, I have used, in most experiments, an F300 hollow tube with an outer diameter of about 9.95 mm and an inner

diameter of 2.85 mm, which has been inserted in our spinning motor. The insertion of a thin tube in the spinning motor can produce a break of the tube at the chuck level, due to the stress experienced by the glass preform, as it is being drawn at high temperature and high spin speeds. Indeed the heat generated inside the furnace is conducted through the glass up to the chuck level (depending on the thermal conductivity of the glass) and its hardness lowers as the temperature increases (see Doremus [1994]). The chuck itself also gets hot and expands, gripping the preform tube too firmly. Besides that, spinning of the preform generates a stress on the external glass surface at the chuck level, because of the radial force generated on the preform. However, in our case the cross sectional area of the tube used was big enough so that breakage of the preform was avoided.
Another technical issue regards the top and bottom irises of the furnace. When high rotation speeds are applied, it is better not to close the top iris of the furnace too much on the preform, because the rotation of the preform can modify the aperture of the iris, and produce a large instability during the drawing. At the other end, even the bottom iris of the furnace must be opened in a way that the spun fibre can vibrate without touching the iris, since this could cause a break of the fibre.
Finally the application of the coating to the spun fibre can represent a problem when high rotation speeds are achieved, since it is difficult to apply the coating homogeneously on the fibre while it is vibrating. The best solution is to use a pressurized coating system, in which the coating is pressurized on the fibre so that its adherence can be improved.

6.3 Spin pitch

Inside the furnace, the preform rotation induces a rotation of the fibre, as it is drawn. After fibre cooling, this twist is "frozen" into the spun fibre and becomes a permanent characteristic. The spin pitch is a measure of this twist, and is defined as the distance between successive twists in the fibre.
It is known from the literature (Payne et al. [1983]) that the spin pitch is given by the ratio between the drawing speed and the spin speed. Although this relationship is very intuitive, a clear systematic confirmation of its validity has never been shown, and the complete independence of the spin pitch on other parameters, such as the feed speed, the drawing temperature, the preform size and the preform geometry has never been confirmed. I demonstrated these points by undertaking three different experiments, as shown in Fig. 6.2.
I have drawn a solid silica F300 rod with a diameter of 20.6 mm and an F300 hollow tube, with an outer diameter of 9.95 mm and an inner diameter of 2.85 mm. For these three experiments, performed using preforms with different sizes and geometry, I have used different values of the feed speed, drawing speed, spin speed and drawing temperature. In all cases I have been able to verify the relation 6.1:

$$d = \frac{W_d}{R} \tag{6.1}$$

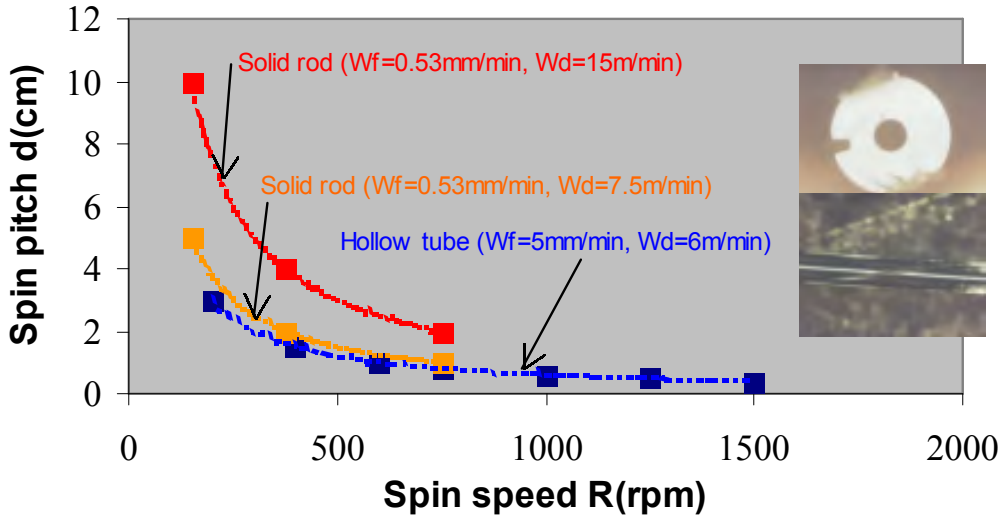

FIGURE 6.2: Spin pitch versus spin speed in 3 different experiments.

where d is the spin pitch, W_d is the drawing speed and R is the rotation speed. Thus I have also demonstrated the independence of the spin pitch on the other drawing parameters. In practice, I have been able to measure the spin pitch by readily making a visible key in the preform by cutting it on its external perimeter, as shown in the inset of Fig. 6.2. The key was 1 mm deep and 1 mm wide. It rotates around the external surface of the fibre with the periodicity of the spin pitch. We can see in the second inset of Fig. 6.2 the longitudinal section of the spun hollow fibre, viewed under an optical microscope. The key is seen as a dark line that spirally rotates around the fibre.

6.4 Spinning effects on a hollow fibre

In order to analyze the effect of spinning on a very simple holey structure, I tested the effects of preform spinning on the air filling fraction (AFF) of a hollow fibre. I used the same tube as in the previous section (outer diameter of 9.95 mm and inner diameter of 2.85 mm) and performed three different experiments, in which I used the same feed speed of 5 mm/min and the same drawing speed of 6 m/min. The results are shown in Fig. 6.3. First of all I found that the circularity of the inner hole is not affected by preform spinning.

We can though see that preform spinning leads to a linear increase of the AFF with the spin speed in the temperature regime of 2100 °C and 2150 °C. However, using a lower drawing temperature of 2050 °C, I could not measure any change in the AFF.

The different effects of the spinning on the fibre hole in the three different temperature regimes, is related to the enhanced viscosity of the glass at low temperature, as explained in Sect. 3.5.2.

The observation that preform spinning can lead to hole expansion could be very useful in the future as it may provide an alternative way to retain the holey structure without the need for pressurizing the HF preform.

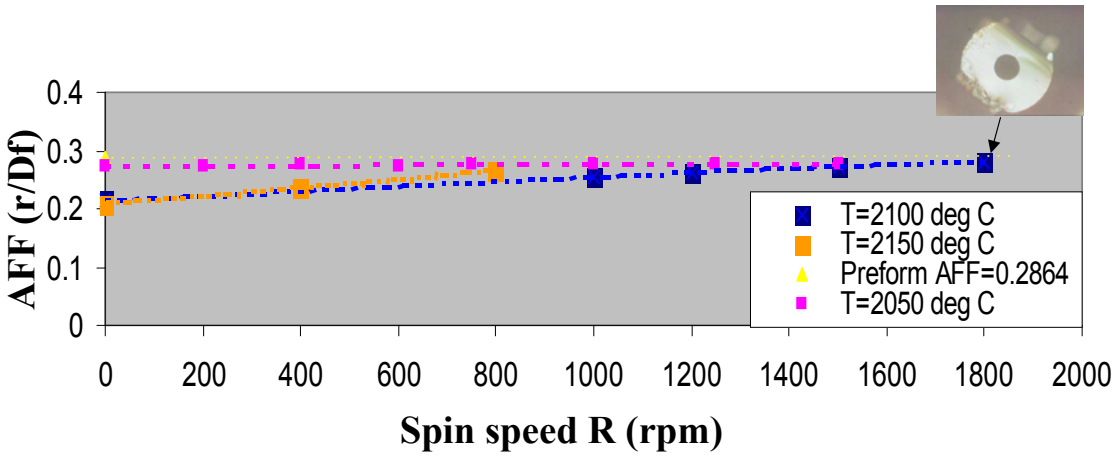

FIGURE 6.3: AFF versus spin speed for 3 hollow fibres fabricated with different temperatures

On the other hand, I have also observed that, using the same high feed speed, preform spinning doesn't have any effect on the AFF of a hollow fibre at a lower drawing temperature. This implies that the spinning of a small mode HF (normally fabricated at a very low temperature and using a similar high feed speed) wouldn't affect its AFF. This point has been demonstrated in Sect. 6.6.

6.5 Spinning effects on an off-centre hole

To make another step towards the understanding of the spinning effects on the fabrication of a HF, I spun a fibre with an off-centre hole. I drilled a hole with a diameter of 2 mm, centering it 5 mm away from the centre of a silica F300 rod, whose diameter was 20.6 mm. I used a drawing speed of 6 m/min, a feed speed of 0.65 mm/min and a drawing temperature of 2000 °C. The results are summarized in Fig. 6.4. As we can see, the behavior of an off-centre hole is quite similar to that of a central hole. Indeed spinning can lead to an increase of the AFF of the hole towards its original value in the preform (i.e. 0.1). I checked the circularity of the hole at all the different spin speeds, measuring the two perpendicular diameters of the hole. Although the hole was positioned largely off-centre I could not measure any deformation of the circularity (as might at first be expected given the radial velocity dependence).
Although a HF has a much more complex structure than our tested hollow fibre, this experiment indicates that preform spinning is likely to allow retention of circular structure within the starting preform.
I experimentally demonstrated this point in the next section.

6.6 A spun holey fibre

The previous experiments gave us information about the correct dependence of the spin pitch on the drawing and spinning parameters (Sect. 6.3), about the modification of

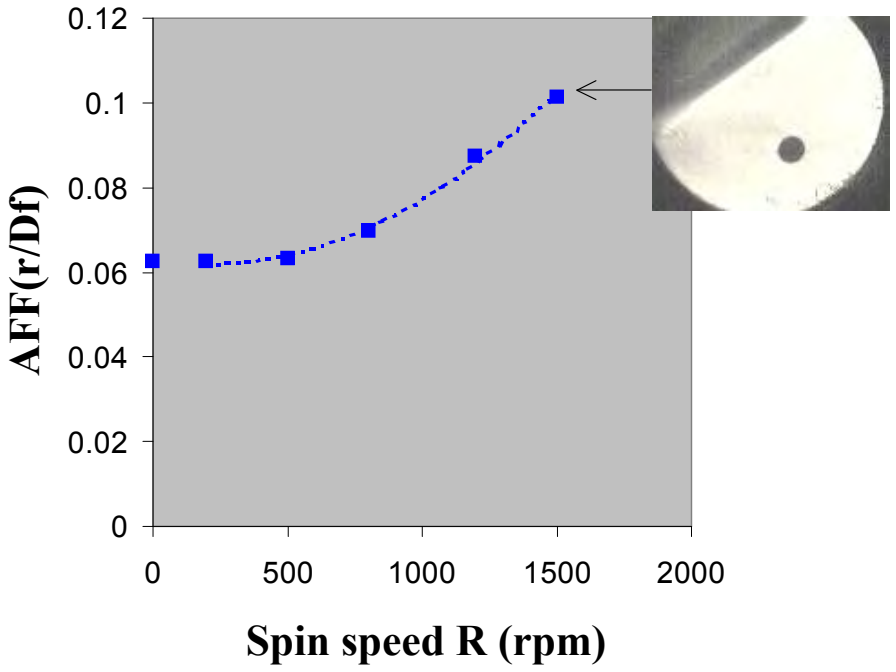

FIGURE 6.4: AFF versus spin speed for an off-centre hole.

the AFF with the spin speed (Sect. 6.4), and about the circularity both of a spun central hole (Sect. 6.4) and of a spun off-centre hole (Sect. 6.5). I then attempted the fabrication of the first spun HF with the conviction that the HF structure would not be affected by spinning both in terms of AFF and in terms of hole ovality, because of the low drawing temperature and high feed speed used. Fig. 6.5 shows different sections of the fabricated spun HF at different spin speeds, corresponding to different spin pitches (according to the equation 6.1). Since all the samples have been taken during the same drawing process, I have indicated, on the right side of the figure, the fibre length, time and preform position corresponding to each sample.

Although the fibre drawing was made at a quite low temperature of 1950 °C, a maximum spin speed of 2000 rpm (the upper limit of our spinning motor) was reached, without breaking the fibre. I used a small silica jacket with an outer diameter of 9.73 mm and an inner diameter of 1.7 mm. The fibre was drawn at a drawing speed of 3.1 m/min, so that the minimum spin pitch achieved was 1.5 mm.

I performed some geometric measurements on the samples taken. Fig. 6.6 shows the evolution of a reference hole pitch, hole size and core diameter with the spin speed. It is not possible to see any variation in the core size, while small variations affect the reference hole size and hole pitch. However, as we can read on the left of Fig. 6.5, each sample corresponds to a particular fibre length L, drawing time t and preform position PP outside the furnace (thus preform length). These factors are responsible for random variations of the HF geometry, due to the internal pressure instability, as discussed in Sect. 3.9.3. Then the cause of the small variations in the hole size, which are independent on the spin speed, cannot be related to the preform spinning. Thus we can conclude

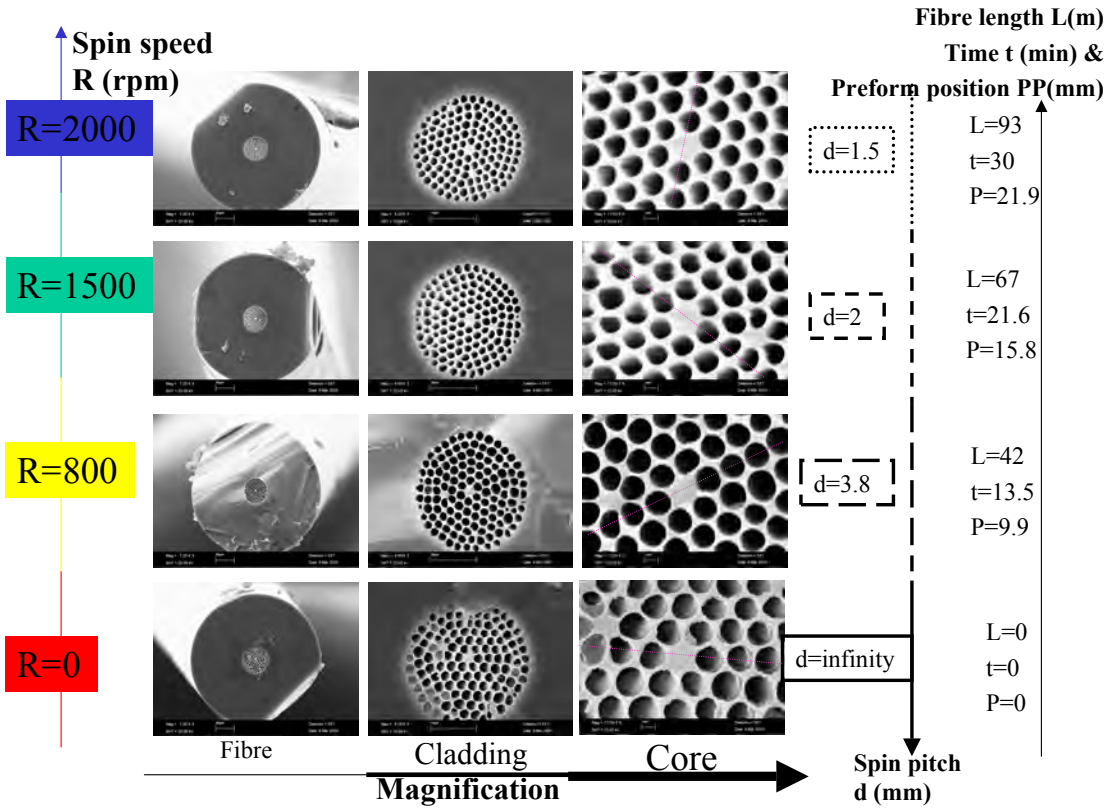

FIGURE 6.5: SEM of 4 HFs drawn sequentially at a temperature T=1950 °C, using the same drawing parameters but different spin speed.

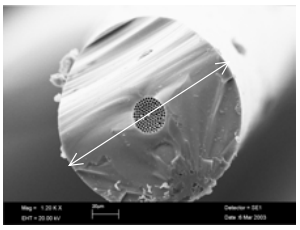

R=800 rpm, measurement of fibre diameter

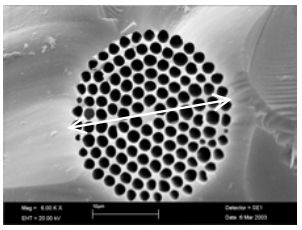

R=800 rpm, measurement of clad diameter

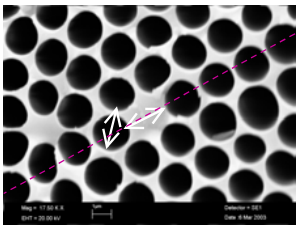

R=800 rpm, measurement of Λ , d and r

Spin speed R(rpm)	Spin pitch d_S (µm)	Fibre diameter D_f (µm)	Max error of D_f (µm)	Clad diameter C (µm)	Max error of C (µm)	Core diameter r (µm)	Reference hole size d (µm)	Reference hole pitch Λ (µm)	Reference air filling fraction d/Λ	Max error of r, d and Λ (µm)
2000	1.5	140.9	1	23.3	0.2	2.13	1.68	2	0.84	0.07
1500	2	139	1	24	0.2	2.13	1.68	1.94	0.86	0.07
800	3.8	140	1	24.8	0.2	2.13	1.74	2	0.87	0.07
0	infinity	141.9	1	26.7	0.2	2.13	2	2.2	0.9	0.07

FIGURE 6.6: Geometric measurements taken on the fibres of Fig. 6.5

that there is no actual influence of the spinning on the geometric characteristics of a small mode HF.
The beat length of the unspun HF (spin speed R=0) was measured to be 0.71 mm, a common value for a highly nonlinear HF with a core size about 2 micron and an AFF of about 0.85. No change in the beat length was measured for the spun HF (R=2000 rpm).
To achieve a lowering of the fibre birefringence, the spin pitch achieved for our spun HF should have been about 10 times lower than the beat length, i.e. 0.07 mm (Payne et al. [1983]). Such a small value of the spin pitch would require the use of a faster spinning motor (i.e. $R > 2000\ rpm$) or the lowering of the drawing speed.
However, if we reduce the drawing speed, the feed speed must also be reduced, in order to keep the same fibre diameter. Moreover the feed speed value need also to be kept high enough to allow retention of the HF structure, as explained in Sect. 3.5.1, or otherwise the drawing temperature should be reduced. Clearly some compromise needs to be reached between these two conflicting requirements.
The most practical way to make a low birefringence (i.e low PMD) HF would be to increase the beat length of the unspun HF.
On one hand, this can be achieved with a more precise stacking, to get a more symmetric geometry. The introduction of automation in the stacking process would provide major help in this direction (see Sect. 3.10.1, Parry and Gray [1986]).
On the other hand, we could increase the core size and decrease the AFF of the HF, but this would be done at the expense of the HF nonlinearity.

6.7 Conclusions

In this chapter I have investigated the possibility to apply the preform spinning technique (Payne et al. [1983]) to the fabrication of HNL-HFs.
The main issues of interest concerned the possibility to spin a holey fibre at a low drawing temperature, to be able to get a holey structure, and, at the same time, it was an open question what would have happened to the inner holes of our HF, while spinning.
Firstly, I made a set of systematic experiments on the most simple holey structure: a hollow fibre.
In Sect. 6.3, I discussed how I empirically found that the spin pitch is given simply by the ratio between the rotation speed and the drawing speed, and is independent on the preform geometry, the feed speed or the drawing temperature.
In Sect. 6.4, I observed the behaviour of preform spinning on a central hole, finding that spinning can lead to hole expansion, at high drawing temperature (2150 °C), while no effect has been noted when the spinning is performed at lower drawing temperature (2050 °C).
In the following Sect. 6.5, I investigated the effects of preform spinning on an off-centre hole. It was an open question whether the circularity of the hole would have been affected in this case. However our experiments left no doubt about this, confirming that

no change in the hole circularity could be achieved. The behaviour of an off-centre hole was similar to the one of an in-centre hole. Indeed, also in this case, I observed hole expansion due to the rotation of the hollow fibre preform.
Finally, in the last Sect. 6.6, I attempted the fabrication of a spun HF. I used a drawing temperature as low as 1950 °C and still managed to spin a HF with a rotation speed up to 2000 rpm. As expected, the HF inner hole circularity was kept and, at the same time, in this temperature regime, I didn't observe any dimensional change of the holes that could be related to the HF preform spinning.
In conclusion, in this chapter, I demonstrated that the preform spinning technique, invented by David Payne in 1981 (Payne et al. [1983], Barlow et al. [1981]), can be successfully applied not only to the fabrication of conventional optical fibers, but also to the fabrication of HFs, which require different drawing parameters (in particular a much lower drawing temperature) and whose inner structure is completely different.
Our birefringence measurements of spun HNL-HFs didn't show any substantial change in birefringence (thus in PMD) between the spun HF and the unspun one. Further developments are required to effectively produce a low birefringence HNL-HF. In particular the production of HNL-HFs with an intrinsically higher beat length (of the order of few cm) should be a fundamental requirement to obtain an effective low birefringence in a spun HF, fabricated as described in this chapter. This may be achieved through an automation of the stacking operation (Parry and Gray [1986]) or through a modification of the HF inner geometry, as the choice of a bigger core size or a lower AFF. But the last point has the drawback of decreasing the effective fibre nonlinearity.
Another possibility could be to modify the fabrication parameters I have used by, for example, using greater spin speed (with a new spinning motor) and, at the same time, lower draw speeds.
Finally, the use of alternative spinning techniques, as the fibre spinning approach invented by Hart et al. [1994], which allows the use of higher drawing speeds and non-constant spin speeds, should allow the achievement of better performances in terms of PMD reduction (Li and Nolan [1998]).
The application of these spinning techniques to the fabrication of HNL-HFs may allow in the future the development of small core HFs with a low PMD.
(Note that, following this work, my colleague Mr John Hayes and others, just recently, have managed to demonstrate PMD reduction in the production of large mode area HFs using preform spinning. A ten-fold increase in beat length from about 1 to 10 m was demonstrated. This preliminary result confirms the validity and applicability of my method.)

Chapter 7

Conclusions and future work

7.1 Conclusions

In addition to a wide range of different exploitation routes, HF technology can be applied to the production of optical fibres with an enhanced nonlinearity 10-100 times greater than in CFs. This is due to the high NA that it is possible to achieve in this novel air/silica structured optical waveguide, which allows the confinement of the fundamental optical mode in a very small effective area (down to 1.5 μm^2).
Moreover this type of HF with high NA and a small core size can present completely novel dispersion properties, such as anomalous dispersion below 1.27 μm or high normal dispersion at 1550 nm. This behaviour arises from the large contribution, in HFs, of the waveguide dispersion to the total dispersion value.
On top of that, HFs , with small core size and high NA, can present extremely high values of birefringence (a beat length less than 1 mm), by simple structural variations.
All of these properties make small core HFs extremely attractive especially for application in highly nonlinear fibre devices.
In this thesis we have, first of all, explored the feasibility of fabricating such HFs with high NA and small core size (chapter 3). Several problems hindered for some time the fabrication of these fibres. One of the first HNL-HF was fabricated by Bennett et al. [1999](Fig. 3.5), at the ORC. In its best section, it had a hole pitch of 1.8 μm and hole size of 0.34 μm, while the fibre diameter was about 300 μm and its length was limited to a few meters. The short length of this fibre and its intrinsic fragility made it unusable for practical laboratory applications in HNL devices. But, especially, the fabrication of this unique HF couldn't be repeated.
We then needed a reliable fabrication method to produce robust, long, standard dimension HFs with an extremely high AFF and a very small core size. The production of these fibres was fundamental to the investigation of possible applications of HF technology in optical communications.
Thus, as discussed in Sect. 3.3, we addressed the fabrication problem of HNL-HFs. The main issue to solve was the closure of the HF holes when, during the drawing stage, their size was reduced from about 1-2 mm to $1-2$ μm. Indeed the surface tension, acting on

the inner walls of the holes, caused them to collapse when their size was decreased to very small values.

We tried to solve this problem in several different ways. By studying the quantitative relations between the HF drawing parameters and the final hole size (Sect. 3.5), we understood the importance to use a high feed speed value and a low temperature during HF drawing.

Moreover we invented a novel HF fibre fabrication approach, based on air clad, two ring structured HF, (Sect. 3.6). This technique allowed the production of HFs with a small core size (about 4 μm).

However the key to reliably fabricate HNL-HFs was found in the successive introduction of a pressurization technique (Sect. 3.7), based on the sealing of the top of the preform prior to fibre drawing. Sealing creates a pressure (of the order of 0.25 psi) inside the HF holes, which can actively balance the effects of the surface tension. First applied to air jacketed HFs, this fabrication method has been successfully employed in the production of very long, full silica jacketed HFs with a core size as small as 1 μm and an AFF as high as 0.95. During this work the effects of pressurization by sealing technique has also been investigated through systematic measurements, showing pressure instability issues and demonstrating the direct dependence of the internal HF pressure on the HF preform length.

Once fabricated, the resulting long and robust HNL-HFs could then be characterized. Extremely high values of nonlinearity were demonstrated in these novel silica/air waveguide structures (up to 70 $W^{-1}km^{-1}$)(Sect. 5.5). At the same time novel dispersion properties were found such as anomalous GVD at 1 μm (Sect. 4.3) and an extremely high normal GVD at 1.55 μm (-453 ps/nm-km) (Sect. 5.4). In particular, by taking advantage of the anomalous dispersion of a HF at 1 μm, we have demonstrated pulse compression and soliton formation at this wavelength, using only a few meters of fibre. We have also measured a high birefringence in all of our fabricated fibres and, as an example, shown the birefringence measurement of a small core HF with a beat length of only 0.44 mm (Sect. 4.5), one order of magnitude smaller than conventional stress induced high birefringent optical fibers (Noda et al. [1986]).

In chapters 4 and 5, we have described the applications of our HFs to high nonlinearity devices. In particular we have demonstrated, in Sect. 4.2, a 2R data regenerator based on only 3.3 m of a HF with an A_{eff} of about 2.8 μm^2. This can be considered to be the first application of a HNL-HF to optical switching (Petropoulos et al. [2001b]).

We then demonstrated, for the first time, a Raman amplifier based on only 75 m of a HF with a core size of 1.5 μm, obtaining internal Raman gains of over 42 dB and a noise figure of about 6 dB. By using the same fibre (and experimental set-up) we also obtained 11 dB extinction ratio in Raman induced all-optical modulation experiments (Sect. 4.6). The idea to make a HF based Raman amplifier (Yusoff et al. [2003]) is very promising, due to the possibility of achieving very high nonlinearity in a HF, which in turns means the possibility to use a short fibre length and significantly reduce the problem of double

Rayleigh scattering (Nissov et al. [1999]).
We have also investigated the Brillouin effect in a HF by demonstrating a 73.5 m based HF Brillouin laser (Sect. 4.7) with a good laser power efficiency of 70% and a Brillouin shifted output power of 110 mW, at a wavelength of 1552.18 nm. In particular we investigated the stimulated Brillouin characteristics of the HF and established that structural variations along the particular HF used were responsible for broadening the Brillouin gain line-shape, and consequently for increasing the Brillouin power threshold. Although these characteristics increased the threshold of our HF Brillouin laser, it was important to realize that HF structural variations (which are normally greater than in CFs, due to the younger technology, the more complex structure and to the smaller geometric characteristics) may be advantageous in applications in which the Brillouin gain should be suppressed.
Wavelength conversion using HFs is the topic of chapter 5. We show that HF technology can be successfully applied to wavelength conversion devices based either on XPM (Sect. 5.3) or FWM (Sect. 5.6).
We first adopted a 6 m anomalous dispersion HF and an apodized FBG filter to demonstrate WDM wavelength conversion using XPM and spectral filtering (Lee et al. [2002b]). However we obtain an error penalty of 4 dB in the wavelength converted soliton pulses transmitted at a data rate of 10 Gbit/s. To overcome this limitation, related to the anomalous dispersion of the HF used at 1550 nm (Nakazawa et al. [1999]), we implement a similar wavelength conversion experiment based on a 5.8 m long, normally dispersive HF (about $-350\ ps/nm-km$). In this case we can achieve an error-free penalty-free multiple wavelength conversion of 10 Gb/s data pulses over a 15 nm bandwidth (Lee et al. [2003b]).
By fabricating a HNL-HF with a reduced negative dispersion of $-30\ ps/nm-km$ (and a record nonlinearity of 70 $W^{-1}km^{-1}$), we demonstrated, in Sect. 5.6, a HF based tunable wavelength converter based on FWM in a 15 m long HNL-HF with a high SBS threshold (Belardi et al. [2002b], Lee et al. [2003a]). Error-free wavelength conversion of 10 Gb/s NRZ data signals over a 10 nm bandwidth was reliably achieved.
These experiments constitute some of the very first applications of HF technology to optical communication systems and were all based on the use of very short fibre lengths, demonstrating the advantage of HNL-HFs in terms of short devices and thus, in the future, low power requirements. This work has produced over 40 scientific publications and two patent applications regarding the novel air-clad HF (Belardi et al. [2002a]) and the idea of a HF based Raman amplifier (Yusoff et al. [2003]).
However several issues must still be addressed for actual integration of HF technology in commercial optical systems. One of these regards the high degree of birefringence of HNL-HFs and the associated problem of PMD. In chapter 6, we address the possible solution to this problem by demonstrating that the preform spinning technique (Payne et al. [1983]), used in the '80s for the production of very low birefringent optical fibers (Barlow et al. [1981]), can be successfully integrated into HF technology. We thus

demonstrate the fabrication of the first spun HF and prove the fundamental consistancy of its geometric parameters compared to the unspun case.

7.2 Future work

Since the first demonstration of continuum generation in a microstructured fibre by Ranka et al. [1999], the enormous possibilities offered by HF technology in the field of nonlinear optics have also been exploited and rapidly developed, in parallel with our work, by other research groups.
One important example is the commercialization of a HF based system for optical frequency metrology (Udem et al. [2002]), which relies on efficient supercontinuum generation in a small core HF.
An important application of HF technology may be related to efficient parametric amplification. Sharping et al. [2002b], at the Northwestern university, in the USA, have already demonstrated an optical parametric oscillator based on four-wave mixing in a 2.1 meter long microstructured fibre, with a 40 nm wavelength tunability, at a wavelength of about 750 nm.
Another research group, at "COM", in Denmark, has successfully demonstrated high speed demultiplexing based on a nonlinear optical loop mirror with a HF. Using a 50 m long HF with a zero dispersion wavelength at 1552 nm, they demonstrated error-free demultiplexing from 160 Gb/s of optical-time-division multiplexing signals transmitted through an 80 km span of standard single mode fiber (Siahlo et al. [2003]).
The prospect of possible commercial applications of HFs in telecommunications is also encouraged by the drastic reduction of HF losses, which has been possible to achieve over the last few years. Indeed recently losses as low as 0.28 dB/km at 1550 nm have been reported by Tajima et al. [2003], at "NTT" in Japan, in a HF with a hole diameter of 4 μm and a hole pitch of 8 μm. This extraordinary achievement brings HF losses down to comparable values to those of standard single mode optical fibers.
While losses in silica based HFs are being effectively reduced, some research is targeted on the fabrication of HFs made by glasses other than silica, to further enhance fibre nonlinear effects. Indeed lead silicate glass HFs have been produced by means of an extrusion technique (Kiang et al. [2002], Ravi Kanth Kumar et al. [2002]). The intrinsic high nonlinearity of soft glasses has allowed the measurement, in a SF57 lead silicate glass HF, of an effective nonlinearity as high as 640 $W^{-1}km^{-1}$ at 1550 nm (Petropoulos et al. [2003]). Furthermore, the optimization of nonlinear and dispersion characteristics of SF6 HFs has led to the demonstration of an ultrabroad supercontinuumn, spanning at least from 350 nm to 2200 nm, in a 75 cm long SF6 HF with a core size of 2.6 μm (Ravi Kanth Kumar et al. [2002]).
Recently a HF has been made also in tellurite glass by Russell's group (Ravi Kanth Kumar et al. [2003]). This material offers a range of useful properties not possessed by silica, such as high refractive index, good infrared transmittance and high optical nonlinearity.

Moreover the Raman gain peak for tellurite glasses is roughly ten times greater and has almost twice the bandwidth when compared to fused silica. Thus it could become an interesting material to make a HF based Raman amplifier.

In the future we should explore further the wide range of possibilities offered by the application of HF technology to glasses other than silica. However the massive nonlinear effects possible in HFs made by non-silica glasses are counterbalanced by their high losses, of the order of few dB/m (Ravi Kanth Kumar et al. [2002], Ravi Kanth Kumar et al. [2003]).
Instead, the losses of our HNL-HFs are likely to decrease, following the work already carried out by Tajima et al. [2003], concerning HFs with a greater core size. If the losses of our HNL-HFs could go down to values comparable to those of standard DSFs, they may practically improve the performance of a full range of highly nonlinear devices. Besides those we have described in this thesis, the application of HNL-HFs with low loss and slightly negative broad flat dispersion may lead to an important improvement in the performance of current parametric amplifiers at 1550 nm. At the same time, a perfect control of the dispersion properties of our HNL-HFs should lead to an extended tunability of actual wavelength conversion devices, also because they can be based on a very short HF lengths.
However, one of the barriers to obtaining efficient parametric processes in our HFs concerns the non-uniformity along their length, as pointed out in Sect. 3.9.3. This is a direct consequence of our HF pressurization method and that consists of the sealing of the preform prior to the drawing stage. So, if we want to overcome this issue, other more controlled pressurization methods should be investigated. Although direct pressurization of a HF preform has already been explored in the past (Fitt et al. [2002]), our improved knowledge of the HF drawing process suggests new practical routes to obtain an externally controlled pressurization of a HF preform.
On the other hand, the possibility to monitor and control the non-uniformity of a HF structure (for example by relating the internal pressure to the preform length, as described in Sect. 3.9.3), may be further investigated in order to use it as a way to suppress the Brillouin gain (Sect. 4.7) and to explore this fundamental nonlinear effect in the novel HF structure.
However, even though HNL-HFs will be made with reduced losses (Tajima et al. [2003]), perfectly designed dispersion (Hansen et al. [2003], Hansen et al. [2002], Reeves et al. [2002]), with high uniformity (Farr et al. [2002]) and with reduced losses for splicing to standard fibres (Hansen et al. [2003], Kerbage et al. [2001]), still one fundamental problem would preclude an actual application of this technology to current optical communication systems. That is the high birefringence of HNL-HFs and the associated problem of PMD. Thus fabrication techniques to actively reduce PMD in HNL-HFs should be developed. We have already demonstrated (chapter 6) that the preform spinning technique (Payne et al. [1983]) is perfectly compatible with HNL-HF technology

and we have already produced a spun HF with a spin pitch as small as 1.5 mm. However this was not enough to actively reduce birefringence of our HFs, because, in our experiment (see Sect. 6.6) the spin pitch to achieve a reduction of the actual HF birefringence should have been at least 20 times lower (Payne et al. [1983]). A practical way to improve our result could be, either to fabricate HNL-HFs with an intrinsic lower birefringence (in the unspun fibre), for example by using an automatic stacking technique (Parry and Gray [1986]), or to improve our fabrication facilities, for example by installing a faster spinning motor.

Moreover the recent availability, at the ORC, of a large bore furnace (about 100 mm) may allow the preparation of a HF preform with bigger dimensions, which may result in an improvement of the regularity of the final HF structure and of the intrinsic HF birefringence.

The fabrication of a low birefringence HNL-HF should definitively constitute a fundamental breakthrough for an actual integration of HF technology into practical optical communication systems.

Appendix A

List of publications

Journal Papers

J. H. V. Price, T. M. Monro, K. Furusawa, **W. Belardi**, J. C. Baggett, S. Coyle, C. Netti, J. J. Baumberg, R. Paschotta, and D. J. Richardson, "UV generation in a pure silica holey fiber"
Applied Physics B 2003 Vol.77 (2) pp.291-298

J. H. Lee,**W. Belardi**, K. Furusawa, P. Petropoulos, Z. Yusoff, T. M. Monro, and D. J. Richardson, "Four-wave mixing based 10Gbit/s tuneable wavelength conversion using a holey fiber with a high SBS threshold"
IEEE Photonics Technology Letters 2003 Vol.15 (3) pp. 440-442

J. H. Lee, Z. Yusoff , **W. Belardi**, M. Ibsen, T. M. Monro, and D. J. Richardson, "A tuneable WDM wavelength converter based on cross phase modulation effects in normal dispersion holey fiber"
IEEE Photonics Technology Letters 2003 Vol.15 (3) pp. 437-439

L. Tartara, I. Cristiani, V. Degiorgio, F. Carbone, D.Faccio, M. Romagnoli, and **W. Belardi**, "Phase-matched nonlinear interactions in a holey fiber induced by infrared super-continuum generation"
Optics Communications 2003 Vol. 215 (1) pp.191-197

J. H. Lee, Z. Yusoff, **W. Belardi**, M. Ibsen, T. M. Monro, and D. J. Richardson, "Investigation of Brillouin effects in small-core holey optical fiber: lasing and scattering"
Optics Letters 2002 Vol.27 (11) pp.927-929

J. H. Lee, P. C. Teh, Z. Yusoff, M. Ibsen, **W. Belardi**, T. M. Monro, and D. J. Richardson, "A holey fiber-based nonlinear thresholding device for optical CDMA receiver performance enhancement"
IEEE Photonics Technology Letters 2002 Vol.14 (6) pp.876-878

J. H. V. Price, **W. Belardi**, T. M. Monro, A. Malinowski, A. Piper, and D. J. Richardson, "Soliton transmission and supercontinuum generation in holey fiber using a diode pumped Ytterbium fiber source"
Optics Express 2002 Vol.10 (8) pp.382-387

Z. Yusoff, J. H. Lee, **W. Belardi**, T. M. Monro, P. C.Teh, and D. J. Richardson, "Raman effects in a highly nonlinear holey fiber: amplification and modulation"
Optics Letters 2002 Vol.27 (6) pp. 424-426

P. Petropoulos, T. M. Monro, **W. Belardi**, K. Furusawa, J. H. Lee, and D. J. Richardson, "2R-regenerative all-optical switch based on a highly nonlinear holey fiber"
Optics Letters 2001 Vol.26 (16) pp.1233-1235

C. W. J. Hillman, W. S. Brocklesby, T. M. Monro, **W. Belardi**, and D. J. Richardson, "Structural and optical characterization of holey fibres using scanning probe microscopy"
Electronics Letters 2001 Vol.37 (21) pp.1283-1284

D. Faccio, A. Busacca, **W. Belardi**, V. Pruneri, P. G. Kazansky, T. M. Monro, D. J. Richardson, B. Grappe, M. Cooper, and C. N. Pannell, "First demonstration of thermal poling in holey fibres"
Electronics Letters 2001 Vol.37 (2) pp.107-108

T. M. Monro, **W. Belardi**, K. Furusawa, J. C. Baggett, N. G. R. Broderick, and D. J. Richardson, "Sensing with microstructured optical fibres"
Journal of Measurement Science and Technology 2001 Vol.12 (7) pp.854-858

J. C. Baggett, T. M. Monro, **W. Belardi**, K. Furusawa, and D.J. Richardson, "Assorted core air-clad fibre"
Electronic Letters 2000 Vol.36 (25) pp.2065-2066

Invited conference presentations

D. J. Richardson, K. Furusawa, H. Ebendorff-Heidepriem, P. Petropoulos, V. Finazzi, J. C. Baggett, **W. Belardi**, T. A. Kogure, J. H. Lee, Z. Yusoff, J. Nilsson, Y. Jeong, J. K. Sahu and T.M. Monro, "Practical applications of holey optical fibers"
OFC 2004, Los Angeles, 22-27 Feb 2004 (accepted)

J. H. Lee, **W. Belardi**, T. M. Monro, and D. J.Richardson "Holey fibre based nonlinear optical devices for telecommunications"

CLEO/QELS 2003, Baltimore, 3-5 Jun 2003

J. H. Lee, D. J. Richardson, Z. Yusoff, **W. Belardi**, and T. M. Monro, "System applications of holey fibers"
LEOS 2002, Glasgow, 10-14 Nov 2002

T. M. Monro, V. Finazzi, **W. Belardi**, K. M. Kiang, J. H. Lee, and D. J. Richardson, "Highly nonlinear holey optical fibres: design manufacture and device applications"
ECOC 2002, Copenhagen, 8-12 Sep 2002

D. J. Richardson, J. H. Lee, Z. Yusoff, **W. Belardi**, K. Furusawa, J. H. V. Price, M. Kiang, K. Frampton, D. Hewak, J. A. Tucknott, R. C. Moore, H. N. Rutt, and T. M. Monro, "Holey fibers for nonlinear fiber devices"
Optical Amplifiers And Their Applications (OAA) 2002, Vancouver, 14-17 Jul 2002

D. J. Richardson, T. M. Monro, **W.Belardi**, and K. Furusawa, "Holey fibers: new opportunities for manipulating light"
OECC 2002, Yokohama, Japan 8-12 Jul 2002

D. J. Richardson, T. M. Monro, **W. Belardi**, and K. Furusawa, "Holey fibers: new possibilities for guiding and manipulating light"
IEEE/LEOS Workshop on Fibre and Optical Passive Components (WFOPC 2002), Glasgow, 5-6 Jun 2002

D. J. Richardson, **W. Belardi**, K. Furusawa, J. H. V. Price, A. Malinowski, and T. M. Monro, "Holey fibers: fundamentals and applications"
CLEO 2002, Long Beach, California 19-24 May 2002

D. J. Richardson, **W. Belardi**, K. Furusawa, and T. M. Monro, "Holey fibres: fundamentals and applications"
CPT 2002, Yurakucho, Tokyo, 15-17 Jan 2002

N. G. R. Broderick, T. M. Monro, D. J. Richardson, and **W. Belardi**, "Practical aspects of holey optical fibres"
OECC/IOCC 2001, Sydney, 1-5 Jul 2001

T. M. Monro, J. C. Baggett, **W. Belardi**, K. Furusawa, J. H. V. Price, and D. J. Richardson, "Holey fibres: Properties applications and future directions"
ICTON 2001, Cracow, Poland 18-21 Jun 2001

J. H. V. Price, **W. Belardi**, L. Lefort, T. M. Monro, and D.J. Richardson, "Nonlinear

pulse compression dispersion compensation and soliton propagation in holey fiber at 1 μm"
Nonlinear Guided Waves and Their Applications 2001, Clearwater, Florida 25-28 Mar 2001

T. M. Monro, **W. Belardi**, K. Furusawa, N. G. R. Broderick, and D. J. Richardson,"Microstructured optical fibres: New opportunities for sensing"
OFS 2000, Venice, 11-13 Oct 2000

Post-deadline conference presentations

W. Belardi, J. H. Lee, K. Furusawa, Z. Yusoff, P. Petropoulos, M. Ibsen, T. M. Monro, and D. J. Richardson, "A 10 Gbit/s tuneable wavelength converter based on four-wave mixing in highly nonlinear holey fibre"
ECOC 2002, Copenhagen, 8-12 Sep 2002

J. H. Lee, Z. Yusoff, **W. Belardi**, M. Ibsen, T. M. Monro, B. Thomsen, and D. J. Richardson, "A holey fiber based WDM wavelength converter incorporating an apodized fiber Bragg grating filter"
CLEO/QELS 2002, Long Beach, California 19-24 Mar 2002

J. H. Lee, P.C. Teh, Z. Yusoff, M. Ibsen, **W. Belardi**, T. M. Monro, and D. J. Richardson, "An OCDMA receiver incorporating a holey fibre nonlinear thresholder"
ECOC 2001, Amsterdam, 30 Sep - 4 Oct 2001

J. H. Lee, Z. Yusoff, **W. Belardi**, T. M. Monro, P. C. Teh, and D. J. Richardson, "A holey fibre Raman amplifier and all-optical modulator"
ECOC 2001, Amsterdam, 30 Sep - 4 Oct 2001

Conference presentations

Z. Yusoff, P. C. Teh, P. Petropoulos, K. Furusawa, **W. Belardi**, T. M. Monro, and D. J. Richardson, "24 channels x 10 GHz multiwavelength pulse source based on supercontinuum generation in highly nonlinear holey fiber"
OFC 2003, Atlanta, 23-28 Mar 2003

Z. Yusoff, J. H. Lee, **W. Belardi**, T. M. Monro, and D. J. Richardson, "Applications of Raman effect in holey fibre"
Photon 2002, Cardiff, 2-5 Sep 2002

W. Belardi, T. M. Monro, J. H. Lee, Z. Yusoff, J. H. V. Price, A. Malinowski, A. Piper, and D. J. Richardson, "Silica holey fibres: fabrication and nonlinear effects"
Photon 2002, Cardiff, 2-5 Sep 2002

C. W. J. Hillman, W. S. Brocklesby, T. M. Monro, **W. Belardi**, and D. J.Richardson, "Optical characterization of holey fibers using NSOM techniques"
Near Field Optics (NFO 7), Rochester, 10-14 Aug 2002

J. H. Lee, Z. Yusoff, **W. Belardi**, T. M. Monro, B. Thomsen, and D. J. Richardson, "Holey fiber based tuneable WDM wavelength converter using cross-phase modulation and filtering"
ECOC 2002, Copenhagen, 8-12 Sep 2002

L. Tartara, I. Cristiani, V. Degiorgio, F. Carbone, D. Faccio, M. Romagnoli, and **W. Belardi**, "Phase matched nonlinear interactions in a holey fiber induced by infrared super-continuum generation"
IQEC 2002, Moscow, 22-28 June 2002

Z. Yusoff, J. H. Lee, **W. Belardi**, M. Ibsen, T. M. Monro, and D. J. Richardson, "A holey fiber based Brillouin laser"
CLEO 2002, Long Beach, California 19-24 May 2002

J. Nilsson, R. Selvas, **W. Belardi**, J. H. Lee, Z. Yusoff, T. M. Monro, D. J. Richardson, K. D. Park, P. H. Kim, and N. Park "Continuous-wave pumped holey fiber Raman laser"
OFC 2002, Anaheim, California 17-22 Mar 2002

W. Belardi, T. M. Monro, J. H. V. Price, J. H. Lee, P. Petropoulos, and D. J. Richardson, "Fabrication and applications of highly nonlinear silica holey fibres"
Quantum Electronics & Photonics (QEP 15), Glasgow, 3-6 Sep 2001

J. C. Baggett, T. M. Monro, **W. Belardi**, and D. J. Richardson, "Assorted core air-clad fibre"
IOP Physics Congress 2001, Brighton, 18-22 Mar 2001

P. Petropoulos, T. M. Monro, **W. Belardi**, K. Furusawa, J.H. Lee, and D. J. Richardson, "A highly nonlinear holey fiber and its application in a regenerative optical switch"
OFC 2001, Anaheim, 17-22 Mar 2001

D. Faccio, A. Busacca, V. Pruneri, P. G. Kazansky, T. M. Monro, **W. Belardi**, D. J. Richardson, B. Grappe, M. Cooper, and C. N. Pannell, "Experimental study of thermal poling in holey fibres"

Nonlinear Guided Waves and Their Applications, Clearwater, Florida 25-28 Mar 2001

J. C. Baggett, T. M. Monro, **W. Belardi**, K. Furusawa, and D. J. Richardson, "Assorted core air-clad fibre"
CLEO 2001, Baltimore, 6-11 May 2001

D. Faccio, A. Busacca, V. Pruneri, P. G. Kazansky, T. M. Monro, **W. Belardi**, D. J. Richardson, B. Grappe, M. Cooper, and C. N. Pannell, "First demonstration of thermal poling in holey fibres"
CLEO 2001, Baltimore, 6-11 May 2001

Patent applications

Z. Yusoff, **W. Belardi**, P. C. The, J. H. Lee, T. M. Monro, D. J. Richardson, "Optical fibre-based devices utilizing the Raman effect"
International publication number: WO 03029851 (publication date 10-04-2003)

W. Belardi, K. Furusawa, T. M. Monro, D. J. Richardson, P. W. Turner,"Holey optical fibres"
International publication number: WO 0216980 (publication date 28-2-2002)

Bibliography

G. P. Agrawal. *Fiber-optics communication systems.* Wiley: New York, 1997.

G. P. Agrawal. *Applications of nonlinear fiber optics.* Academic Press: New York, 2001a.

G. P. Agrawal. *Nonlinear fiber optics (3rd edition).* New York: Academic Press, 2001b.

O.L. Anderson. Cooling time of strong glass fibers. *J. Appl. Phys.*, 29:9–12, 1958.

K. Aoki, H.T. Miyazaki, H. Hirayama, K. Inoshita, T. Baba, N. Shinya, and Y. Aoyagi. Three-dimensional photonic crystals for optical wavelengths assembled by micromanipulation. *Appl. Phys. Lett.*, 81:3122–3124, 2002.

T. Appenzeller, I. Amato, R. Crawford, G. Graff, G. M. Freedman, D.and Whitesides, J.P. Mathias, C.T. Seto, J.A. Stroscio, D.M. Eigler, M. Sundaram, S.A. Chalmers, P.F. Hopkins, A.C. Gossard, K.D. Wise, and K. Najafi. Special section of "science" : Engineering a small world: from atomic manipulation to microfabrication. *Science*, 254:1300–1342, 1991.

M. Asghari, I. H. White, and R. V. Penty. Wavelength conversion using semiconductor optical amplifiers. *J. Lightwave Technol.*, 15:1181–1190, 1997.

O. Aso, S. Arai, T. Yagi, M. Tadakuma, Y. Suzuki, and S. Namiki. Broadband four-wave mixing generation in short optical fiber. *Electron. Lett.*, 36:709–711, 2000.

M. Asobe, T. Kanamori, and K. Kubodera. Ultrafast all-optical switching using highly nonlinear chalcogenide glass fiber. *IEEE Photon. Technol. Lett.*, 4:362–365, 1992.

J. C. Baggett, T. M. Monro, K. Furusawa, and D. J. Richardson. Comparative study of large mode holey and conventional fibers. *Opt. Lett.*, 26:1045–1047, 2001.

N. P. Bansal and R. H. Doremus. *Handbook of glass properties.* New York: Academic Press, 1986.

A. J. Barlow, J. J. Ramskov-Hansen, and D. N. Payne. Birefringence and polarization mode-dispersion in spun single-mode fibers. *Appl. Opt.*, 20:2962–2968, 1981.

S. Bateson. Critical study of the optical and mechanical properties of glass fibers. *J. Appl. Phys.*, 29:13–21, 1958.

P.C. Becker, N. A. Olsson, and J. R. Simpson. *Erbium-doped fiber amplifiers.* Academic Press, 1999.

W. Belardi, K. Furusawa, T. M. Monro, D. J. Richardson, and P. Turner. Holey optical fibres. *World Intellectual Property Organization (patent application)*, (WO 02/16980), 2002a.

W. Belardi, J. H. Lee, K. Furusawa, Z. Yusoff, P. Petropoulos, M. Ibsen, T. M. Monro, and D. J. Richardson. A 10 Gbit/s tuneable wavelength converter based on four-wave mixing in highly nonlinear holey fibre. *ECOC*, paper PD1.2 (postdeadline), 2002b.

P. J. Bennett, T. M. Monro, and D. J. Richardson. Toward practical holey fiber technology: fabrication, splicing, modeling, and characterization. *Opt. Lett.*, 24:1203–1205, 1999.

F. Bernabid, J. C. Knight, G. Antonopoulos, and P. St. J. Russell. Stimulated Raman scattering in hydrogen-filled hollow-core photonic crystal fiber. *Science*, 298:399–402, 2002.

T. A. Birks, J. C. Knight, and P. St. J. Russell. Endlessly single-mode photonic crystal fiber. *Opt. Lett.*, 22:961–963, 1997.

T. A. Birks, D. Mogilevtsev, J. C. Knight, and P. St. J. Russell. Dispersion compensation using single-material fibers. *IEEE Photon. Technol. Lett.*, 11:674–676, 1999.

T. A. Birks, P. J. Roberts, P. St. J. Russell, and D. J. Atkin. Full 2-D photonic bandgaps in silica/air structures. *Electron. Lett.*, 31:1941–1942, 1995.

M. Born and E. Wolf. *Principles of optics.* Cambridge University Press, New York, 1999.

A. Boskovic, S. V. Chernikov, J. R. Taylor, L. Gruner-Nielsen, and O. A. Levring. Direct continuous-wave measurement of n_2 in various types of telecommunication fiber at 1.55 μm. *Opt. Lett.*, 21:1966–1968, 1996.

G. Bouwmans, R. M. Percival, W. J. Wadsworth, J. C. Knight, and P. St. J. Russell. High power Er:Yb fiber laser with very high numerical aperture pump-cladding waveguide. *Appl. Phys. Lett.*, 83:817–818, 2003.

F. Brechet, P. Roy, J. Marcou, and D. Pragnoux. Single mode propagation into depressed core-index photonic-bandgap fibre designed for zero-dispersion propagation at short wavelengths. *IEEE Electron. Lett.*, 36:514–515, 2000.

N. G. R. Broderick, T. M. Monro, P. J. Bennett, and D. J. Richardson. Nonlinearity in holey optical fibres: measurement and future opportunities. *Opt. Lett.*, 24:1395–1397, 1999a.

N. G. R. Broderick, H. L. Offerhaus, D. J. Richardson, R. A. Sammut, J. Caplen, and L. Dong. Large mode area fibres for high power applications. *J. Opt. Fibre Technol.*, 5:185–196, 1999b.

J.K. Chandalia, B.J. Eggleton, R.S. Windeler, S.G. Kosinski, X. Liu, and C. Xu. Adiabatic coupling in tapered air-silica microstructured optical fiber. *IEEE Photon. Technol. Lett.*, 13:52–54, 2001.

A.T. Clausen, L. Oxenlowe, C. Peucheret, H. N. Poulsen, P. Jeppersen, S. N. Knudsen, and L. Gruner-Nielsen. 10 GHz return-to-zero pulse source tunable in wavelength with a single or multiwavelength output based on four wave mixing in a newly developed highly nonlinear fiber. *IEEE Photon. Technol. Lett.*, 13:70–72, 2001.

R. F. Cregan, B. J. Mangan, J. C. Knight, T. A. Birks, and P. St. J. Russell. Photonic bandgap guidance in optical fibers. *Science*, 285:1537–1539, 1999.

R.H. Doremus. *Glass science.* John Wiley & Sons Inc., 1994.

H. Ebendorff-Heidepriem, P. Petropoulos, V. Finazzi, K. Frampton, R.C. Moore, D.J. Richardson, and T. M. Monro. Highly nonlinear bismuth-oxide-based glass holey fiber. *submitted for OFC*, 2004.

B.J. Eggleton, P.A. Krug, L. Poladian, and F. Ouellette. Long periodic superstructure Bragg gratings in optical fibres. *Electron. Lett.*, 30:1620–1622, 1994.

B.J. Eggleton, P.S. Westbrook, C.A. White, C. Kerbage, R.S. Windeler, and G.L. Burdge. Cladding-mode-resonances in air-silica microstructure optical fibers. *J. Lightwave Technol.*, 18:1084–1100, 2000.

B.J. Eggleton, P.S. Westbrook, R.S. Windeler, S. Spalter, and T.A. Strasser. Grating resonances in air-silica microstructured optical fibers. *Opt. Lett.*, 24:1460–1462, 1999.

R.P. Espindola, R.S. Windeler, A. A. Abramov, B.J. Eggleton, T.A. Strasser, and D.J. DiGiovanni. External refractive index insensitive air-clad long period fibre grating. *Electron. Lett.*, 35:327–328, 1999.

D. Faccio, A. Busacca, W. Belardi, V. Pruneri, P. G. Kazansky, T. M. Monro, D. J. Richardson, B. Grappe, M. Cooper, and C. N. Pannell. Demonstration of thermal poling in holey fibres. *Electron. Lett*, 37:107–8, 2001.

L. Farr, J. C. Knight, B. J. Mangan, and P. J. Roberts. Low loss photonic crystal fibre. *ECOC*, paper PD3 (postdeadline), 2002.

X. Feng, T.M. Monro, P. Petropoulos, V. Finazzi, and D. Hewak. Soho (solid holey) fiber. *ECOC*, paper We1.7.2, 2003.

A. Ferrando, E. Silvestre, J. J. Miret, and P. Andres. Nearly zero ultraflattened dispersion in photonic crystal fibers. *Opt. Lett.*, 25:790–792, 2000.

A. Ferrando, E. Silvestre, J. J. Miret, J. A. Monsoriu, M. V. Andres, and P. St. J. Russell. Designing a photonic crystal fiber with flattened chromatic dispersion. *Electron.Lett.*, 35:325–327, 1999.

V. Finazzi, T. M. Monro, and D. J. Richardson. Fundamental properties of small core holey fibers. *ECOC*, paper We1.7.6, 2003a.

V. Finazzi, T. M Monro, and D. J. Richardson. The role of confinement loss in highly nonlinear silica holey fibers. *IEEE Photon. Technol. Lett.*, 15:1246–1248, 2003b.

V. Finazzi, T. M. Monro, and D. J. Richardson. Small-core silica holey fibers: nonlinearity and confinement loss trade-offs. *J. Opt. Soc. Am. B*, 20:1427–1436, 2003c.

V. Finazzi, T.M. Monro, and D.J. Richardson. Confinement loss in highly nonlinear holey optical fibres. *OFC*, paper ThS4, 2002.

A. D. Fitt, K. Furusawa, T. M. Monro, C. P. Please, and D. J. Richardson. The mathematical modelling of capillary drawing for holey fibre manufacture. *J. Engineering Mathematics*, 43:201–27, 2002.

J.G. Fleming, S.Y.; Lin, I. El-Kady, R. Biswas, and K.M. Ho. All-metallic three-dimensional photonic crytal with a large infrared bandgap. *Nature*, 417:52–55, 2002.

K. Furusawa, A. N. Malinowski, J. H. V. Price, T. M. Monro, J. K. Sahu, J. Nilsson, and D. J. Richardson. A cladding pumped ytterbium-doped fiber laser with holey inner and outer cladding. *Opt. Express*, 9:714–20, 2001.

A. Galtarossa, B. S. Marks, C.R. Menyuk, L. Palmieri, and A. Pizzinat. Low PMD fibers. *LEOS*, paper TuB1.2, 2003a.

A. Galtarossa, L. Palmieri, A. Pizzinat, B.S. Marks, and C. R. Menyuk. An analytical formula for the mean differential group delay of randomly birefringent spun fibers. *J. Lightwave Techn.*, 21:1635–1643, 2003b.

A. Ghatak and K. Thyagarajan. *Introduction to fiber optics.* Cambridge: Academic Press, 1998.

I. C. Goyal, A. K. Ghatak, and R. K. Varshney. Dispersion compensating fibers. *ICTON*, paper Mo.A.5, 2002.

D. F. Grosz, C. Mazzali, S. Celaschi, A. Paradisi, and H. L. Fragnito. Modulation instability induced resonant four-wave mixing in WDM systems. *IEEE Photon. Technol. Lett.*, 11:379–381, 1999.

L. Gruner-Nielsen, S. N. Knudsen, T. Veng, B. Edvold, and C. C. Larsen. Design and manufacture of dispersion compensating fibre for simultaneous compensation of dispersion and dispersion slope. *OFC*, 2:232 –234, 1999.

G.C. Gupta, R.E. Tench, O. Mizuhara, L.L. Wang, N.N. Dang, N. Chand, B. Mason, A. Ougazzaden, and C.W. Lentz. 3.2 Tbit/s (40 ch × 80 Gb/s) transmission over 1000 km with 100 km span (25 dB loss) and 0.8 bit/s/Hz of spectral efficiency. *OFC*, paper TuA5, 2002.

K. P. Hansen, J. R. Folkenberg, C. Peucheret, and A. Bjarklev. Fully dispersion controlled triangular-core nonlinear photonic crystal fiber. *OFC*, paper PD2-1 (postdeadline), 2003.

K.P. Hansen, J.R. Jensen, C. Jacobsen, H.R. Simonsen, J. Broeng, P.M.W. Skovgaard, and A. Petersson. Highly nonlinear photonic crystal fiber with zero-dispersion at 1.55 μm. *OFC*, paper FA9-1 (postdeadline), 2002.

J. Hansryd, F. Dross, M. Westlund, P. A. Antrekson, and S. N. Knudsen. Increase of the SBS threshold in a short highly nonlinear fiber by applying a temperature distribution. *J. Lightwave Technol.*, 19:1691–1697, 2001.

A.C. Hart, R.G. Huff, and K.L. Walker. Method of making a fiber having low polarization mode dispersion due to a permanent spin. *United States Patent*, 5,298,047, 1994.

K. O. Hill, Y. Fujii, D. C. Johnson, and B. S. Kawasaki. Photosensitivity in optical fibre waveguides: Application to reflection filter fabrication. *Appl. Phys. Lett.*, 32:647–649, 1978.

K. O. Hill, B. Malo, F. Bilodeau, D. C. Johnson, and J. Albert. Bragg gratings fabricated in monomode photosensitive optical fiber by UV exposure through a phase mask. *Appl. Phys. Lett.*, 62:1035–1037, 1993.

K.O. Hill, B. Malo, K.A. Vineberg, F. Bilodeau, D.C. Johnson, and I Skinner. Efficient mode conversion in telecommunication fibre using externally written gratings. *IEE Electron. Lett.*, 26:1270–1272, 1990.

K. M. Ho, C. M. Chan, C. T.and Soukoulis, R. Biswas, and M. Sigalas. Photonic band gaps in three dimensions: New layer-by-layer periodic structures. *Solid State Commun.*, 89:413–416, 1994.

K. M. Ho, C. T. Chan, and C. M. Soukoulis. Existence of a photonic gap in periodic dielectric structures. *Phys. Rev. Lett.*, 65:3152–3155, 1990.

M. Ibsen and R. Feced. Broadband fibre Bragg gratings for pure third-order dispersion compensation. *OFC*, paper FA7, 2002.

K. Imoto, M. Sumi, G. Toda, and T. Suganuma. Optical fiber drawing method with gas flow controlling system. *J. Lightwave Technol.*, 7:115–121, 1989.

K. Inoue and H. Toba. Wavelength conversion experiment using fiber four-wave mixing. *IEEE Photon. Technol. Lett.*, 4:69–72, 1992.

J. D. Joannopoulos, R. D. Meade, and J. N. Winn. *Photonic Crystals.* Princeton University Press, 1995.

J. D. Joannopoulos, P. R. Villeneuve, and S. Fan. Photonic crystals: putting a new twist on light. *Nature*, 386:143–149, 1997.

S. John. Strong localization of photons in certain disordered dielectric superlattices. *Phys. Rev. Lett.*, 58:2486–2489, 1987.

S.G. Johnson and J.D. Joannopoulos. Three-dimensionally periodic dielectric layered structure with omnidirectional photonic band gap. *Appl. Phys. Lett.*, 77:3490–3492, 2000.

P. Kaiser and H. W. Astle. Low-loss single material fibers made from pure fused silica. *Bell Syst. Tech. J.*, 53:1021–1039, 1974.

G. Kakarantzas, T. A. Birks, and P. St. J. Russell. Structural long-period gratings in photonic crystal fibers. *Opt. Lett.*, 27:1013–1015, 2002.

G. Kakarantzas, A. Ortigosa-Blanch, T. A. Birks, P. St. J. Russell, L. Farr, F. Couny, and B. J. Mangan. Structural rocking filters in highly birefringent photonic crystal fiber. *Opt. Lett.*, 28:158–160, 2003.

F. P. Kapron, D. B. Keck, and R. D. Maurer. Radiation losses in glass optical waveguides. *Appl. Phys. Lett.*, 17:423–425, 1970.

R. Kashyap. *Fiber Bragg Gratings.* Accademic Press, San Diego (CA), 1999.

C. Kerbage, A. Hale, A. Yablon, S. Windeler, and B. J. Eggleton. Integrated all-fiber variable attenuator based on hybrid microstructure fiber. *App. Phys. Lett.*, 79:3191–3193, 2001.

K. M. Kiang, K. Frampton, T. M. Monro, R. Moore, J. Tuchnott, D. W. Hewak, D. J. Richardson, and H. N. Rutt. Extruded single mode non-silica glass holey optical fibers. *Electron. Lett.*, 38:546–547, 2002.

S. J. Kim, J. H. Han, J. S. Lee, and C. S. Park. Intensity noise suppression in spectrum-sliced incoherent light communication systems using a gain-saturated semiconductor optical amplifier. *IEEE Phot. Technol. Lett.*, 11:1042–1044, 1999.

J. C. Knight, J. Arriaga, T. A. Birks, A. Ortigosa-Blanch, W. J. Wadsworth, and P. St. J. Russell. Anomalous dispersion in photonic crystal fiber. *IEEE Photon. Technol. Lett.*, 12:807–809, 2000.

J. C. Knight, T. A. Birks, R. F. Cregan, P. St. J. Russell, and J. P. De Sandro. Large mode area photonic crystal fibre. *Electron. Lett.*, 34:1347–1348, 1998a.

J. C. Knight, T. A. Birks, Russell P. St. J., and D. M. Atkin. All-silica single-mode optical fiber with photonic crystal cladding. *Opt. Lett.*, 21:1547–1549, 1996.

J. C. Knight, J. Broeng, T. A. Birks, and P. St. J. Russell. Photonic bandgap guidance in optical fibers. *Science*, 282:1476–1478, 1998b.

T. F. Krauss. Planar photonic crystal waveguide devices for integrated optics. *Phys. Stat. Sol. (a)*, 197:688–702, 2003.

T. F. Krauss, R. M. De La Rue, and S. Brand. Two dimensional photonic bandgap structures operating at near infrared wavelengths. *Nature*, 383:699–702, 1996.

B.T. Kuhlmey, T.P. White, G. Renversez, D. Maystre, L.C. N. Botten, C.M. de Sterke, and R.C. McPhedran. Multipole method for microstructured optical fibers. ii. implementation and results. *J. Opt. Soc. Am. B*, 19:2331–40, 2002.

S. Kyriacou, C.E. Polymeropoulos, and V. Sernas. Accelerated cooling of optical fibers. *Mat. Res. Soc. Symp. Proc.*, 172:49–54, 1990.

J. H. Lee, W. Belardi, K. Furusawa, P. Petropoulos, Z.; Yusoff, T.M. Monro, and D.J. Richardson. Four-wave mixing based 10-Gb/s tunable wavelength conversion using a holey fiber with a high SBS threshold. *IEEE Phot. Techn. Lett.*, 15:440–42, 2003a.

J. H. Lee, Z. Yusoff, W. Belardi, M. Ibsen, T. M. Monro, and D. J. Richardson. Investigation of Brillouin effects in small-core holey optical fiber: lasing and scattering. *Opt. Lett.*, 27:927–9, 2002a.

J. H. Lee, Z. Yusoff, W. Belardi, M. Ibsen, T. M. Monro, and D. J. Richardson. A tunable WDM wavelength converter based on cross-phase modulation effects in normal dispersion holey fiber. *IEEE Photon. Technol. Lett.*, 15:437–439, 2003b.

J. H. Lee, Z. Yusoff, W. Belardi, M. Ibsen, T.M. Monro, B. Thomsen, and D.J. Richardson. A holey fiber based WDM wavelength converter incorporating an apodized fiber Bragg grating filter. *CLEO*, paper: CPDB5 (postdeadline), 2002b.

J.H. Lee, Z. Yusoff, W. Belardi, T.M. Monro, P.C. Teh, and D.J. Richardson. A holey fibre Raman amplifier and all-optical modulator. *ECOC*, paper PDA 1.1 (postdeadline), 2001.

P.J. Lemaire, R.M. Atkins, V. Mizrahi, and W.A. Reed. High pressure H_2 loading as a technique for achieving ultrahigh UV photosensitivity and thermal sensitivity in GeO_2 doped optical fibres. *Electron. Lett.*, 29:1191–1193, 1993.

M.J. Li and D.A. Nolan. Fiber spin-profile designs for producing fibers with low polarization mode dispersion. *Opt. Lett.*, 23:1659–1661, 1998.

T. Li. *Optical fiber communications.* Academic Press Inc., 1985.

J. Limpert, T. Schreiber, S. Nolte, H. Zellmer, A. Tunnermann, R. Iliew, F. Lederer, J. Broeng, G. Vienne, A. Petersson, and C. Jacobsen. High power air-clad large mode area photonic crystal fiber laser. *Opt. Expr.*, 11:818–823, 2003.

S.Y. Lin, J.G. Fleming, D.L. Hetherington, B.K. Smith, R. Biswas, K.M. Ho, M.M. Sigalas, W. Zubrzycki, S.R. Kurtz, and J. Bur. A three-dimensional photonic crystal operating at infrared wavelengths. *Nature*, 394:251–253, 1998.

C. Lopez. Materials aspects of photonic crystals. *Advanced Materials*, 15:1679–1704, 2003.

W. N. MacPherson, M. J. Gander, R. McBride, J. D. C. Jones, P. M. Blanchard, J. G. Burnett, A. H. Greenaway, B. Mangan, T. A. Birks, J. C. Knight, and P. St. J. Russell. Remotely addressed optical fibre curvature sensor using multicore photonic crystal fibre. *Optics Commun.*, 193:97–104, 2001.

W. N. MacPherson, J. D. C. Jones, B. J. Mangan, J. C. Knight, and P. St. J. Russell. Two-core photonic crystal fibre for doppler difference velocimetry. *Optics Commun.*, 223:375–380, 2003.

P. V. Mamyshev. All-optical data regeneration based on self-phase modulation effect. *ECOC*, pages 475–476, 1998.

B. J. Mangan, J. C. Knight, T. A. Birks, P. St. J. Russell, and A. H. Greenaway. Experimental study of dual-core photonic crystal fibre. *Electron. Lett.*, 36:1358–1359, 2000.

G. Meltz, W.W. Morey, and W.H. Glen. Formation of Bragg gratings in optical fibers by a transverse holographic method. *Opt. Lett.*, 14:823–825, 1989.

D. Mogilevtsev, T. A. Birks, and P. St. J. Russell. Group-velocity dispersion in photonic crystal fibers. *Opt. Lett.*, 23:1662–1664, 1998.

T. M. Monro, W. Belardi, K. Furusawa, J. C. Baggett, N. G. R. Broderick, and D. J. Richardson. Sensing with microstructured optical fibres. *Meas. Sci. Technol.*, 12: 854–858, 2001.

T. M. Monro, P. J. Bennett, N. G. R. Broderick, and D. J. Richardson. Holey fibers with random cladding distributions. *Opt. Lett.*, 25:206–208, 2000.

T. M. Monro, D. J. Richardson, N. G. R. Broderick, and P. J. Bennett. Dispersion in holey optical fibers. *WDM Topics*, 29, 1999a.

T. M. Monro, D. J. Richardson, N. G. R. Broderick, and P. J. Bennett. Holey optical fibers: an efficient modal model. *J. Lightwave Technol.*, 17:1093–1101, 1999b.

K. Nagayama, M. Kakui, M. Matsui, T. Saitoh, and Y. Chigusa. Ultra-low-loss (0.1484 dB/km) pure silica core fibre and extension of transmission distance. *Electron. Lett.*, 38:1168–1169, 2002.

S. R. Nagel, J. B. MacChesney, and K. L. Walker. An overview of the modified chemical vapor deposition MCVD process and performance. *IEEE J. Quantum Electron.*, 18: 459–475, 1982.

N. Nakazawa, H. Kubota, and K. Tamura. Random evolution and coherence degradation of a high-order optical soliton train in the presence of noise. *Opt. Lett.*, 24:318–320, 1999.

S. Namiki and Y. Emori. Ultrabroad-band Raman amplifiers pumped and gain equalized by wavelength-division-multiplexed high-power laser diodes. *IEEE J. Sel. Top. Quantum Electron.*, 7:3–16, 2001.

L. E. Nelson. Optical fibers for high capacity WDM, long-haul systems. *IEICE Trans. Electron.*, E86-C:693–698, 2003.

M. D. Nielsen and N. A. Mortensen. Photonic crystal fiber design based on the V-parameter. *Opt. Expr.*, 11:2762–2768, 2003.

M. Nissov, K. Rottwitt, H. D. Kidorf, and M. X. Ma. Rayleigh crosstalk in long cascades of distributed unsaturated Raman amplifiers. *Electron. Lett.*, 35:997–8, 1999.

J. Noda, K. Okamoto, and Y. Sasaki. Polarization-maintaining fibers and their applications. *J. Ligthwave Technol.*, LT-4:1071–89, 1986.

S. Noda, K. Tomoda, N. Yamamoto, and A. Chutinan. Full three-dimensional photonic bandgap crystals at near-infrared wavelengths. *Science*, 289:604–606, 2000.

P. Ohlen, B. E. Olsson, and D. Blumenthal. Wavelength dependence and power requirements of a wavelength converter based on XPM in a dispersion-shifted optical fiber. *IEEE Photon. Technol. Lett.*, 12:522–524, 2000.

T. Okuno, M. Onishi, T. Kashiwada, S. Ishikawa, and M. Nishimura. Silica-based functional fibers with enhanced nonlinearity and their applications. *IEEE J. Sel. Top. Quantum Electron.*, 5:1385–1391, 1999.

A. Ortigosa-Blanch, J. C. Knight, W. J. Wadsworth, J. Arriaga, B. J. Mangan, T. A. Birks, and P. St. J. Russell. Highly birefringent photonic crystal fibers. *Opt. Lett.*, 25:1325–1327, 2000.

A. Othonos and K. Kalli. *Fiber Bragg Gratings.* Artec House, Boston, 1999.

U.C. Paek. Free drawing and polymer coating of silica glass optical fibers. *Transactions of the ASME*, 121:774–788, 1999.

H. Papamichael and J. N. Miaoulis. Heat transfer in the heating region of the optical fiber drawing process. *SPIE*, 2287:11–20, 1994.

I. R. Parry and P. M. Gray. Instrumentation in astronomy VI. *ed D.L. Crawford, Proc. SPIE*, 627:118, 1986.

D. N. Payne, R. J. Mansfield, J. J. Ramskov-Hansen, M. R. Hadley, and A. J. Barlow. Optical fibres and their manufacture. *World Intellectual Property Organization*, (WO83/00232), 1983.

P. Petropoulos, T. Monro, H. Ebendorff-Heidepriem, K. Frampton, R. Moore, H. Rutt, and D. J. Richardson. Soliton-self-frequency-shift effects and pulse compression in an anomalously dispersive high nonlinearity lead silicate holey fiber. *OFC*, paper PD0.3 (postdeadline), 2003.

P. Petropoulos, T. M. Monro, W. Belardi, K. Furusawa, J. H. Lee, and D. J. Richardson. A 2R-regenerative all-optical switch based on a highly nonlinear holey fiber. *Opt. Lett.*, 26:1233–5, 2001a.

P. Petropoulos, T. M. Monro, W. Belardi, K. Furusawa, J. H. Lee, and D. J. Richardson. A highly nonlinear holey fiber and its application in a regenerative optical switch. *OFC*, paper TuC, 2001b.

H. G. Pfaender. *Schott guide to glass*. Chapman & Hall, 1996.

J. H. V. Price, W. Belardi, L. Lefort, T. M. Monro, and D. J. Richardson. Nonlinear pulse compression, dispersion compensation, and soliton propagation in holey fiber at 1 μm. *NLGW*, paper WB1, 2001a.

J. H. V. Price, W. Belardi, T. M. Monro, A. Malinowski, A. Piper, and D. J. Richardson. Soliton transmission and supercontinuum generation in holey fiber using a diode pumped ytterbium fiber source. *Opt. Expr.*, 10:382–387, 2002.

J.H.V.P. Price, K. Furusawa, T.M. Monro, L. Lefort, and D.J. Richardson. A tunable. femtosecond pulse source operating in the range 1.06-1.33 microns based on an Yb doped holey fiber amplifier. *CLEO*, paper CPD1, 2001b.

M. Qi and H. I. Smith. Achieving nanometer-scale, controllable pattern shifts in X-ray lithography using an assembly-tilting technique. *J. Vacuum Science & Technol. B*, 20:2991–2994, 2002.

J. K. Ranka, R. S. Windeler, and A. J. Stentz. Efficient visible continuum generation in air-silica microstructure optical fibers with anomalous dispersion at 800 nm. *CLEO*, paper CPD8-1 (postdeadline), 1999.

J. K. Ranka, R. S. Windeler, and A. J. Stentz. Visible continuum generation in air-silica microstructure optical fibers with anomalous dispersion at 800 nm. *Opt. Lett.*, 25: 25–27, 2000.

V. V. Ravi Kanth Kumar, A. K. George, J. C. Knight, and P.St. J. Russell. Tellurite photonic crystal fibre. *Opt. Expr.*, 11:2641–2645, 2003.

V. V. Ravi Kanth Kumar, A. K. George, W. H. Reeves, J. C. Knight, P. St. J. Russell, F. G. Omenetto, and F. G. Taylor. Extruded soft glass photonic crystal fiber for ultrabroad supercontinuum generation. *Opt. Expr.*, 10:1520–1525, 2002.

W. H. Reeves, J. C. Knight, P. St. J Russell, and P. J. Roberts. Demonstration of ultra-flattened dispersion in photonic crystal fibers. *Opt. Expr.*, 10:609–613, 2002.

G.F. Round and V.K. Garg. *Applications of fluid dynamics*. London: Edward Arnold, 1985.

P. St. J. Russell. Photonic band gaps. *Physics world*, August:37–42, 1992.

P. St. J. Russell. Photonic crystal fibers. *Science*, 299:358–362, 2003.

J. K. Sahu, C. C. Renaud, K. Furusawa, R. Selvas, J. A. Alvarez-Chavez, D. J. Richardson, and J. Nilsson. Jacketed air-clad cladding pumped ytterbium-doped fibre laser with wide tuning range. *Electron. Lett.*, 37:1116–1117, 2001.

T. Sakamoto, F. Futami, K. Kikuchi, S. Takeda, Y. Sugaya, and S. Watanabe. All optical wavelength conversion of 500 fs pulse train by using a nonlinear optical loop mirror composed of a highly nonlinear DSF. *Photon. Technol. Lett.*, 13:502–504, 2001.

S. Y. Set, B. Dabarsyah, C. S. Goh, K. Katoh, Y. Takushima, K. Kikuchi, Y. Okabe, and N. Takeda. A widely tunable fiber Bragg grating with a wavelength tunability over 40 nm. *OFC*, MC4, 2001.

E. B. Shand. *Modern materials*, volume 6. Academic press: New York, 1968.

D.N. Sharp, M. Campbell, E.R. Dedman, M.T. Harrison, R.G. Denning, and A.J. Turberfield. Photonic crystals for the visible spectrum by holographic lithography. *Opt. Quant. Electron.*, 34:3–12, 2002.

J. E. Sharping, M. Fiorentino, A. Coker, P. Kumar, and R. S. Windeler. Four-wave mixing in microstructure fiber. *Opt. Lett.*, 26:1048–1050, 2001.

J. E. Sharping, M. Fiorentino, P. Kumar, and R. S. Windeler. All-optical switching based on cross-phase modulation in microstructure fiber. *IEEE Photon. Technol. Lett.*, 14: 77–79, 2002a.

J. E. Sharping, M. Fiorentino, P. Kumar, and R. S. Windeler. Optical parametric oscillator based on four-wave mixing in microstructure fiber. *Opt. Lett.*, 27:1675–1677, 2002b.

R. M. Shelby, M. D. Levenson, and P. W. Bayer. Resolved forward Brillouin scattering in optical fibers. *Phys. Rev. Lett.*, 54:939–942, 1985.

L. P. Shen, W. P. Huang, G. X. Chen, and S. S. Jian. Design and optimization of photonic crystal fibers for broad-band dispersion compensation. *IEEE Photon. Technol. Lett.*, 15:540–542, 2003.

K. Shiraki, M. Ohashi, and M. Tateda. SBS threshold of a fiber with a Brillouin frequency shift distribution. *J. Lightwave Technol.*, 14:50–57, 1996.

A. I. Siahlo, L. K. Oxenlowe, A. T. Berg, K. S.and Clausen, P. A. Andersen, C. Peucheret, A. Tersigni, P. Jeppesen, K. P. Hansen, and J. R. Folkenberg. A

high-speed demultiplexer based on a nonlinear optical loop mirror with a photonic crystal fiber. *IEEE Photon. Technol. Lett.*, 15:1147–1149, 2003.

C. Simonneau, P. Bousselet, G. Melin, L. Provost, and C. Moreau. High power air-clad photonic crystal fiber cladding-pumped EDFA for WDM applications in the C-band. *ECOC*, paper Th4.1.2 (postdeadline), 2003.

C. M. Smith, N. Venkataraman, M. T. Gallagher, D. Muller, J. A. West, N. F. Borrelli, D. C. Allan, and K. W. Koch. Low loss hollow core silica/air photonic bandgap fibre. *Nature*, 424:657–659, 2003.

R. G. Smith. Optical power handling capacity of low loss optical fibers as determined by stimulated Raman and Brillouin scattering. *Appl. Optics*, 11:2489–2494, 1972.

S. P. Smith, F. Zarinetchi, and S. Ezekiel. Narrow-linewidth stimulated Brillouin fiber laser and applications. *Opt. Lett.*, 16:393–395, 1991.

H. S. Sozuer and J. P. Dowling. Photonic band calculations for woodpile structures. *J. Mod. Opt.*, 41:231–239, 1994.

R. Stegeman, L. Jankovic, H. Kim, C. Rivero, G. Stegeman, K. Richardson, P. Delfyett, Y. Guo, A. Schulte, and T. Cardinal. Tellurite glasses with peak absolute raman gain coefficients up to 30 times that of fused silica. *Opt. Lett.*, 28:1126–1128, 2003.

K. Suzuki, H. Kubota, S. Kawanishi, M. Tanaka, and M. Fujita. Optical properties of low-loss polarization maintaining photonic crystal fiber. *Opt. Expr.*, 9:676–680, 2001.

K. Tajima, J. Zhou, K. Kurokawa, and K. Nakajima. Low water peak photonic crystal fibre. *ECOC*, paper Th4.1.6 (postdeadline), 2003.

Y. Tanaka and K. Hotate. Analysis of fiber Brillouin ring laser composed of single-polarization single-mode fiber. *J. Lightwave Technol.*, 15:838–844, 1997.

C. L. Tang. Saturation and spectral characteristics of the Stokes emission in the Stimulated Brillouin process. *J. Appl.Phys.*, 37:2945–2955, 1966.

R. W. Tkach, A. R. Chraplyvy, and R. M. Derosier. Spontaneous Brillouin scattering for single-mode optical fibre characterization. *Electron. Lett.*, 22:1011–1013, 1986.

R. J. Tonucci, B. L. Justus, A. J. Campillo, and C. E. Ford. Nanochannel array glass. *Science*, 258:783–785, 1992.

Th. Udem, R. Holzwarth, and T. W. Hansch. Optical frequency metrology. *Nature*, 416: 233–237, 2002.

N. Venkataraman, M. T. Gallagher, C. M. Smith, D. Müller, J. A. West, and J. C. Koch, K. W.and Fajardo. Low loss (13 dB/km) air core photonic band-gap fibre. *ECOC*, paper PD1, 2002.

W. J. Wadsworth, J. C. Knight, A. Ortigosa-Blanch, J. Arriaga, E. Silvestre, and P. St. J. Russell. Soliton effects in photonic crystal fibres at 850 nm. *Electron. Lett.*, 36:53–55, 2000.

W. J. Wadsworth, J. C. Knight, and P. St. J. Russell. Large mode area photonic crystal fibre laser. *CLEO*, paper CWC1, 2001.

W. J. Wadsworth, R. M. Percival, G. Bouwmans, J. C. Knight, and P. St. J. Russell. High power air-clad photonic crystal fibre laser. *Opt. Expr.*, 11:48–53, 2003.

S. Watanabe and F. Futami. All-optical signal processing using highly nonlinear optical fibers. *IEICE Trans. Commun.*, 84-B:1179–1189, 2001.

S. Watanabe, T. Naito, and T. Chikama. Compensation of chromatic dispersion in a single mode fiber by optical phase conjugation. *IEEE Photon. Technol. Lett.*, 5:92–94, 1993.

M. J. Weber. *Handbook of optical materials.* CRC press, 2003.

I. H. White, R. V. Penty, M. Webster, Y. J. Chai, A. Wonfor, and S. Shahkooh. Wavelength switching components for future photonics networks. *Communications Magazine*, 40:74–81, 2002a.

T. P. White, R. C. McPhedran, C. M. de Sterke, L. C. Botten, and M. J. Steel. Confinement losses in microstructured optical fibers. *Opt. Lett.*, 26:1660–1662, 2001.

T.P. White, B.T. Kuhlmey, R.C. McPhedran, D. Maystre, G. Renversez, C.M. de Sterke, and L.C. Botten. Multipole method for microstructured optical fibers. i. formulation. *J. Opt. Soc. Am. B*, 19:2322–30, 2002b.

J.A.R. Williams, I. Bennion, and L. Zhang. The compression of optical pulses using self-phase-modulation and linearly chirped Bragg-gratings in fibers. *IEEE Photon. Technol.Lett.*, 7:491–493, 1995.

Y. Xu and A. Yariv. Loss analysis of air-core photonic crystal fibers. *Opt. Lett.*, 28: 1885–1887, 2003.

E. Yablonovitch. Inhibited spontaneous emission in solid-state physics and electronics. *Phys. Rev. Lett.*, 58:2059–2062, 1987.

E. Yablonovitch. Photonic band-gap structures. *J. Opt. Soc. Am. B*, 10:283–295, 1993.

E. Yablonovitch. Photonic bandgap based designs for nano-photonic integrated circuits. *IEDM*, paper 1.3.1:17–20, 2002.

E. Yablonovitch, T.J. Gmitter, and K. M. Leung. Photonic band structure: The face-centered-cubic case employing nonspherical atoms. *Phys. Rev. Lett.*, 67:2295–2299, 1991.

T. Yamamoto, E. Yoshida, and M. Nakazawa. Ultrafast nonlinear optical loop mirror for demultiplexing 640 Gbit/s TDM signals. *Electron. Lett.*, 34:522–528, 1998.

A. Yariv and P. Yeh. *Optical waves in crystals*. Wiley, New York, 1984.

P. Yeh, A. Yariv, and C. Hong. Electromagnetic propagation in periodic stratified media. *J. Opt. Soc. Am.*, 67:423–448, 1977.

P. Yeh, A. Yariv, and E. Marom. Theory of Bragg fiber. *J. Opt. Soc. Am.*, 68:1196–1201, 1978.

J. Yu and P. Jeppersen. 80 Gb/s wavelength conversion based on cross-phase modulation in high-nonlinearity dispersion-shifted fiber and optical filtering. *IEEE Photon. Technol. Lett.*, 13:833–835, 2001.

J. Yu, X. Zheng, C. Peucheret, A. T. Clausen, H. N. Poulsen, and P. Jeppersen. 40 Gb/s all-optical wavelength conversion based on a nonlinear optical loop mirror. *J. Lightwave Technol.*, 18:1001–1006, 2000.

Z. Yusoff, W. Belardi, P. C. Teh, J. H. Lee, T. M. Monro, and D. J. Richardson. Optical fibre-based devices utilising the Raman effect. *World Intellectual Property Organization (patent application)*, (WO 03/029851), 2003.

Z. Yusoff, J. H. Lee, W. Belardi, T. M. Monro, P. C. Teh, and D. J. Richardson. Raman effects in a highly nonlinear holey fiber: amplification and modulation. *Opt. Lett.*, 27: 424–6, 2002a.

Z. Yusoff, J.H. Lee, W. Belardi, T.M. Monro, P.C. Teh, and D.J. Richardson. A holey fibre Brillouin laser. *CLEO*, paper CMJ7, 2002b.